CRANFIELD INSTITUTE OF TECHNOLOGY

SCHOOL OF MECHANICAL ENGINEERING

DEPARTMENT OF FLUID ENGINEERING AND INSTRUMENTATION

TOTAL TECHNOLOGY

PhD THESIS

Academic Year 1989-1992

THEORETICAL AND COMPUTATION MODELLING OF POLYMER SEAL LIFE

by

Mrs Tsz Hang Emily Ting Ho

Supervisors : Dr. John Hemp
Dr. John Mapes
Dr. Bernard Nau
Prof. Mike Sanderson

SUMMARY

Elastomer seals are widely used in the petroleum industry. Seal failure can be very expensive, due to losses in production and high maintenance costs. Another aspect of this problem is the difficulty in predicting the working life, of a specific elastomeric seal in a specific application, at the design stage. The objective of the present work is to develop the theoretical and computational seal life model to assist reliable prediction of seal life.

Seal life computer software has been developed to model fluid ingress into elastomeric seals and the resulting long term material property changes caused by volume swell and chemical reaction between elastomer and ingressed fluid. The approach used is to model diffusion using a finite element method. This permits application to a wide range of seal geometries. The mathematical model of diffusion is coupled with chemical reaction equations of second order to model chemical ageing processes in the seal. To model the effects of swell, volume of absorbed fluid is coupled with Young's modulus. Physical, as opposed to chemical, stress relaxation is not incorporated since the short time scale of this enable direct measurements to be made.

The software has been tested against experimental data for a number of elastomer / operating condition combinations. Satisfactory agreement is obtained for ethylene propylene diene (EPDM) and nitrile rubber aged in air or high pressure water; nitrile and hydrogenated nitrile rubber (HNBR) aged in high temperature, high pressure hydrocarbon liquid.

The software has also been found useful for calculating required soak time in planning rig tests for the study of explosive decompression caused by absorbed gas in elastomers.

Pending further development of the software, long term prediction of retained sealing force of O-rings in high temperature, high pressure water is calculated from compression set by a semi-empirical approach. Results are compared with experimental data.

ACKNOWLEDGEMENTS

I wish to express my gratitude to the following persons and institutions :

- To the members of the support panel - Prof. M.Sanderson, Dr. J. Hemp, Dr. J. Mapes, Dr. B.S.Nau and Mr. C. Armstrong, for their advice, penetrating comments and constructive criticisms which led to the fruitful results of the current PhD project.

- To Dr. B.S. Nau and Mr. R. Flitney of BHRG for educating me with the industrial reality in the field of fluid sealing.

- To Dr. R. Campion, Mr. G Morgan, Dr. A Stevenson and Mr. C. Derham of MERL for guiding me to the fascinating world of polymer, and allowing me to use their experimental results for validations.

- To Dr. A. Mak for initially suggesting me to take up a PhD course, and then for the supportive encouragement throughout the three years.

- To Mr. R Tang for kindly checking the grammar of the thesis.

- To my dear parents for their love and for my education to University.

- To my darling husband, Dr. W.P. Ho, for helping out in the graphics presentation software, and for his bearing of me for three years not doing much housework.

CONTENTS

LIST OF FIGURES

NOTATIONS

A	Helmoholtz free energy	N mm (or mJ)
A_a	Cross-section area of aged rubber	mm^2
A_o	Cross-section area of unused rubber	mm^2
B_p	Eflux on the boundary	[conc.] mm^2/sec
b	Contact width of an O-ring	mm
C	Fractional compression of an O-ring	-
C_1, C_2	Elastic constant in Mooney-Rivlin equation	-
C_s	Compression set	%
c	Fluid concentration in rubber for gas	$\frac{mm^3 \text{ gas}}{mm^3 \text{rubber}}$
	for liquid	g liquid/g rubber
c_∞	Equilibrium fluid concentration of rubber	g liquid/g rubber
c_1	Specific heat capacity	J/K kg
D	Diffusion coefficient	mm^3/sec
d	Diameter	mm
E	Young's Modulus	N/mm^2
E_a	Activation energy for chemical reaction	J/kg mole
E_d	Activation energy for diffusion coefficient	J/kg mole
e_1	Cohesive-energy density (c.e.d.) values for liquid	N/mm^2
e_2	Cohesive-energy density (c.e.d.) values for polymer	N/mm^2
e_T	Thermal expansion (strain)	-
F	Retained interference force	%
f	Tensile force	N
G	Shear Modulus	N/mm^2
$\Delta G1$	Total free energy of dilution	N mm / mol
ΔH_1	Heat of dilution	N mm / mol
ΔH_{sr}	Heat of solution of rubber	J/kg mole

I_1, I_2, I_3	Rivlin strain invariants	-
K	Heat conductivity	mJ/sec mm^3 K
k	Boltzmann constant	J/K
k_c	Chemical reaction rate in aged rubber	/ [conc.] / sec
k_1	Number of moles of liquid in the swollen polymer	mole
L	Molar latent heat of evaporation	J/kg
l	Bond length in polymer chain	mm
M	Compression Young's modulus	N/mm^2
M_c	Number average molecular weight between crosslinks	-
M_o	Bulk compliance of polymer materials	mm^2/N
M_p	Potential modulus change (M_{max} - M)	N/mm^2
N	Number of network chains per unit volume	-
N_i, N_j	Shape functions	-
n	Total number of bonds in a polymer chain	-
n_1	Fluid concentration required to form one crosslink	-
n_2	Number of crosslink sites required to form one crosslink	-
P	Permeation coefficient	mm^2/sec/bar
p	Pressure	bar
p_i	Partial pressure	bar
p_o	Arbitrary hydrostatic stress	N/mm^2
p(x,y,z)	The probability function per unit volume describing the statistical properties of randomly jointed chain.	-
Q	Heat energy	N mm (or mJ)
R	Gas constant	J/K kg mole
r	Radius	mm
S	Entropy	J/kg K
S_i	Sink term in diffusion equation	[conc.] mm / sec
s	Solubility coefficient of gas	/bar

T	Temperature in Kelvin	K
Tg	Glass-transition temperature	K
t	Time	sec
t_1, t_2, t_3	Principal stresses	N/mm^2
U	Internal energy	N mm (or mJ)
u,w	Displacement in two perpendicular directions	mm
V	Molar volume	mm^3/mol
V_1	Molar volume of the solvent	mm^3/ mol
V_p	Volume of the swollen rubber	mm^3
V_s	Volume of the liquid absorbed	mm^3
v_2	Volume fraction of the polymer	-
W	Work done	N mm (or mJ)
x,y,z	3 perpendicular directions in Cartesian coordinate	-
Y(t)	Potential reaction sites at time t	-
z_1, z_2	2 integration point for Gaussian quadrature formula	-

α	Thermal expansion coefficient	/K
α_L	Thermal expansion coefficient of rubber in leather form	/K
α_G	Thermal expansion coefficient of rubber in glass form	/K
δ	Solubility parameter	$(N/mm^2)^{1/2}$
σ	Stress	N/mm^2
ρ	Density	g/mm^3
υ	Poisson's ratio	-
χ_1	Flory-Huggins polymer-solvent dimensionless interaction term	-

$\lambda_1, \lambda_2, \lambda_3$	Extension ratios	-
ε	Strain	-
τ	Time interval	sec
ϕ	Restricted volume for the movement of a rubber molecule	mm^3
φ	Free volume in polymers	mm^3/g
θ	Unknown function in differential equations	-
ξ	A location in between a time step	-
β, η, ζ	Area coordinates of a triangular finite element	-

the full names for different polymer types :

EPDM	ethylene propylene diene
high ACN NBR	high acrylonitrile butadiene
HNBR	hydrogenated nitrile
TFE/P	tetrafluoroethylene propylene

1. INTRODUCTION

1.1 Introduction to Seal Life Project

Polymer/elastomer seals are widely used in the petroleum industry and for other high duty applications. They are located in subsea equipment, process valves, pumps and transportation pipelines, to seal multi-phase hydrocarbon fluids at high temperatures and pressures. With new offshore platforms constructed in water very much deeper than before, drilling to greater depths in extreme environments, and the application of much more sensitive and delicate instruments for monitoring production, high performance seals are demanded to minimize maintenance cost and maximize reliability. Premature seal failure can be potentially catastrophic, while replacement of these seals is prohibitively expensive and difficult.

These seals are exposed to service fluids made up of steam, gases and hydrocarbon fluids in a multi-phase mixture. Under normal operational conditions, the seals are subjected to pressures up to 1000 bar and temperatures from ambient to above 200°C. During transient blow-down conditions, service temperature can fall to -90°C.

The present PhD work is part of a bigger project, the Seal Life Project, in which engineers and scientists from BHR group and MERL work with the support from the petroleum industry and seal manufacturers, to develop the methodology required for predicting elastomer seal life. The Seal Life Project includes four main areas :

i. Review & Definition
   - a study of existing knowledge in subject areas relevant to the project.

ii. Fundamental Experimental Programme
   - a study in basic science of physical, chemical, diffusion and fracture properties of elastomer materials used in seal
   (carried out by the Materials Engineering Research Laboratory MERL)

iii. Computer Modelling
   - a suite of computer programs developed as an aid in the prediction of useful life of seals in service

iv. Seal Functional Test

- performance tests on actual seals operating in representative service conditions to provide seal life performance data to cross-reference fundamental material experiments and to validate the computer model.

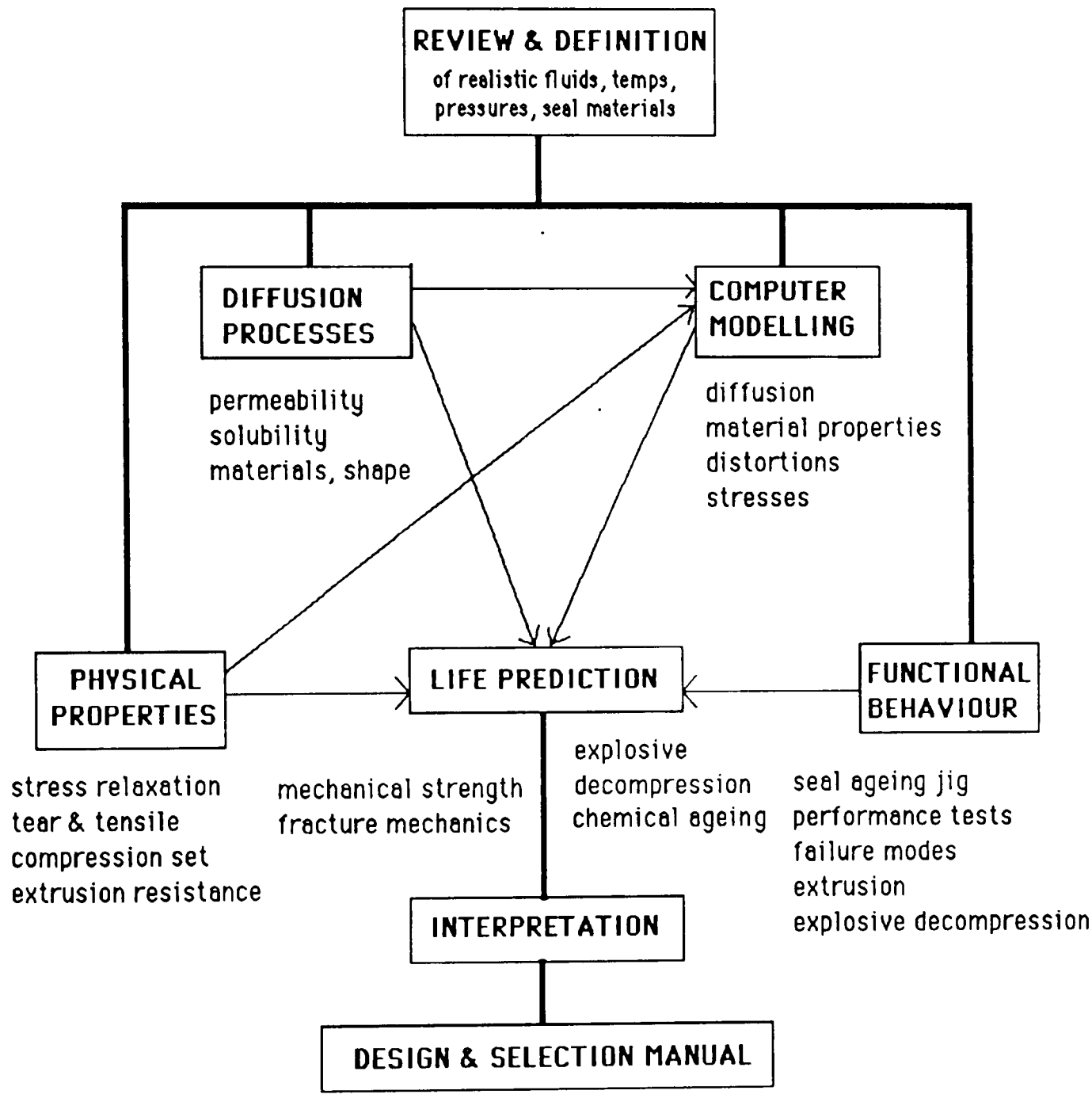

Fig 1.1 Structure of the Seal Life Project

Each of the four tasks is significant in its own right, as well as dovetailing with other tasks, as shown in Fig 1.1. The deliverables of the project include:

i. All Seal Performance Data to provide directly usable information, as well as the basis for predictive modelling of seal life.

ii. A Seal Life Prediction Manual which will have the most up-to-date and

useful information on the subject, including information derived form literature and the results of the test programme.

iii. The Computer Software developed for predicting seal life from known material information.

1.2 Introduction to Thesis

The present PhD work concentrates on the theoretical and computational modelling of elastomer seal life. Chapter 2 starts with a brief description on seal failure. Then, it explains how computer modelling can assist seal life prediction. The approach to develop the software, the program validation method and the computer tools used for development are also defined.

Since a complete model for predicting seal life has not been available, the literature review in Chapter 3 looks into the existing models for individual factors affecting seal life. The established theories for computing diffusion, property losses and dimensional changes are then analysed, selected and inter-related in Chapter 4. Chapter 5 details how the finite element method can be used to solve derived theoretical equations.

The selection of numerical and computational methods for the Seal Life Software is a balance of stability, accuracy and efficiency. User-friendly facilities also need to be included in the software. These are reported in Chapter 6. Chapter 7 presents the validation work that has been carried out for the software. Results are analysed. The software is then used to understand seal behaviours, and to predict seal life. In Chapter 8, retained force is calculated from compression set by a semi-empirical approach.

It is always important that research projects are well managed so as to deliver results on schedule and on budget. Chapter 9 records on how the Seal Life Project was managed, values the performance and suggests scope for further improvement. In Chapter 10, the procedures to predict functional seal life in applications are summarized. The overall advance in seal life prediction is discussed and concluded. Possible further work to enhance seal life prediction is given in Chapter 11.

2. OBJECTIVES

The present PhD work develops a suite of computer software, the Seal Life Software, to assist the prediction of the useful life of seals in service.

Failure of seals occurs due to a variety of different mechanisms. Possible failure mechanisms include :

i. rubber fracture in explosive decompression conditions,
ii. loss of material in extrusion,
iii. loss in contact stress due to chemical or physical ageing, to a degree where sealing can no longer be maintained.

The first two types of failure are mainly short term where simulation tests may be possible. The final one is, however, long term and there is a limited amount of quantifiable information on seal failure due to degradation of material. The Seal Life Software developed is aimed to predict this type of failure mode, although the diffusion module of the software can be used to determinate the required duration for simulating explosive decompression tests, and the computed fluid concentration distribution in seal can help to quantify and locate cracks in explosive decompression.

Seal Life Software takes into account seal shape, the diffusion of fluids into the seal, and the chemical reaction between rubber compounds and ingressed fluids as shown in Fig 2.1, to model the variation of material properties with time.

Computer modelling of material properties in elastomers with time and temperature is an area which has just been attended by engineers and chemists after the space shuttle (Challenger) accident in 1986. An overall consideration of polymer seal life where diffusion, stress analysis and material behaviour are mutually coupled is novel. Existing work has considered some, rather than the full range of factors which could contribute to seal life. A very important part of the present PhD project is to review a wide spectrum of factors so as to establish a model which takes into account all factors, and inter-relates them in an accountable manner. Then numerical

methods are studied to solve the mathematical model, and software is developed to apply the model to practical applications.

As part of an industrial orientated research project, the resource backup, industrial relevance and applicability of the computer program are ensured.

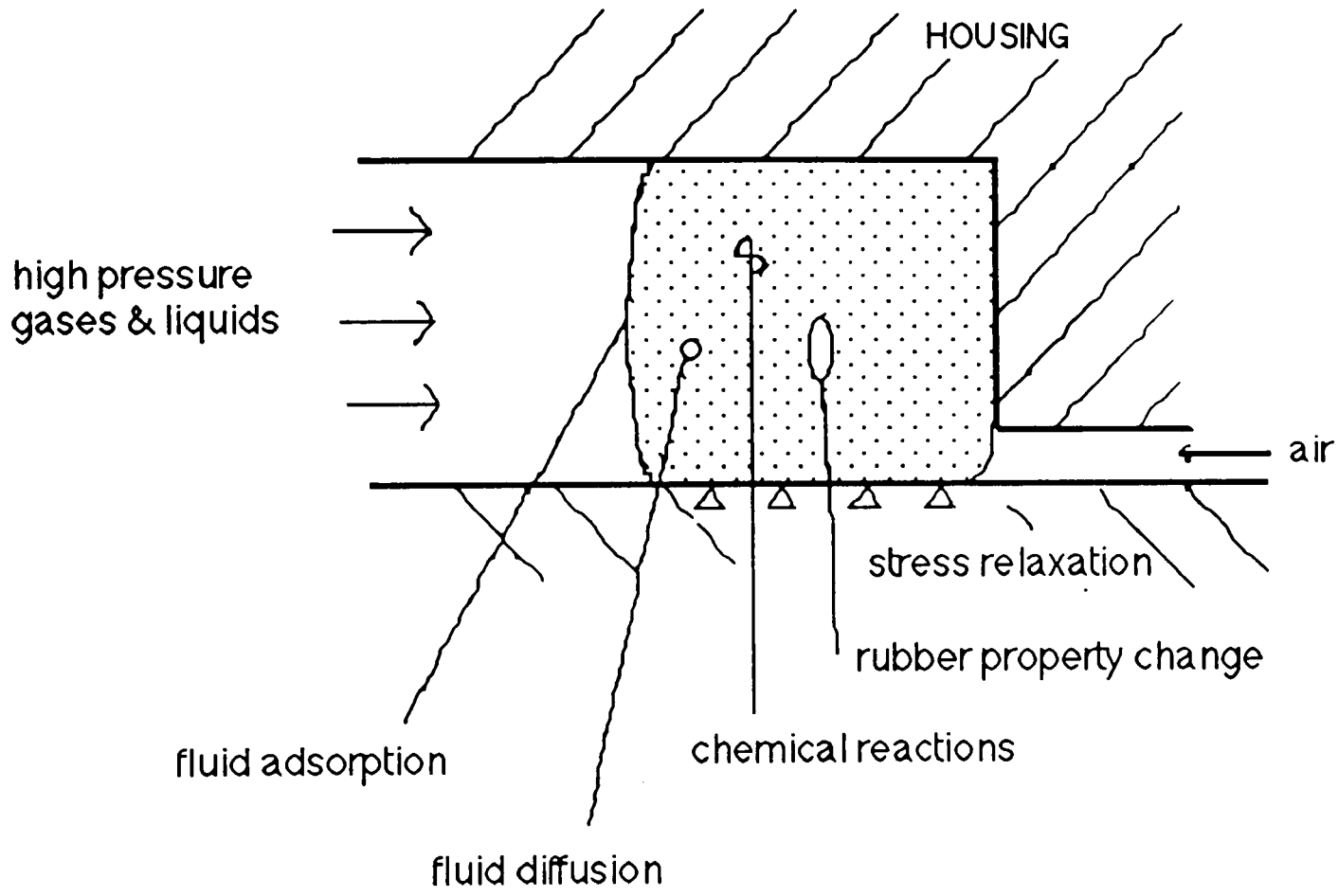

Fig 2.1 A deformed O-ring in its housing

2.1 Software Overview

The adopted approach to the PhD project is to consider individual factors separately, and develop 'stand alone' functional modules using common data files for data input and output. The 'stand alone' modules are:

- Diffusion
- Material Properties
- Graphics Interface

The final seal life software will comprise of all the listed modules for

predicting seal life, as shown in Fig 2.2. The approximate shape of the deformed polymer seal under specified pressure and temperature will be fed into the diffusion module for modelling the adsorption of fluids on surface of the seal and the spreading of fluids through the seal. The obtained local fluid concentrations will determine the local material properties of the seal, varying with time due to physical and chemical processes. These material properties can be fed into numerical stress-strain equations, or commercial finite element stress-strain package, to calculate the variation of sealing contact-stress with time.

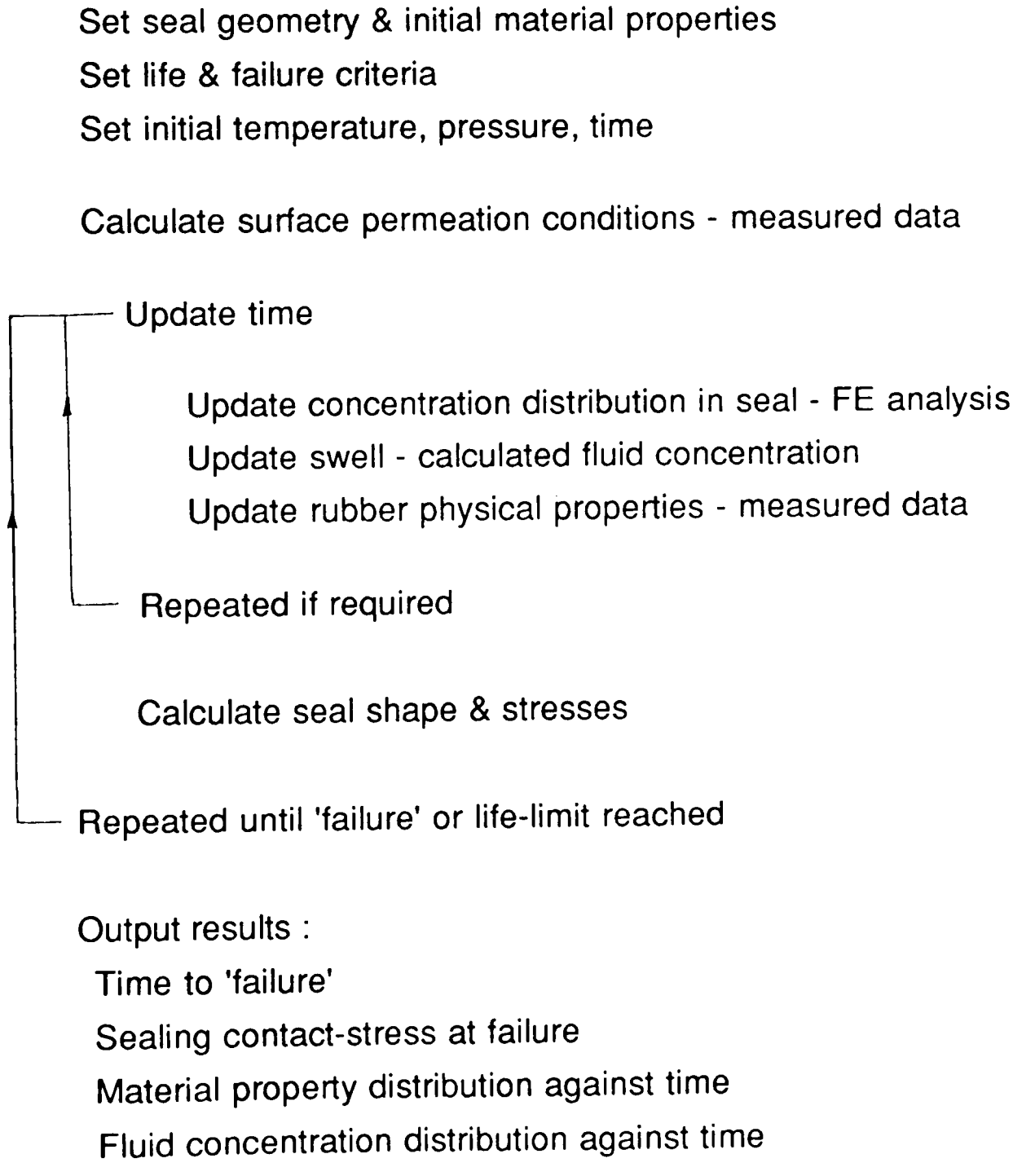

Fig 2.2 The overall computer program structure

Both the diffusion coefficients and material properties of rubber change with time, and vary spatially in service seals as fluids diffuse into the rubber. Vulcanized rubber used in seal production has extensive cross-linked structure to provide short-term properties and dimensional stability. However, the seals undergo long-term property and dimensional changes when soaked in fluids of high temperature and subjected to high stress. In the Seal LIfe Software, the coefficients for property and dimensional changes will be derived from experimental studies of seal materials in service fluids, and stored in a common data file to be used by every module in the software.

The output of computer analysis will be verified with analytical solutions, experimental data and seal function test results.

2.2 Facilities for Program Validation

The development of the computer software has to be based on theories derived from research work on basic properties of rubber and sealing technology. These theories are combined to build up a methodology for predicting seal life. The software development is therefore carried out alongside laboratory experiments and seal function testing. Brief descriptions of the test facilities and the relevant test results from the laboratory experiments are presented in Chapter 7 - Program Validation. Tables of relevant seal function test results are also included in the Chapter. Detail information on the seal function test rig facilities are provided in Appendix 4.

2.3 Computer Tools

The Seal Life Software is written in standard FORTRAN 77 to be run on desktop computers with large memory and hard disk capacity. Its graphics interface is developed separately using the graphics facilities of Macintosh desktop computer.

3. LITERATURE REVIEW

Rubber is widely used offshore by the petroleum industry. Hindmarch (1) reviewed some of the commonest rubber products used offshore, including hoses, coatings and insulations, seals, downhole motors with elastomeric stator, pumpdown completion equipment and other engineering components. Rubber possesses an unique ability of being able to stretch to five to ten times its original length and then retract rapidly to near its original dimensions when the stress is removed. This elastomeric behaviour makes it most useful in application where high strength material such as metals and ceramics become inappropriate.

Natural rubber has been known and used for over 100 years. However, it is mainly synthetic rubbers being used in high duty offshore industry, due to their relative higher strength, chemical inertness, lower flammability, wide service temperature range and high electrical resistivity. MRPRA (2) summarized in a table the strengths and weaknesses of some synthetic rubbers in comparison with natural rubber.

A wide range of synthetic polymers has been developed for industrial, military and aerospace applications. Allen (3) gave a retrospect to the development of science and technology in polymers. Evans (4) reviewed the properties and characteristics of synthetic polymers used in seals. Some examples were : high, medium and low acrylonitrile content nitrile rubbers, carboxylated nitrile rubbers, ethylene propylene rubbers for water and stream, fluorosilicones for aerospace application, oil resistant fluorocarbons etc. Application of seals using the described materials can be static, rotary or reciprocating. Seal configurations include the widely used circular section (O-rings), V or U sections, T sections and X rings. Seal performance depends on material as well as design criteria such as stretch, swell and shrinkage.

The traditional methods to assess seal life include :

i. by previous experience of similar applications,
ii. by functional seal tests - usually accelerated and extrapolated to long

term,

iii. by material property tests followed by subjective interpretation.

There is however little reliable information available to apply method (i) to cover the wide variety of seal materials, configurations, sizes and service conditions.

Parker and Raines (5) applied method (ii) to life prediction. They measured compression set, stress relaxation and leakage in accelerated tests, and then applied Arrhenius equation to 'day to failure', without necessarily understanding the failure mechanism. This method may be useful in individual applications, but does not advance the technology. Chemical reactions occurring at higher temperatures do not necessarily happen at lower temperatures. And as with method (i), a wide variety of seal materials, configurations, sizes and service fluids would require extensive testing for all the different combination of conditions.

Palmer (6) studied the representation of stress relaxation measurement to seal performance - leakage, compared with other material properties such as volume swell, compression set, low temperature brittle point and the Gehman T10 value. He found differences between compression set and compression stress relaxation. He concluded compression stress relaxation provided the best indication of seal performance, with minor exceptions. In fact, the two methods measure different effects or the same effect to a different extent, degree of representation of each method depends on what the dominating effects are. Therefore, in general, both have to be considered to establish seal performance.

Method (iii) is controversial as there is little agreement on which material properties to focus on. Commonly-used properties are tensile strength, elongation at break, hardness, tear resistance and volume swell. These were the measurements done by Seregely, Nagy and Pfisztner (7) to study ageing of elastomers under simulated offshore conditions. These is however no definition for how to interpret these material properties to represent seal performance.

Existing research on seal life prediction, taking account of material, diffusion and stress analysis is still at a very early stage of development. Individual factors affecting seal life can have well-established technology. Works have been performed to model O-ring deformation and contact stress with temperature dependent material properties. The ageing of rubber in aggressive media, however, was not considered, was incomplete, or was not validated against actual sealing performance in service. A mathematical or computer model that can apply to different geometries and service conditions will be most useful to the industry. Stevenson (8) provided an overview of the different factors required in predicting seal life.

The objective of the present PhD project is to combine the established knowledge on relevant subjects to predict seal life. Therefore, in these literature studies, I shall first summarize the available research to model seal life, and explain the limitation in applying them to sealing technology and different failure modes. Then I shall present the established science on diffusion, elastic properties and deformation of elastomer compounds, which will form the base of the theory for predicting seal life in Chapter 4.

3.1 Combination of Material, Diffusion and Stress Analysis to Predict Seal Life

Traditionally, rubber components are relatively cheap and occasional replacement is acceptable. But in the case of offshore, nuclear or space applications, where replacement is extremely difficult, reliable prediction of the performance of rubber materials in applications is most important.

One of the earliest elastomer seal life prediction studies was performed by nuclear industry, in which failure can lead to high cost, and in the extreme, safety hazards. Blakeston, Tomblin and Ward (9) carried out ageing tests on ethylene propylene rubber seals in pressurized, high temperature water with dissolved oxygen. They tested small size seals in laboratory to monitor changes in weight, volume, hardness and compression set. They also measured leakage and 'standoff' on a few of the small size O-rings.

'Standoff' was defined as the amount by which an O-ring projected from its groove. Then, they had long term endurance sealing tests for full-sized seals in laboratory and in the Winfrith reactor as opportunity allowed. The endurance tests could last for 30,900 and 24,900 hrs. Arrhenius technique was used to predict long term compression set of elastomers satisfactorily. A number of other types of elastomers were tested, including ethylene propylene terpolymer, ethylene acrylic compounds, perfluoroelastomers and specially conditioned grades of fluorocarbon compounds.

The authors did not try to understand the reason for observed behaviour, such as hardness increase in the first 1000 hours and then decrease to less than the original values after 2500 hour. They attempted to find the best available material for their applications. Fluids in nuclear industry are limited to a few types - water, air, oxygen and nitrogen. Results showed that materials performed better as seals in service than in the smaller sizes seals tested in laboratory. This probably was the effect of diffusion which delayed ageing in full-sized seals. It is for the same reasons that diffusion calculation will be included in the current PhD project.

Metcalfe, Baset, Lesco and Selander (10) modelled the behaviour of space shuttle solid rocket booster O-rings, supported step-by-step by experimental work. A large-displacement, incompressible, viscoelastic finite element model was used to model squeeze during assembly of a booster case joint, followed by relaxation, recovery and pressurization. Transient temperature effects were also explained and quantified.

He looked into a critical period, of the order of half a second, during the ignition transient when rapid pressurization and structural deformation could occur. The effect of temperature was relatively insignificant for uniaxial tension of V96 fluorocarbon O-ring in the test timescale. He used Neo-Hookean model to represent rubber elasticity, and Prony expansion (a summation of exponential decay terms) to represent relaxation. Correlations of stress relaxation data with the model were good for up to 20% strain. He used the same model for predicting viscoelastic behaviours such as uniaxial creep, and uniaxial recovery after reduction of load. Viscoelastic behaviours

occurred in the transition zone between glasslike and rubberlike consistency.

"Sluggishness" occurred at low temperature. Modulus, stress relaxation characteristic were affected, and performance of the booster O-ring at ignition depended to some degree on its complete time-temperature-squeeze history. A conventional 'master curve' and 'WLF log timeshift' relationship by Ferry (11) was used for the temperature effect in relaxation.

Metcalfe aimed to model momentary behaviour of rocket booster O-rings. He however had taken into account some very important seal life factors at low temperatures, such as relaxation and viscoelastic behaviour, with extensive experimental work for validation. The work did not look into ageing which would take longer time to occur.

Wadiak, Bond, Cyr, Fields, Ferguson, Swenson (12) collaborated in developing a finite element methodology to predict age-related mechanical property and structural performance changes in high performance polymers. They modelled two mechanisms in polymer ageing processes - i) diffusion, ii) the chemical reaction of chemical species in polymers, at constant temperature and density. They intended to predict the eventual location and extent of the chemical contamination, but they did not study the effect of ageing on mechanical performance. They commented that data on the relationship between critical chemical species concentrations and mechanical properties were required to perform structural or other modelling to assess performance changes due to ageing. Elaborate experimental procedures and equipment would be required to determine these experimental data.

3.2 Material Properties

Treloar (13) described rubber as succession of hydrocarbon units in chains. The structure of rubber is characterized by :

i. the presence of long-chain molecules, with freely rotating links;
ii. weak secondary forces between the molecules (as in a liquid);
iii. an interlocking of the molecules at a few places along their length to form a three-dimensional network.

Condition (i) provides the ability of high extensibility of rubber. Weak intermolecular forces in condition (ii) allow individual chains to take up the variety of statistical conformations upon which the phenomenon of rubber-like elasticity ultimately depends. The presence of cross-linkages or junction points between chains, described in condition (iii), produces a coherent network in which all molecules are linked together to stay as a solid. These cross-linkages between chains are normally introduced by the process of vulcanization.

The double bonds in these chains largely determine the chemical reactivity of each molecule and its ability to react with sulphur or other reagents in the vulcanization process. They are also responsible for the susceptibility of the rubber molecule to oxidation or other degradative reactions leading to a deterioration of physical properties (ageing).

The properties we are particularly interested in are the elastic behaviour, and the diffusion and adsorption of fluids in rubber.

3.2.1 Elastic Behaviour

Cowie (14) summarized the elastic behaviour of rubber as below:

i. the elastic modulus of an ideal rubber increases as the temperature of the rubber increases,
ii. rubber gives out heat (reversibly) when stretched,
iii. rubber held in the stretched state, under a constant load, contracts (reversibly) on heating.

In simple mechanistic terms, the elastic modulus is a measure of the resistance to the uncoiling of randomly oriented, torsionally vibrating chains in rubber under stress. Application of stress eventually tends to untangle the chains and align them in the direction of the stress, but an increase in temperature will increase the thermal motion of the chains and make them harder to reorientate. This leads to a higher elastic modulus.

Observation (ii) and (iii) are called Gough-Joule effects which were first discovered in 1806. They can be explained in thermodynamics terms, from basic concept of kinetic theory of elasticity. These are well documented in Treloar (13) and Flory (15).

The deformation of a rubber (at constant temperature) is associated with a reduction of entropy, with no change in internal energy.

$$dW = dU - dQ \quad \text{.....(3.1)}$$

thus $dW = -dQ$ for $dU = 0$ at constant T

The work done by the stretching force being necessarily positive, it follows that dQ, the heat absorbed, is negative. i.e. heat is evolved on extension. The amount of the heat evolution is exactly equal to the work done on the rubber by the applied force. If the heat is not emitted but is retained, it will cause a rise in temperature $-dQ/c_1$, where c_1 is the heat capacity (specific heat) at constant length.

For a mechanism involving only change in entropy, scientists in 1930's and 1940's concluded that the tension in stretched rubber (at constant length) should be proportional to the absolute temperature. However, thermal expansivity of the unstrained rubber would reduce the strain or relative extension of a constant length piece of rubber with increasing temperature, resulting in a reduction of the applied force. Extension calculated on unstrained length at temperature of measurement should therefore be used to eliminate the thermoelastic inversion effect.

Theoretically, Shear Modulus G can be estimated by Gaussian statistics,

$$G = NkT \quad \text{.....(3.2)}$$

where N is the number of network chains per unit volume,

k is the Boltzmann constant

Effect of temperature on Young's modulus was one of the factors analysed after the space shuttle (Challenger) accident. Metcalfe, Baset, Lesco and Selander (10) modelled the dynamic response of O-rings to pressurization, relaxation and recovery, taking into account the change of Young's modulus with temperature.

$$E = E_r [1 + (T-T_r)/T_r - 3\alpha(T-T_r)] \quad \text{.....(3.3)}$$

where α is the thermal expansion coefficient,

and r signifies reference temperature values.

3.2.2 Fluid Diffusion and Adsorption

Rubber subjected to high pressure fluids for any length of time will take up fluids by adsorption. These fluids diffuse into the bulk of the material with which they may interact chemically and physically. Fluid diffusion therefore plays a key role in determining the seal's contact stress and sealing ability.

Van Amerongen (16) summarized the fundamentals of solubility, permeation, and diffusion of liquids and gases in elastomers. He discussed the effect of crosslinks, polar groups and fillers on rate of diffusion. He explained diffusion can be a limiting factor in ageing, and the gas permeability of a multi-layer slab depends on the permeability of its components.

Southern (17) reviewed the theory of liquid diffusion in rubber. He studied the effect of rubber compounds and the nature of liquid in determining the diffusion coefficient, and finally the effect of the presence of liquid on the physical properties of the rubber.

In the determination of swelling properties, the concept of cohesive-energy density has been widely applied to understand the role of molecular interactions in polymer-liquid mixture, see Rodriguez (18), Bateman (19) and

Young (20). Cohesive energy density (c.e.d.) is defined as the energy required to separate all the molecules in a given material from one another. For many non-polar liquid mixtures, the heat of dilution ΔH_1 (for component 1) is expressed as

$$\Delta H_1 = V_1 (e_1^{1/2} - e_2^{1/2})^2 v_2^2 \quad \text{.....(3.4)}$$

in which e_1 and e_2 are respective c.e.d. values for liquid and polymers, v_2 is the volume fraction of the polymers.

According to the equation, ΔH_1 is always positive and is at its minimum when $e_1 = e_2$. A consequence of this is that swelling of a given polymeric material in a variety of liquids is maximum when the c.e.d. of the liquid is equal to that of the polymeric material. In the literature, the square root of the c.e.d. is represented by the 'solubility parameter' denoted by the symbol δ.

Beerbower, Kaye and Pattison (21) explained how δ can be used to predict the fluid/elastomer incompatibility. Elastomers in fluids can be roughly classified by the following categories : i) non-swell, ii) swell to between 25% to 50%, iii) swell to between 50% to 100%, iv) swell of over 100%. The scheme is however not accurate enough for seal life prediction when diffused fluid can change material properties, and possibly cause chemical reaction with polymer compounds.

Mathematical techniques have been well established to model fluid diffusion in polymeric materials. Adkins (22) explained how a general differential equation could be built from Fick's first and second law. Crank (23) derived differential equations for fluid diffusion with chemical reactions. He also solved the differential equations for simple geometries, such as sphere, cylinder etc., using general mathematics functions. Zienkiewicz (24,25), Hinton & Owen (26,27) detailed how to solve the differential equation using finite element method. Conner and Brebbia (28), Burnett (29) described different methods used for modelling time-dependent differential equation, and commented on their stability and efficiency in implementation.

Ellis, McCauley and Mark (30) used finite element analysis to model

concentration-dependent diffusion of water in a polymeric material - polycarbonate. He considered variable surface concentration, using the equation :

$$c(x_1,y) = c_\infty(1-e^{-\beta t}) \quad \text{.....(3.5)}$$

where c_∞ is the equilibrium concentration, t is the time and β is a constant The predicted concentration distribution with time was validated against experimental data obtained using a radio-tracer method. Variable surface concentration assumption provided significant better overall fit to the experimental data. Ellis also modelled stress with finite element method. He said that the next stage of his work would be to combine diffusion and mechanical programs to model diffusion in stressed systems.

Crank and Park (31) considered temperature effect on diffusion. It is widely accepted that diffusion coefficients of gas and liquid obey the relationship

$$D = D_o \exp(-E_d/RT) \quad \text{.....(3.6)}$$

where D_o and E_d are pre-exponential factor and activation energy respectively

One of the many experiments that supported the Arrhenius behaviour of diffusion coefficient of polymers was carried out by Harper and Naeem (32).

Van Krevelen (33) mentioned the above relationship of diffusion coefficient. In addition, he said that the solubility coefficient of gases in rubber also depended on temperature,

$$s = s_o \exp(-\Delta H_{sr}/RT) \quad \text{.....(3.7)}$$

where H_{sr} is the heat of solution in rubber.

Roy and Reddy (34) developed a finite element program to analyse plane and axisymmetric adhesively bonded joints. Penetrant sorption was calculated using diffusion coefficient based on the concept of free volume. According to this theory, the diffusion coefficient D for a polymeric material above its glass transition temperature is given by

$$D = \frac{D_o}{T_o} T \exp\left\{\frac{B}{f_o}\left[\frac{3(\alpha T+\gamma c^n) + (e - 1/3M_o\sigma)}{f_o + 3(\alpha T+\gamma c^n) + (e - 1/3M_o\sigma)}\right]\right\} \quad \text{.....(3.8)}$$

where M_o is the bulk compliance of the material, T is the temperature, f_o is the free volume fraction, B is a material constant, α is the linear coefficient of thermal expansion, γ is the linear coefficient of expansion due to moisture, N is an exponent for the saturated state and e is the transient component of the mechanically induced dilational strain.

This definition of diffusion coefficient is very involved. Roy and Reddy (34) demonstrated the solution agreed very well with analytical solution, and had good capabilities for prediction over a range of geometries, external loads and environmental conditions. However, the validation against actual sealing performance in service was incomplete. As a first approach, Crank and Park (31) and Van Krevelen (33) equations are adopted in preparing input data for the Seal Life Software to take account of the most significant environmental factor (temperature) affecting diffusion.

Campion and Morgan (35) measured permeation rate P experimentally to investigate permeation and diffusion of gases at high pressures (3600 psi, 6100 psi) and at temperatures between 50°C to 150°C.The equation used is:

$$P = Ds \quad \text{.....(3.9)}$$

They recorded reduction in permeation rate at high pressures. They suggested it was due to a pressure-induced compaction of the polymers, causing their molecular chains to pack closely together, reducing the free volume available within the polymers for gaseous diffusion. A small deviation from Arrhenius behaviour also occurred. They suggested the cause was the rise of Tg affecting results from lower temperatures but not on those at higher temperatures. As diffusion at high pressure is most common in sealing, the diffusion properties obtained from data measured at the exposure pressure are recommended for input into modelling seal life to improve accuracy.

3.3 Decay of Material Properties

The material properties of rubber will decay in service. Under strained conditions, this decay can be divided into two components, physical decay and chemical decay, as shown in Fig 3.1. The former is associated with slippage and rearrangement of the elastomer network, and the latter is associated with chemical changes, such as the breakage of the load-bearing chains or crosslinks in the elastomer structure.

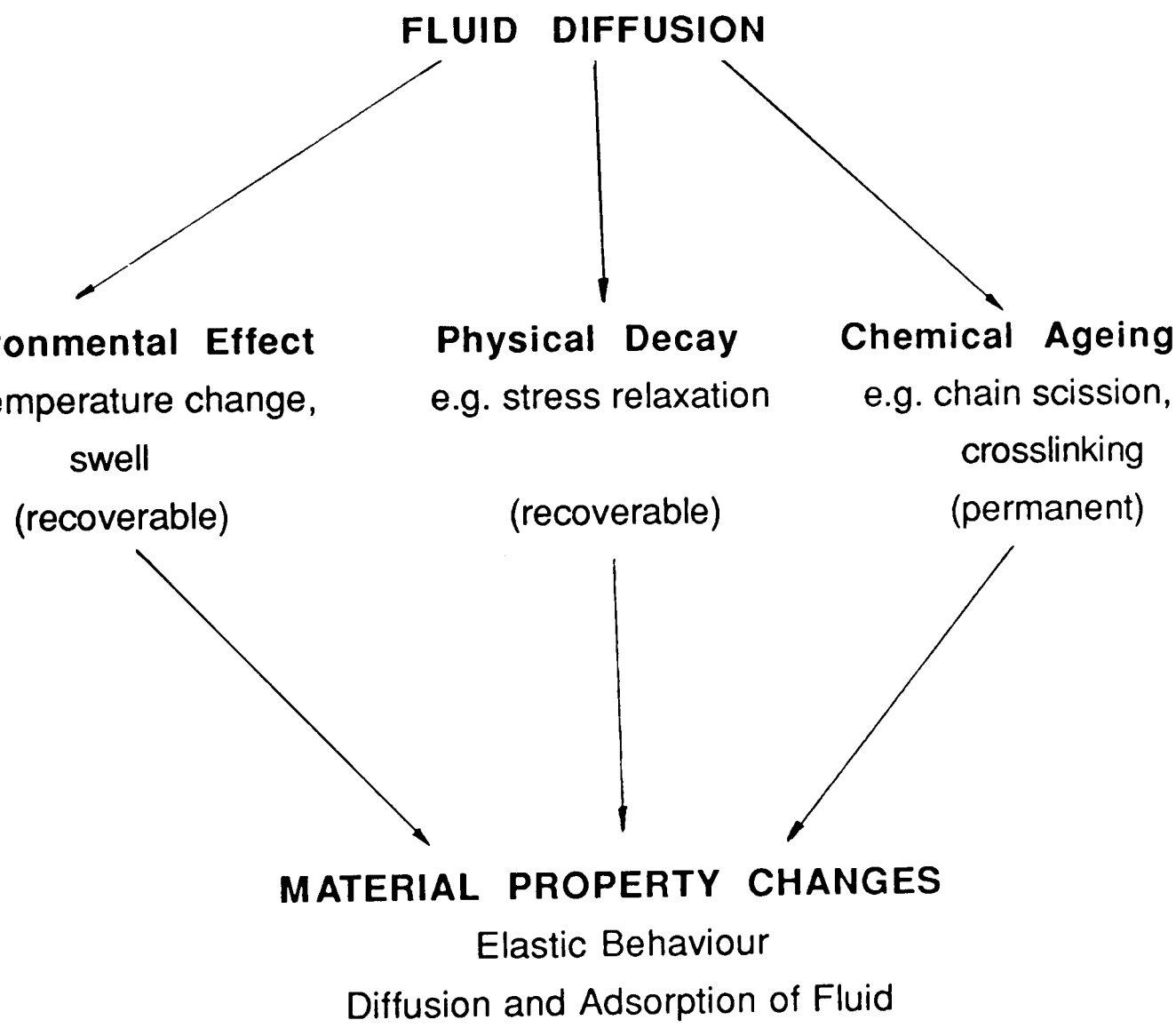

Fig 3.1 Material Property Decay of Rubber

3.3.1 Physical Decay of Material Properties

Physical decay is in principle recoverable. It is relatively rapid initially, but slows down with time. Derham (36) did some stress relaxation work at room temperature on three general purpose elastomers, and showed that physical stress relaxation decreased linearly with the logarithm of time.

$$(\sigma_o - \sigma_t) / \sigma_t = A \log (t/t_o) \quad \text{.....(3.10)}$$

He commented that physical relaxation rates were high near to the glass transition region where molecular motion was sluggish. The relaxation rates decreased as the temperature raised and the molecules became more mobile. In general, he found that a short duration test of a few days, was sufficient to measure the physical stress relaxation at any temperature.

Derham (36,37) also investigated the effect of water absorption on stress relaxation. He found that the physical stress relaxation rates of natural rubber and general purpose elastomers were increased significantly by the absorption of 1% or less of water, compared with those of the dry material. However in his latest work for the Seal Life Project, he found the presence of water in oil resistant elastomers had no significant effect in physical stress relaxation rates.

Another factor affecting the physical rate was the degree and type of crosslinking. Increasing crosslink density decreased the rate of relaxation. Derham (38) also showed that the presence of fillers introduced additional relaxation mechanisms.

3.3.2 Chemical Decay of Material Properties

a. Effect of Chemical Ageing on Material

Derham (36) commented that chemical relaxation would dominate over physical relaxation at high temperatures, longer times and aggressive media applications. The rate of chemical relaxation is normally found to be approximately linear with time, but it slows down when oxygen cannot diffuse fast enough into the specimen to sustain the maximum possible rate of chemical reaction. Under these conditions the reaction is said to be 'diffusion controlled'.

Brydson (39) identified the process of some common chemical reactions caused by the absorption of oxygen. These included :

i. chain breakdown (chain scission),
ii. cross-link breakdown (cross-link scission),
iii. cross-link formation,
iv. the development of polar groups (which affect electrical insulation properties) and
v. the development of chromophoric (colour forming) moieties in elastomers.

Rodriguez (18) studied some degradative effects :

i. Scission
ii. Depolymerization
iii. Cross-linking
iv. Bond changes
v. Side-group changes

and tried to establish a preliminary mathematical formulation for describing the rate of the reactions.

Blow (40) reviewed the change of material properties of elastomers with time and temperature due to ageing. Change of hardness, 'modulus' (stress at a stated elongation) and tensile strength measured at room temperature, are all widely used to assess the degree of deterioration. Hardness and modulus

changes are important, since softening will lead to increased deformation and extrusion of the seal from its housing, and hardening will reduce the ability of the seal to conform to irregular surface.

For sealing applications, the effect of prolonged heating on the elastic properties such as creep, set and stress relaxation are probably more significant than tensile strength deterioration.

Criteria, although arbitrary, can be adopted, such as the time to produce a certain % loss of property at a given temperature or the temperature to produce a certain % loss of property at a given time. These enable different rubbers to be compared. Blow (40) commented that accelerated tests performed at high temperature might not give true picture of the deterioration of rubber, as some chemical reactions occurred in accelerated tests do not operate at the lower temperature. It is desirable to carry out tests at several temperatures and for several times.

Southern and Thomas (41) suggested that increase in degree of crosslinking could considerably reduce the equilibrium concentration c_∞ of rubber. The diffusion coefficient, however showed a relatively slight change. The variation in their experiments was 10%.

Hermann R. (42) looked into the effects of absorbed water on the physical properties (Young's Modulus) of stretched and compressed acrylics. He found that Young's Modulus suffered reductions of up to 25% when the water content was at equilibrium. The loss in Young's Modulus did not completely recover when the water was removed by drying. The irreversible damage for the stretched acrylic was approximately 6% whereas in compressed material the damage lay around 8%.

b. Measuring Chemical Ageing

In general, many types of chemical attack are possible because of the wide variety of chemical species and polymeric substrates. The better studied reactions are those that cause change in molecular weight, such as chain scission, cross-link breakdown, cross-link formation.

Brydson (39) mentioned four experimental methods to measure the oxidative ageing of polymer networks, they were :

i. stress-relaxation measurements;
ii. use of the Mullins equation;
iii. measurement of the fraction of gel rendered soluble on ageing;
iv. radiochemical techniques.

Out of the four methods, the stress-relaxation technique is most well established. It is an extension of the use of equilibrium modulus measurements to measure the concentration of stress-bearing chains. In continuous stress-relaxation experiment, new cross-links are formed under strained position and therefore will not contribute to the stress-supporting network of the test sample. In intermittent stress-relaxation tests, a sample is only strained during measurement. The new cross-links are formed when the sample is at rest, and therefore do contribute to the stress-supporting network. The difference in results obtained in continuous and intermittent experiments provides a measure of the extent of cross-linking during oxidation.

Although the new cross-links formed in strained sample do not contribute to the stress-supporting network, they can cause set - i.e. some degree of deformation remains when the imposed strain is removed from the material, the material cannot fully recovered to its original shape.

The stress-relaxation method gives satisfactory results for natural rubber latex, uncross-linked natural rubber, uncross-linked gutta percha and peroxide-cured vulcanizates. However, divergent results are obtained for sulphur-cured vulcanizates.

Sperling (43) used equilibrium swelling theory, the Flory-Rehner Equation, to measure the crosslinking of rubber, and therefore predict the elastic modulus of aged rubber. The Flory-Rehner equation may be written as :

$$- [\ln(1-v_2) + v_2 + \chi_1 v_2^2] = V_1 N [v_2^{1/3} - v_2/2] \quad \text{.....(3.11)}$$

where v_2 is the volume fraction of polymers in the swollen material,

V_1 is the molar volume of the solvent,

N is the number of active network chain segments per unit volume,

χ_1 is the Flory-Huggins polymer-solvent dimensionless interaction term.

The use of the Flory Equation however requires the interaction term χ_1 to be known. This puts a severe restriction on the application of the method, see Sheehan and Bisio (44). χ_1 appears to be a constant independent of N with tertiary peroxide-cured rubbers, but its value is affected by the type, level and time of cure with sulphur-based systems.

To summarize experimental measurement of chemical ageing, different types of rubber have different dominating degradative effect, and require different methods of measurement. Peroxide-cured systems generally have main-chain scission rather than cross-link scission. Stress-relaxation and solvent swollen methods measure ageing effectively. In unaccelerated sulphur systems, both cross-linking and chain scission occur, and ageing measurement is very difficult. Tetramethyl thiuram disulphide systems have good ageing properties, their ageing is normally determined by additives.

3.4 Elastic Deformation

A rubber seal in application will be very much distorted from its original shape. The understanding of elastic deformation in rubber, the knowledge of contact area, stresses and strains both in initial straining and in working conditions, and their development in time is important for determining the effect of material property change to polymer seal life.

3.4.1 Formulation 1 : Linear Incompressible

Rubber is made up of long-chain molecules with freely rotating links, and therefore exhibits different elasticity behaviour from metal or ceramic. Gaussian distribution function is used to describe the elasticity of rubber molecules in each single long-chain. Assuming one end of the chain is fixed at a point in vulcanized rubber, its cross-links restrict the motion of the other end to a small volume element $d\phi$. Under such restriction, Treloar (13) defined the entropy S of the chain as :

$$S = k \ln \{ p(x,y,z)\, d\phi \} \quad \text{.....(3.12)}$$

and the probability function per unit volume describing the statistical properties of randomly jointed chain with n bonds (including double bonds), bond length l is :

$$p(x,y,z) = (b^3/\pi^{3/2}) \exp(-b^2r^2) \quad \text{.....(3.13)}$$

where $b^2 = 3/2nl^2$ ..... (3.14)

Combine the two expressions yields

$$S = k \{ \ln (\text{constant}) - b^2r^2 + \ln d\phi \}$$

$$= a - kb^2r^2 \quad \text{.....(3.15)}$$

where a is an arbitrary constant that includes the constant volume element $d\phi$

r is the distance between the ends of a chain

The work required to move one end of the chain from a distance r to a distance r+dr with respect to the other is equal to the change in Helmoholtz free energy

$$dW/dr = dA/dr = -TdS/dr = - k'Tb^2r \quad \text{.....(3.16)}$$

and the tensile force f acting along the direction of r is

$$f = dW/dr = -k'Tb^2r = -(3k'T/2nl^2)r \quad \text{.....(3.17)}$$

The tension is thus shown to be proportional to the chain end separation r, and the molecule may be regarded as possessing an elasticity governed by Hooke's law. This linear force-extension relation is subject to the same limitations as the Gaussian distribution function from which it was derived. It is therefore valid only so long as the distance between the ends of the chain is not so large as to be comparable with its fully extended length.

Johannesson (45,46) used analytical solution to model O-ring deformation. He calculated the pressure distribution in an O-ring contact using experimental displacement data, based on a linear relationship between stress and strain. The peak contact stress calculated was generally lower than experimental results.

The general computational method adopted for stress-strain analysis, particularly for complex shape components, is **Finite Element Method**. Its application in rubber is however made difficult by the nonlinearities due to large deformations, nonlinear behaviour of rubber material, the indeterminate nature of the contact area and a Poisson's ratio υ approaching 0.5, which lead to numerical instability in conventional displacement finite element.

Linear finite element modelling has been applied successfully to compute stresses accurately and reliably for some incompressible or nearly incompressible solid. Herrmann (47) introduced a stress-displacement mixed formulation method. It employed the theorem of minimum potential energy and used linear analysis. The variational equation derived is :

$$\delta \sum_{n=1}^{N} \int_{Bn}\int\int \{G[\mu_1{}^2 - 2\mu_2 + 2\upsilon H\mu_1 - \upsilon(1-2\upsilon)H^2 - 6\upsilon e_T H - 2\mu_1 e_T] - F_i u_i\}\, d\upsilon - \int_{S1a}\int P_i u_i\, dS = 0 \quad \text{.....(3.18)}$$

where G is the shear modulus,

F_i is the body force component,
P_i is the applied surface forces,
υ is Poisson's ratio,
μ_1 and μ_2 are strain invariants,
H is the pressure function and $H = 3\sigma_m / 2G(1+\upsilon)$ .....(3.19)
σ_m is the mean pressure and $\sigma_m = (\sigma_1 + \sigma_2 + \sigma_3)/3$ .....(3.20)
e_T is the thermal expansion and $e_T = \int_{To}^{T} \alpha \, dT'$ .....(3.21)
α is thermal expansion coefficient = $1/l \, (dl/dT)$ .....(3.22)

Kikuchi (48) used selectively-reduced integration for 'unlocking' the large bulk modulus term in linear finite element incompressible problems.

Zienkiewicz (49) documented the latest development in mixed formulation which included stress-strain-displacement mixed form, and discussed their stability.

Salita (50) developed a simple finite element model to approximate the response of an axisymmetric O-ring in a rectangular joint groove. The equilibrium deformation was determined by equating the accumulated strain energy to the work done by pressure forces; and the resiliency (rate-dependent) effects were simulated by introducing a dashpot term whose coefficient was assumed to be proportional to stiffness. The resulting stiffness equations were linear, and therefore much faster than a commercial contact analysis package - ABAQUS. He also used 36 simple concentric triangular elements with nodes only on the periphery and the centre - A much simpler mesh than most adopted in the literature.

In linear elasticity, it is assumed that the ratio of the change of distance between neighbouring points of the body resulting from the deformation to their distance in the undeformed state may be neglected in comparison with unity. O-rings exhibit substantially elastic behaviour with typical initial compression of 20% when the above assumption is invalid. It is therefore advisable to study available theory of elasticity which do not make the assumption.

3.4.2 Formulation 2 : Non Linear Incompressible

We shall now describe three non-linear formulations :

a. Neo-Hookean Model (Treloar 13)

Rubber elasticity ultimately depends on individual chains joined into a network structure. A stress-strain relationship for a rubber network can be derived from the Gaussian distribution function based on a number of assumptions. They are :

i. the rubber is incompressible;
ii. all chains have the same molecular weight;
iii. no energy is stored in stretched, distorted or broken bonds;
iv. the rubber was cross-linked in the unstretched state;
v. the network deforms in an affine manner - i.e. the coordinates expressing the relative average positions of network junctions must change in proportion to the changes in macroscopic dimensions of the specimen;
vi. the distortion is small enough for Gaussian statistics;
vii. all chains are tied to the network at their ends, or some small correction is needed to account for the free chain ends.

The resulting equation for the work of deformation is

$W = -TdS$

$= 1/2NTk (\lambda_1^2 + \lambda_2^2 + \lambda_3^2 - 3)$ .....(3.23)

where $\lambda_1, \lambda_2, \lambda_3$ are the extension ratios.

and NTk can be identified as the Shear modulus G

thus $W = 1/2G (\lambda_1^2 + \lambda_2^2 + \lambda_3^2 - 3)$ .....(3.24)

This is called the Neo-Hookean method.

The general stress-strain relation derived from statistical network theory involves only a single material constant or modulus, which is related to the degree of cross-linking or number of chains per unit volume of the network. This stress-strain relation was verified with the actual properties of rubber by

Treloar (13) for different types of strain, including (i) simple extension, (ii) uniaxial compression or equi-biaxial extension, and (iii) shear. In each case, the stress-strain curve converged towards the theoretical values as the strain was reduced. The data for equi-biaxial extension agreed very closely with the theoretical form up to quite large values of the strain, when the extended sides were 3 times their original length, and the compressed side was 1/9 of its original value. On the other hand, the data for extension and shear both deviated markedly from the theory at relatively small values of strain. The upturn of stresses at very large strains (over 500%) greatly exceeded the theoretical predictions. This was interpreted as the network approaching its limiting extension where the use of Gaussian distribution for network chain displacement is no longer applicable. It was noted that the compression data fitted the theoretical curve over a much greater fraction of the range covered than the data for simple extension.

b. Mooney-Rivlin Model (Eirich 51, Williams 52)

In order to obtain a more accurate mathematical formulation for the general properties of rubber, a phenomenological method of approach can be employed. Such a method is not based on molecular or structural concepts, but presents the properties of the material in the most general and complete form so as to avoid false deductions based on inadequate data.

Mooney suggested the earliest significant phenomenological theory of large elastic deformations. His theory is based on the following assumptions:

i. the rubber is incompressible, and isotropic in the unstrained state;
ii. Hooke's law is obeyed in simple shear, or in a simple shear superimposed on a plane transverse to prior uniaxial extension or compression.

From considerations of symmetry, Mooney's strain-energy function is defined as :

$$W = C_1 (\lambda_1^2 + \lambda_2^2 + \lambda_3^2 - 3) + C_2 (1/\lambda_1^2 + 1/\lambda_2^2 + 1/\lambda_3^2 - 3) \quad .....(3.25)$$

which contains the two elastic constants C_1 and C_2.

This equation is identical to the form derived from the Gaussian network theory with $C_2 = 0$ and $2C_1 = G = NkT$.

However, results from Mooney's theory deviated from simple extension experimental data. In particular, the deviation is of the same kind, and of the same order of magnitude as the deviation for statistical theory.

Rivlin developed a formulation based on the following assumptions :

i. the rubber is incompressible, and isotropic in the unstrained state;

ii. the strain energy is unaltered by a rotation of the body through 180°.

The simplest possible even-powered functions which satisfy these requirements are :

$$I_1 = \lambda_1^2 + \lambda_2^2 + \lambda_3^2 \quad \text{..... (3.26)}$$

$$I_2 = \lambda_1^2 \lambda_2^2 + \lambda_2^2 \lambda_3^2 + \lambda_1^2 \lambda_3^2 \quad \text{..... (3.27)}$$

$$I_3 = \lambda_1^2 \lambda_2^2 \lambda_3^2 \quad \text{..... (3.28)}$$

These three expressions are termed strain invariants where $I_3 = 1$ for incompressibility. The strain-energy function for an incompressible isotropic elastic material may therefore be expressed as the sum of a series of I_1 and I_2 terms.

$$W = \Sigma C_{ij} (I_1-3)_i (I_2-3)_j \quad \text{..... (3.29)}$$

The first of these terms represents the form of strain-energy function derived from the Gaussian network theory. And the first two terms yield the Mooney-Rivlin equation with constants $C_1 = \partial W / \partial I_1, C_2 = \partial W / \partial I_2$

The principal stresses corresponding to a pure homogeneous strain of the most general type may be derived as

$$t_i = 2 \{ \lambda_i^2 (dW/dI_1) - 1/\lambda_i^2 (dW/dI_2)\} + p \quad \text{.....(3.30)}$$

where p is an arbitrary hydrostatic stress. And the three principal stress differences are

$$t_1 - t_2 = 2 (\lambda_1^2 - \lambda_2^2) \{dW/dI_1 + \lambda_3^2 (dW/dI_2)\} \quad \text{.....(3.31)}$$

$$t_2-t_3 = 2(\lambda_2^2-\lambda_3^2)\{dW/dI_1 + \lambda_1^2(dW/dI_2)\} \quad \text{.....(3.32)}$$

$$t_3-t_1 = 2(\lambda_3^2-\lambda_1^2)\{dW/dI_1 + \lambda_2^2(dW/dI_2)\} \quad \text{.....(3.33)}$$

Experiments of Rivlin and Saunders showed that it is reasonable to assume dW/dI_1 is a constant, while dW/dI_2 is a function of I_2 independent of I_1. Therefore, the assumption of C_2 as a constant in Mooney's equation is not always appropriate. Mooney's equation suits experimental data best when the dW/dI_2 is small in comparison with the dW/dI_1 term, i.e. when the case studied has a high I_2 value correspond to a low dW/dI_2 value.

For an O-ring inside a housing, using a plane strain assumption, we can say that the value of I_2 is higher when the initial interference is high. That is the accuracy of the theoretical model (Mooney-Rivlin) improves with increasing interference.

c. Alternative Forms of Strain-Energy Function

Other authors expanded the Rivlin type of formulation to include higher order terms in I_1-3 and I_2-3, to obtain a more appropriate general method of characterizing the properties of a rubber for engineering. The attempts were unsuccessful. Gent and Thomas put forward a more realistic formula;

$$W = C_1(I_1-3) + k\ln(I_2-3) \quad \text{.....(3.34)}$$

in which $dW/dI_1 = C_1$, $dW/dI_2 = k'/I_2$ corresponding to a non-linear dependence of dW/dI_2 on I_2.

3.4.3 Solution of Strain-Energy Equations

Oden (53) used finite element method to solve different expanded forms of Rivlin's strain-energy function which include higher order terms in I_1-3 and I_2-3. Newton-Raphson method is adopted for non-linear iteration. His work was extensive and complicated.

In seal applications, Medri, Molari and Strozzi (54) applied Mooney-Rivlin law to specify non-linear elastic material behaviour during the deformation of

an O-ring between two plates, excluding time domain and using a plane strain assumption. George, Strozz and Rich (55) reviewed the available methods for O-ring stress analysis, including analytical, experimental and computational methods. He also developed computer software using the Neo-Hookean model, and found that it was adequate for such purposes. Metcalfe, Baset, Lesco and Selander (10) analysed the behaviour of space shuttle solid rocket booster O-rings using both Mooney-Rivlin and Neo-Hookean models, with plane strain approximation. He found that a Mooney-Rivlin model would give more discrepancy than the Neo-Hookean model. The Neo-Hookean model was therefore selected for his work.

Green and English (56) studied the strain-energy equation. They found neo-Hookean model is suitable for describing material behaviour of deformed O-rings. However, numerical instabilities developed when Poisson's ratio approached 0.5, especially when restrained O-rings were analysed. They suggested the use of reduced integration for cases with high localized hydrostatic stresses.

From the work of the above researchers, it seems Neo-Hookean model is most suitable for describing the non-linear material behaviour of elastomeric O-rings. In cases of numerical instability when Poisson's ratio approaches 0.5, reduced integration can be applied to improve solutions.

3.5 Contact Analysis

The analysis of an elastomeric O-ring during squeeze and pressurization also involves determination of contact boundaries.

Medri, Molari and Strozzi (54) compared contact width calculated from various analytical models with experimental data. The analytical models considered included :

i. Lindley's semi-empirical characteristic

$$\frac{b}{d} = \left(\frac{6}{\pi}\left(1.25\,C^{1.5} + 50\,C^{6}\right)\right)^{1/2}$$

where b is the actual contact width

d is the cord diameter of the O-ring

C is the fractional compression

ii. Hertizan analysis

$$\frac{b}{d} = \left(\frac{6}{\pi}\left(1.25\,C^{1.5}\right)\right)^{1/2}$$

iii. A simple, purely empirical model proposed by Lindley viz : -

$$\frac{b}{d} = 2.4\,C$$

iv. An empirical model proposed by Wendt

$$\frac{b}{d} = 1.5\,C^{2}/3$$

v. A model proposed by Gorelik and Feld'man

$$\frac{b}{d} = 2\,C + 0.15 \qquad \text{for} \quad 0.1 \leq C \leq 0.425$$

$$\frac{b}{d} = (2\,C + 0.15)^{2} \qquad \text{for } 0.425 \leq C \leq 0.45$$

The conclusion was that all models give very similar results below 20% compression. Above 20% the agreement is also good except for model (ii). The correlation of the models with the experimental values is excellent. However, no analytical methods exist which will cope with laterally constrained O-ring geometries.

Medri, Molari and Strozzi (53) suggested a numerical solution using load increments. A structure was loaded by increments to bring a new node into contact each time, until the total amount of force was reached. The method required a lot of computing time. He therefore proposed to split the contact problem into two parts. The linear part proceeded by displacement increments, contact was taken into account by putting a 'roller' constraint on the contact line if the displaced node went on or beyond it. In the nonlinear part, the load and displacement of the unilateral contact nodes were related by 3 dimensional constants. He claimed convergence was good, but required small compressibility assumption in dealing with incompressible materials.

Salita (50) determined contact surface with iterative application of boundary constraints. At least one node was initially constrained along the boundary. Then deformation was calculated. No nodes might pass through the walls. The worst offenders were constrained to move onto the wall, and deformation calculation repeated until all nodes lay within the boundary.

Pascoe, Mottershead and Hellen (57) reviewed the major displacement finite element contact methods in current use, and commented on their relative strengths and weaknesses. He said that contact modelling using finite element method could include a wide variety of problems. It is important to identify the form of contact problem you have. From his guidelines, O-ring in a housing can be classified as a 2-D sticking contact with changing boundary. He suggested load application would be best in increments as in standard non-linear analysis. This approach allows reasonable tracking of the load history and is not restricted to one boundary condition change per load step. There are predominantly three main methods of including the contact conditions in the system of finite element equations :

i) Penalty methods
   It is relatively straightforward to implement into existing finite element schemes. However, the user has to pre-define the gap stiffness, which cannot be too high or too low in real application.

ii) Lagrange multipliers

No gap elements are necessary. Extra rows and columns are added representing the normal and tangential nodal displacement constraint, to apply sticking conditions for a node. Its main disadvantages are that the order of the system of equations increases and the banded nature of the equations may be lost, extra coding is also necessary to monitor the relative positions, the normals and tangents of the touching nodes.

iii) Transformation matrix method

The displacement constraint to be imposed on a system is formed into a transformation matrix. A disadvantage is that a complete change in the reduced stiffness matrix is necessary, for each change of contact condition. Thus a full re-inversion is required.

Method (i) is an approximate method and as such iteration for a particular contact stage may be necessary. Methods (ii) and (iii) can apply the displacement constraints exactly in one stage, but not for cases involve overlaps if method (iii) is used

Gap elements are used in method (i) to simulate contact between two surfaces by generating restoring forces when the two surfaces approach each other and by removing the contact forces when the two surfaces move away form each other. This means that gap elements have two stiffness values associated with them, a finite value when the surfaces are in contact, and zero when the surfaces are not. The user-defined stiffness of gap elements is a key parameter. If the stiffness value is too small, overlap occurs. If the stiffness value is too large, no solution may be yielded because bouncing occurs. Rizzo (58) suggested stiffness should be determined by simple comparison of the stiffness to those of associated spar elements. If a gap element has stiffness 100 times greater than that of one spar, then the displacement calculated has a 1 percent error.

For long term seal life prediction, analytical method provides an approximate, initial O-ring geometry. Finite element analysis is however required for accurate geometry calculation in special cases.

3.6 Finite Element Application in Rubber Industry

Finite element application in rubber industry is very common. Derby, Collins and Moses (59) applied finite element method to analyse rubber curing. Heat is applied to the outside of rubber during curing. In dealing with large rubber parts, a compromise must be made between over-curing the outside and under-curing the inside. Finite element modelling is useful in determining the minimum press time based on avoiding porosity at the coolest point, or in justifying the modification required for moulds at the design stage.

Nelson (60) incorporated finite element method into computer aided design systems in automotive industry. He used finite element method to predict how fast air would leak out of automobile tyres of various designs. He used a commercial finite element package ABAQUS to compare the suitability of different rubber compounds in automobile exhaust hanger service.

Morman and Pan (61) used ABAQUS to calculate nonlinear stress distribution and static force-deflection response of a suspension bushing, and an engine mount. They concluded that finite element analysis for automotive engineering was far superior to closed-form equations in accuracy and in the ability to produce detailed information for design consideration.

Competition in the automotive industry requires increasingly refined component design, and decreasing development times. Fursdon (62) described how Avon Automotive Components Division used ABAQUS in design stage to predict stiffness of engine mount, cord reinforced components and wiper blade, to study deformed shape of fluid chamber and stresses in a diaphragm component which formed a seal and flexible piston within a brake actuator. He said that finite element analysis allowed accurate prediction to be made systematically for geometries beyond the scope of approximate design formula. However, a component is specified both by the design geometry and the appropriate material data. It is normally the collection of the material data which poses the main difficulty. He anticipated that the use of finite element stress analysis coupled with appropriate durability data will facilitate increased understanding of fatigue life performance of standard rubber compounds.

4. DEVELOPMENT OF THEORETICAL METHOD

Fluid diffusion and material ageing are closely related. As an illustration, consider a small volume of rubber near the centre of a seal. Its chemical reaction rate will depend on the availability of free reactant (e.g. fluid diffusant). There are various possibilities :

i. If fluid diffuses in faster than it reacts, the ageing process is chemical reaction rate limited.

ii. (a) If the reverse is true, then ageing is limited by the diffusion rate.

(b) The availability of fluid is also dependent on its saturated concentration in the rubber. If this is low then a diffusion limited situation is more likely than if it is high.

Type (ii) situations can result in considerable spatial variation in ageing through the body of the seal. Conversely, type (i) can result in a relatively uniform distribution ageing through the seal. For example, carbon dioxide has a high solubility and low reaction rate compared with oxygen, so these two gases are likely to demonstrate type (i) and (ii) behaviour respectively. Similar considerations may be applied to the interpretation of possible explosive decompression damage.

Specific manifestations of fluid diffusion and adsorption, property and dimensional changes caused by physical and chemical ageing processes will be considered in turn in this Chapter. Part of the established theory has been previously published by Ho et al (ref. 63).

4.1 Fluid Adsorption and Diffusion

Elastomers subjected to high pressure fluid for any length of time take up fluid. The first stage of ingress, surface adsorption, is essentially instantaneous for practical temperatures and purposes. This stage forms the practical boundary conditions of the present computer modelling.

The next stage, the diffusion of fluid into the body of the sample until the fluid equilibrium concentration in the rubber is reached, is often of considerable duration. This is governed by differential equation (4.1) for an axisymmetric model or (4.2) for a 3-dimensional model.

$$\partial c/\partial \tau = \partial/\partial z\,[\,D_z(\partial c/\partial z)] + 1/r\,\{\partial/\partial r\,[D_r r(\partial c/\partial r)]\} + S_i \quad \text{.....(4.1)}$$

$$\partial c/\partial \tau = \partial/\partial x\,[\,D_x\,(\partial c/\partial x)\,] + \partial/\partial y\,[D_y(\partial c/\partial y)] + \partial/\partial z\,[D_z(\partial c/\partial z)] + S_i \quad \text{.....(4.2)}$$

where D_x, D_y, D_z, D_r are the diffusion coefficients in the specified direction,
c is the concentration of fluid in its host,
$d\tau$ is the time interval,
r is the radius,
z is the longitudinal length in axisymmetric model,
x, y, z are the rectangular Cartesian coordinates,
S_i is the sink term.

Each succeeding layer eventually achieves equilibrium in time, until the whole sample is finally at its equilibrium concentration. The steady state condition can be fully described by equation (4.3) or (4.4).

$$\partial/\partial z\,[\,D_z(\partial c/\partial z)] + 1/r\,\{\partial/\partial r\,[D_r r(\partial c/\partial r)]\} + S_i = 0 \quad \text{.....(4.3)}$$

$$\partial/\partial x\,[\,D_x\,(\partial c/\partial x)\,] + \partial/\partial y\,[D_y(\partial c/\partial y)] + \partial/\partial z\,[D_z(\partial c/\partial z)] + S_i = 0 \quad \text{.....(4.4)}$$

The diffusion coefficients can vary spatially and temporarily, due to the ageing of rubber caused by chemical interactions with fluids. To take into account the change of diffusion coefficients in applying finite element method, each element should possess its own diffusion coefficient which is updated with time.

Equations (4.1) to (4.4) can be derived from Fick's 1st and 2nd Law of Diffusion as shown in Appendix 1.

4.1.1 Difference between Liquid and Gas Adsorption

Liquid and gas behave differently in the first stage of ingress - adsorption. Liquid adsorption relies on a balance of the chemical potentials of external contacting liquid, and liquid dissolved in the elastomer. Therefore it is largely pressure independent. Gases, on the other hand, have to dissolve on to the surface of elastomers, and this process is highly pressure dependent until the densities of gases approach the liquid range.

Mass uptake measurements at ambient pressure are performed (at MERL) to determine the equilibrium concentration of liquids in elastomers. These data are fed into the diffusion module as the boundary conditions for rubber seals.

The gas concentration (c) on polymer surface is directly proportional to pressure (p); this is Henry's Law

$$c = sp \quad \text{.....(4.5)}$$

where constant s is the solubility coefficient in bar^{-1}

In gas mixtures, the concentration (c_i) of constituent 'i' absorbed at the surface of the polymers is directly proportional to its partial pressure (p_i).

$$c_i = sp_i \quad \text{.....(4.6)}$$

The partial pressure (p_i) is determined by Dalton's Law, being expressed in terms of the molar fraction of constituent 'i' and the total pressure (p):

$$p_i = p * m_i / (m_1 + m_2 + m_3 + ...+ m_i + ...) \quad \text{.....(4.7)}$$

Therefore, the concentration of constituent i at the surface of polymers is

$$c_i = s * p * m_i / (m_1 + m_2 + m_3 + ...+ m_i + ...) \quad \text{.....(4.8)}$$

A solution of gas in liquid can be treated similarly.

4.1.2 Diffusion Property Changes

The magnitude of the solubility coefficient s increases with absolute temperature (T) according to equation (3.7) :

$$s = s_0 \exp (-\Delta H_{sr}/RT)$$

where R is the Gas Constant, and the heat of solution ΔH_{sr} comprises the sum of the heat of condensation and the heat of mixing with the polymer.

Equilibrium concentration and diffusion coefficient also change with temperature and pressure as discussed in Section 3.2.2. The current project emphasizes on modelling ageing when seals are in a stable environment for a long period of time. Therefore, the proposed computer model will only handle cases with limited changes in temperature and pressure during seal life. It is necessary to determine the service fluid pressure and temperature, and then input the corresponding values of equilibrium concentration, diffusion coefficient, and soak time for computer analysis. Information and data are available from permeation experimental test report (ref 64) and liquid uptake report (ref 65) by Campion and Morgan.

The present computer model also handles change of equilibrium concentration and diffusion coefficient in aged rubber, caused by chemical interactions between polymer and ingressed fluids. It allows users to enter empirical equilibrium concentration and diffusion coefficient with respect to crosslink density (C.L.D.). More details are discussed in Section 4.2.2.

4.2 Property Losses

All rubbers are subjected to ageing with increasing time at high temperature. The rate of ageing varies widely depending upon the elastomer base, the additive recipe of the rubber compound, and the contact medium.

Ageing can be characterized as temporary (physical) and permanent (chemical), and many appear as property losses and dimensional changes (deformation). Material properties such as elastic modulus (E), Poisson's ratio (υ), diffusion coefficient (D), solubility coefficient (s), equilibrium liquid concentration (c_∞) change with temperature and time, while shape and volume of rubber change due to compression set, liquid uptake and thermal expansion.

4.2.1 Property Changes Due to Physical Effects

Property of material can change due to a number of physical effects as summarized in Fig 4.1. These are generally recoverable when the physical effects are removed.

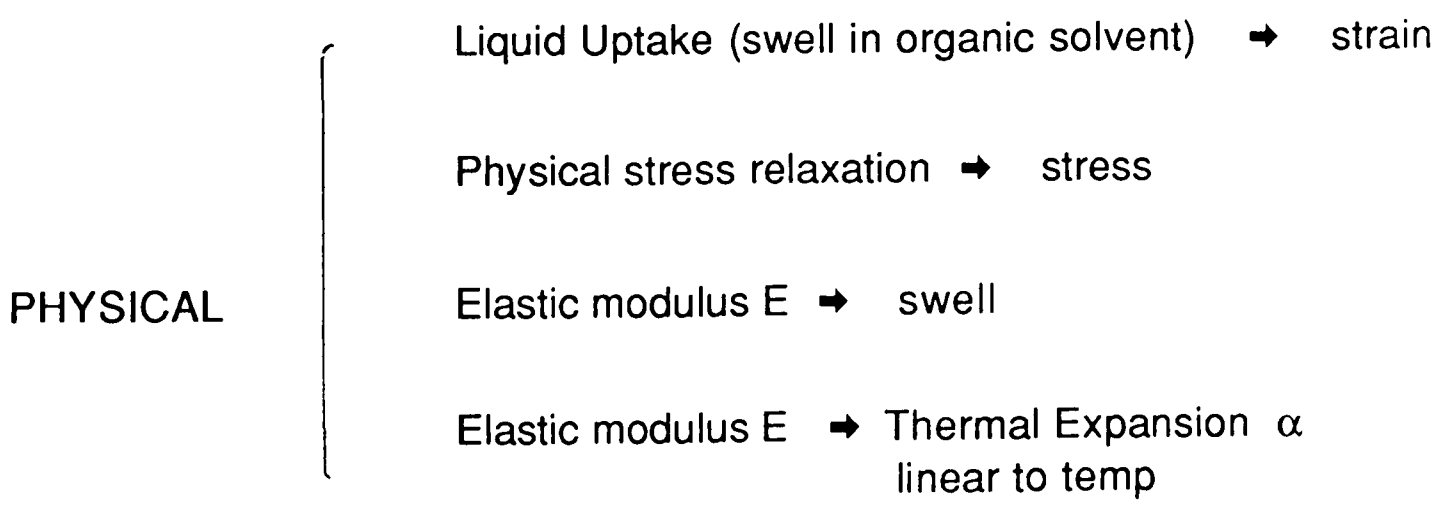

Fig 4.1 Physical effects

a. Physical Stress Relaxation

When strain is applied to polymer, it can result in reorientation of the molecular network, disengagement and rearrangement of chain

entanglements, breaking of bonds due to secondary valence forces between chains, between filler particles, or between chains and filler particles, and particularly for filled elastomers, due to the previous stress history of the material. Physical property losses can be measured by stress relaxation experiment. This is characterized as linear stress decrease with the logarithm of time,

$$(\sigma_o - \sigma_t) / \sigma_t = A \log (t/t_o) \quad \text{..... (4.9)}$$

based on two assumptions:

i. the physical stress relaxation rate is constant within the operational temperature range.
ii. the change of crosslink density has insignificant effect on the physical stress relaxation.

The first assumption is justified as long as the service temperature is well above (30°C to 40°C) the Tg of the material. The second assumption is true in normal service conditions. When the crosslink density becomes too high, the material will be brittle and unsuitable for sealing.

In service at high temperatures and long soak times, chemical relaxation will dominate over physical relaxation. Therefore, physical relaxation need not be included in the modelling of long term ageing. However, in data obtained from short term experiments the physical effect must be determined and subtracted to obtain an accurate determination of the chemical processes.

b. Equilibrium Concentration in Stressed Rubber

Equilibrium concentration (c_∞) of liquid in elastomeric seals depends on strain. The volume of liquid uptake by an elastomer can be increased by stretching it and decreased by applying compressive strain to it.

Liquid uptake is better explained with the Gibbs free energy of the system due to the transfer of unit quantity (1 mol) of liquid from the liquid phase to a very large quantity of the mixed phase. In cross-linked polymers, it is necessary to take into account the configurational entropy of the network.

The total free energy of dilution can therefore be expressed as

$$\Delta G1 = \Delta G1_m + \Delta G1_e \quad \text{..... (4.10)}$$

where $\Delta G1_m$ represents the free energy of dilution for the polymers in the state prior to cross-linking

$$\Delta G1_m = RT \ \{ \ln(1-v_2) + v_2 + \chi_1 v_2^2 \} \quad \text{..... (4.11)}$$

in which the parameter χ_1 includes a component χ_o due to entropy

and $\Delta G1_e$ corresponds to the change of free energy (per mole of liquid absorbed) due to the associated elastic expansion of the network.

$$\Delta G1_e = \Delta W / k_1 = \rho RT(V_1 v_2^{1/3}) / M_c \quad \text{..... (4.12)}$$

in which : k_1 is the number of moles of liquid in the swollen polymers ,

ρ is the density of the dry rubber

V_1 is the molar volume of the swelling liquid and $1/v_2 = 1 + k_1 V_1$

M_c is the average molecular weight between crosslinks

and M_c^{-1} is usually identified as crosslink density

From equation (4.10), the total free energy of dilution is :

$$\Delta G1 = RT \ \{ \ln(1-v_2) + v_2 + \chi_1 v_2^2 + \rho(V_1 v_2^{1/3}) / M_c \ \}$$

and for equilibrium swell :

$$\Delta G1 = RT \ \{ \ln(1-v_2) + v_2 + \chi_1 v_2^2 + \rho(V_1 v_2^{1/3}) / M_c \ \} = 0 \quad \text{..... (4.13)}$$

$$\text{the normal stresses } t_1 = t_2 = t_3 = 0 \quad \text{..... (4.14)}$$

$$\lambda_1 \lambda_2 \lambda_3 = 1 / v_2 \quad \text{..... (4.15)}$$

Application of tensile stress will increase the amount of swell. The relationship between normal stresses (t_1, t_2, t_3) and swell ratio can be expressed as :

$$t_1 = RT \ \{ \ln(1-v_2) + v_2 + \chi_1 v_2^2 + \rho(V_1 v_2 \lambda_1^2) / M_c \ \} / V_1 \quad \text{..... (4.16)}$$

$$t_2 = t_3 = RT \ \{ \ln(1-v_2) + v_2 + \chi_1 v_2^2 + \rho(V_1) / \lambda_1 M_c \ \} / V_1 = 0 \quad \text{..... (4.17)}$$

the quantity which determines the direction of the change of swell is the hydrostatic pressure component of the applied stress. For a simple

hydrostatic pressure this leads to a reduction of swell with increasing pressure. Conversely, a tensile stress, for which the hydrostatic pressure component is negative, is expected to lead to an increase in swell.

Also the change of liquid uptake $\Delta V/V$ is proportional to the square of the torsional strain. For a good swelling agent $\Delta V/V$ is negative - i.e. the swelling decreases on twisting.

For an O-ring in a housing, its boundaries are restrained by metal and high pressure fluids, equilibrium concentration is therefore likely to be lower than free volume swell. In this first attempt to model seal life, empirical unconstrained volume swell data are used. Initial contact stress prediction would therefore be higher than actual by allowing more liquid uptake, but in the long term, predicted stress would be lower than actual as in reality less chemical reaction occurs. Rubber O-rings with high initial swell are not recommended for real application, so the model will predict shorter life in general.

c. Young's Modulus Change Due to Swell

When rubber swells, its modulus will be reduced. This can be explained from the statistical network theory of rubber elasticity.

Initial change of entropy dS_o corresponding to linear extension ratio λ_o is

$$dS_o = -1/2\ NK(3\lambda_o^2 - 3) \quad \text{..... (4.18)}$$

The total entropy change dS_o' in passing from the unstrained unswollen state to the strained swollen state, based on Gaussian Statistics, would be

$$dS_o' = -1/2\ Nk\ (\lambda_1^2 \lambda_o^2 + \lambda_2^2 \lambda_o^2 + \lambda_3^2 \lambda_o^2 - 3) \quad \text{..... (4.19)}$$

The entropy of deformation from the swollen network is

$$dS' = dS_o' - dS_o$$
$$= -1/2\ Nk\ \lambda_o^2\ (\lambda_1^2 + \lambda_2^2 + \lambda_3^2 - 3)$$

$$= -1/2\ Nk\ v_2^{-2/3} (\lambda_1^2 + \lambda_2^2 + \lambda_3^2 - 3) \quad \text{(4.20)}$$

where v_2 is the volume fraction of polymers in the swollen rubber.

The entropy of deformation from the unswollen network is

$$dS = v_2\, dS' = -1/2\ Nk\ v_2^{1/3} (\lambda_1^2 + \lambda_2^2 + \lambda_3^2 - 3) \quad \text{(4.21)}$$

The strain energy function for the swollen rubber in terms of the extension ratios measured in the swollen state becomes :

$$W = -TdS = 1/2\ NkT\ v_2^{1/3} (\lambda_1^2 + \lambda_2^2 + \lambda_3^2 - 3) \quad \text{(4.22)}$$

And Neo-Hookean Model states that for unswollen rubber

$$W = 1/2\ NkT (\lambda_1^2 + \lambda_2^2 + \lambda_3^2 - 3) \quad \text{(4.23)}$$

$$G = NkT \quad \text{(4.24)}$$

Therefore, the modulus in the swollen state G' can be expressed in terms of the modulus in the unswollen state G :

$$G' = v_2^{1/3} G \quad \text{(4.25)}$$

d. Young's Modulus Change Due to Temperature

According to the Joule-Gough effect, the elastic modulus of elastomers increases in proportion to absolute temperature. Taking into account temperature effect, Young's modulus at evaluated temperature is

$$E = E_r [1 + (T-T_r)/T_r - 3\alpha(T-T_r)] \quad \text{(4.26)}$$

where α is the thermal expansion coefficient,

and r signifies reference temperature values.

4.2.2 Property Changes Due to Chemical Effects

Property changes due to chemical effects (Fig 4.2) are normally irreversible, accelerated by temperature, and predominant in long term.

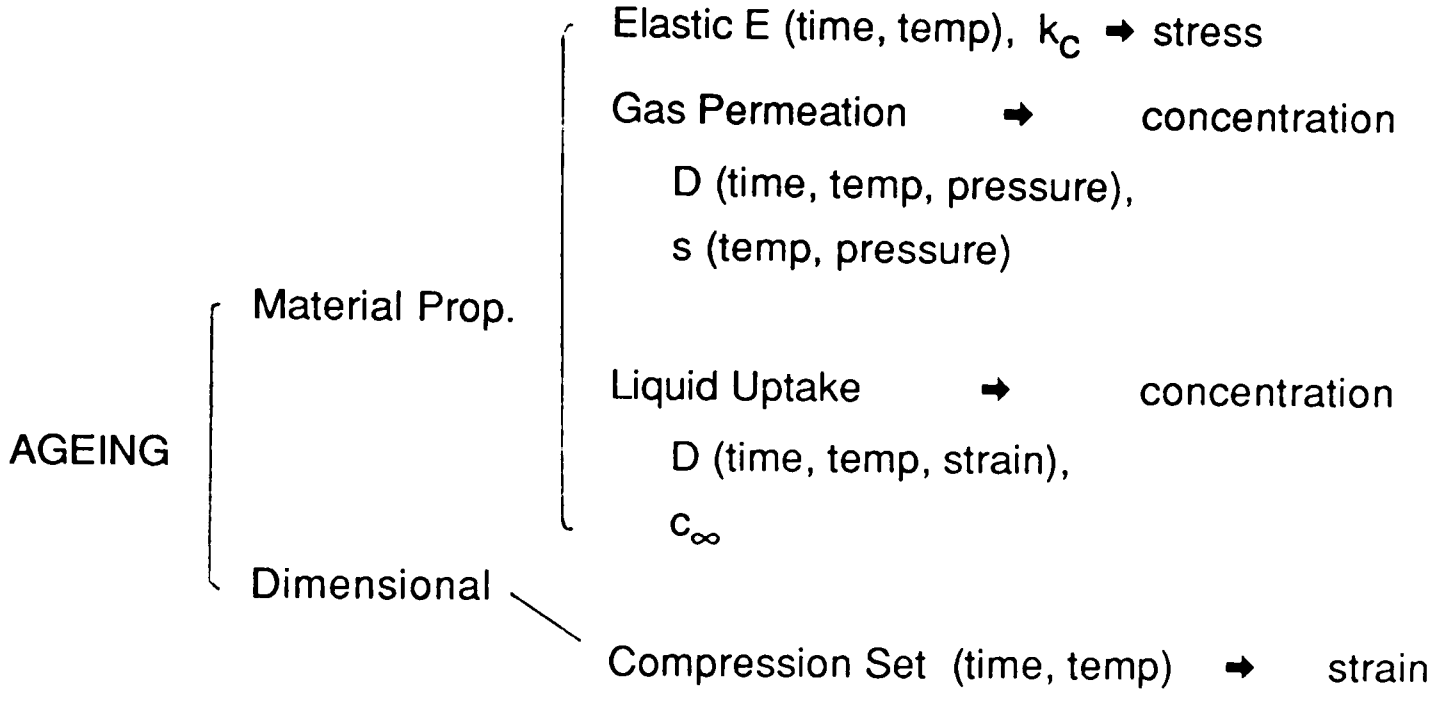

Fig 4.2 Ageing effects

a.Young Modulus

Young modulus (E) of rubber depends on time and temperature. When absorbed fluids react with polymer chains, in some cases new crosslinks are formed (see Fig 4.3), and the Young's Modulus of the material increases. In other cases, chain scission occurs and the Young's Modulus of the material decreases. These chemical reactions are normally accelerated by an increase in temperature. From basic chemistry, a chemical reaction can be written as :

n_1 reactant molecules + n_2 potential reaction sites ------>1 crosslink
where n_1 and n_2 are integers

Assume oxidation as a specific example,

then oxygen reaction rate is $\frac{d\,O(t)}{dt} = -k_c\, Y(t)\, O(t)$ ..... (4.27)

where Y(t) is the potential reaction sites at time t

the reaction rate coefficients $k_c = Ae^{(-E_a/RT)}$ .....(4.28)

E_a is the activation energy,

R is the gas constant and T is absolute temperature.

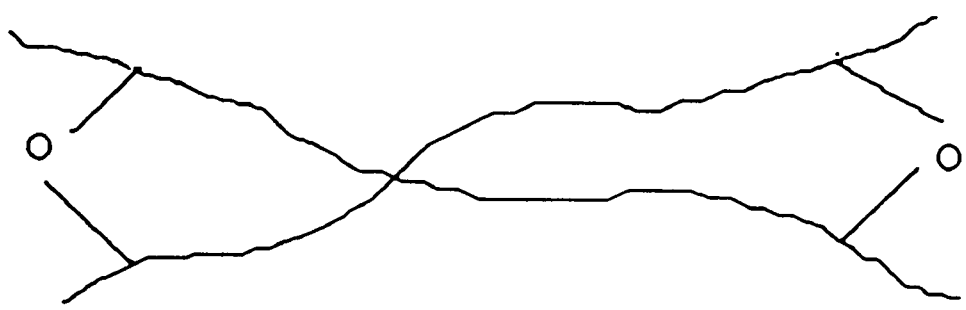

Fig 4.3 The formation of crosslinks between polymer chains

When diffusion and chemical reaction are coupled together, the oxygen concentration at time t, denoted by O(t) is given by the following two equations :

$$\frac{d\,O(t)}{dt} = \frac{d}{dx} D_x \frac{d\,O(t)}{dx} + \frac{d}{dy} D_y \frac{d\,O(t)}{dy} - \Sigma\, k_c\, Y(t-\partial t)\, O(t) \quad \text{..... (4.29)}$$

and

$$\frac{d\,Y(t)}{dt} = -\frac{n_1}{n_2} k_c\, Y(t)\, O(t) \quad \text{..... (4.30)}$$

where n_1 / n_2 is the rate of fluid consumption to reaction sites consumption

Young's modulus at time t is linearly related to crosslink density (C.L.D.):

$$E(t) = a\,[\,C.L.D.\,(t)\,] - b$$
$$= a\,[\,C.L.D.\,(t) - C.L.D.(0)\,] + E_0 \quad \text{..... (4.31)}$$

or linearly related to the consumption of reaction sites in chain scission :

$$E(t) = a\,Y(t) - b$$
$$= a\,[\,Y(t) - Y(0)\,] + E_0 \quad \text{..... (4.32)}$$

The resultant change in Young modulus will affect the contact stress of rubber O-rings in a housing.

b. Liquid Uptake Properties

In an aged elastomer seal, liquid uptake properties such as diffusion coefficient (D) and equilibrium concentration (c_∞) change with time as crosslink formation or chain scission occurs. Temperature determines rate of chemical reactions, and hence controls the change of liquid uptake properties. Liquid uptake in turn modifies the strain of the seal constrained in its housing groove.

c. Gas Permeation Properties

Gas permeation properties, such as diffusion coefficient (D) and solubility coefficient (s) at constant temperature and pressure may also change with time, as a result of crosslink formation or chain scission occurred in aged rubber. In the present computer modelling, regular updated of the liquid uptake and gas permeation properties are performed, based on laboratory data obtained from rubber sample measurements.

$$\frac{s - s(t_1)}{s(t_2) - s(t_1)} = \frac{\text{C.L.D. } (t) - \text{C.L.D. } (t_1)}{\text{C.L.D } (t_2) - \text{C.L.D. } (t_1)} \quad \text{.....(4.33)}$$

where C.L.D.(t_1) and C.L.D.(t_2) are measured crosslink densities of rubber aged for different periods of time,

$s(t_1)$ and $s(t_2)$ are the corresponding solubility coefficients from experimental results,

s is the solubility coefficients of an aged rubber with crosslink density C.L.D. (t).

4.3 Dimensional Changes

Physical dimensional change in unconstrained rubber is normally homogeneous. However, deformation occurs when rubber or rubber-like material is constrained. This deformation is incompressible and non-linear. Furthermore, chemical dimensional change is normally associated with deformation.

4.3.1 Dimensional Changes Due to Physical Effects

a. Swelling

The phenomenon of the swelling of rubber in a typical solvent is analogous to the mixing of two mutually soluble low molecular weight liquids which do not interact chemically. It is a purely physical mixing or interdiffusion process in which the two components may be regarded as chemically neutral.

For the 1st approximation, the increase in volume of swollen rubber may be assumed equal to the volume of liquid absorbed.

$$v_2 = V_p/(V_s + V_p) \quad \text{.....(4.34)}$$

where v_2 is the volume fraction of polymers in the swollen rubber

V_p is the volume of the unswollen rubber

V_s is the volume of the liquid absorbed

However, because of free volume existing in rubber, the volume of the swollen rubber is likely to be less than $(V_s + V_p)$, as some of the absorbed liquid occupies the free volume between rubber molecules. The amount of free volume (φ) in rubber depends on the rubber temperature relative to Tg. It can be predicted from the following equation :

$$\varphi = (\alpha_L - \alpha_G)\, T = (\Delta\alpha)T \quad \text{..... (4.35)}$$

where α_L is the thermal expansion coefficient of the rubber in leather form,

α_G is the thermal expansion coefficient of the rubber in glass form.

In real conditions, swollen volume will lie in between the extreme conditions of (i) assuming that the volumes are additive and (ii) subtracting all free volume from condition (i). Estimations for these conditions, plus some measurements on dimensional changes during swelling in toluene were performed by MERL on EPDM and high ACN NBR materials. Preliminary research showed that the actual value made a 40/60 proportion with the two extremes, being nearer the additive limit. In the proposed computer model, we shall use a 50/50 average between the two extremes when data are available, or use the additive limit when free volume data are not available.

b. Thermal Expansion

Thermal expansion of rubber occurs almost instantly. It depends on the thermal expansion coefficient (α) of the material, and the temperature of the rubber which is equal to the temperature of its contact medium in an ageing problem.

$$\Delta l = \alpha \, l \, \Delta T \quad \text{..... (4.36)}$$

4.3.2 Large Strain Axisymmetric Deformation

Deformation of rubber is best described by invariants in terms of strain components which are independent of the co-ordinate system used. The three principle extension ratios in an axisymmetric model are

$$\lambda_\theta = r/r_o = \varepsilon_\theta + 1 \quad \text{..... (4.37)}$$

$$\lambda_r = \partial r/\partial r_o = \varepsilon_r + 1 \quad \text{..... (4.38)}$$

$$\lambda_z = \partial z/\partial z_o = \varepsilon_z + 1 \quad \text{..... (4.39)}$$

where

$$\varepsilon_\theta = u/r_o \quad \text{..... (4.40)}$$

$$\varepsilon_r = \partial w/\partial r_o \quad \text{..... (4.41)}$$

$$\varepsilon_z = \partial w/\partial z_o \quad \text{..... (4.42)}$$

For incompressible material, its volume remains constant during deformation

$$\lambda_\theta \lambda_r \lambda_z = 1 \quad \text{..... (4.43)}$$

Assume the material is perfectly elastic, all the work done will be stored in the form of strain energy for an isothermal deformation. The strain energy per unit volume W may be expressed as a function of three strain invariants.

$W(I_1,I_2,I_3)$ where the invariants are written as

$$I_1 = \lambda_\theta^2 + \lambda_r^2 + \lambda_z^2 \quad (4.44)$$

$$I_2 = (1/\lambda_\theta^2) + (1/\lambda_r^2) + (1/\lambda_z^2) \quad (4.45)$$

$$I_3 = \lambda_\theta^2 \lambda_r^2 \lambda_z^2 = 1 \quad (4.46)$$

From Williams (51), the rubber stress-strain relationship

$$p_\theta = 2C_1\lambda_\theta^2 - 2C_2/\lambda_\theta^2 + p_o \quad (4.47)$$

$$p_r = 2C_1\lambda_r^2 - 2C_2/\lambda_r^2 + p_o \quad (4.48)$$

$$p_z = 2C_1\lambda_z^2 - 2C_2/\lambda_z^2 + p_o \quad (4.49)$$

where p_θ, p_r, p_z are the principal stresses, and p_o is an arbitrary hydrostatic pressure.

$$p_\theta - p_r = 2C_1\lambda_\theta^2 - 2C_2/\lambda_\theta^2 - 2C_1\lambda_r^2 + 2C_2/\lambda_r^2$$

$$= 2C_1(\lambda_\theta^2 - \lambda_r^2) \quad (4.50)$$

when $C_2=0$

And the usual equilibrium equation is satisfied at every point in the strained state so that $dp_r/dr + (p_r-p_\theta)/r = 0$ (4.51)

$$dp_r/dr = 2C_1(\lambda_\theta^2 - \lambda_r^2)/r \quad (4.52)$$

$$p_r = 2C_1 \int (\lambda_\theta^2 - \lambda_r^2)\, dr/r \quad (4.53)$$

4.3.3 Dimensional Changes Due to Chemical Effects

The formation of new crosslinks at a strained position can cause compression set. These new crosslinks do not contribute to the original stress-supporting network, but strengthen the test sample at the strained position. When the applied force is removed, the newly formed crosslinks will restrict the ability of the aged rubber to return to its original shape .

a. Uniaxial Elongation or Compression

For an incompressible rubber :

$\lambda_1 \lambda_2 \lambda_3 = 1$ ..... (4.54)

$\lambda_2 = \lambda_3 = \sqrt{1/\lambda_1}$ ..... (4.55)

Hence the work done in extension $W = GA_o/2 [\lambda_1^2 + (2/\lambda_1)-3]$

and for $A_o=1$ $W = G/2 [\lambda_1^2 + (2/\lambda_1)-3]$ ..... (4.56)

the tension force $f = \partial W/\partial\lambda_1 = G (\lambda_1 - 1/\lambda_1^2)$ ..... (4.57)

the stress $t = \lambda_1 (\partial W/\partial\lambda_1) = G (\lambda_1^2 - 1/\lambda_1) + p_o$ ..... (4.58)

Consider a rubber strip compressed to a constant length l and left to age,

since rubber is incompressible, $A_o l_o = A_a l_a$ ..... (4.59)

$l/(A_o l_o) = l/(A_a l_a)$ ..... (4.60)

$\lambda_o/A_o = \lambda_a/A_a$ ..... (4.61)

where A_o is the original unstrained cross-sectional area,

A_a is the unstrained cross-sectional area of the aged rubber,

l_o is the original length of the rubber,

l_a is the unstrained length of the aged rubber,

λ_o is the extension ratio for the original strip held at constant length l

λ_a is the extension ratio for the aged strip held at constant length l

Berry, Scanlan and Watson (66) expressed the retained force ratio (fa/fo) of the aged rubber in terms of its set length and its original length :

$$\frac{f_a}{f_o} = \frac{G_a A_a (\lambda_a - 1/\lambda_a^2)}{G_o A_o (\lambda_o - 1/\lambda_o^2)} = \frac{G_a \lambda_a (\lambda_a - 1/\lambda_a^2)}{G_o \lambda_o (\lambda_o - 1/\lambda_o^2)} = \frac{G_a (\lambda_a^2 - 1/\lambda_a)}{G_o (\lambda_o^2 - 1/\lambda_o)}$$

..... (4.62)

where fa is the applied force on the original rubber

fo is the applied force on the aged rubber

The newly formed crosslinks in a strained position do not contribute to the original stress-supporting network. For the calculation of % retained force,

G_a is assumed to be equal to G_o for hardened rubber. However, when chain scissions occur, Ga should be the softened value.

b. Plane Strain Analogue

When the same theory is applied to seals, for simplification we first assume a plain strain condition. That is when an elastomeric ring is cut across one section on its circumference and straightened. By applying the incompressible equation (4.54)

$$\lambda_1 \lambda_2 \lambda_3 = 1$$

and

$$\lambda_2 = 1/\lambda_1 \quad \text{..... (4.63)}$$

$$\lambda_3 = 1 \quad \text{..... (4.64)}$$

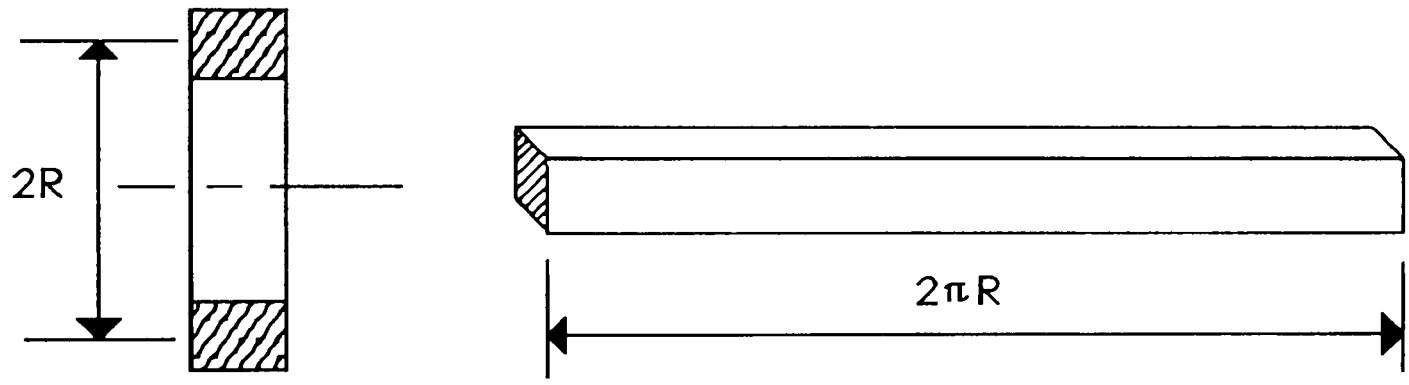

where $\lambda_3 = \lambda_z = 1$

Fig 4.4 A straightened elastomeric ring

The work done in extension is $W = GA_0/2\,[\lambda_1^2 + (1/\lambda_1^2) + 1 - 3]$

for Ao=1 in term of extension ratios $W = G/2\,[\lambda_1^2 + (1/\lambda_1^2) - 2]$ ..... (4.65)

the tension force $f = \partial W/\partial \lambda_1 = G\,(\lambda_1 - 1/\lambda_1^3)$ ..... (4.66)

the stress $t = \lambda_1\,(\partial W/\partial \lambda_1) = G\,(\lambda_1^2 - 1/\lambda_1^2) + p_o$ ..... (4.67)

Using equation (4.61), the retained force ratio (f_a/f_o) of the aged rubber is expressed in term of the set length and the original length of the rubber as :

$$\frac{f_a}{f_o} = \frac{G_a A_a (\lambda_a - 1/\lambda_a^3)}{G_o A_o (\lambda_o - 1/\lambda_o^3)} = \frac{G_a \lambda_a (\lambda_a - 1/\lambda_a^2)}{G_o \lambda_o (\lambda_o - 1/\lambda_o^2)} = \frac{G_a (\lambda_a^2 - 1/\lambda_a^2)}{G_o (\lambda_o^2 - 1/\lambda_o^2)}$$

..... (4.68)

c. Constant Hoop Extension Ratio

When the nominal diameter of an elastomeric ring is of the same magnitude as its section diameter, a plain strain assumption may not give satisfactory results. It should be treated as an axi-symmetric problem. For simplification, $\lambda_3 = \lambda_\theta = R/R_o$, the hoop extension ratio of the O-ring.

For $\lambda_1 \lambda_2 \lambda_3 = 1$

$$\lambda_2 = R_o/R\lambda_1 \quad \text{..... (4.69)}$$

$$\lambda_3 = R/R_o \quad \text{..... (4.70)}$$

Hence the work done in extension $W = GA_o/2\,[\,\lambda_1^2 + (R_o^2/R^2\lambda_1^2) + R^2/R_o^2 - 3]$

for $A_o=1$, $W = G/2\,[\,\lambda_1^2 + (R_o^2/R^2\lambda_1^2) + R^2/R_o^2 - 3]$ ..... (4.71)

the tension force $f = \partial W/\partial \lambda_1 = G\,(\lambda_1 - R_o^2/R^2\lambda_1^3)$ ..... (4.72)

the stress $t = \lambda_1\,(\partial W/\partial \lambda_1) = G\,(\lambda_1^2 - R_o^2/R^2\lambda_1^2) + p_o$ ..... (4.73)

The empirical model for entering into the computer model to calculate contact stress with time, using measured set dimensions, is

$$\frac{f_a}{f_o} = \frac{G_a A_a (\lambda_a - R_a^2/R^2\lambda_a^3)}{G_o A_o (\lambda_o - R_o^2/R^2\lambda_o^3)} = \frac{G_a (\lambda_a^2 - R_a^2/R^2\lambda_a^2)}{G_o (\lambda_o^2 - R_o^2/R^2\lambda_o^2)}$$

..... (4.74)

5. NUMERICAL METHOD

The diffusion equation is in fact a form of generalized Poisson equation. Equations of this type are commonly solved by either finite difference or finite element methods. The latter is chosen based on the following reasons :

i. the finite element method is versatile in dealing with irregular seal geometry.
ii. treatment of boundary conditions is easier with the finite element methods
iii. higher order approximations can be relatively easier to obtain.

The main drawback of the finite element method is the difficulty in determining the coefficients for the approximating equations. In the present project, these coefficients will be defined from understanding the basic science of seal material, based on experimental data obtained from material rig tests and related material research.

Chemical reaction occurring between ingressed fluid and rubber can be incorporated into general diffusion equations by finite element method. This will be detailed in this chapter. The same mesh will be used for diffusion and chemical reaction calculation. This can simplify data input and storage.

5.1 Solution to Fluid Diffusion

It is possible to arrive mathematically at a finite element approximation directly from the differential equations governing an engineering problem. The advantage of such method is that:

a. The search for a 'functional' equivalent to the known differential equation is made unnecessary.
b. The method can be extended to a range of problems for which a 'functional' may not exist, or has not been discovered.

Consider the problem of solving approximately a set of differential equations which the unknown function $\{\theta\}$ has to satisfy in the region V,

with the governing equation $A(\{\theta\})= 0$

and boundary condition $C(\{\theta\})= 0$ to be satisfied on boundary S.

If a trial function which satisfies the boundary conditions is written in the general form $\{\theta\}_a = [N]\{\theta\}$ .....(5.1)

in which [N] are prescribed functions of co-ordinates and $\{\theta\}$ is a set of n parameters, then in general $A(\{\theta\}_a)= R \neq 0$

The best solution of the unknown function will be to reduce the residual R to a minimum at all points of V (Zienkiewicz 24,25) such that

$\int_V WR\, dV= 0$ .....(5.2)

where W is some function of the co-ordinates. We can write this as a set of simultaneous equations :

$\int W_i A([N]\{\theta\})\, dV = 0$ .....(5.3)

where W_i is the known as the weighting function which is made equal to the global shapes function $\{N_i\}$ in Galerkin's method.

5.1.1 Galerkin's Residual Method in Cartesian Coordinates

Applying the Galerkin's residual method (Zienkiewicz 24,25) to solve the 2-dimensional steady state differential equation (see eq.4.4) :

$$\partial/\partial x(D_x * (\partial\theta/\partial x)) + \partial/\partial y(D_y * (\partial\theta/\partial y)) + S_i = 0 \quad \text{..... (5.4)}$$

The associated functional F which will give a least value of its residual R at all points of A is

$$F = \int_A \{\{ \partial/\partial x(D_x * (\partial\theta/\partial x)) + \partial/\partial y(D_y * (\partial\theta/\partial y)) + S_i \} * N_i \} dA \text{..... (5.5)}$$

Integration by parts states that :

$$_{xL}\int^{x_R} u\, dv = (uv)x_R - (uv)x_L - {}_{xL}\int^{x_R} v\, du \quad \text{.....(5.6)}$$

Thus $\iint \{ D_x * N_i * (\partial/\partial x(\partial\theta/\partial x)) \} dxdy$

$$= {}_{yB}\int^{y_T} \{(D_x * N_i * (\partial\theta/\partial x))x_R - (D_x * N_i * (\partial\theta/\partial x))x_L \} dy$$
$$- \iint \{D_x * (\partial\theta/\partial x) * (\partial N_i/\partial x)\} dxdy$$
$$= \int_\varphi \{(D_x * N_i * n_x(\partial\theta/\partial x))x_R + (D_x * N_i * n_x(\partial\theta/\partial x))x_L \} d\varphi$$
$$- \iint \{D_x * (\partial\theta/\partial x) * (\partial N_i/\partial x)\} dxdy$$
$$= \int_\varphi \{(D_x * N_i * n_x * (\partial\theta/\partial x)\} d\varphi - \iint \{D_x * (\partial\theta/\partial x) * (\partial N_i/\partial x)\} dxdy$$

.....(5.7)

where n_x is the direction cosine between the normal and x direction

Similarly in the y direction, we can write :

$$\iint \{ D_y * N_i * (\partial/\partial y(\partial\theta/\partial y)) \} dxdy$$
$$= \int_\varphi \{(D_y * N_i * n_y * (\partial\theta/\partial y)\} d\varphi - \iint \{D_y * (\partial\theta/\partial y) * (\partial N_i/\partial y)\} dxdy$$

And the eflux B_p on the boundary is $D\, \partial\theta/\partial n - B_p = 0$ .....(5.8)

$$[D_x(\partial\theta/\partial x)n_x + D_y(\partial\theta/\partial y)n_y] - B_p = 0 \text{.....(5.9)}$$

$$\int_\varphi N_i [D_x(\partial\theta/\partial x)n_x + D_y(\partial\theta/\partial y)n_y] d\varphi - \int_\varphi N_i B_p d\varphi = 0 \text{.....(5.10)}$$

The equation 5.5 becomes

$$F = \int_A \{ (D_x^* (\partial\theta/\partial x)^* \partial N_i/\partial x) + (D_y^* (\partial\theta/\partial y)^* \partial N_i/\partial y) + S_i^* N_i\} dA + \int_\varphi N_i B_p d\varphi$$

with $\theta = [N_i, N_j, ...] \{\theta\}^e = [N]\{\theta\}^e$ .....(5.11)

$$\partial\theta/\partial x = [\partial N/\partial x] \{\theta\}^e$$ .....(5.12)

$$\partial\theta/\partial\theta_i = N_i$$ ..... (5.13)

The finite element equation to be solved is therefore

$$F = \int_A \{ D_x^* ((\partial N_i/\partial x)^*\theta_i + (\partial N_j/\partial x)^*\theta_j + ...) * \partial N_i/\partial x$$
$$+ D_y^* ((\partial N_i/\partial y)^*\theta_i + (\partial N_j/\partial y)^*\theta_j + ...) * \partial N_i/\partial y) + S_i^* N_i\} dA + \int_\varphi N_i B_p d\varphi$$
$$= 0$$ ..... (5.14)

where i,j,....are nodal points of each element

In three dimensions by identical procedure, we can write :

$$\iint \{ D_x * N_i * (\partial/\partial y(\partial\theta/\partial x)) \} dxdydz$$
$$= \int\varphi \{(D_x * N_i * n_x^* (\partial\theta/\partial x)\} d\varphi - \iint \{D_x * (\partial\theta/\partial x) * (\partial N_i/\partial x)\} dxdydz$$

Therefore the discretised finite element equation to be solved is :

$$F = \int_V \{ D_x^* ((\partial N_i/\partial x)^*\theta_i + (\partial N_j/\partial x)^*\theta_j + ...) * \partial N_i/\partial x$$
$$+ D_y^* ((\partial N_i/\partial y)^*\theta_i + (\partial N_j/\partial y)^*\theta_j + ...) * \partial N_i/\partial y$$
$$+ D_z^* ((\partial N_i/\partial z)^*\theta_i + (\partial N_j/\partial z)^*\theta_j + ...) * \partial N_i/\partial z) + S_i^* N_i\} dV + \int_\varphi N_i B_p d\varphi$$
$$= 0$$ ..... (5.15)

The forced boundary conditions on domain θ :

$$C(\{\theta\}) = \theta - \theta_p = 0$$ ..... (5.16)

where θ_p is the prescribed values of concentration

The choice of [N] in functional F should be such that $N_i = 0$ on domain θ (to be shown in section 5.1.3).

5.1.2 Galerkin's Residual Method in Axisymmetric Coordinates

Hinton and Owen (26,27) applied the Galerkin's residual method to solve the axisymmetric steady state diffusion equation (4.3)

$$\partial/\partial z\,[\,D_z(\partial\theta/\partial z)] + 1/r\,\{\partial/\partial r\,[D_r r(\partial\theta/\partial r)]\} + S_i = 0$$

The associated functional F which will give a least value of its residual R at all points of V is

$$F = \int_V \{\{\ \partial/\partial z\,[\,D_z(\partial\theta/\partial z)] + 1/r\,\{\,\partial/\partial r\,[D_r r(\partial\theta/\partial r)]\,\} + S_i\ \}\ *\ N_i\,\}\,dV \quad \text{.....(5.17)}$$

and in axisymmetric problems, $dV = 2\pi r dA$ .....(5.18)

Therefore, following a procedure similar to that in section 5.1.1 :

$$F = \int_A \{\{\ \partial/\partial z\,[\,D_z r(\partial\theta/\partial z)] + \partial/\partial r\,[D_r r(\partial\theta/\partial r)] + S_i{}^* r\ \}\ *\ N_i\,\}\,dA$$

$$= \int_A \{(D_z{}^*\ r^*(\partial\theta/\partial z)^*\partial N_i/\partial z) + (D_r{}^* r^*(\partial\theta/\partial r)^*\partial N_i/\partial r) + r^* S_i{}^* N_i\}dA$$

$$+ \int_\varphi N_i B_p r d\varphi$$

$$= \int_A \{\ D_z{}^* r^*\ ((\partial N_i/\partial z)^*\theta_i + (\partial N_j/\partial z)^*\theta_j + ...)\ *\ \partial N_i/\partial z$$

$$+ D_r{}^* r^*\ ((\partial N_i/\partial r)^*\theta_i + (\partial N_j/\partial r)^*\theta_j + ...)\ *\ \partial N_i/\partial r) + r\ *\ S_i\ *\ N_i\}dA$$

$$+ \int_\varphi N_i B_p r d\varphi$$

$$= 0 \quad \text{.....(5.19)}$$

where $\theta = [N_z, N_r, ...] \begin{vmatrix} \theta_z \\ \theta_r \end{vmatrix} = [N]\{\theta\}_e$ .....(5.20)

5.1.3 Fixed Value (Dirichlet) Boundary Condition

To fit the curved irregular seal boundary with good accuracy but minimum number of elements, six-noded quadratic triangular elements are used. One of the elements is shown below :

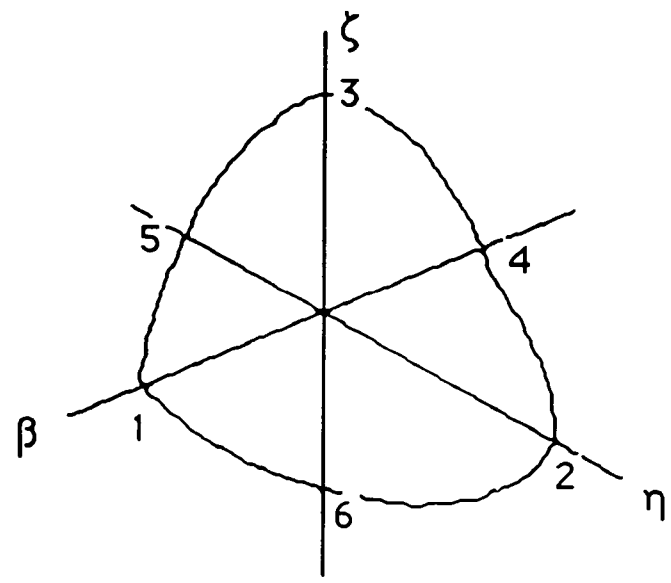

At node 1 $\beta = 1, \quad \eta = 0$
At node 2 $\eta = 1, \quad \beta = 0$
At node 6 $\beta = 0.5, \eta = 0.5$ for condition $\zeta = 0, \eta = 1 - \beta$

Fig 5.1 A six-noded quadratic triangular element in a skew planner coordinate system (β, η, ζ).

Steady state equation (5.19) can be written as

$$[K][\theta] = [F] \qquad (5.21)$$

where [K] is the stiffness matrix, [θ] is the unknown,

and the functional part $[F] = \int_V \{S_i^* N_i\} dV + \int_\varphi N_i B_p r d\varphi$

Expressing equation (5.21) in terms of a six-noded quadratic triangular element gives :

$$\begin{pmatrix} k_{11} & k_{12} & k_{13} & k_{14} & k_{15} & k_{16} \\ k_{21} & k_{22} & k_{23} & k_{24} & k_{25} & k_{26} \\ k_{31} & k_{32} & k_{33} & k_{34} & k_{35} & k_{36} \\ k_{41} & k_{42} & k_{43} & k_{44} & k_{45} & k_{46} \\ k_{51} & k_{52} & k_{53} & k_{54} & k_{55} & k_{56} \\ k_{61} & k_{62} & k_{63} & k_{64} & k_{65} & k_{66} \end{pmatrix} \begin{pmatrix} \theta_1 \\ \theta_2 \\ \theta_3 \\ \theta_4 \\ \theta_5 \\ \theta_6 \end{pmatrix} = \begin{pmatrix} f_1 \\ f_2 \\ f_3 \\ f_4 \\ f_5 \\ f_6 \end{pmatrix} \qquad (5.22)$$

If one of the boundary conditions is that θ_3 equals a known constant C, equation (5.22) can be written to

$$\begin{bmatrix} k_{11} & k_{12} & 0 & k_{14} & k_{15} & k_{16} \\ k_{21} & k_{22} & 0 & k_{24} & k_{25} & k_{26} \\ 0 & 0 & 1 & 0 & 0 & 0 \\ k_{41} & k_{42} & 0 & k_{44} & k_{45} & k_{46} \\ k_{51} & k_{52} & 0 & k_{54} & k_{55} & k_{56} \\ k_{61} & k_{62} & 0 & k_{64} & k_{65} & k_{66} \end{bmatrix} \begin{bmatrix} \theta_1 \\ \theta_2 \\ C \\ \theta_4 \\ \theta_5 \\ \theta_6 \end{bmatrix} = \begin{bmatrix} f_1 - k_{13} C \\ f_2 - k_{23} C \\ C \\ f_4 - k_{43} C \\ f_5 - k_{53} C \\ f_6 - k_{63} C \end{bmatrix} \quad \text{.....(5.23)}$$

and the unknown θ_i can be obtained by solving the above matrix equation.

There must be at least one fixed value (Dirichlet) boundary condition known to solve a matrix of simultaneous equations in a finite element model, otherwise no unique solutions can be obtained.

5.1.4 Flux (Neumann) Boundary Condition

$\int_\varphi N_i B_p d\varphi$ is the amount of substance flowing through the total surface area at a given time. It can be used to describe rubber soaking in liquid, and taking up liquid until saturation. This is also the function representing surface heat loss in heat conduction.

Applying partial differential equations to solve $d\varphi = \sqrt{(dx^2+dy^2)}$ .....(5.24)

$$dx = (\partial x/\partial\beta)d\beta + (\partial x/\partial\eta)d\eta + (\partial x/\partial\zeta)d\zeta \quad \text{.....(5.25)}$$

$$dy = (\partial y/\partial\beta)d\beta + (\partial y/\partial\eta)d\eta + (\partial y/\partial\zeta)d\zeta \quad \text{.....(5.26)}$$

where β, η and ζ are area coordinates, and they are dependent on each other :

$$\beta + \eta + \zeta = 1 \quad \text{.....(5.27)}$$

Since $\zeta=0$ on side 162, $\eta=1-\beta$

$$\partial x/\partial\beta = \partial/\partial\beta\,(N_1x_1 + N_2x_2 + N_3x_3 + N_4x_4 + N_5x_5 + N_6x_6) \quad \text{.....(5.28)}$$

$$= (4^*\beta\text{-}1)x_1 + 4\zeta x_5 + 4\eta x_6$$

$$= (4^*\beta\text{-}1)x_1 + (4\text{-}4\beta)x_6 \quad \text{.....(5.29)}$$

N_1, N_2, ... are shape functions as shown in appendix 2

$$\partial x/\partial\eta = (4^*\eta\text{-}1)x_2 + 4\zeta x_4 + 4\beta x_6$$

$$= (4\text{-}4^*\beta\text{-}1)x_2 + 4\beta x_6$$

$$= (3\text{-}4^*\beta)x_2 + 4\beta x_6 \quad \text{.....(5.30)}$$

$$\partial x/\partial\zeta = (4^*\zeta\text{-}1)x_3 + 4\eta x_4 + 4\beta x_5$$

$$= -x_3 + 4^*\eta x_4 + 4\beta x_5$$

$$= -x_3 + (4\text{-}4^*\beta)x_4 + 4\beta x_5 \quad \text{.....(5.31)}$$

and $(\partial x/\partial\beta)d\beta = [(4^*\beta\text{-}1)x_1 + (4\text{-}4\beta)x_6]\, d\beta$ .....(5.32)

$(\partial x/\partial\eta)d\eta = [(3\text{-}4^*\beta)x_2 + 4\beta x_6]\, \text{-}d\beta$ .....(5.33)

$(\partial x/\partial\zeta)d\zeta = 0$ .....(5.34)

therefore, $dx = [(4^*\beta\text{-}1)x_1 + (4\text{-}4\beta)x_6 - (3\text{-}4^*\beta)x_2 - 4\beta x_6]\, d\beta$

$$= [(-x_1 + 4x_6 - 3x_2) + (4x_1 - 8x_6 + 4x_2)\beta]\, d\beta \quad \text{.....(5.35)}$$

similarly, $dy = [(-y_1 + 4y_6 - 3y_2) + (4y_1 - 8y_6 + 4y_2)\beta]\, d\beta$ .....(5.36)

the Functional term for natural boundary conditions becomes

$$\int_\varphi N_i B_p d\varphi = B_{p1} \int_1^6 N_i d\varphi + B_{p2} \int_6^2 N_i d\varphi$$

$$= B_{p1} \int_0^{0.5} f_i(\beta) d\beta + B_{p2} \int_{0.5}^1 f_i(\beta)\, d\beta \quad \text{.....(5.37)}$$

where $f_i(\beta) = N_i \sqrt{[(-x_1 + 4x_6 - 3x_2) + (4x_1 - 8x_6 + 4x_2)\beta]^2}$

$$+ [(-y_1 + 4y_6 - 3y_2) + (4y_1 - 8y_6 + 4y_2)\beta]^2$$

Consider each boundary in two halves, the new coordinate system z is defined:

$\beta = (z+1)/4$, $d\beta = dz/4$ when $z=-1$, $\beta=0$; $z=1$, $\beta=0.5$

$\beta = (z+3)/4$, $d\beta = dz/4$ when $z=-1$, $\beta=0.5$; $z=1$, $\beta=1$

and using a standard 2-point Gaussian quadrature formula of the form

$$ {}_{-1}\int^{1} f(z)dz = w_1 f(z_1) + w_2 f(z_2) \quad \text{.....(5.38)} $$

where $z_1 = -0.57735,\ z_2 = 0.57735$

$$ \int_{\varphi} N_i B_p d\varphi = 1/4\ B_{p1}[w_1 f_i((z_1+1)/4) + w_2 f_i((z_2+1)/4)] $$
$$ + 1/4\ B_{p2}[w_1 f_i((z_1+3)/4) + w_2 f_i((z_2+3)/4)] \quad \text{.....(5.39)} $$

with

$$ f_i((z+1)/4) = N_i \sqrt{\ [\ (-x_1 + 4x_6 - 3x_2) + (4x_1 - 8x_6 + 4x_2)\ (z+1)/4]^2} $$
$$ + [(-y_1 + 4y_6 - 3y_2) + (4y_1 - 8y_6 + 4y_2)\ (z+1)/4\ ]^2 $$
$$ = N_i \sqrt{\ [\ (-x_1 + 4x_6 - 3x_2 + x_1 - 2x_6 + x_2) + (x_1 - 2x_6 + x_2)z]^2} $$
$$ + [(-y_1 + 4y_6 - 3y_2 + y_1 - 2y_6 + y_2) + (y_1 - 2y_6 + y_2)z]^2 $$
$$ = N_i \sqrt{\ [(2x_6 - 2x_2) + (\ x_1 - 2x_6 + x_2)z]^2} $$
$$ + [(2y_6 - 2y_2) + (y_1 - 2y_6 + y_2)z]^2 \quad \text{.....(5.40)} $$

$$ f_i((z+3)/4) = N_i \sqrt{\ [\ (-x_1 + 4x_6 - 3x_2) + (4x_1 - 8x_6 + 4x_2)\ (z+3)/4\ ]^2} $$
$$ + [(-y_1 + 4y_6 - 3y_2) + (4y_1 - 8y_6 + 4y_2)\ (z+3)/4\ ]^2 $$
$$ = N_i \sqrt{\ [\ (-x_1 + 4x_6 - 3x_2 + 3x_1 - 6x_6 + 3x_2) + (x_1 - 2x_6 + x_2)z]^2} $$
$$ + [(-y_1 + 4y_6 - 3y_2 + 3y_1 - 6y_6 + 3y_2) + (y_1 - 2y_6 + y_2)\ z\ ]^2 $$
$$ = N_i \sqrt{\ [\ (2x_1 - 2x_6) + (x_1 - 2x_6 + x_2)z]^2} $$
$$ + [(2y_1 - 2y_6) + (y_1 - 2y_6 + y_2)\ z\ ]^2 \quad \text{.....(5.41)} $$

The relevant shape functions N_i written in terms of z, for $\beta = (z+1)/4$ are

$N_1 = \beta(2\beta-1) = 1/4(z+1)((z+1/2)-1) = (z+1)(z-1)/8$

$N_2 = (1-\beta)(1-2\beta) = 1/4(4-z-1)(1-(z+1)/2) = (3-z)(1-z)/8$

$N_3 = 0$

$N_4 = 0$

$N_5 = 0$

$N_6 = 4\beta(1-\beta) = 1/4(z+1)(4-z-1) = (z+1)(3-z)/4$

and for $\beta=(z+3)/4$ are :

$N_1 = \beta(2\beta-1) = 1/4(z+3)((z+3/2)-1) = (z+3)(z+1)/8$

$N_2 = (1-\beta)(1-2\beta) = 1/4(4-z-3)(1-(z+3)/2) = (1-z)(-1-z)/8$

$N_3 = 0$

$N_4 = 0$

$N_5 = 0$

$N_6 = 4\beta(1-\beta) = 1/4(z+3)(4-z-3) = (z+3)(1-z)/4$

Input N_i and f(z) into the basic equation (5.39)

$$\int_{\varphi} N_i B_p d\varphi = 1/4\, B_{p1}[w_1 f_i((z_1+1)/4) + w_2 f_i((z_2+1)/4)]$$
$$+ 1/4\, B_{p2}[w_1 f_i((z_1+3)/4) + w_2 f_i((z_2+3)/4)]$$

$$= 1/4\, B_{p1}\{w_1 \begin{bmatrix} (z_1+1)(z_1-1)/8 \\ (3-z_1)(1-z_1)/8 \\ 0 \\ 0 \\ (z_1+1)(3-z_1)/4 \end{bmatrix} \sqrt{[(2x_6-2x_2)+(x_1-2x_6+x_2)z_1]^2 + [(2y_6-2y_2)+(y_1-2y_6+y_2)z_1]^2}$$

$$+ w_2 \begin{bmatrix} (z_2+1)(z_2-1)/8 \\ (3-z_2)(1-z_2)/8 \\ 0 \\ 0 \\ (z_2+1)(3-z_2)/4 \end{bmatrix} \sqrt{[(2x_6-2x_2)+(x_1-2x_6+x_2)z_2]^2 + [(2y_6-2y_2)+(y_1-2y_6+y_2)z_2]^2}\}$$

$$+ 1/4\, B_{p2} \{w_1 \begin{Bmatrix} (z_1+3)(z_1+1)/8 \\ (1-z_1)(-1-z_1)/8 \\ 0 \\ 0 \\ 0 \\ (z_1+3)(1-z_1)/4 \end{Bmatrix} \sqrt{\,[\,(2x_1-2x_6)+(x_1-2x_6+x_2)z_1]^2 + [(2y_1-2y_6)+(y_1-2y_6+y_2)\,z_1\,]^2}$$

$$+ w_2 \begin{Bmatrix} (z_2+3)(z_2+1)/8 \\ (1-z_2)(-1-z_2)/8 \\ 0 \\ 0 \\ 0 \\ (z_2+3)(1-z_2)/4 \end{Bmatrix} \sqrt{\,[\,(2x_1-2x_6)+(x_1-2x_6+x_2)z_2]^2 + [(2y_1-2y_6)+(y_1-2y_6+y_2)\,z_2\,]^2\,\}} \quad \text{.....(5.42)}$$

Axisymmetric problems can be solved with the same method, and the Functional term for natural boundary conditions in equation (5.37) becomes

$$\int_\varphi N_i B_p r d\varphi = B_{p1}\, {}_1\!\int^6 r N_i d\varphi + B_{p2}\, {}_6\!\int^2 r N_i d\varphi$$

$$= B_{p1}\, {}_0\!\int^{0.5} f_i(\beta)\, d\beta + B_{p2}\, {}_{0.5}\!\int^1 f_i(\beta)\, d\beta \text{.....(5.43)}$$

where $f_i(\beta) = N_i \begin{Bmatrix} y_1 \\ y_2 \\ y_3 \\ y_4 \\ y_5 \\ y_6 \end{Bmatrix} \sqrt{\,[\,(-x_1+4x_6-3x_2)+(4x_1-8x_6+4x_2)\beta]^2 + [(-y_1+4y_6-3y_2)+(4y_1-8y_6+4y_2)\beta]^2}$

5.1.5 Convection Boundary Condition

When gases escape from a surface into a closed volume (e.g. evaporation from surface), the mass flow B_p through the surface is not constant, but depends on the surface concentration θ_s and the ambient concentration θ_∞.

$$B_p = h\,(\theta_s - \theta_\infty) \quad \text{.....(5.44)}$$

In rubber seal application, the above equation will be useful in calculation of emission through a narrow extrusion gaps of a certain length with the surface concentration θ_s not known, similar to heat gained or lost on a surface by convection. Derivation of h for emission in free surface will be, however, much more complicated.

the Functional term for convection boundary conditions becomes

$$\begin{aligned}\int_\varphi N_i B_p d\varphi &= \int_\varphi N_i\, h\, \theta_s\, d\varphi - \int_\varphi N_i\, h\, \theta_\infty\, d\varphi \\ &= h\int_\varphi N_i\,[N]\,[\theta]\,d\varphi - h\int_\varphi N_i\,\theta_\infty\,d\varphi \\ &= (h\int_\varphi \{N_i\}^T\{N\}\,d\varphi)\,[\theta] - h\int_\varphi \{N\}^T\theta_\infty\,d\varphi \quad \text{.....(5.45)}\end{aligned}$$

When the two terms are added to the functional F. The extended functional F becomes,

$$\begin{aligned}\partial F/\partial\theta_i = \int_V \{ & D_x{}^* ((\partial N_i/\partial x)^*\theta_i + (\partial N_j/\partial x)^*\theta_j + ...) * \partial N_i/\partial x \\ & + D_y{}^* ((\partial N_i/\partial y)^*\theta_i + (\partial N_j/\partial y)^*\theta_j + ...) * \partial N_i/\partial y) + S_i{}^* N_i\} dV \\ & + h\int_\varphi Ni\,[N]\,[\theta]\,d\varphi + \int_\varphi N_i(B_p - h\,\theta_\infty)\,d\varphi \\ = 0 & \quad \text{.....(5.46)}\end{aligned}$$

Therefore replacing B_p by $(B_p - h\,\theta_\infty)$ in the natural boundary equations (5.37) and (5.43) will include the effect of ambient temperature/concentration.

$$\int_\varphi N_i(B_p - h\theta_\infty)\,d\varphi = (B_{p1} - h_1\theta_\infty)\,{}_0\int^{0.5} f_i(\beta)d\beta + (B_{p2} - h_2\theta_\infty)\,{}_{0.5}\int^{1} f_i(\beta)d\beta$$

$$\text{.....(5.47)}$$

where $f_i(\beta) = N_i \sqrt{[(-x_1 + 4x_6 - 3x_2) + (4x_1 - 8x_6 + 4x_2)\beta]^2}$

$$+ [(-y_1 + 4y_6 - 3y_2) + (4y_1 - 8y_6 + 4y_2)\beta]^2 \text{ for 3-dimensional cases}$$

$$\text{or} \qquad f_i(\beta) = N_i \begin{Bmatrix} y_1 \\ y_2 \\ y_3 \\ y_4 \\ y_5 \\ y_6 \end{Bmatrix} \sqrt{[(-x_1 + 4x_6 - 3x_2) + (4x_1 - 8x_6 + 4x_2)\beta]^2}$$

$$+ [(-y_1 + 4y_6 - 3y_2) + (4y_1 - 8y_6 + 4y_2)\beta]^2$$

for axisymmetric cases.

The surface temperature/concentration dependent term $h \int_\varphi N_i [N] [\theta] d\varphi$ can be calculated as the natural boundary equations

$$h\int_\varphi \{N\}^T\{N\}d\varphi = h_1 \int_1^6 \{N\}^T\{N\}d\varphi + h_2 \int_6^2 \{N\}^T\{N\}d\varphi$$

$$= h_1 \int_0^{0.5} f_i(\beta)d\beta + h_2 \int_{0.5}^1 f_i(\beta)\, d\beta \qquad (5.48)$$

where $f_i(\beta) = \{N\}^T\{N\} \sqrt{[(-x_1 + 4x_6 - 3x_2) + (4x_1 - 8x_6 + 4x_2)\beta]^2}$

$$+ [(-y_1 + 4y_6 - 3y_2) + (4y_1 - 8y_6 + 4y_2)\beta]^2$$

Using the standard 2-point Gaussian Quadrature Integration

$$h\int_\varphi \{N\}^T\{N\}d\varphi = 1/4\, h_1[w_1 f_i((z_1+1)/4) + w_2 f_i((z_2+1)/4)]$$

$$+ 1/4\, h_2[w_1 f_i((z_1+3)/4) + w_2 f_i((z_2+3)/4)] \qquad (5.49)$$

where $z_1 = -0.57735$, $z_2 = 0.57735$

$$f_i((z+1)/4) = \{N\}^T\{N\} \sqrt{[(2x_6 - 2x_2) + (x_1 - 2x_6 + x_2)z]^2}$$

$$+ [(2y_6 - 2y_2) + (y_1 - 2y_6 + y_2)z]^2$$

$$f_i((z+3)/4) = \{N\}^T\{N\} \sqrt{[(2x_1 - 2x_6) + (x_1 - 2x_6 + x_2)z]^2}$$

$$+ [(2y_1 - 2y_6) + (y_1 - 2y_6 + y_2)\, z]^2$$

The equation $h\int_\varphi \{N\}^T\{N\}d\varphi$ is written in full in Appendix 3.

The corresponding axisymmetric equation is

$$h\int_\varphi r\,\{N\}^T\{N\}d\varphi = h_1 \int_1^6 r\{N\}^T\{N\}d\varphi + h_2 \int_6^2 r\{N\}^T\{N\}d\varphi$$

$$= h_1 \int_0^{0.5} f_i(\beta)d\beta + h_2 \int_{0.5}^1 f_i(\beta)\, d\beta \qquad (5.50)$$

$$\text{where} \quad f_i(v) = \{N\}^T\{N\} \begin{Bmatrix} y_1 \\ y_2 \\ y_3 \\ y_4 \\ y_5 \\ y_6 \end{Bmatrix} \sqrt{[(-x_1 + 4x_6 - 3x_2) + (4x_1 - 8x_6 + 4x_2)\beta]^2 + [(-y_1 + 4y_6 - 3y_2) + (4y_1 - 8y_6 + 4y_2)\beta]^2}$$

The complete numerical equation for steady state axisymmetric mass transfer is

$$\partial F/\partial\theta_i = \int_V \{ D_x^* r * ((\partial N_i/\partial x)^*\theta_i + (\partial N_j/\partial x)^*\theta_j + ...) * \partial N_i/\partial x + D_y^* r * ((\partial N_i/\partial y)^*\theta_i + (\partial N_j/\partial y)^*\theta_j + ...) * \partial N_i/\partial y) + S_i * r * N_i\} dA + h\int_\varphi r N_i [N] [\theta] d\varphi + \int_\varphi N_i r(B_p - h\,\theta_\infty) d\varphi = 0 \quad (5.51)$$

where N_i, N_j are the shape functions as shown in appendix 1

$\int_V \{ S_i * r * N_i\} dA$ is the sink term

$h \int_j r N_i [N] [\theta] d\varphi$ is the surface concentration dependent term

$\int_\varphi r N_i B_p d\varphi$ is the fixed flux boundary term

$-\int_\varphi r N_i h \theta_\infty d\varphi$ is the natural boundary term that includes the effect of natural concentration.

Arrange equation (5.51) in the form of $[K]\{\theta\} = \{F\}$

then

$$[K][\theta] = \int_A \{ D_x^* r * ((\partial N_i/\partial x)^*\theta_i + (\partial N_j/\partial x)^*\theta_j + ...) * \partial N_i/\partial x + D_y^* r * ((\partial N_i/\partial y)^*\theta_i + (\partial N_j/\partial y)^*\theta_j + ...) * \partial N_i/\partial y \} dA + h\int_\varphi r N_i [N] [\theta] d\varphi$$

$$[F] = -\int_A \{S_i * r * N_i\} dA - \int_\varphi r N_i (B_p - h\,\theta_\infty) d\varphi$$

5.1.6 Partial Discretization for Time Dependent Analysis

Consider fluid diffusion in the transient state, a time-dependent term representing concentration storage $b(\partial\theta/\partial\tau)$ has to be included in the governing differential equations.

In matrix representation, equation (5.11) $\theta = [N_i, N_j, ...] \{\theta\}^e$

equation (5.12) $\partial\theta/\partial t = [N_i, N_j, ...] \{\partial\theta/\partial\tau\}^e$

the term for axis-symmetric differential equation is

$$F_{add} = \int \{b * r * \partial\theta/\partial\tau * N_i\} dA$$

$$= \int \{b\, r\, [N] \{\partial\theta/\partial\tau\}^e * N_i\} dA$$

$$= \int \{b\, r\, [N] \{\partial\theta/\partial t\}^e [N]^T\} dA$$

$$= (\int b\, r\, [N]^T [N]\, dA) \{\partial\theta/\partial t\}^e \quad \text{.....(5.52)}$$

where the first term is a scalar, and we can write

$$F_{add} = [B] \{\partial\theta/\partial t\}^e \quad \text{.....(5.53)}$$

with $[B] = \int b\, [N]^T [N]\, dV$

Then the transient equation arrived at is

$$[K]\{\theta\} = [B] \{\partial\theta/\partial t\} + \{F\} \quad \text{.....(5.54)}$$

where

$$[K][\theta] = \int_A \{ D_x * r * ((\partial N_i/\partial x)*\theta_i + (\partial N_j/\partial x)*\theta_j + ...) * \partial N_i/\partial x$$

$$+ D_y * r * ((\partial N_i/\partial y)*\theta_i + (\partial N_j/\partial y)*\theta_j + ...) * \partial N_i/\partial y \}\, dA$$

$$+ h \int_\varphi r\, N_i\, [N]\, [\theta]\, d\varphi$$

$$[F] = - \int_A \{S_i * r * N_i\}\, dA - \int_\varphi r N_i (B_p - h\, \theta_\infty)\, d\varphi$$

$$[B] = \int_A \{ N_i * r * b * N_j\}\, dA$$

5.2 Solution to Chemical Reaction

Many types of chemical attack are possible because of the wide variety of chemical species and polymeric substrates. We shall now consider the two simplest types of chemical reactions : the first-order reaction and the second-order reaction.

In both cases, the chemical reaction term can be added to the diffusion equation as a sink term which depends on fluid concentration.

5.2.1 First Order Chemical Reaction

When a first-order reaction occurs with fluid diffusion problem, and the rate of removal of diffusing substance is $k_c * c$, where k_c is a constant, then the governing differential equation becomes

$$\partial c/\partial \tau = \partial/\partial x [D_x (\partial c/\partial x)] + \partial/\partial y [D_y(\partial c/\partial y)] + \partial/\partial z [D_z(\partial c/\partial z)] - k_c * c \quad .....(5.55)$$

The new sink term is

$$= - \int_A \{ r * S_i * N_i \} dA$$

$$= - \int_A \{ r * k_c * [N] [\theta] * N_i \} dA$$

$$= - (\int_A r * k_c * [N]^T [N] dA) [\theta] \quad .....(5.56)$$

Equation (5.54) therefore is redefined as :

$$[K]\{\theta\} = [B] \{\partial\theta/\partial t\} + \{F\} .....(5.57)$$

where

$$[K][\theta] = \int_A \{ D_x * r * ((\partial N_i/\partial x)*\theta_i + (\partial N_j/\partial x)*\theta_j + ...) * \partial N_i/\partial x$$

$$+ D_y * r * ((\partial N_i/\partial y)*\theta_i + (\partial N_j/\partial y)*\theta_j + ...) * \partial N_i/\partial y$$

$$- k_c * r * [N]^T [N] [\theta] \} dA + h \int_\varphi r N_i [N] [\theta] d\varphi$$

$$[F] = - \int_A \{S_i * r * N_i\} dA - \int_\varphi r N_i (B_p - h \theta_\infty) d\varphi$$

$$[B] = \int_A \{ N_i * r * b * N_j\} dA$$

5.2.2 Second Order Chemical Reaction

The chemical reaction term from section 4.2.2, $\Sigma\, k_c\, Y(t-\partial t)\; O(t)$, can be written as :

$$-\int_A \{\, r * S_i * N_i \,\}\, dA$$

$$= -\int_A \{\, r * k_c * Y(t-\partial t) * [N]\,[\theta] * N_i \,\}\, dA$$

$$= -\left(\int_A r * k_c * Y(t-\partial t) * [N]^T\,[N]\, dA\right)[\theta] \quad \text{.....(5.58)}$$

where $[\theta]$ represents fluid concentration O(t)

Equation (5.54) therefore is redefined as :

$$[K]\{\theta\} = [B]\,\{\partial\theta/\partial t\} + \{F\} \quad \text{.....(5.59)}$$

where

$$[K][\theta] = \int_A \{\, D_x * r * ((\partial N_i/\partial x)*\theta_i + (\partial N_j/\partial x)*\theta_j + ...) * \partial N_i/\partial x$$

$$+ D_y * r * ((\partial N_i/\partial y)*\theta_i + (\partial N_j/\partial y)*\theta_j + ...) * \partial N_i/\partial y$$

$$- k_c * r * Y(t-\partial t) * [N]^T\,[N]\,[\theta]\,\}\, dA$$

$$+ h \int_\varphi r\, N_i\, [N]\,[\theta]\, d\varphi$$

$$[F] = -\int_A \{S_i * r * N_i\}\, dA - \int_\varphi r N_i (B_p - h\,\theta_\infty)\, d\varphi$$

$$[B] = \int_A \{\, N_i * r * b * N_j\}\, dA$$

In second order chemical reaction, the potential reaction sites also have to be updated with time. The differential equation (4.30) that governs the using up of the potential reaction sites :

$$\frac{d\,Y(t)}{dt} = -\frac{n_1}{n_2}\, k_c\; Y(t)\; O(t)$$

can also be written in the form of

$$[K]\{\theta\} = [B]\,\{\partial\theta/\partial t\} \quad \text{.....(5.60)}$$

where

$$[K][\theta] = \int_A \{\, -k_c * (n_1 / n_2)* r * O(t) * [N]^T\,[N]\,[\theta]\,\}\, dA$$

$$[B] = \int_A \{\, N_i * r * N_j\}\, dA$$

and $[\theta]$ now represents potential crosslink sites, Y(t)

5.2.3 Chemical reaction change material properties

Material properties in seals are likely to be varying spatially as a result of limited supply of active ingredients for chemical reactions in ageing processes. It is therefore essential that the Seal Life Software has spatially varying material properties.

The elastic modulus of swollen rubber can be calculated from mass uptake using the equation:

$$\text{new modulus} = \left(\frac{100 * \rho_s}{100 * \rho_s + \text{concentration} * \rho_r - 0.5\, \rho_r \rho_s \varphi_r * 100}\right)^{1/3} * \text{old modulus} \quad \text{.....(5.61)}$$

where % concentration = 100 x mass of solvent / mass of rubber,

ρ_s is the density of the solvent,

ρ_r is the density of the rubber,

φ_r is the free volume in the rubber.

5.3 Solution to Time Dependent Equation

5.3.1 Method I : Mid-Difference Method (Trapezoidal Rule)

To solve $\partial\theta/\partial\tau$, assume that in each small interval of time $d\tau$, the values of $\partial\theta/\partial\tau$ vary linearly with time,

$$\{\theta\}_\tau = \{\theta\}_{\tau-d\tau} + (\{\partial\theta/\partial t\}_{\tau-d\tau} + \{\partial\theta/\partial t\}_\tau) * d\tau/ 2$$

$$\text{or } \{\partial\theta/\partial t\}_\tau = - \{\partial\theta/\partial t\}_{\tau- d\tau} + (\{\theta\}_\tau - \{\theta\}_{\tau-d\tau}) * 2/d\tau \quad (5.62)$$

Substituting into the transient equation (5.54)

$$[K]\{\theta\}_\tau = [B] (- \{\partial\theta/\partial\tau\}_{\tau-d\tau} + (\{\theta\}_\tau - \{\theta\}_{\tau-d\tau}) * 2/d\tau) + \{F\}_\tau$$

$$([K] - [B]* 2/d\tau) \{\theta\}_\tau = - [B] (\{\partial\theta/\partial t\}_{\tau-d\tau} + \{\theta\}_{\tau-d\tau} * 2/d\tau) + \{F\}_\tau$$

$$[K'] \{\theta\}_\tau = [B'] _{\tau-d\tau} + \{F\}_\tau \quad (5.63)$$

Thus, $\{\theta\}_\tau$ can be evaluated by solving the system of simultaneous equations provided the values of $\{\theta\}_{\tau-d\tau}$ and $\{\partial\theta/\partial t\}_{\tau-d\tau}$ are known. At the first step only the values of $\{\theta\}_{\tau=0}$ are usually known. The value of $\{\delta\theta/ \delta\tau\}$ at any time including $\tau=0$ can be determined by solving the fundamental transient equation

$$[K] \{\theta\}_\tau = [B] \{\partial\theta/\partial\tau\}_\tau + \{F\}_\tau \quad (5.64)$$

$$- [B] \{\partial\theta/\partial\tau\}_\tau = - [K] \{\theta\}_\tau + \{F\}_\tau \quad (5.65)$$

Therefore, the transient differential equation to be solved becomes

$$([K] - [B]* 2/d\tau) \{\theta\}_\tau = -[K]\{\theta\}_{\tau-d\tau} + \{F\}_\tau - [B] (\{\theta\}_{\tau-d\tau} * 2/d\tau) + \{F\}_\tau$$

$$([K] - [B]* 2/d\tau) \{\theta\}_\tau = - ([K] + [B] * 2/d\tau) \{\theta\}_{\tau-d\tau} + 2*\{F\}_\tau \quad (5.66)$$

The mid-difference method is very popular : (Zienkiewicz 25, 67), (Conner and Brebbia 28) and (Burnett 29). Its accuracy is $0(D\tau^2)$; i.e., its asymptotic rate of convergence is $d\tau^2$. However, for typical time-step sizes the solutions

are frequently characterized by oscillations. Although the oscillations die out as the solution steps forward, it is not suitable for a diffusion model where the results at each step are as important as the steady state results.

5.3.2 Method II : Weighted Method

Considering the transient equation (5.54)

$$[K]\{\theta\} = [B]\{\partial\theta/\partial\tau\} + \{F\}$$

At a location in the time step denoted by a dimensionless parameter ξ (Burnett 29) :

$$[K]\{\theta\}_\xi = [B]\{\partial\theta/\partial\tau\}_\xi + \{F\}_\xi \quad \text{.....(5.67)}$$

where $\xi = (\tau - \tau_{n-1})/ \Delta\tau_n \qquad (\Delta\tau_n=\tau_n-\tau_{n-1})$

Approximate expressions for $\{\theta\}_\xi$, $\{\partial\theta/\partial\tau\}_\xi$, $\{F\}_\xi$ can be obtained by approximating $\{\theta(\tau)\}$ and $\{F(\tau)\}$ by linear polynomials over step.

$$\{\theta\}_\xi = (1-\xi)\{\theta\}_{n-1} + \xi\{\theta\}_n \quad \text{.....(5.68)}$$

$$\{F\}_\xi = (1-\xi)\{F\}_{n-1} + \xi\{F\}_n \quad \text{.....(5.69)}$$

$$\{\partial\theta/\partial\tau\}_\xi = -\{\theta\}_{n-1}/\Delta\tau_n + \{\theta\}_n/\Delta\tau_n = (\{\theta\}_n - \{\theta\}_{n-1})/\Delta\tau_n \quad \text{.....(5.70)}$$

therefore, the transient equation becomes

$$[K](1-\xi)\{\theta\}_{n-1} + [K]\xi\{\theta\}_n = ([B]\{\theta\}_n - [B]\{\theta\}_{n-1})/\Delta\tau_n + (1-\xi)\{F\}_{n-1} + \xi\{F\}_n$$

$$([K]\xi - [B]/\Delta\tau_n)\{\theta\}_n = -([B]/\Delta\tau_n + [K](1-\xi))\{\theta\}_{n-1} + (1-\xi)\{F\}_{n-1} + \xi\{F\}_n \quad \text{.....(5.71)}$$

The above equation can represent three common methods

$\xi = 0$: forward difference method

$\xi = 1/2$: mid-difference method

$\xi = 1$: backward difference method

Forward difference method is explicit, and therefore computationally very fast. However, it is potentially unstable. Very small time steps have to be used to ensure stability. It is found to be impractical for our application. Mid-difference method has been discussed in section 5.3.1. Backward difference method is "well behaved" and reliable, but not always optimal from a computational efficiency standpoint. ξ is therefore chosen to be 0.899 for balancing both reliability and efficiency.

6.0 IMPLEMENTATION OF COMPUTER SOFTWARE

The computer used in software development is Macintosh IIx with 4Mb Ram, 80Mb hard disk, Motorola 68030 microprocessor and Motorola 68882 floating-point coprocessor for performing calculations with high precision, and a colour monitor to display colour graphics.

Software used for development are the operating system version B1-6.0.5, finder version B1-6.1.5, and the Absoft 'Fortran' package "MacFortran/020".

6.1 Software System Structure

The software package 'SEAL-LIFE' comprises a set of three programmes :

I. 'SPECTRE' : the main seal life program .
   Language : standard Fortran 77.
   Function : models fluid diffusion, chemical reaction and change of young modulus.

II. 'SCALE' : the mesh pre-processor.
   Language : standard Fortran 77.
   Function : scales a standardised finite element mesh for O-rings of different size.

III. 'SEALIFE' : the post-processor.
   Language : Fortran 77 plus Macintosh "Tool Box" graphics.
   Function : generates colour-graphics maps and time-plots.

In the next few pages are simple flow charts (Fig 6.1, 6.2, 6.3) showing the structure of each of the three programmes. SPECTRE is the main seal life evaluation program, and details of the equations used have already been included in Chapter 5. SCALE provides simple scale up and down facilities to generate finite element mesh of different size O-ring. A standard mesh is used in the O-ring analysis. SEALIFE allows users to have a diagrammatic view of the results obtained from SPECTRE. This is important as the large amount of digital data cannot be readily understood.

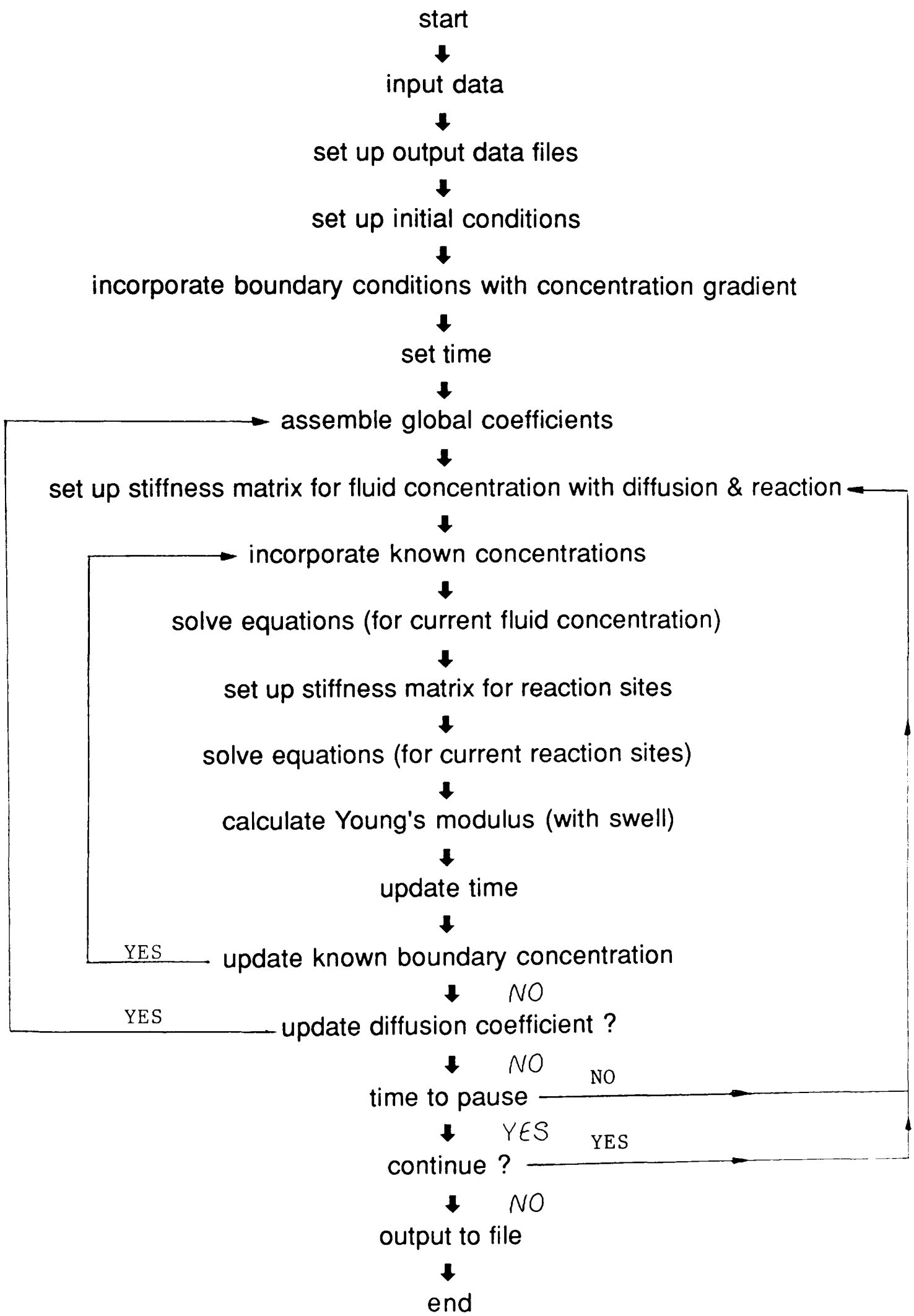

Fig 6.1 Program structure of SPECTRE

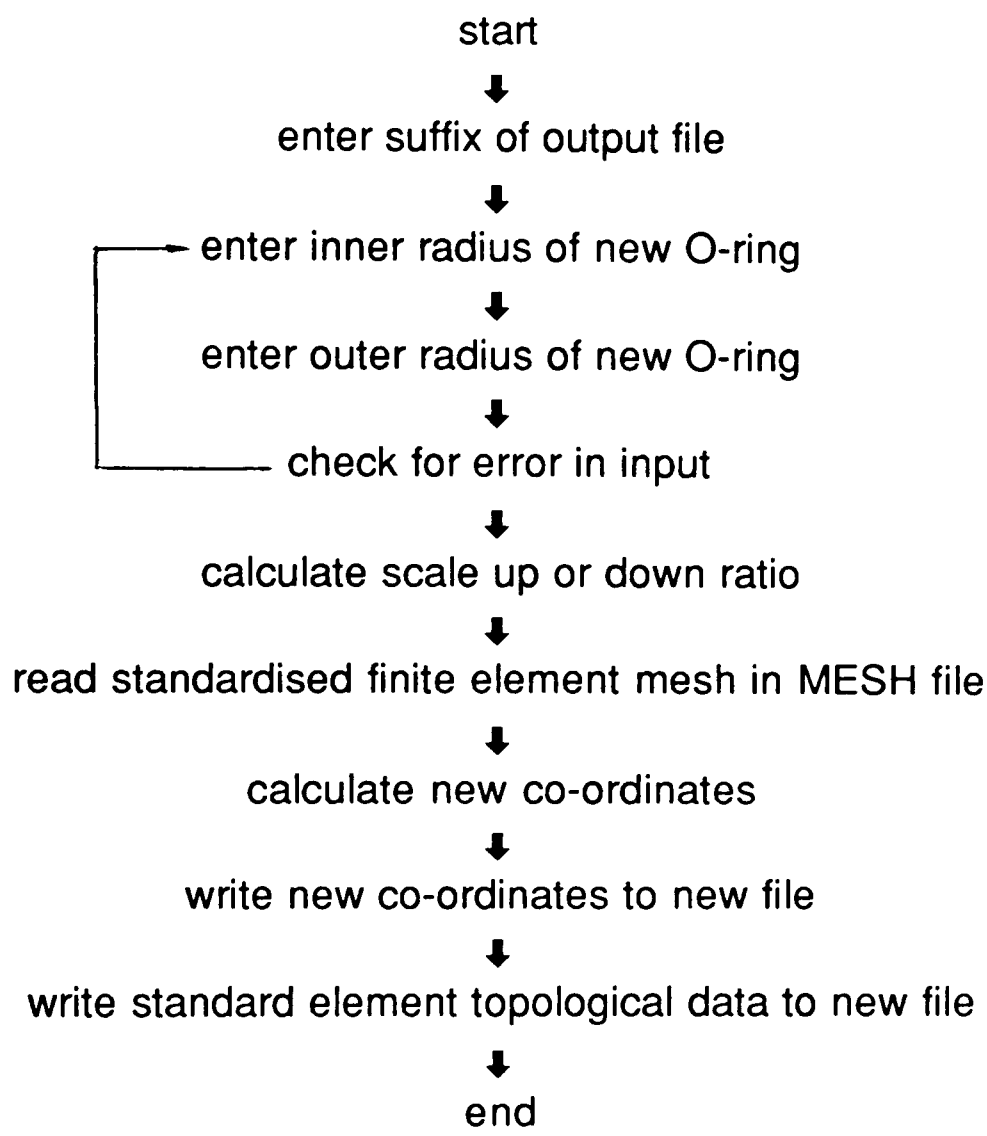

Fig 6.2 Program structure of SCALE

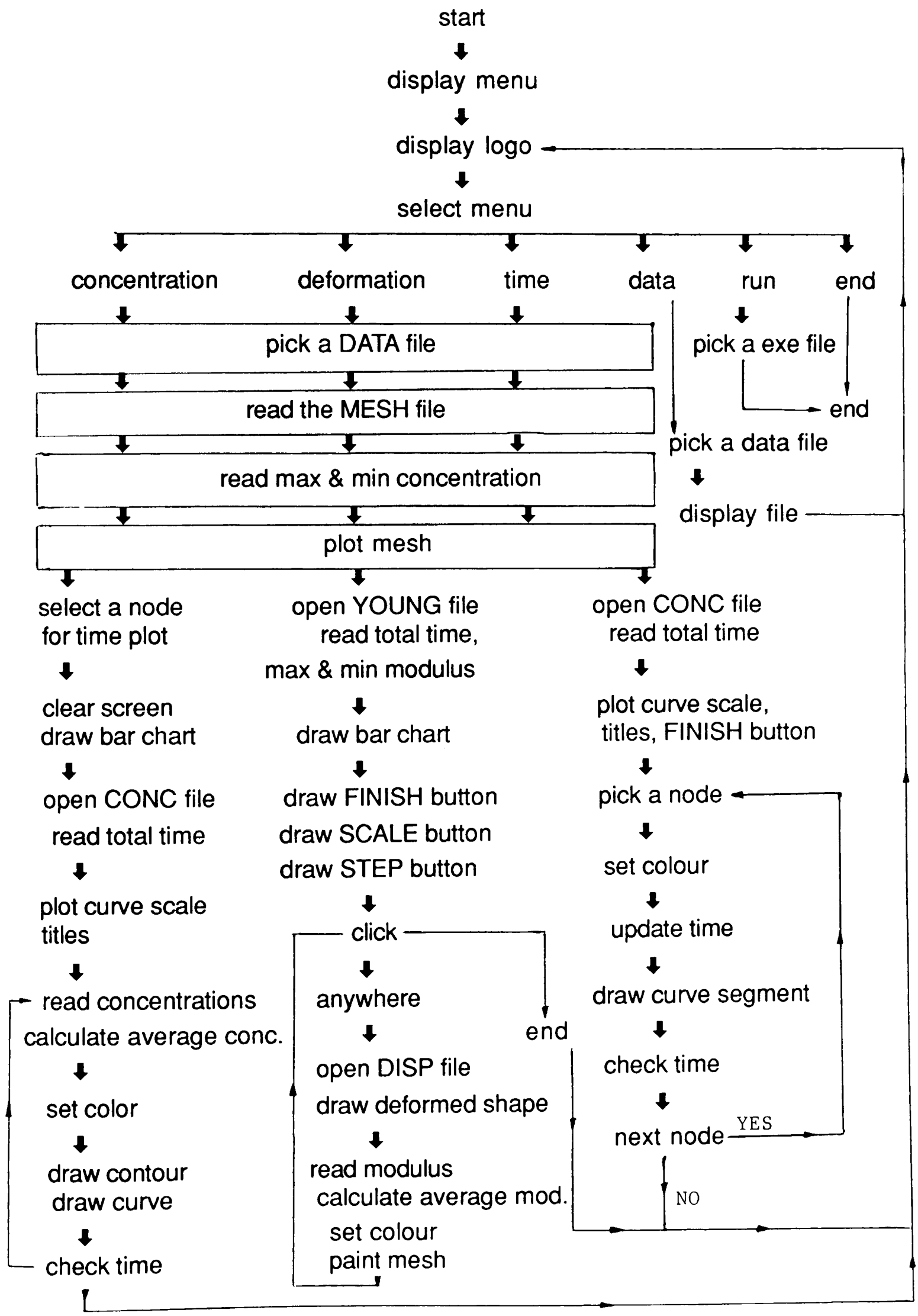

Fig 6.3 Program structure of SEALIFE

6.2 Data Handling

A common set of data files are shared by the three programmes. They are :

program name	input files	output files	graphics display
SPECTRE	MESH.suffix DATA.suffix (START.suffix)	CONC.suffix CLIN.suffix DCOEF.suffix YOUNG.suffix START.suffix	-
SCALE	MESH	MESH.suffix	-
SEALIFE	MESH.suffix DATA.suffix CONC.suffix YOUNG.suffix	-	Yes

The data file 'MESH' is the standard input file to the program 'SCALE' for generating data files with finite element mesh of different size O-rings. 'MESH' is included in the master disk for SEAL-LIFE software.

The suffix of all other data files is run-specific to identify each run or data set. For program 'SPECTRE', the output filenames have the same suffix as the corresponding input data files.

All data files have a standard prefix. The prefix indicates what type of data is being stored in the particular file :

MESH.suffix

this stores the node and element topological data.

DATA.suffix

this stores the following duty-specific information, material information, and run-control data :

a) Duty

- fluid type

- polymer type
- service temperature
- service pressure
- service duration

b) Fluid properties
- initial diffusion coefficient
- initial fluid concentration

c) Polymer properties
- initial Young's Modulus

d) Run control data
- size of time step
- number of time steps between storage of data to files

The data file also includes any combination of the following data sets, a....f, as required :

a) Fixed boundary conditions (Dirichlet)
- fluid concentration at boundary
- number of nodes with saturated concentration (maximum 40 for each fluid concentration), and nodal number
- other known concentrations

A maximum of 10 different fluid concentration sets is allowed.

For each case : concentration, number of nodes, the nodal number.

b) Concentration gradient at boundary (Neumann)
- number of sides with known concentration gradient (maximum 20)
- concentration gradient, nodal number at each end.

c) Swell data
- density of polymers
- density of fluid
- free volume of polymers

d) Thermal data
- thermal expansion coefficient

e) Ageing data

- rate of change in Young's Modulus E with crosslink density
- chemical reaction rate, or constant for reaction rate and activation energy
- table of diffusion coefficient and saturated concentration change (in ratio) with crosslink density

f) Sink

- element number with sink, value of the sink.

CONC.suffix stores fluid concentration distribution with time.

CLIN.suffix

this stores crosslink density distribution with time, for chemical reaction option only.

DCOEF.suffix

this stores diffusion coefficient distribution with time, for varying diffusion property option only.

YOUNG.suffix

this stores Young's Modulus distribution with time, for chemical reaction and swell options.

START.suffix

this stores data at the last time step, for future restart.

6.3 User-Friendliness

Finite Element calculation can generate long lists of data for different locations and for different times. It is most difficult to interpret the data without graphics assistance. The development of the graphics post-processor had to be carried out very early on in the project, so that results obtained from intermediate states can be understood.

6.4 Programme Efficiency

6.4.1 Optimum O-ring Mesh

To fit the curved irregular seal boundary with good accuracy but minimum number of elements, six-noded quadratic triangular elements are used in the finite element modelling. While uniform mesh is most suitable for describing diffusion and chemical reaction, a layer of finer boundary elements is preferred in contact boundary analysis to determine changing boundary. As a result, a standard mesh for O-ring section is selected as shown in Fig 6.4. Nodal numbers in the mesh are also arranged with minimum bandwidth. This will band the system of equations and reduce calculation as will be discussed in the next section.

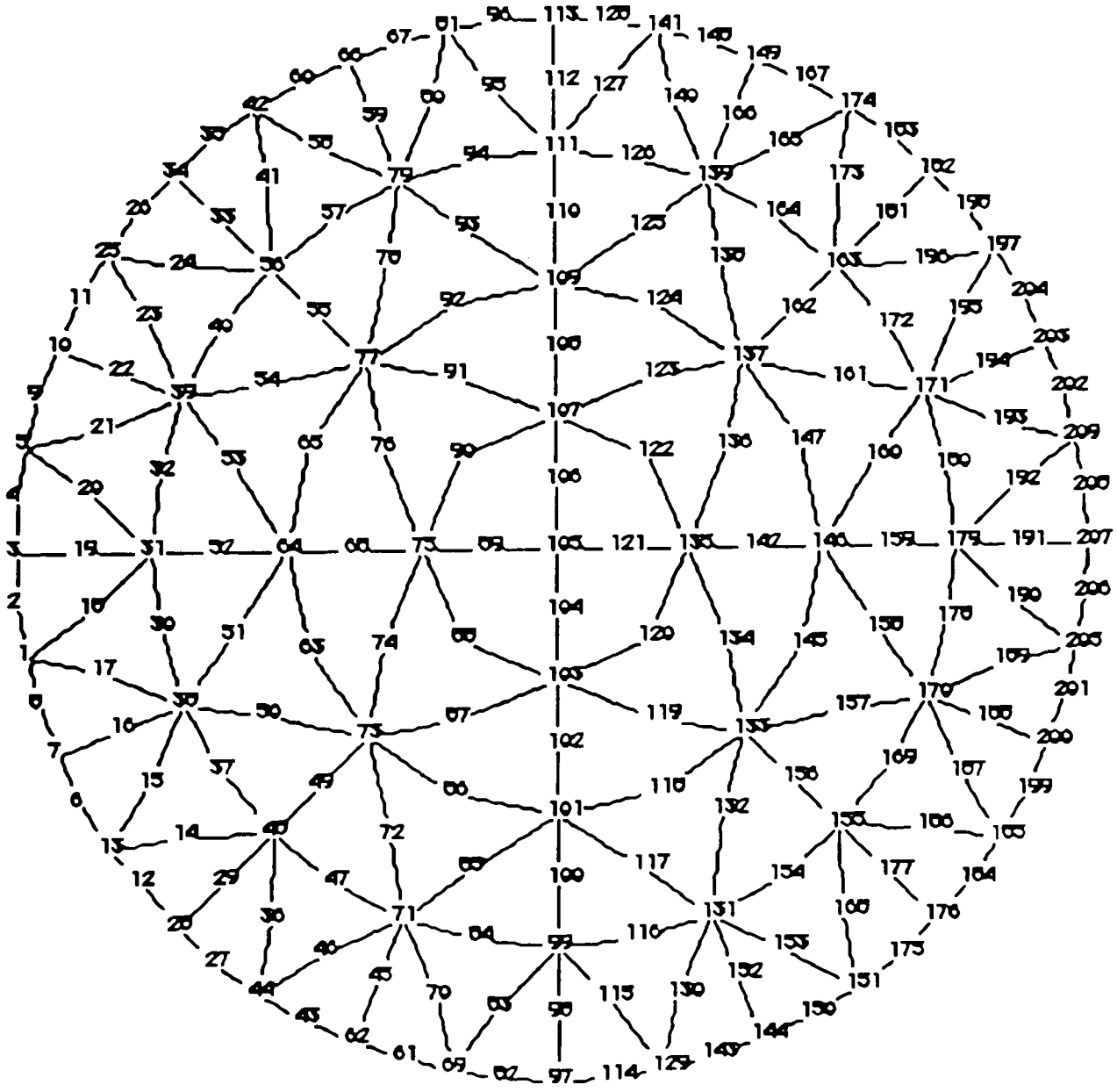

Fig 6.4 Standard finite element mesh for an O-ring

6.4.2 Modified Gaussian Elimination Technique

Finite element method gives rise to a system of linear equations. This system of equations is banded and symmetrical. Modified version of Gaussian Elimination Technique with two stages can be used to solve the equations. The two stages are :

i. Forward Elimination - the matrix is converted into a triangular matrix, with the lower triangle equal to zero
ii. Back Substitution - the upper triangle is reduced to a unity matrix

To eliminate repeat calculation for constant information, global coefficients are stored with time-dependent data added each time-step to permit evaluation of the current stiffness matrix (see flow chart in Fig 6.1). Global coefficients only need to be recalculated when diffusion coefficients change due to chemical reactions.

6.4.3 Varying Time Steps

Fluid diffusion rate changes with time, depending on the concentration gradient. Chemical reaction rate also depends on the amount of available reactant ingredients. As a result, both fluid diffusion and chemical reaction are likely to change more rapidly in the initial stage, but slow down in the longer term. Varying time-steps would be more appropriate to avoid reduce accuracy in the beginning or reduce efficiency in later time steps. In the present computer program, users are asked to input a multiplier for varying the time-steps.

6.5 Programming Stability and Accuracy

As discussed in section 5.3.2, an implicit method to obtain solutions without oscillations must be used for studying time-dependent fluid diffusion in seals. Backward difference method is stable and reliable, and therefore chosen rather than forward difference or mid-difference methods, which may be computationally faster.

There are also checks in the program for instability of concentration, suggesting increase time step intervals if necessary.

6.6 Sizes of the Data Files

Finite element analysis can generate a lot of data in time-dependant analysis when small time steps are used. Incorporated into the Seal-Life Software is the option for users to specify number of time steps between storage of data to files to keep down the sizes of data files. Moreover, only relevant data files will be updated. e.g. the CLIN.suffix file will only be updated when the chemical reaction option has been selected, the DCOEF.suffix file will only be updated when varying diffusion property option has been supplied by the input files.

7. PROGRAM VALIDITY AND APPLICATION

The sealing ability of a elastomeric seal can be indicated by its elastic modulus, compression set and retained force. The Seal-Life Software can model fluid ingress into elastomeric seals and the resulting long term material property changes, caused by volume swell and by chemical reaction between elastomer and the ingressed fluid. Long term prediction of compression set and retained force (stress relaxation) will be handled by a semi-empirical approach in Chapter 8. In the present Chapter, we shall examine the validity of the software for the prediction of concentration distribution and changes in modulus (normally linear compression modulus).

Primary validation of the software has been carried out on a module by module basis. Where possible, well established analytical solutions are used as a basis for comparison. For instance, the thermal analogue of the diffusion equations has been extensively studied in the literature and this provides a valuable basis for validation. Analytical solutions necessarily relate only to the more amenable geometries but when these are successfully reproduced by the diffusion software, this gives confidence in the latter. In addition comparisons have been made with actual experimental measurements for fluid diffusion in elastomers on simple test geometries.

Quantitative validation of the complete system is carried out after confidence has been gained from primary validation. Its main aims is to demonstrate that the proposed computing method can be applied to real service conditions and predict seals performance reliably.

Data for comparison with computed prediction of diffusion behaviour are available from the Seal Life Project, where MERL has generated data for a series of rubber compounds, called benchmark materials, as follows :

#1	EPDM
#2	low ACN NBR
#3	high ACN NBR
#4	HNBR
#5	Hydrin C

#6	Viton E60C
#7	Viton GFLT
#8	VTR 6279
#9	Kalrez
#10	Aflas

All figures for Chapter 7 are presented at the end of the Chapter.

7.1 Diffusion Module Validation

7.1.1 Steady State Thermal Analogue

The finite element diffusion module, including its facilities for various types of boundary conditions, can be tested by comparing computed results with the analytical thermal analogue for simple geometries. Data are widely available for thermal applications. Some tests for rectangular Cartesian coordinate geometries are shown in Fig. 7.1 - 7.3, and for axisymmetric geometries in Fig. 7.4 - 7.6. Curved boundaries tests are shown in Fig. 7.7 - 7.8.

These comparisons were all very satisfactory, computed results being within 1% of the expected values.

7.1.2 Time Dependent Thermal Analogue

Carslaw and Jaeger (68) used the Laplace transformation method to deal with heat conduction problems in simple geometries. Data obtained from the present transient finite element program are compared with Carslaw and Jaeger results as follow:

i. Change of the centre temperature (v) with time for a slab of thickness 2l, with zero initial temperature, and constant surface temperature (V) on both sides.
ii. Change of the centre temperature (v) with time for a sphere of diameter 2l, with zero initial temperature, and constant surface temperature (V).

The mesh used for test i is shown in Fig 7.9, and the comparison is presented in Fig 7.10. The results are in non-dimensional form (t is time, $\kappa = K/\rho c_p$ where κ is the thermal diffusivity, K is the heat conductivity, ρ is the density and c_p is the specific heat). According to Fig 7.10, there is a close agreement between Carslaw and Jaeger's results and the finite element results using a coarse mesh for straight boundaries.

In test ii, three levels of mesh refinement are used in the finite element modelling test. Fig 7.11 clearly shows that fineness of mesh is significant for accuracy with curved boundaries. The three meshes used are included in Fig 7.12 - 7.14.

7.1.3 Gas Permeability Rig Comparison

Sample sheets of polymers were subjected to a permeation test in a permeation rig as shown in Fig 7.15, located at MERL. The sheets had area $0.8cm^2$ exposed to pressurized gas, but their thicknesses varied and were measured carefully for each test. These thicknesses and the test procedures are documented by Campion and Morgan (64).

The permeation laboratory test measured the low pressure P_2 on one side of the sample polymer sheet against time, while the other side of the sheet was subjected to constant high pressure. The gas flow rate dq/dt could then be calculated by the following equation

$$dq/dt = (\partial P_2/\partial t)_V \ (273V_{LP}) / T_{LP} \quad \text{.....(7.1)}$$

where V_{LP} and T_{LP} were volume and ambient temperature of the low pressure reservoir.

Diffusion coefficient D was obtained by Campion and Morgan (64) using the following equation

$$D=h^2/6\tau \quad \text{.....(7.2)}$$

where τ was the time lag, h was the thickness of the polymer sheet

The solubility coefficient s was then calculated from

$(dq/dt)_{steady} = DAs\ (P_1-P_2)/h$ .....(7.3)

where P_1 and P_2 were the high and low pressures,

h was the thickness of the sample

A was the cross sectional area

The steady state values for dq/dt in cm^3/hr were recorded in Campion and Morgan report (64) table 1, while D and s were recorded in table 6. With the measured dimensions (sample thickness and area), and D and s values as input, the computer model can calculate dq/dt against time.

For benchmark material #10 (Aflas) at 2500psi, 100°C, the steady state dq/dt value obtained experimentally was $19.2cm^3/hr$, i.e. $5.333mm^3/s$, while the computed steady state dq/dt value was $5.343mm^3/s$, The difference was therefore about 0.19%. This close agreement was expected as the case was simple one dimensional diffusion.

Furthermore, from equation (7.1) and the computed dq/dt values against time, we could obtain the corresponding P_2 against time. The values were plotted with the experimental value of P_2 in Fig 7.16. The two curves agree very well. This is promising as the input D and s values are from steady state data, but the computed transient data based on this data match the experimental transient readings.

7.1.4 Modelling of Rig Tests

An O-ring in a housing subjected to pressurized gas will take up the shape of the housing as shown in Fig 2.1. The gas dissolves in the surface of the O-ring, and diffuses through the O-ring to the lower concentration side. It eventually soaks the whole O-ring, only a tiny part of the gas escapes through the extrusion gap in the housing.

It is important that the seals are fully saturated before gas decompression takes place, since only saturated seals can represent seals in service which are usually subjected to very long soak times. The computer program has therefore been used in planning the associated rig tests for the study of explosive decompression. The original gas exposure time was extended from 0.5 hour to 96 hours when computed results revealed saturation times could be as long as 61 hours, under the test conditions.

The model used is an undeformed O-ring with equilibrium CO_2 concentration as the mathematical boundary condition over half of its periphery, and zero eflux on the other half as shown in Fig 7.17. The standard mesh shown in Fig 6.4 is used. The O-ring is of 25.4mm outside diameter and 5.33mm section.

Fig 7.18 and 7.19 show computed CO_2 concentration distributions along the central line of the cross-section at half hour, and one hour respectively, for benchmark materials #1, #3, #7, #10 at 100 °C, 2500psi (173 bar). In each case, benchmark #3 (high ACN NBR) O-ring shows the lowest CO_2 concentration throughout its section. Benchmark #1 (EPDM) O-ring is next lowest, while both benchmark #7 (Viton GFLT) and #10 (Aflas) O-rings have a much higher CO_2 concentration, particular at the section close to the pressure boundary. There is also a crossover in CO_2 concentration between #7 (Viton GFLT) and #10 (Aflas) within the O-ring section. This can be explained by the higher diffusion coefficient , but lower equilibrium concentration of benchmark #7 (Viton GFLT) as compared with #10 (Aflas).

According to Fig 7.18 and 7.19, all O-rings are far from equilibrium after an hour soak in CO_2 at 2500psi, 100 °C. When the concentrations at the centre of each O-ring are plotted against time in Fig 7.20, it shows that benchmark #3 (high ACN NBR) take 8 hours to achieve 70 parts of S.T.P. CO_2 for one part of polymer volume, benchmark #1 (EPDM) takes about 2.5 hours, and either benchmark #7 (Viton GFLT) or #10 (Aflas) takes only an hour. The time required for each of the four benchmark O-rings to achieve equilibrium are tabulated in Fig 7.21. Benchmark #7 (Viton GFLT) O-ring is first to reach equilibrium, while benchmark #3 (high ACN NBR) is the last.

The CO_2 concentrations along the central line of benchmark #1 (EPDM) O-rings at 100 °C, with two pressure levels - 2500 psi and 10000 psi after one hour soak are plotted in Fig 7.22. Increasing pressure from 2500 psi to 10000 psi at 100 °C on benchmark #1 (EPDM) O-rings increases slightly the CO_2 concentration across the O-rings.

Fig 7.23 show the concentrations of benchmark #3 (high ACN NBR) O-rings at 2500psi, but two temperature levels - 100 °C and 130 °C respectively. The graphs show that much more CO_2 gas can permeate into the O-rings by increasing the temperature from 100 °C to 130 °C at 2500psi.

7.1.5 Liquid Uptake

Liquid uptake were measured on sheet samples of elastomers by Campion and Morgan (65). These samples were completely immersed in benchmark liquids, and were withdrawn briefly for weighing at certain time intervals, until the equilibrium mass uptake (m_∞) was reached. D_{av}, an "average" or representative D at the point of 50% mass uptake was then evaluated from the equation below:

$$0.5 = (2/h)\ (D_{av}\, t_{av} / \pi\ )^{1/2} \qquad \text{.....(7.4)}$$

$$\text{i.e.} \quad D_{av} = \frac{\pi}{t_{av}} \cdot \left(\frac{h}{4}\right)^2 \qquad \text{.....(7.5)}$$

Validation tests for the computer program use D_{av} and equilibrium mass uptake (m_∞) of benchmark materials #1, #2, #3, #4, #5, #10 soaked in toluene as input to the finite element program. D_{av} is taken as the diffusion coefficient throughout the computed liquid uptake process. The results are shown in Fig 7.24. The computed half periods and the experimental half period t_{av} are tabulated in Fig 7.25 and compared. There is approximately 1% difference between the two sets of values. The difference is acceptable as calculations are performed in time steps. In addition, the actual D can be concentration-dependent.

7.1.6 Modelling of Methanol Uptake in Viton E60C

It is a common practice to introduce methanol into gas well head for a short period of time to dissolve any methane hydrates that have formed, see Pugh and Goodson (69). The methanol treatment may last for 20 minutes to 12 hours. One of the commonly available elastomers in oilfield applications, Viton E60C, has been reported to swell as much as 80% in methanol. This can significantly reduce the strength of Viton E60C seals, and therefore easily damage the seals if any housing movements occur during the methanol soak period.

Using the solubility and diffusion coefficients for methanol uptake at 2500 psi and 23°C from Campion and Morgan (65) table 6, the softening of 5.33mm section Viton E60C O-ring is modelled and shown in Fig 7.26 and Fig 7.27. Fig 7.26 shows that the diffusion of methanol into the O-ring takes a considerable duration. The O-ring is not saturated after 1 month soak. Fig 7.27 shows that with one hour methanol treatment, methanol would have diffused to about 1/8 of the section of the O-ring, and the modulus of the boundary layer has dropped from the original value of 7.56 MPa to approximately 7MPa because of swell. After 14 hours soak, methanol would have diffused to about 1/4 of the section of the O-ring, and the modulus of the boundary layer has dropped to approximately 5MPa. This indicates the O-ring has very much reduced strength at this stage. We therefore predict that housing movements can easily damage the swollen O-ring with 14 hours soak, but not necessarily the O-ring with an hour soak.

7.2 Chemical Reaction Validation

The computer model incorporates the interaction of chemical reaction effects with diffusion. Chemical interactions between fluids and elastomers can be very complex. In the present work it is only possible to introduce a simple 1^{st} or 2^{nd} order model. This is assumed to represent a dominant reaction which might involve crosslink formation or scission, main chain scission etc., depending on the chemical nature of the fluid and elastomer, and the temperature and pressure. The theory based on consumption of diffusing fluid species for chemical reaction with polymer chains. By coupling diffusion with chemical reactions, the distribution of chemically active fluid species could be predicted.

The chemical reaction module was validated against simple chemical analogue and ageing measurements on nitrile rubber supplied by Ministry of Defence.

7.2.1 Simple Chemical Analogue

One test of the validity of the chemical reaction prediction of the model is to make comparison with a simple case having a analytical solution as follows. S.V. Fagg (70) considered a bimolecular reaction in which two substances A and B combine to form new substance C. The rate of formation of molecules of C may be conceived most simply as being proportional to the probability of one molecule of A meeting one molecule of B in suitable conditions. In a constant volume, this probability is proportional to the number of A and B available. The chemical reaction equation is :

$$n_1 A + n_2 B \text{ -------> } C \quad \text{.....(7.6)}$$

let N is number of molecules of new substance C formed

a is initial number of molecules of A

b is initial number of molecules of B

k_c is reaction rate

$$\frac{dN}{dt} = \frac{k_c}{n_1} [a - n_1 N] [b - n_2 N] \quad \text{.....(7.7)}$$

the analytical solution for $n_1 = 1$, $n_2 = 1$, $k_c' = k_c/n_1$ is

$$N = ab \{1 - e^{-(a-b)k_c't}\} / \{ a - be^{-(a-b)k_c't}\} \quad \text{.....(7.8)}$$

Results from the diffusion-reaction software are compared with this analytical solution as shown in Fig 7.28 for two time-step sizes. In general, the diffusion-reaction module agrees well with analytical results, and its performance improves with smaller time-steps. This agreement establishes that the computer model accurately represents the above type of chemical reaction.

7.2.2 Ageing of Nitrile Rubber

This section demonstrates that the chemical reaction model adequately describes the ageing of nitrile rubber in air. This is made possible by the supply of experimental results from Ministry of Defence, Holton Heath. The test pieces were put in an oven for various durations and then taken out for tear strength, modulus, hardness and crosslink density measurements. Material input data required for the computer program were :

i. potential reaction sites at t =0, Y(0)
ii. reaction rate k_c which can be obtained from the following equation

$$k_c = Ae^{(-E_a/RT)} \quad \text{.....(7.9)}$$

From experimental measurement, initial crosslink density [C.L.D.] was,

[C.L.D.] = 5.263 x 10^{-5} g moles crosslinks / g mole rubber vulcanizate

When approaching a fully crosslinked condition, after 272 days in 125°C, the measured crosslink density was :

[C.L.D.] = 89.940 x 10^{-5}

It is therefore assumed that when fully oxidized : **[C.L.D.]** $\approx$**100.0 x 10^{-5}**

and at t=0 : potl. reaction sites **Y(0)** $\approx$ **95.0 x 10^{-5}**

To obtain **chemical reaction rate k_c** at a fixed temperature using equation (4.30), and assuming that when Y(t) is a large number, and supply of oxygen is plentiful, then :

$$\frac{d\,Y(t)}{dt} = -\frac{n_1}{n_2} k_c\, Y(t)\, O(t) \approx \text{constant} \quad \text{.....(7.10)}$$

where O(t) is the concentration of oxygen at time t,

n_1/n_2 is the ratio of oxygen concentration to crosslink sites consumption

and $\ln k_c = \ln A - E_a/RT$ .....(7.11)

In Fig 7.29-7.33, measured crosslink densities are plotted against time, at each temperature to find the reaction rates. These are as follows :

Temperature (K)	reaction rate (cross-link density /day)
343	0.013
358	0.061
373	0.224
398	1.199
423	4.039

A plot ln(slope) against 1/RT (see Fig 7.34) is, linear and yields values for A and Ea. Using these values in equation (7.11), the reaction rate k_c at any temperature is found.

In addition, the measured modulus was plotted against crosslink density, and found to have a linear relationship (Fig 7.35). This was then incorporated into the computer model. Crosslink densities were obtained from Flory-Rehner equation (see equation 3.11 and 4.13) using volume fraction measured from equilibrium toluene swell.

Following through the above procedures, modulus versus time relation were computed for the MoD nitrile compound at several temperatures. The results are shown in Fig 7.36 - 7.40 together with experimental measurement. The agreement is good and demonstrates that the chemical reaction equations, and the modulus versus crosslink density relation, built into the computer program adequately simulate the behaviour of a real nitrile rubber. The deviations appear mainly due to experimental scatter.

7.3 Material Property Changes in Seals

O-rings in real applications will be subjected to both fluid ingress and ageing. The two processes can have adverse effects on material properties. The Seal-Life Software can predict long term material property changes in seals using :

i) results from fluid diffusion tests and tensile ageing tests performed on geometrically simple test pieces,

or

ii) results from fluid diffusion tests performed on geometrically simple test pieces, and data from medium term seal ageing tests.

Examples are included in this section for three different fluids and four different benchmark materials. They are :

EPDM, high ACN NBR	in distilled water
EPDM, high ACN NBR	in air
high ACN NBR, HNBR, Viton E60C	in 10% toluene/90% iso-octane

Other cases will also be briefly discussed in which the use of Seal-Life Software to predict long term material properties change of seals is unnecessary or inappropriate. These include :

Viton E60C, Aflas	in air

7.3.1 Seals in Water

O-ring hardness has been measured in rig tests at BHR group (Appendix 4) after exposure to 100°C, 173 bar water for 168 hour, 336 hour, 720 hour, 1560 hour, 2160 hour and 4320 hour. The hardness of these O-rings are plotted against time in Fig 7.41-7.44. EPDM and Aflas had little hardness change, high ACN NBR had an initial rise and then leveled out, Viton E60C had little change initially, but softened in long term.

a. High ACN NBR O-ring

A best fit curve is drawn through the experimental measurements on high ACN NBR O-rings to characterize material property behaviour during ageing. The most probable cause for the increase of hardness in water is chemical reaction between rubber and oxygen already stored in the rubber, and between rubber and oxygen diffusing into the rubber from the water. Both would be considered in the following :

a.1) Origin of oxygen

Assume oxygen was dissolved into the rubber at 25°C :

the concentration of oxygen dissolved in the rubber , c_O

= solubility coefficient x partial pressure

= 0.054 cm^3 oxygen / cm^3 rubber x 0.21

= <u>0.01134 cm^3 oxygen / cm^3 rubber</u>

It is also possible that oxygen was diffusing into the rubber from the water. Consider ideal gas has volume ratio 2.4465 x 10^{-2} m^3/mol

Assume oxygen was dissolved into water at 25°C :

Oxygen concentration in water

= 2.69 x 10^{-7} mol / g water

= (2.69 x 10^{-7} x 2.4465 x 10^4) cm^3 oxygen / g water

= <u>0.00658 cm^3 oxygen / g water</u>

a.2) Assume hardening was due to the oxygen stored in the rubber only :

Compression Young's Modulus (M) values of O-rings from BHR Group rig tests are deduced from hardness measurement. A chemical reaction rate for the oxygen in the rubber can be calculated from the rate of decay of modulus shown in Fig 7.45, as follows :

$$\frac{dM}{dt} = \frac{(7.8 - 6.9)}{100} = 0.009 \text{ MPa/hr}$$

$$\frac{dM}{dt} = \frac{(8.7 - 6.9)}{200} = 0.009 \text{ MPa/hr}$$

It can be seen that the oxygen level in the rubber is high for the first 200 hours, since the rate of decay is relatively constant for the period.

From equation (4.30) : $$\frac{d M_p}{dt} = - \left(\frac{n_1}{n_2}\right) k_c M_p c \quad \text{..... (7.12)}$$

where M_p is the potential modulus change at time t, M_{max} - M
c is the fluid concentration,
k_c is the chemical reaction rate,
n_1/n_2 is the rate of oxygen consumption to modulus delay

Assume maximum possible modulus change is 100 MPa and using the initial concentration of oxygen (c = 0.01134), we have from equation (7.12) :

$$-0.009 = - (n_1/n_2) k_c [100] [0.01134]$$

$$(n_1/n_2) k_c = 7.937 \times 10^{-3} / \text{hr}$$

From equation (4.27), we can also write : $$\frac{dc}{dt} = - k_c M_p c \quad \text{..... (7.13)}$$

from which $$\int \frac{dc}{c} = -k_c \int M_p \, dt \quad \text{..... (7.14)}$$

$$\ln \left(\frac{c_t}{c_{t=0}}\right) = -k_c M_p t \quad \text{..... (7.15)}$$

From Fig 7.45, 1/3 of modulus change occurs in the first 200 hours indicating about 1/3 of the oxygen has been used up in the period, therefore equation (7.15) gives :

$$\ln (2/3) = - k_c [100] [200]$$

$$k_c = 2.027 \times 10^{-5}/\text{hr}$$

$$= 5.63 \times 10^{-9}/\text{s}$$

and $n_1/n_2 = 390$

The unknown constant k_c and (n_1/n_2) are now both defined.

When the Seal-Life Software is applied using the constants derived above, the calculated modulus changes with time are as shown in Fig 7.45 in dotted lines (experimental results are plotted in solid symbol). The difference between the computed values and the experimental values are under 10% below 1000 hours, and then steadily rise to 20% at 4000 hours. One

possible reason for the increasing discrepancy with time in the above calculation is that additional oxygen becomes available in rubber from that dissolved in water. This would be studied in two different ways as follows.

a.3) Assume oxygen diffused in and out of rubber from/to the water depending on the concentration of oxygen in rubber :

Diffusion coefficient of oxygen in 25°C water = 2.10×10^{-5} cm^2/sec

Diffusion coefficient of oxygen in 25°C high ACN NBR = 0.136×10^{-6} cm^2/sec

Diffusion coefficient of oxygen in 100°C high ACN NBR = 5.517×10^{-6} cm^2/sec

It is therefore assumed that the supply of oxygen from water to the surface of rubber is plentiful when necessary.

no. of mol of oxygen in $1m^3$ of ideal gas at 25°C = 1/0.024465 = 40.875

no. of mol of oxygen in $1m^3$ of water at 25°C = $2.69 \times 10^{-7} \times 10^6$ = 0.269

However, no. of mol of oxygen in fixed volume decrease with temperature, from standard text book, Perry (71a) :

no. of mol of oxygen in $1m^3$ of ideal gas at 100°C = 1/0.03067 = 32.61

no. of mol of oxygen in $1m^3$ of water at 100°C

$\approx$ proportionality constant for Henry's law / molecular weight of solvent

$= (2.996 \times 10^{-6} / 18) \times 10^6$

= 0.166

mol fraction of oxygen in water to in air at 100°C = 0.166 / 32.61 = 0.00509

The equilibrium oxygen concentration of rubber in water, c_{oinw}

= solubility coefficient at 100°C x mol fraction

= 0.0785 x 0.00509 cm^3 oxygen / cm^3 rubber

= 3.996×10^{-4} cm^3 oxygen / cm^3 rubber

This value is much lower than the original oxygen concentration in rubber before ageing.

When the seals were installed (get in contact with water) and then heated up, both seals and water were over-saturated with oxygen. For simplification, it is assumed that oxygen diffusing out of rubber is limited in the short term, in long term oxygen will diffuse from water into rubber when the stored oxygen in rubber is used up. This calculation should provide an upper bound for ageing estimation.

Using varying concentration in the computer model gives the results shown in Fig 7.45. This shows that when the ageing effect of rubber due to oxygen from the diffusing water is added to the original values, the deviation from the experimental values is kept to about 12% even at 4000 hours.

a.4) Assume additional oxygen is supplied to the rubber by the diffusion of water into the rubber :

Consider oxygen being carried by water diffusing into the rubber, oxygen concentration in the rubber is updated with time :

Density of high ACN NBR = 0.98 g/cm^3

Equilibrium mass uptake of water at the tested conditions is 6%

Then the concentration of oxygen in rubber, c_{wo}

= $(2.69 \times 10^{-7} \times 2.4465 \times 10^{4})$ cm^3 oxygen x 0.06 / $(0.98)^{-1}$ cm^3 rubber

= $\underline{3.87 \times 10^{-4}\ cm^3\ oxygen / cm^3\ rubber}$

Diffusion coefficient of water = 8×10^{-8} cm^2/s

The amount of oxygen carried by the diffusing water into the rubber would be less and slower than the amount of oxygen diffusing into the rubber driven by oxygen concentration gradient. This shall therefore not be considered in the computer calculation.

b. High ACN NBR Rectangular Ring

Using the values $k_c = 5.63 \times 10^{-9}$, $n_1/n_2 = 390$, $c_O = 0.01134$, $c_{oinw} = 0.0004$ and $D = 5.52 \times 10^{-6}$ cm^2/sec, we can predict the modulus change of a larger, rectangular seal. Computed results in Fig 7.46 show that modulus change is

slower in the larger seals, as the supply of oxygen from water is reduced by the lower ratio of wetted-surface to volume for the large rectangular seal.

c. EPDM O-ring

Modulus of EPDM O-rings in 100°C water deduced from hardness had a lot of scatter as plotted in Fig 7.47. Two patches of manufactured EPDM O-rings with different material properties, original hardness of 72 IRHD and of 83 IRHD, were used. The change in modulus of EPDM over a long period of time is generally small. The modulus gradually dropped over a long period of time mainly due to the adsorption and diffusion of water into the rubber. This is because of the slow diffusion coefficient, but relatively high saturated concentration of oxygen in EPDM. At the test conditions,

equilibrium mass uptake of water is 9.3 %

diffusion coefficient of water in EPDM = 0.334×10^{-8} cm^2/s

From EPDM pieces tested in MERL, the modulus of EPDM increases significantly in high temperature air, but not in water. The most probable explanation is that chemical reaction between EPDM and oxygen increase hardness of the rubber, but significant amount of oxygen is required for the reaction. The following is to use EPDM test pieces data to define the unknown constant k_c and (n_1/n_2) for the condition. First, the origin of oxygen is considered.

c.1) Origin of oxygen

Assume oxygen was dissolved into the rubber at 25°C :

the concentration of oxygen dissolved in the EPDM rubber

= solubility coefficient x partial pressure

= 0.130 cm^3 oxygen / cm^3 rubber x 0.21

= <u>0.0273cm^3 oxygen / cm^3 rubber</u>

Ideal gas has volume ratio 2.4465×10^{-2} m^3/mol

Assume oxygen was dissolved into water at 25°C, the amount of oxygen in each g of water = 0.00658 cm^3 oxygen / g water

c.2) Assume hardening was due to the oxygen stored in the rubber only :

From EPDM test pieces : Modulus after 1 week = 4.34 MPa

Modulus after 12 week = 5.70 MPa

Increase in modulus = 5.70 - 4.34 = 1.36MPa

Within such time, the original oxygen concentration in EPDM (0.0273 cm^3 oxygen / cm^3 rubber) was used up.

Consider $$\frac{dM_p}{dt} = \frac{n_1}{n_2} \left(\frac{dc}{dt}\right) \quad \text{..... (7.16)}$$

$$dM = (n_1/n_2)\, dc$$

$$1.36 = (n_1/n_2)\,(0.0273)$$

$$n_1/n_2 = 50$$

From equation (7.15) : $$\ln\left(\frac{c_t}{c_{t=0}}\right) = -k_c M_p t$$

assume maximum modulus change (M_p) = 100 MPa,

and 95% original fluid concentration consumed in the first 12 week time :

$$\ln(0.05) = -k_c [100] [12 \times 7 \times 24 \times 3600]$$

$$k_c = 4.13 \times 10^{-9}/s$$

The unknown constant k_c and (n_1/n_2) are now both defined.

The modulus change in EPDM due to chemical reaction and swell is computed using the constants derived above. Results are as shown in Fig 7.47 - EPDM experienced a slight rise in modulus initially when it reacted with the oxygen already stored in the rubber. The modulus gradually dropped over a long period of time mainly due to the adsorption and diffusion of water into the rubber.

c.3) Assume oxygen diffused in and out of rubber from / to the water depending on the concentration of oxygen in rubber :

Diffusion coefficient of oxygen in 25°C water = 2.10×10^{-5} cm^2/sec

Diffusion coefficient of oxygen in 25°C EPDM = 0.146×10^{-5} cm^2/sec

Diffusion coefficient of oxygen in 100°C EPDM = 2.012×10^{-5} cm^2/sec

The supply of oxygen from water to the surface of rubber is limited.

The boundary oxygen concentration of rubber in water, c_{oinw}
= solubility coefficient x mol fraction

= 0.130 x 0.00509 cm^3 oxygen / cm^3 rubber

= 6.617×10^{-4} cm^3 oxygen / cm^3 rubber

This value is much lower than the original oxygen concentration in rubber before ageing.

Both the seals and water were over-saturated with oxygen when ageing started. For simplification, it is assumed that oxygen diffusing out of rubber is limited in the short term, in long term oxygen will diffuse from water into rubber when the stored oxygen in rubber is used up.

From both experimental and computational results shown in Fig 7.47, material property change of EPDM in 100°C water appears to be insignificant.

c.3.) Assume additional oxygen is supplied to the rubber by the diffusion of water into the rubber :

Consider density of EPDM = 1.10 g/cm^3

Then, the concentration of oxygen in rubber

= $(2.69 \times 10^{-7} \times 2.4465 \times 10^{4})$ cm^3 oxygen x 0.093 / $(1.10)^{-1}$ cm^3 rubber

= $\underline{6.68 \times 10^{-4}\ cm^3\ oxygen / cm^3\ rubber}$

The amount of oxygen carried by the diffusing water into the rubber would be much slower than the amount of oxygen diffusing into the rubber driven by oxygen concentration gradient, therefore need not be included in the computer calculation.

c.4). Arrhenius relationship

Water tests are also performed at 173 bar, 70°C and 155°C for 720 hour.

Modulus deduced from hardness measurements are checked on Arrhenius

relation, see Fig 7.48-7.50. It is possible that modulus of Viton E60C follow Arrhenius. Modulus of EPDM has little change with time, and those of high ACN NBR and Aflas are inclusive. 155°C probably is too high a temperature for high ACN NBR, resulting in complete material failure at 155°C. Aflas normally has very slow chemical reaction rate, but high physical relaxation. Therefore, measured Aflas values may be dominated by physical effects.

7.3.2 O-rings in atmospheric air

Tensile tests were performed on test pieces by MERL to characterize the change of modulus with time due to air ageing at 70°C, 100°C, and 155°C at 1 bar, results being shown in Fig 7.51. Chemical reaction rates of EPDM and high ACN NBR can be evaluated to model O-rings in 100°C air.

a. High ACN NBR and EPDM O-rings

a.1) Reaction rate k_c

<u>from High ACN NBR test pieces</u>

Standard fluid diffusion and adsorption properties for common fluids and polymers between 25°C to 60°C are available in polymer handbooks. The information is used to calculate the fluid diffusion and adsorption properties of high ACN NBR in air at 100°C, based on equation 3.6 and 3.7.

the concentration of oxygen in high ACN NBR at 100°C
= 0.0785 x 0.21 cm^3 oxygen / cm^3 rubber
= 0.0165 cm^3 oxygen /cm^3 rubber

From Fig 7.51, $\frac{dM}{dt}$ = 12 / (2000 x 60 x 60)
= 1.667 x 10^{-6} MPa /s

Assuming maximum modulus = 100,
n_1/n_2 value is same as in water = 390

and there is a constant supply of oxygen to keep up the concentration in the rubber piece,

using equation (7.12) : $$\frac{d M_p}{dt} = - \left(\frac{n_1}{n_2}\right) k_c M_p c$$

gives : $$1.667 \times 10^{-6} = - (390)\, k_c\, [100]\, [0.0165]$$

$$k_c = - 2.59 \times 10^{-9}/s$$

<u>from EPDM test pieces</u>

When similar calculation are performed for EPDM in 100°C air,

From Fig 7.51, $\frac{dM}{dt} = 3.5 / (1000 \times 60 \times 60)$

$= 9.722 \times 10^{-7}$ MPa /s

From standard fluid diffusion and solubility coefficient in polymer handbooks, the concentration of oxygen in EPDM at 100°C

$= 0.114 \times 0.21$ cm^3 oxygen / cm^3 rubber

$= 0.0239$ cm^3 oxygen /cm^3 rubber

Using equation (7.12), and assuming :

maximum modulus = 100,

n_1/n_2 value is same as in water = 50

and there is a constant supply of oxygen to keep up the concentration in the rubber piece : $9.722 \times 10^{-7} = - 50\, k_c\, [100]\, [0.0239]$

$$k_c = 9.00 \times 10^{-9}\ /s$$

a.2) Computed predictions on O-rings

With the constant derived above, the Seal-Life Software calculated continuous hardening in ageing EPDM and high ACN NBR O-rings. The evaluated modulus at 100°C, 1 month (720 hour) after tests were compared with modulus deduced from the hardness of O-rings aged in BHR group test rig, as shown in Fig 7.52 and 7.53. In both cases, the quantitative agreements are very good. In particular for high ACN NBR when chemical reaction is fast, ageing in seals is diffusion controlled. The 2mm tensile test

pieces aged very quickly, but ageing in seals would be slower depending on the supply of reactants. The Software has successfully allowed for diffusion.

a.3) Arrhenius relationship

Modulus measured from tensile test samples at 70°C, 100°C and 155°C are plotted against inverse of absolute temperature in Fig 7.54. EPDM seems to follow Arrhenius relationship after 1 week soak, but not after 12 week soak.The equation for EPDM after 1 week soak is :

$$E = 40.4 \exp(-687/T)$$

High ACN NBR appears not to follow Arrhenius relationship after 1 week, or 12 week soak. The tensile test pieces are relatively thin, of 2mm thickness only. They were saturated with test fluids quickly. Fluid concentration across each piece should be fairly uniform. If their material properties do not follow Arrhenius, we have insufficient confidence to predict modulus change in temperatures other than the ones we measured - 70°C, 100°C and 155°C. In section 7.2.2, we have shown that modulus of one type of Nitrile rubber follows Arrhenius satisfactory at 150°C after four day tests. But the high ACN NBR samples appears to have been substantially destroyed in 155°C air after 1 week. This confirms the limitation of using high temperature accelerated tests to predict long term seal life for some materials in certain fluids.

b. Viton E60C and Aflas O-rings

Tensile tests performed on Viton E60C and Aflas in 100°C air have no significant effects on modulus, as shown in Fig 7.55. Therefore, modulus prediction with software is not necessary. This agrees with the little change in hardness for O-rings of the two materials tested in BHR group test rig.

	hardness before test	hardness after test
Viton E60C flange O-ring	79	77.5
Viton E60C spigot O-ring	78	77.5
Aflas flange O-ring	71	71.5
Aflas spigot O-ring	72	71.5

7.3.3 Seals in 10% toluene / 90% iso-octane

Tensile tests were also carried out to characterize the change of modulus with time in 10% toluene/ 90% iso-octane due to ageing at 70°C, 100°C, and 155°C at 1 bar. Measured modulus values had a more complex trend than those from air tests. One main reason is the additional effect of rubber swell in hydrocarbon liquid. Modulus after 1 week and 12 week are plotted against inverse of absolute temperature in Fig 7.56, the graphs do not follow Arrhenius relations, and values after 1 week tests were dominated by swell.

a. High ACN NBR O-ring

Liquid uptakes tests were performed in MERL on high ACN NBR rubber pieces at 70°C and 155°C, at 1 bar and 173 bar to specify diffusion coefficient and equilibrium mass uptake. By extrapolation to 100°C, 1 bar,

mass uptake of high ACN NBR = 7.7%

Diffusion coefficient of high ACN NBR = 28.7×10^{-8} cm^2/s

Average the Young' s modulus values measured from tensile tests in Fig 7.57:

$$\frac{dM}{dt} \approx 0.0023 \text{ MPa / hr} = 6.39 \times 10^{-7} \text{ MPa / s}$$

This is the rate of modulus change caused by chemical reaction only, assuming that the rubber pieces are always saturated with fluid, and therefore modulus do not change with time due to swell after initially short period of time.

Using equation (7.12) :

$$\frac{d M_p}{dt} = - \left(\frac{n_1}{n_2}\right) k_c M_p c$$

Assume maximum possible modulus change is 140 MPa; the supply of iso-octane / toluene for the 2mm thin sheet is plentiful, the equilibrium concentration of iso-octane / toluene is the saturated value (7.7%), we have :

$$\left(\frac{n_1}{n_2}\right) k_c = 6.39 \times 10^{-7} / 140 / 7.7 = 5.93 \times 10^{-10} \quad \ldots\ldots\ldots\ldots\ldots\ldots\ldots\ldots (7.17)$$

a.1) Assume insignificant amount of fluid being used by chemical reaction.

A key factor affecting ageing in O-rings from that in thin tensile test pieces is the time-scale required to attain equilibrium, due to differences in shape and volume. From pure diffusion calculation:

MERL tensile test piece attain 99% saturation in 30 hour
attain 95% saturation in 17 hour

Centre of O-rings tested in BHR group attain 95% saturation in 400 hour
attain 82% saturation in 220 hour

and different parts of the O-ring have different fluid concentration until saturation. Therefore, even if chemical reaction does not used up much ingressed fluid, the modulus change in the O-ring can be significantly different from that of a thin sheet. This case can be studied by the Seal Life Software using a relatively high value for ($n_1/n_2 = 1$) and a low value for k_c (5.93×10^{-10}) which satisfy equation (7.17). Results for this are shown in Fig 7.57. They look reasonably agreeable with experimental O-ring data, considering the sensitivity of modulus change to hardness measurements.

a.2) Assume significant amount of fluid being used by chemical reaction.

When the supply of reactant for chemical reaction is limited by diffusion. The equilibrium fluid concentration in the rubber has to be smaller than the saturated value. The rate of modulus change caused by chemical reaction is slower than that in a thin sheet. From equation (7.12)

$$c_{equilibrium} = \frac{\frac{dM_{pc}}{dt}}{\left(\frac{n_1}{n_2}\right) k_c [140]} \quad \text{..... (7.18)}$$

where $\frac{dM_{pc}}{dt}$ is the rate of modulus change caused by reaction only.

From equation (7.14), $\int \frac{dc}{c} = -k_c \int M_p \, dt$

$$\ln\left(\frac{c_{eq}}{c_0}\right) = -k_c M_p [t_{eq} - t_0] \quad \text{..... (7.19)}$$

where c_{eq} is the equilibrium fluid concentration of the rubber with thick depth,
c_o is the saturated fluid concentration of the rubber,
t_{eq} is the time required for the thick piece of rubber to achieve equilibrium,
t_o is the time required for the thin piece of rubber to achieve equilibrium.

By extrapolation, diffusion coefficient and equilibrium mass uptake of high ACN NBR rubber at 100°C, 173 bar,

mass uptake of high ACN NBR = 6.36%

Diffusion coefficient of high ACN NBR = 9.32×10^{-8} cm^2/s

Consider the Young' s modulus change of BHR Group O-rings from 400 hour to 720 hour soak :

$$\frac{dM}{dt} \approx 1.875 \times 10^{-3} \text{ MPa / hr}$$

Using equation (7.17) and (7.18), $c_{eq} = 6.27$

Putting $c_{eq} = 6.27$ into equation (7.19) :

$$\ln\left(\frac{6.27}{6.36}\right) = -k_c [140] [400 - 0] \quad \text{..... (7.19)}$$

$$k_c = 2.44 \times 10^{-7}$$

and from equation (7.17) : $\frac{n_1}{n_2} = 0.00243$

the Seal-Life Software calculated initial reduction of modulus due to swell, and continuous hardening due to ageing at 173 bar, using the constant derived above. The evaluated modulus at 100°C 1 month (720 hour) and 2 month (1440 hour) after tests were compared with modulus values deduced from the hardness of O-rings tested in BHR group test rig. The results shown in Fig 7.58 does not improve that obtained from the first assumption of insignificant amount of fluid being used up, for this fluid/elastomer combination. The first assumption is justify. This also demonstrates that prediction by Seal Life Software depends on the accuracy of the available experimental data to define material property.

b. HNBR O-ring

Similar work were performed on HNBR rubber at 70°C. The diffusion coefficient and equilibrium mass uptake measured for HNBR at 1 bar are :

mass uptake of HNBR = 11.7%

Diffusion coefficient of HNBR = 28.6×10^{-8} cm^2/s

Average the Young' s modulus values measured from tensile tests in Fig 7.58:

$\frac{dM}{dt} \approx 0.00025$ MPa / hr = 6.94×10^{-8} MPa / s

Assume maximum possible modulus change = 160, and consider equation (7.12) :

$$\left(\frac{n_1}{n_2}\right) k_c = 6.94 \times 10^{-8} / 160 / 11.7 = 3.71 \times 10^{-11} \quad \text{..... (7.20)}$$

By extrapolation of diffusion coefficient and equilibrium mass uptake of HNBR rubber to 70°C, 173 bar,

mass uptake of HNBR = 9.79%

Diffusion coefficient of HNBR = 9.3×10^{-8} cm^2/s

From pure diffusion calculation,

MERL tensile test piece attain 95% saturation in 12 hour

Centre of O-rings testsed in BHR group attain 95% saturation in 440 hour

82% saturation in 220 hour

The change of modulus of HNBR with time is computed assuming insignificant fluid being used up by chemical reaction with a low value for k_c (3.71×10^{-11}), and a high value for $\frac{n_1}{n_2} = 1$

The results obtained is shown in Fig 7.59 and compared with modulus deduced from the hardness of O-rings tested in BHR group test rig. It appears that some significant amount of fluid can be used up by chemical reaction. Initially, the modulus reduction caused by swell is smaller because equilibrium concentration of the rubber is lower than the saturated value. However, chemical hardening will be less than the above 1st approximation

in long term. One more experimental result at soak hour longer than 720 hour is required in this case to define the material behaviour using method shown in section 7.3.3 a.2.

c. Viton E60C O-ring

Calculation is also performed on Viton E60C at 155°C, assuming chemical reaction does not used up much ingressed fluid. The data used for deriving constants for computer input are :

mass uptake of Viton E60C at 155°C, 1 bar = 6.0%

Diffusion coefficient of Viton E60C at 155°C, 1 bar = 217×10^{-8} cm^2/s

mass uptake of Viton E60C at 155°C, 173 bar = 4.93%

Diffusion coefficient of Viton E60C at 155°C, 173 bar = 44.4×10^{-8} cm^2/s

For a 2mm thick piece of rubber,

$$\frac{dM}{dt} \approx \frac{(26.9 - 5.0)\ MPa}{10 \times 7 \times 24\ hr} = 0.0130\ MPa / hr$$

Using equation (7.12) and assume maximum potential modulus change = 100,

$$\left(\frac{n_1}{n_2}\right) k_c = 0.0130 / 3600 / 100 / 6.0 = 6.02 \times 10^{-9} \quad \text{..... (7.21)}$$

The derived constants are :

chemical reaction rate $k_c = 6.02 \times 10^{-9}$

$$\frac{n_1}{n_2} = 1$$

The modulus of unaged Viton E60C O-rings deduced from hardness is much higher than the initial modulus measured from tensile test, as shown in Fig 7.59. For tested O-rings, there was a substantial initial reduction in hardness that cannot be explained by swell only. There is therefore doubt in applying general hardness to modulus relationship to Viton, which has high glass transition temperature. A new graph for specifying hardness to modulus in Viton E60C is drawn in Fig 7.60, using Potts (71b) data measured from

unaged O-rings. No improvement resulted from using this graph.

Viton E60C is normally classified as high duty material for hydrocarbon applications. The material is resistant to hydrocarbon in short or medium term, longer material and O-rings tests are required to establish the reasons for the difference between computed and experimental values.

d. High ACN NBR V-ring

Following the calculation of material properties changes in high ACN NBR O-rings (of approx. 5.333mm section), the available chemical reaction constants $k_c = 5.93 \times 10^{-10}$, $n_1/n_2 = 1$, and diffusion data $c_\infty = 6.36\%$, $D = 9.32 \times 10^{-8}$ cm^2/s were used to predict material behaviour of a larger size (10mm section) V-ring. The difference of material properties with time for two different types of seals are shown in Fig 7.61.

7.4 Conclusions from Computer Validation and Application

The Seal-Life Software contained two parts - the diffusion and the reaction modules. Results from the diffusion module have been validated against exact solutions for thermal diffusion in simple geometries (section 7.1.1 and 7.1.2), gas permeation in a thin sheet (section 7.1.3) and liquid uptake in rectangular slabs (section 7.1.5), the agreement is excellent in all cases. The diffusion module has since then been used to calculate required soak time in planning rig tests for the study of explosive decompression caused by absorbed gas in elastomers (section 7.1.4), and to calculate the reduction in material strength (modulus) of swollen elastomers in liquids (section 7.1.6). These are real applications commonly occurred in designing seals and predicting seal life. The diffusion module has proved to handle these aspects of seal life prediction most capably.

Results from the chemical module have been validated against exact solutions for bimolecular reaction (section 7.2.1), and ageing of nitrile rectangular slabs due to crosslink formation (section 7.2.2). They agree very

well in both cases. This demonstrates the program can describe simple 1st and 2nd order chemical reaction adequately.

When the diffusion and reaction modules are combined to model modulus of high ACN NBR seals in air (section 7.3.2.a), water (section 7.3.1.a) and 10% toluene / 90% iso-octane (section 7.3.3.a), computed values agreed with experimental values closely. High ACN NBR has most severe hardening in air, less in water or 10% toluene / 90% iso-octane. The hardening in water more or less leveled out after 2000 hour soak. In long term, hardening in air or 10% toluene / 90% iso-octane is likely to be more serious than in water.

Computed and experimental modulus for EPDM agree that severe hardening occurred with long term soak in air, while O-rings have little material change in water, possibly some softening in long term due to the uptake of water by EPDM. The computed method can be used to calculate values of HNBR in 10% toluene / 90% iso-octane too.

Viton E60C has no significant modulus change in water or air, but has substantial initial softening in 10% toluene / 90% iso-octane which cannot be completely explained and predicted by the Seal Life Software. In long term, hardening occurred at high temperature (155°C) which can be modelled by the Software. We conclude that the reliability of the results obtained from the Seal Life Software for Viton E60C is only moderate since we have not completely understand the behaviour of Viton E60C in such conditions.

The Seal-Life Software requires characterized material property behaviours as input data to model long term material change in seals of different shapes. These data appear to be least available for fluoroelastomers such as Viton. Therefore, the application of the Software to fluoroelastomers is limited, while the application to other types of elastomers (EPDM, nitrile and HNBR) are very good.

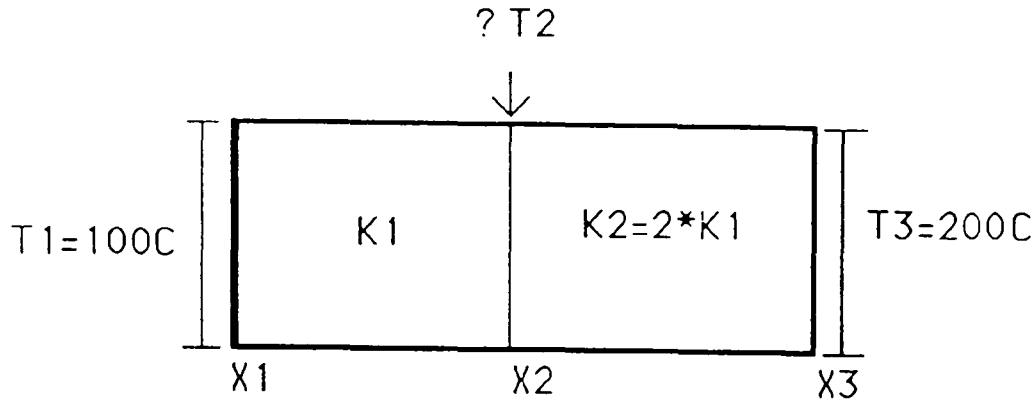

Other boundaries - zero flux

Dimensions: X12 = X1-X2
X23 = X2-X3
X12 = X23 = X13/2

Analytical solution:
T2 = 166.67C

Figure 7.1 Thermal analogue of diffusion for a 2-material plate

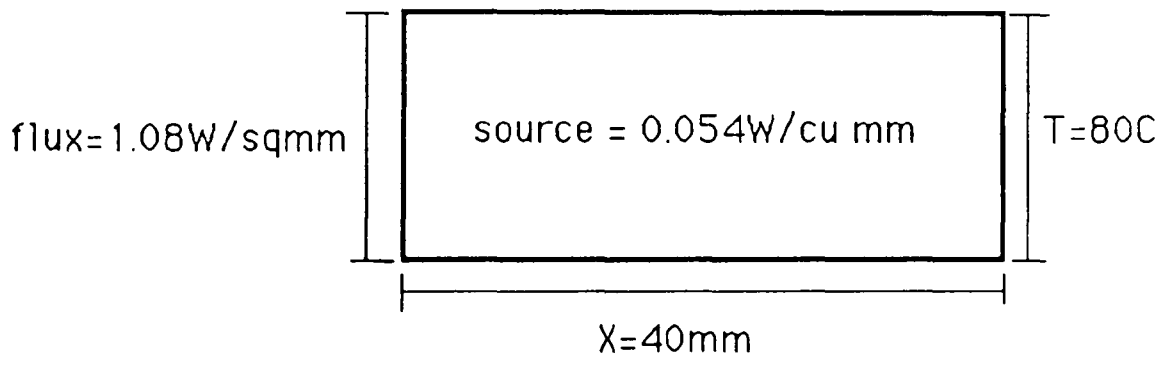

Other boundaries - zero flux
K=0.0054W/mmK

Analytical solutions:
T=1430 C at X=10mm
T=1080 C at X=20mm
T= 630 C at X=30mm

Figure 7.2 Thermal analogue of diffusion for plate with source

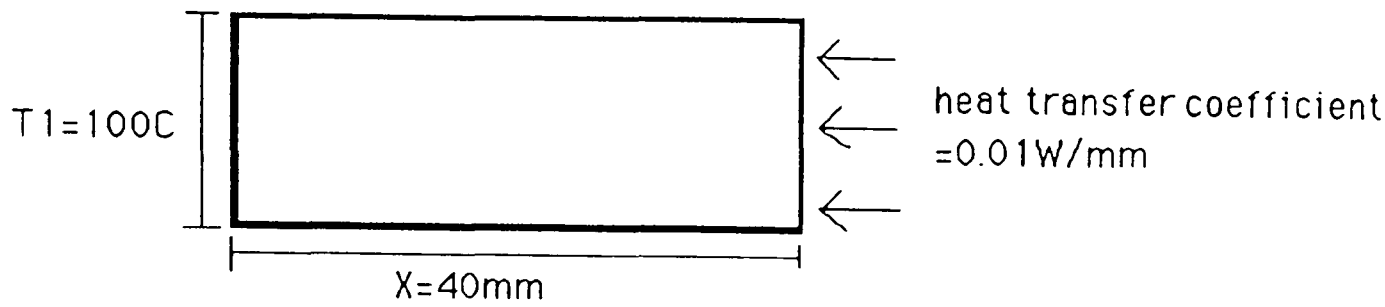

Other boundaries - zero flux
ambient temperature = 20C
K=0.1W/mmK

Analytical solutions:
T=180C at X=40mm
T=140C at X=20mm
T=120C at x=10mm

Figure 7.3 Thermal analogue of diffusion for plate with heat transfer boundary condition

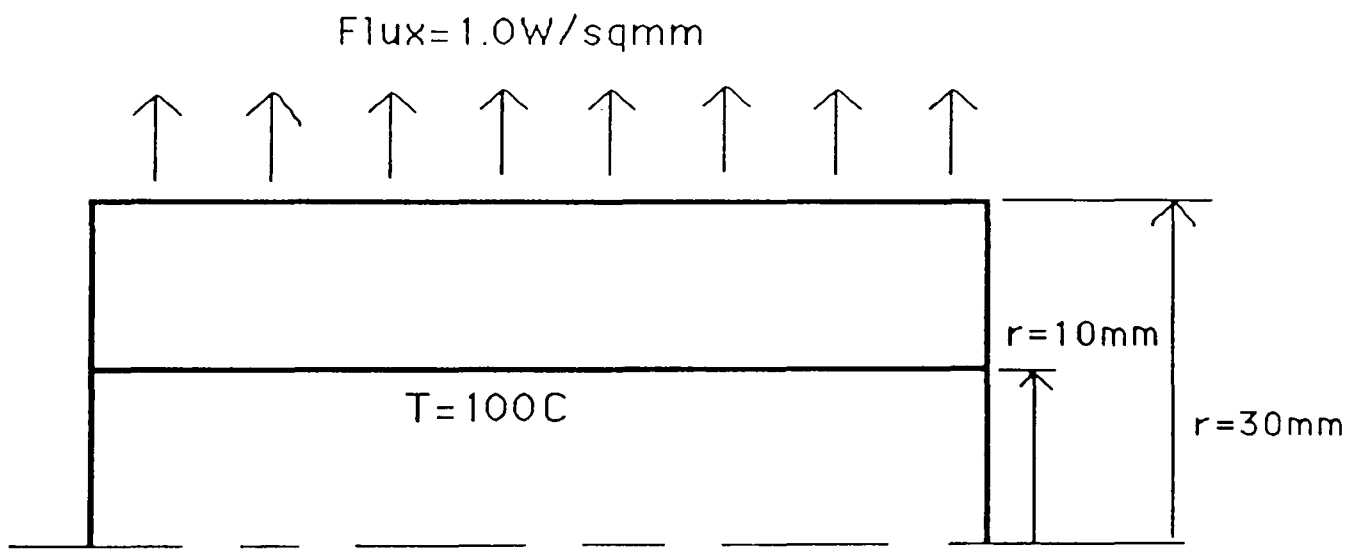

K=0.1W/mmK
Other boundaries - zero flux

Analytical solutions:
T=-229.6C at r=30mm
T=-108.0C at r=20mm

Figure 7.4 Axisymmetric thermal analogue of diffuison for a cylinder with fixed flux boundary

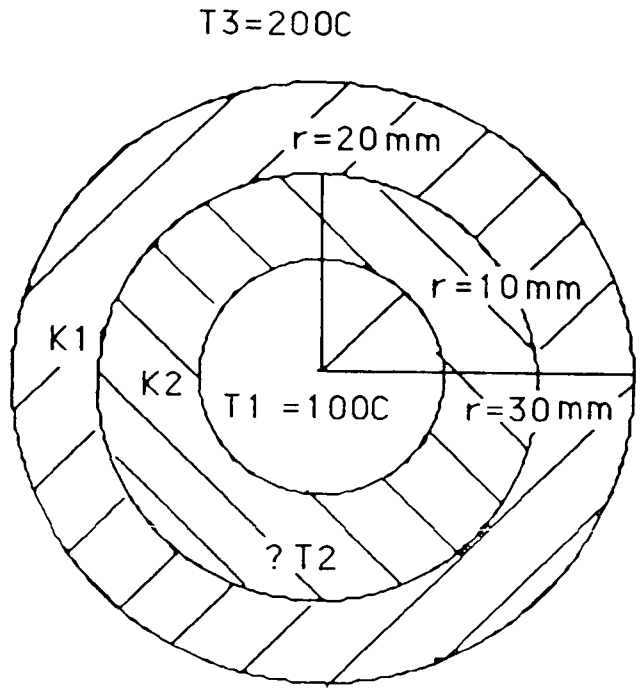

K1 = 0.1W/mmK, K2 = 0.2W/mmK

Analytical solution:
T2 = 177.37C at r = 20mm

Figure 7.5 Axisymmetric thermal analogue of diffusion for a 2-material cylinder

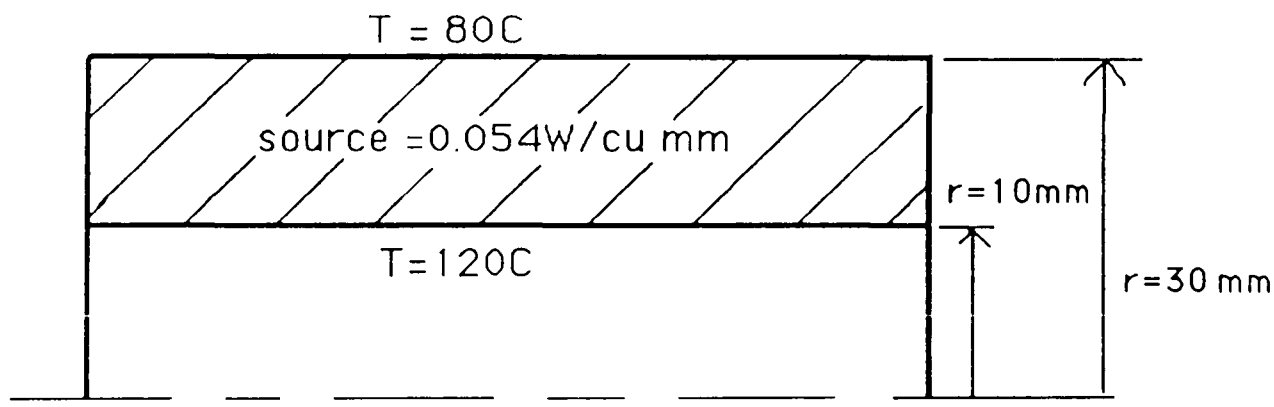

K=0.054 W/mmK
Other boundaries -zero flux

Analytical solutions:
T = 145.9C at r=20mm
Max Temp = 149.9C at r=17.06mm

Figure 7.6 Axisymmetric thermal analogue of diffusion for a cylinder with a source

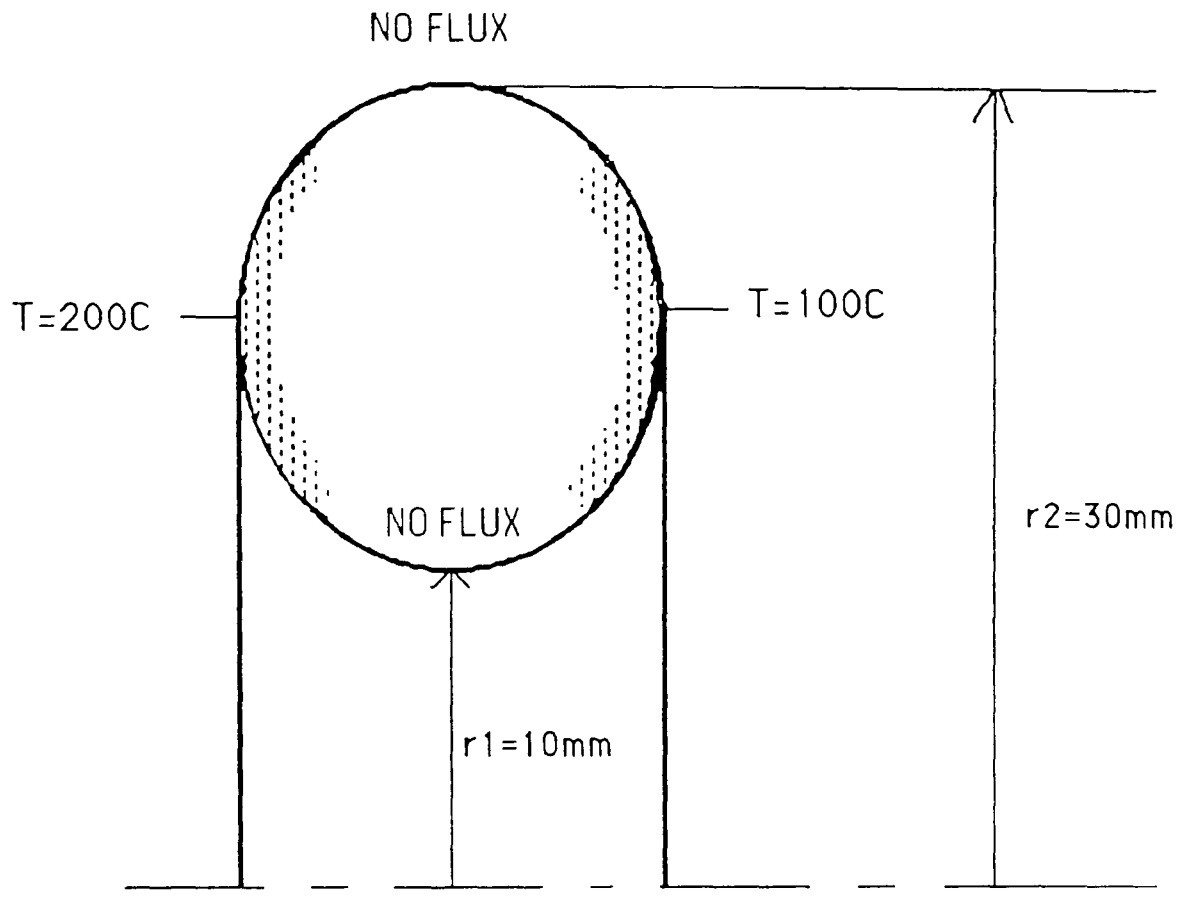

K=0.1W/mmK

Temp at centre = 150C

Analytical solutions:

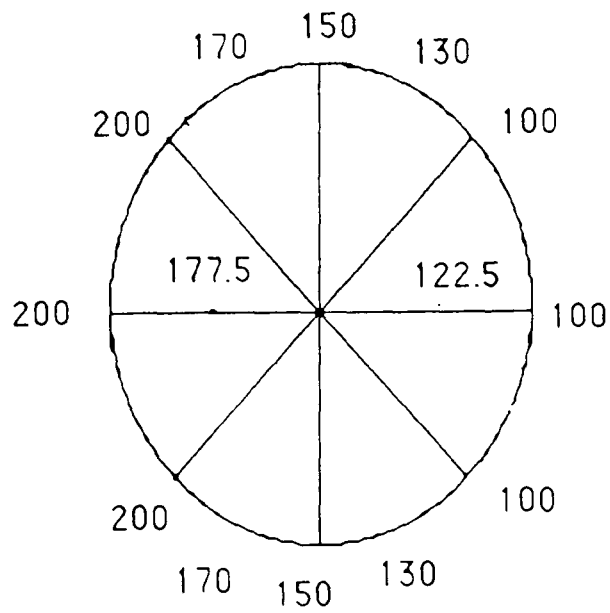

Figure 7.7 Diffusion model of O-ring with flux boundary conditions: axial flow

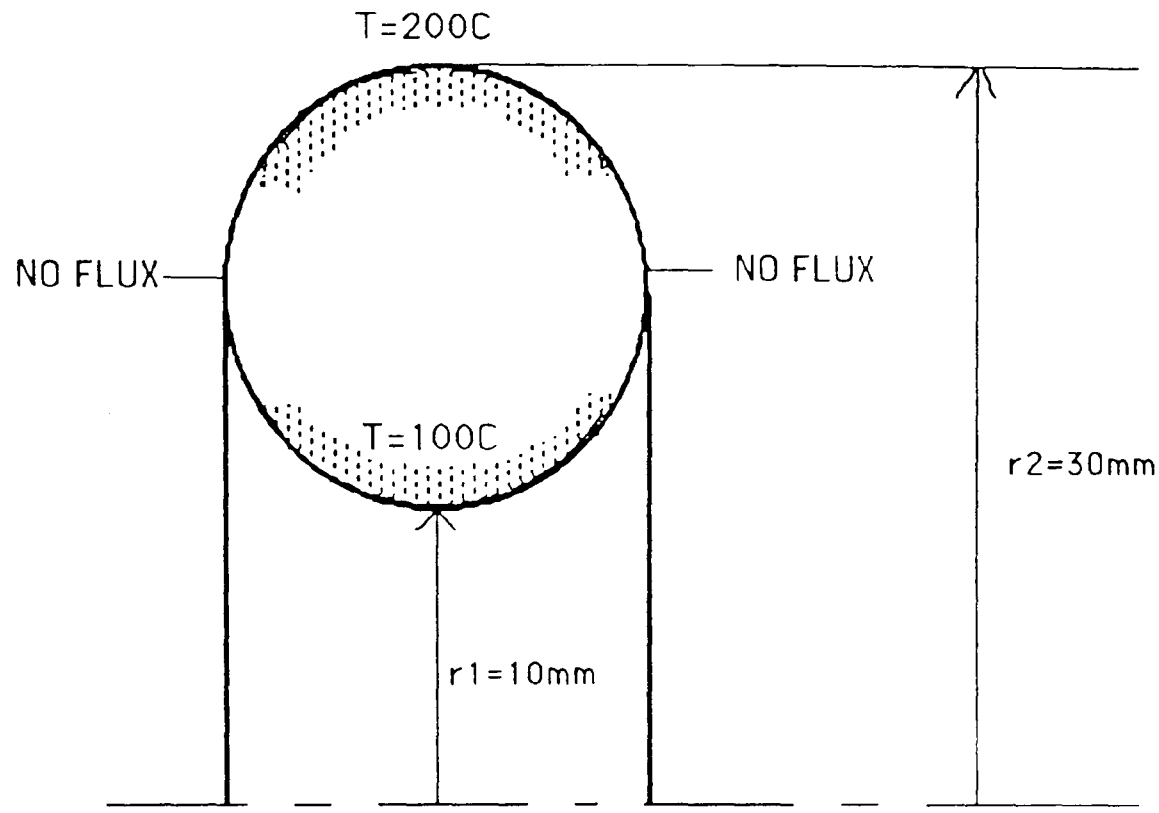

K=0.1W/mmK

Analytical solution:
Temp at centre = 150C

Figure 7.8 Diffusion model of O-ring with flux boundary conditions : radial flow

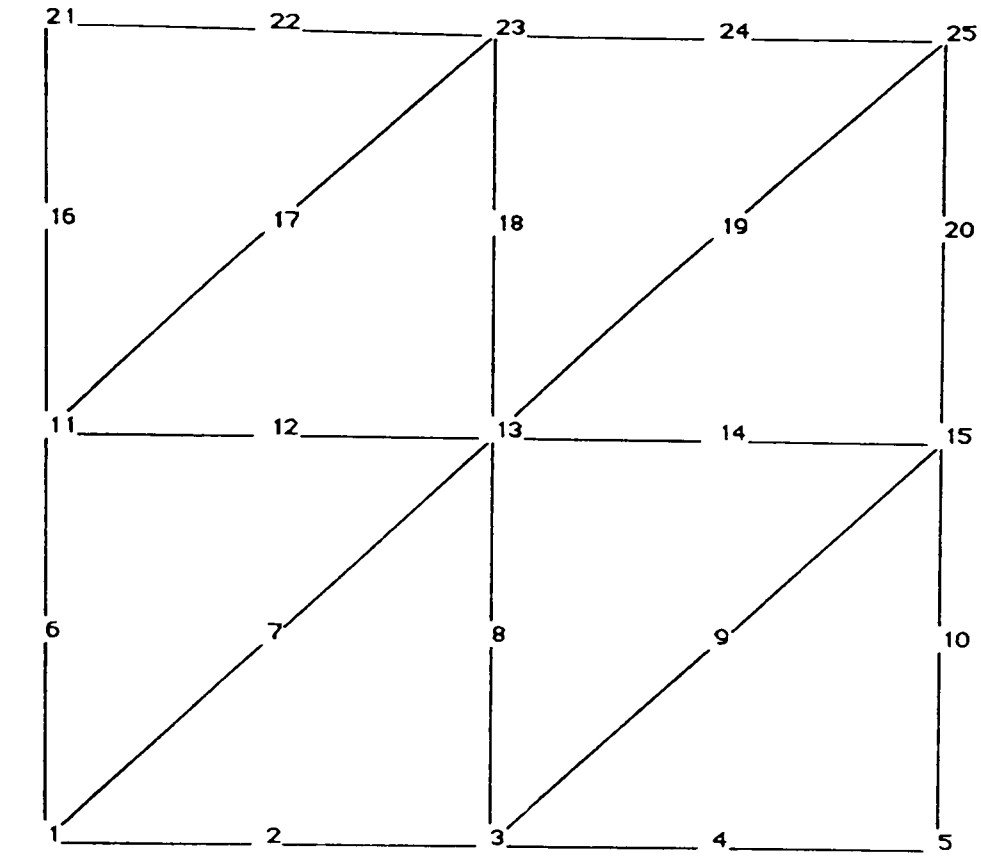

Figure 7.9 Mesh of the slab

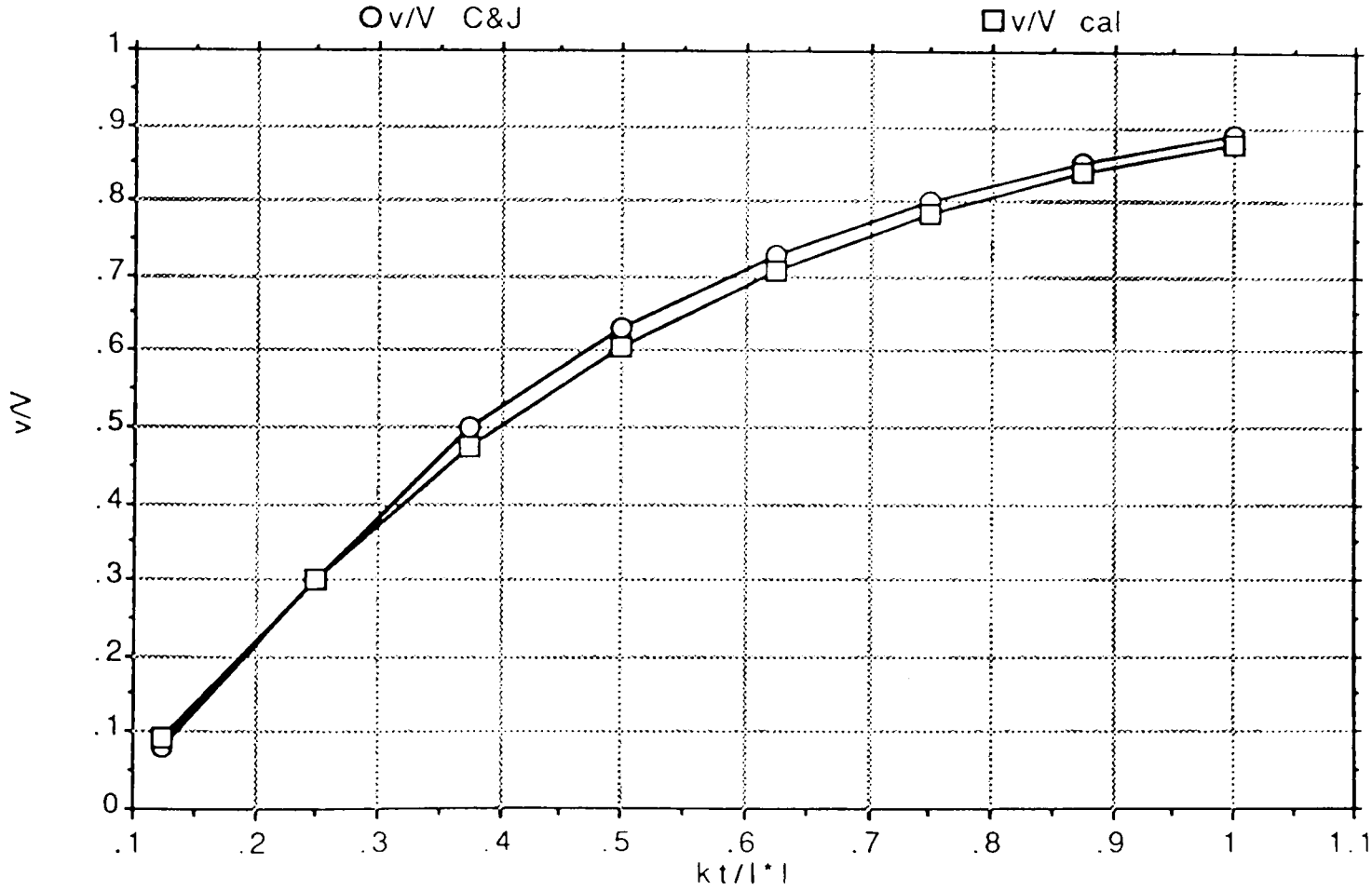

Figure 7.10 Transient thermal analogue : comparison of analytical (C&J) and computed values (cal) at centre of a slab

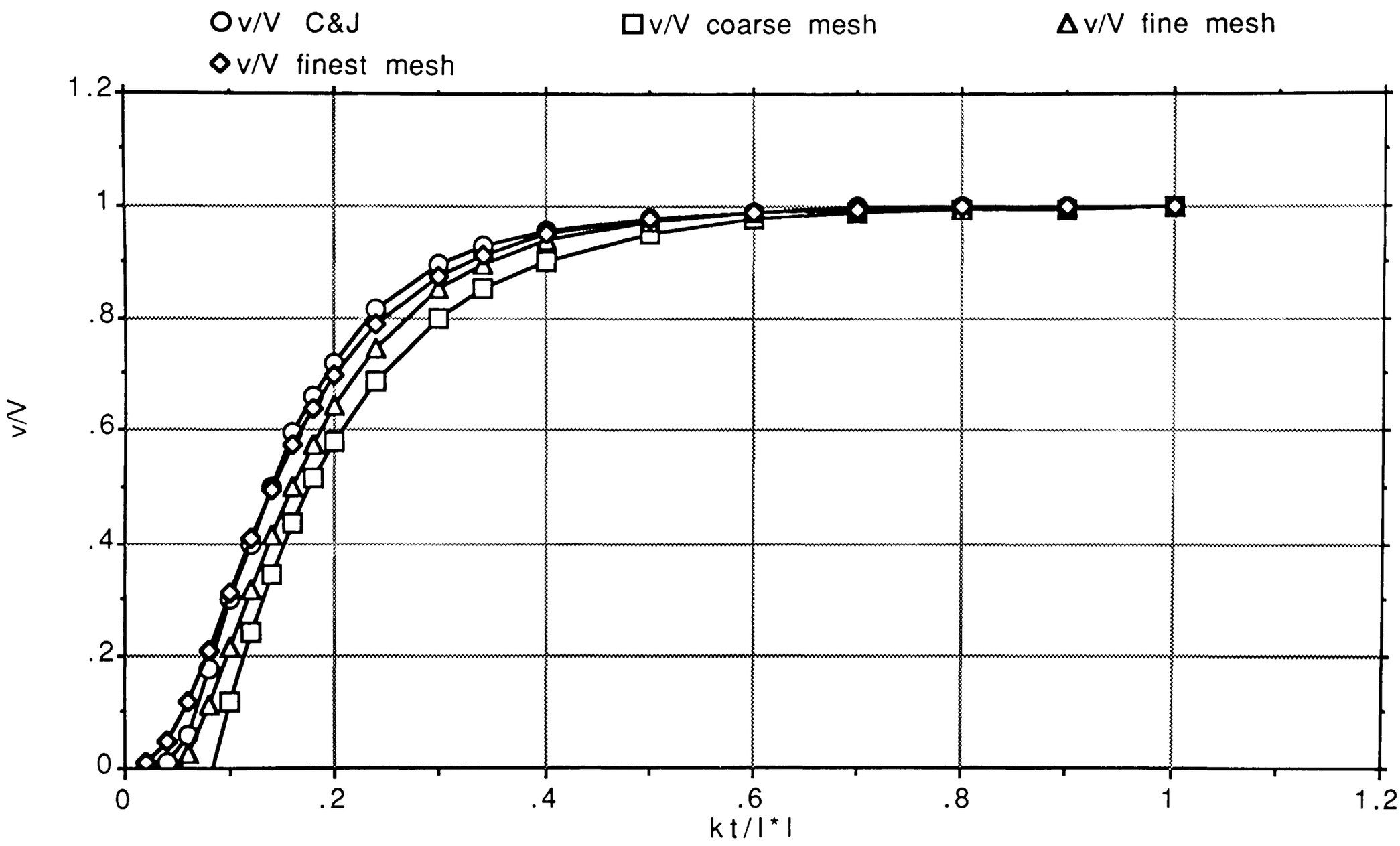

Fig 7.11 Transient thermal analogue : comparison of analytical (C&J) and computed values, 3 mesh sizes, at centre of a sphere

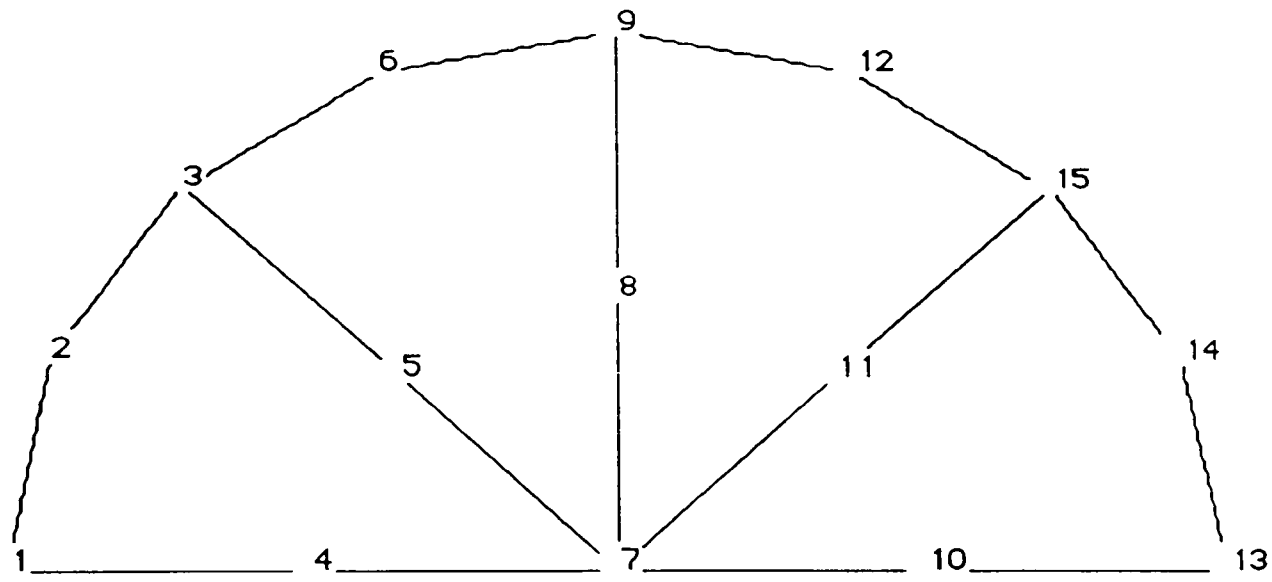

Figure 7.12 Mesh for sphere analogue (Figure 7.11) : coarse

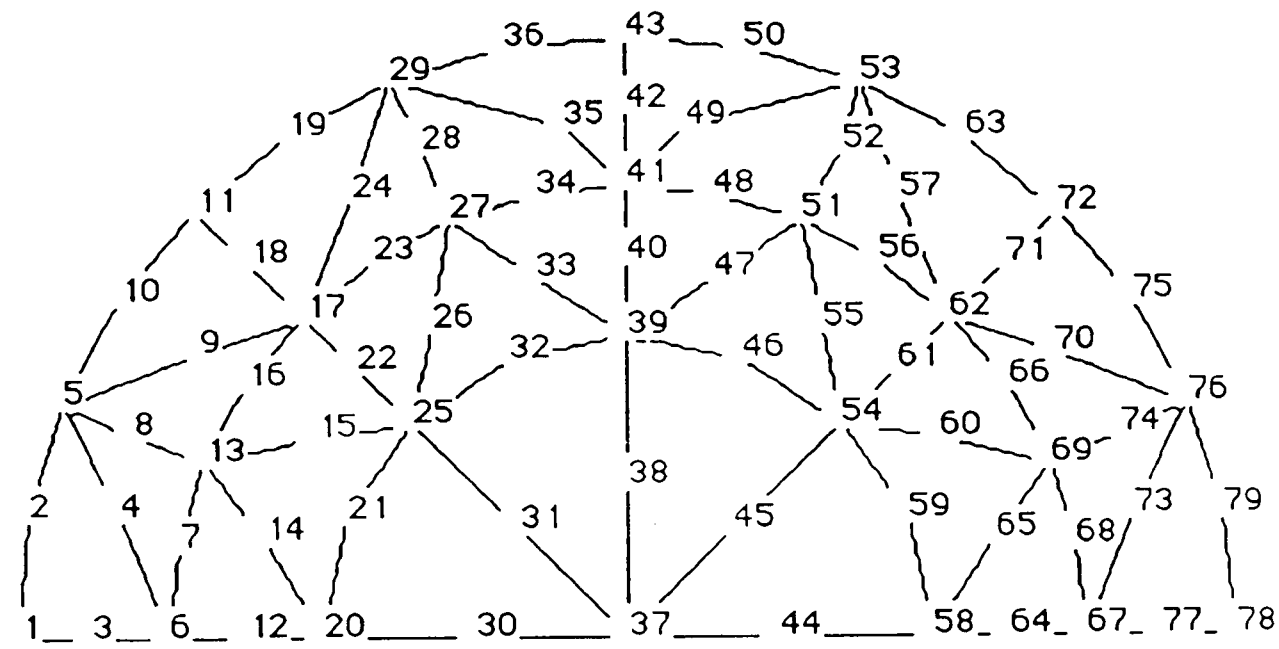

Figure 7.13 Mesh for sphere analogue (Figure 7.11) : medium

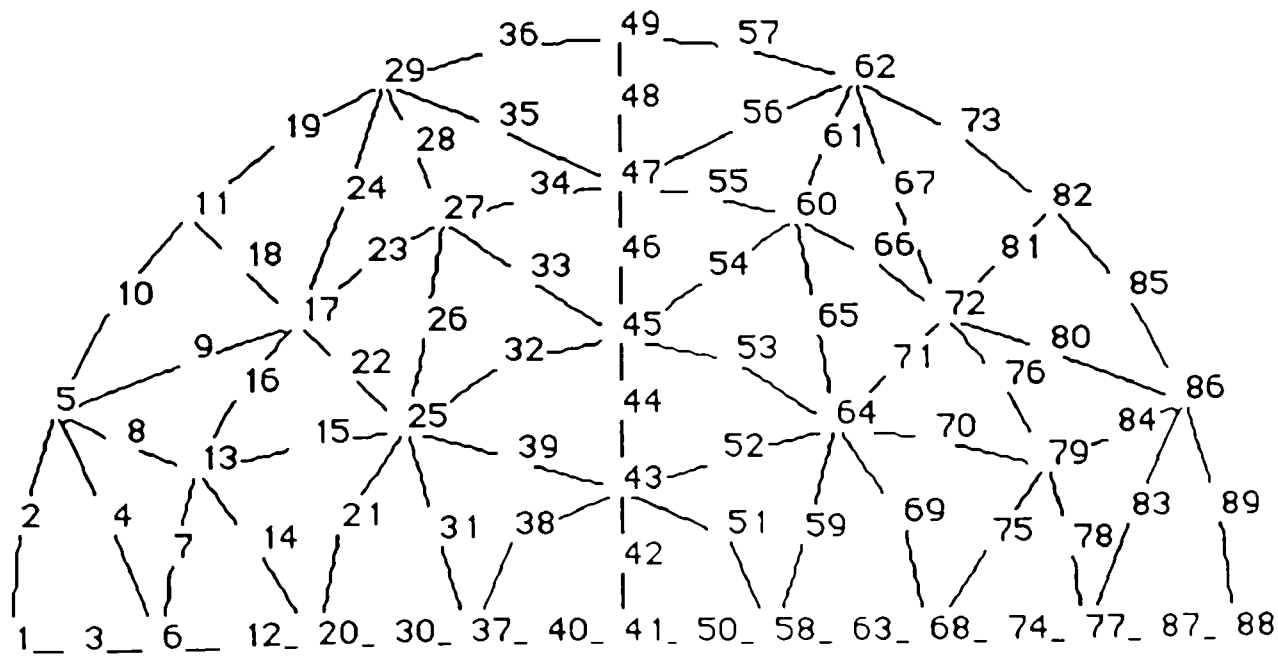

Figure 7.14 Mesh for sphere analogue (Figure 7.11) : fine

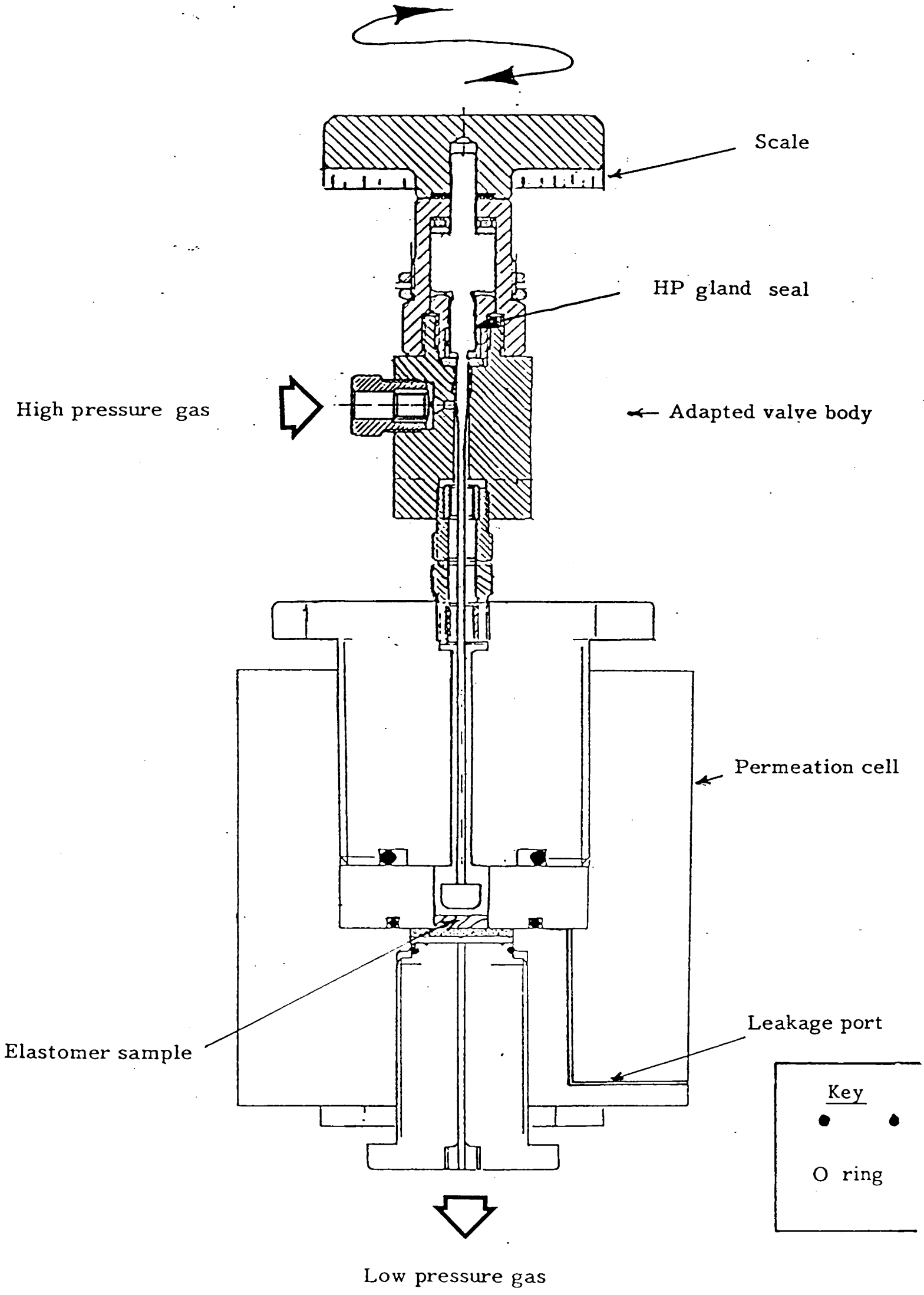

Figure 7.15 MERL gas permeation test rig

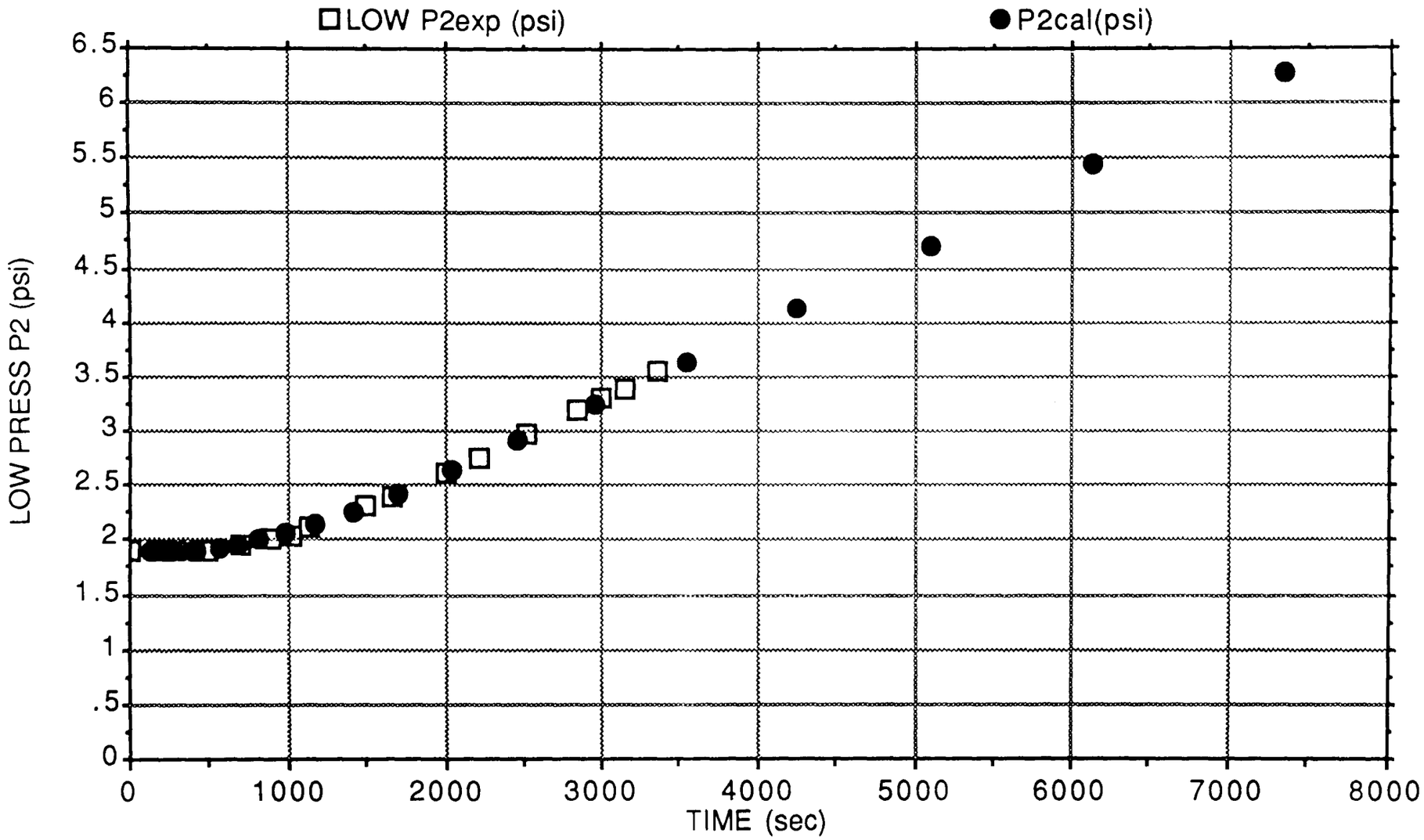

Figure 7.16 Gas Permeation Test : comparison of measured (exp) and computed (cal) results

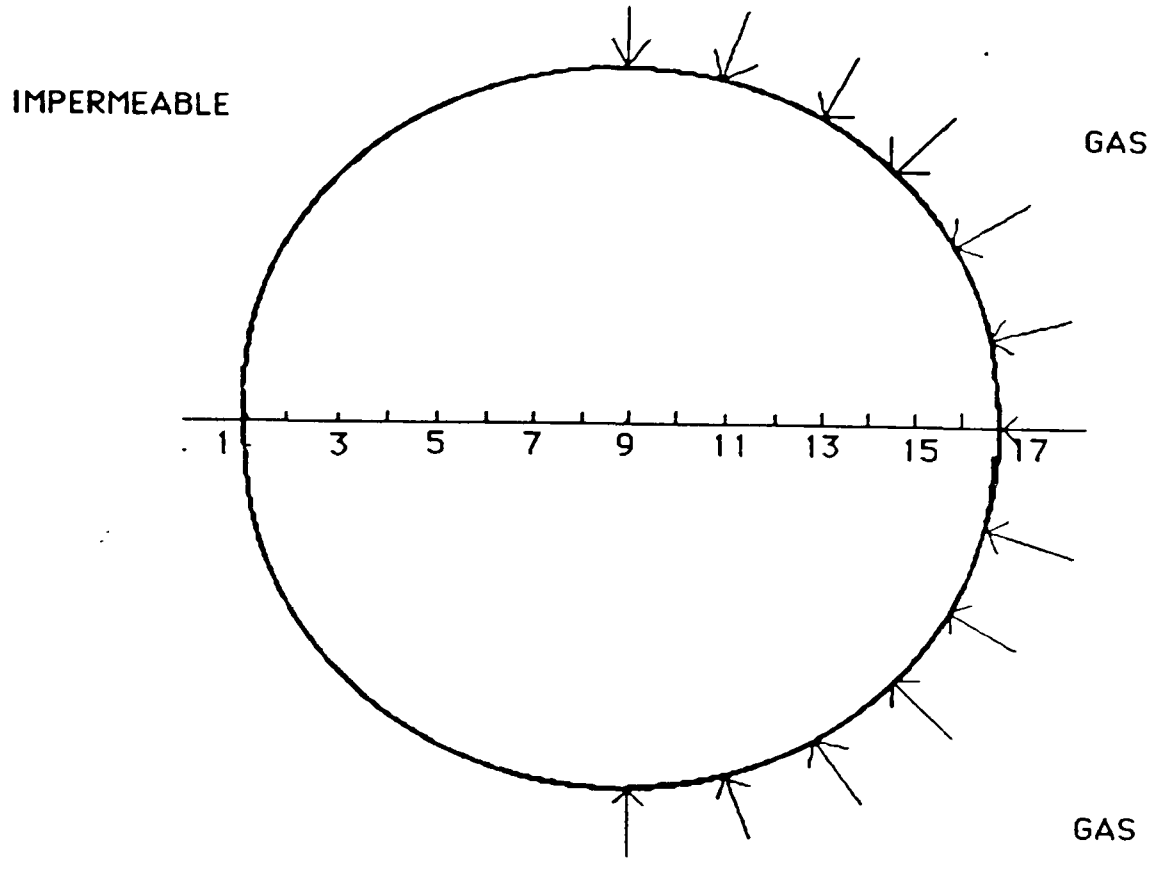

Figure 7.17 Model for diffusion of gas into an undeformed O-ring

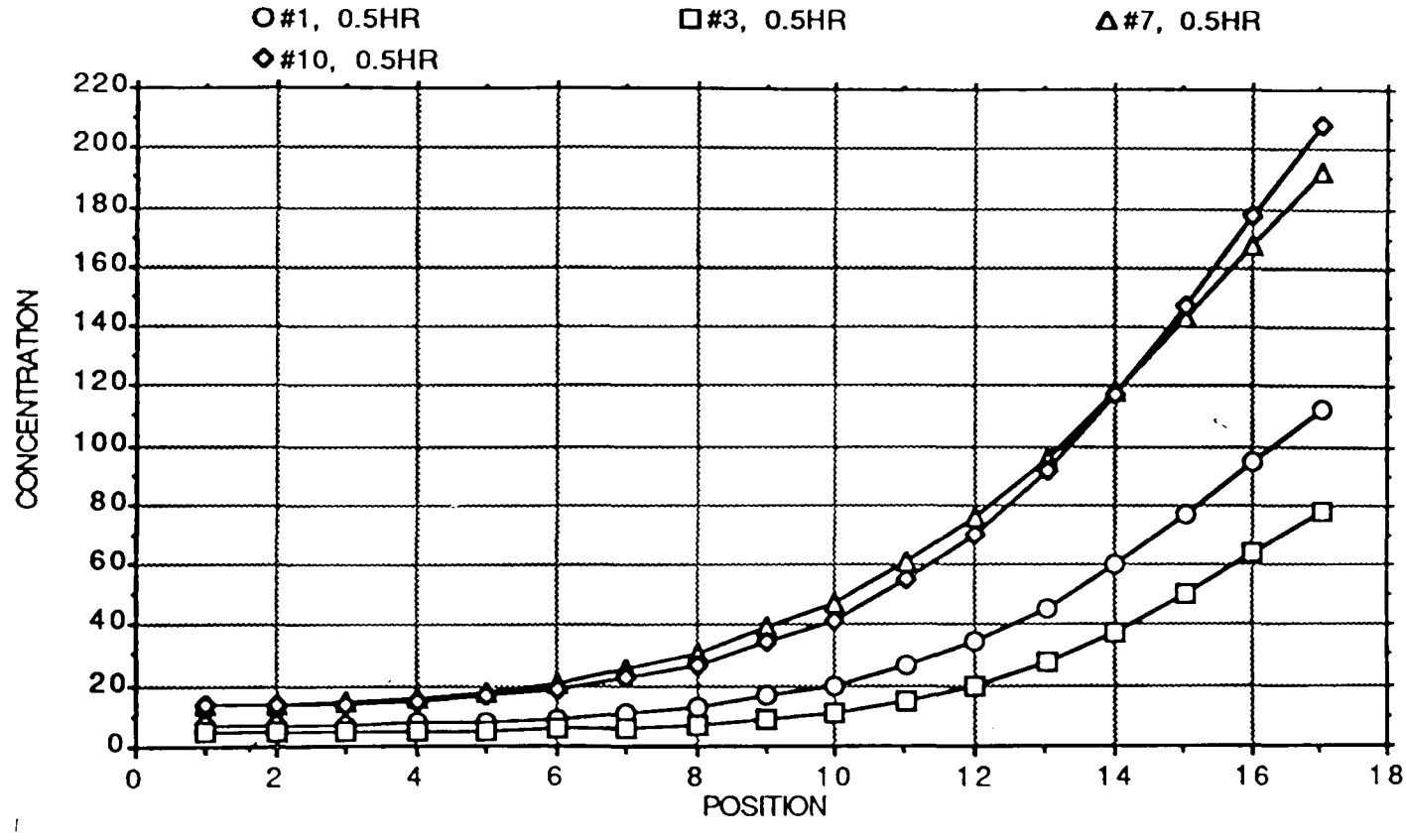

Figure 7.18 Gas uptake : Computed distributions of concentration along the centreline of an O-ring for Benchmark Materials 1,3,7 and 10 after 30 minutes. [carbon dioxide, 172bar, 100°C]

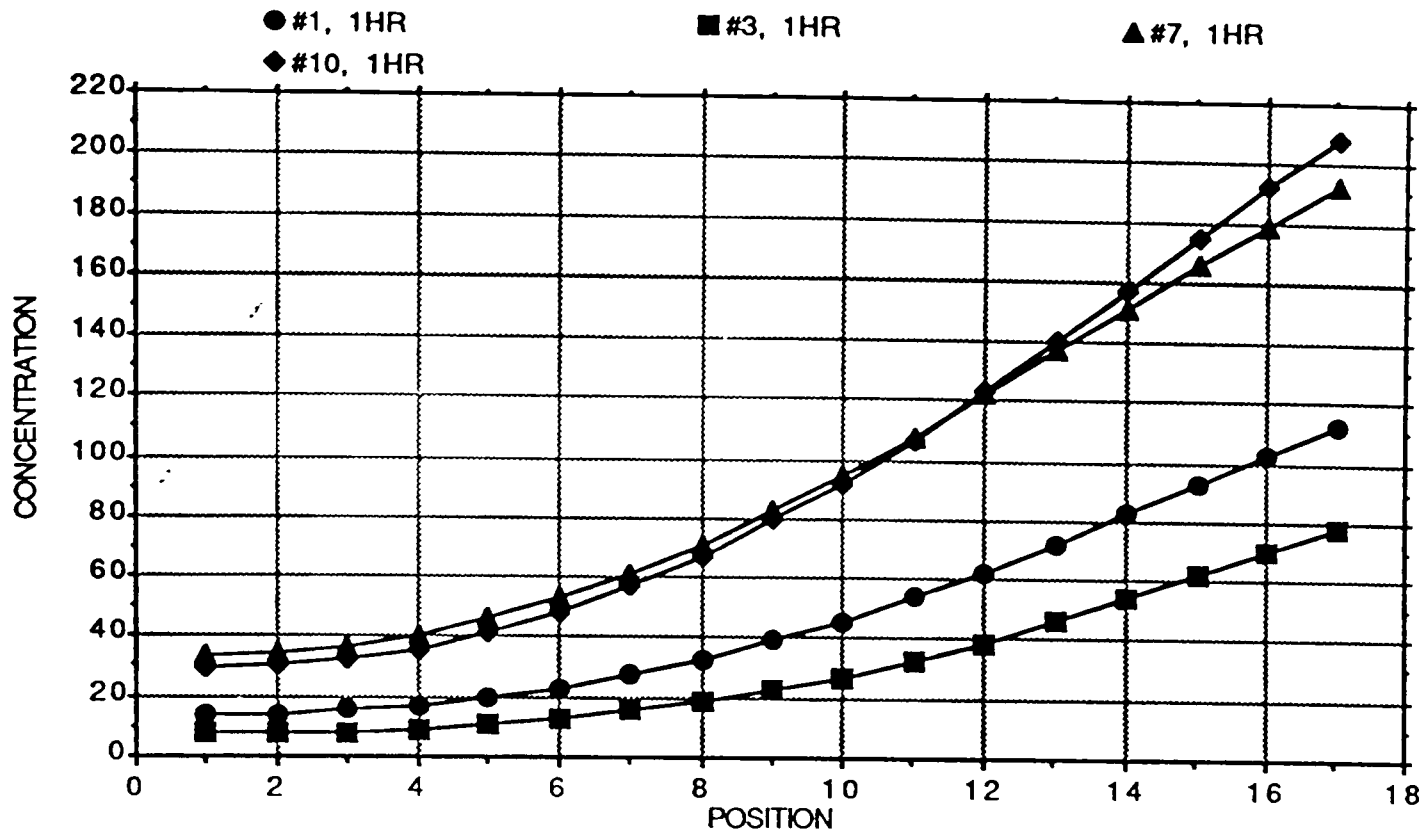

Figure 7.19 Gas uptake : Computed distributions of concentration along the centreline of an O-ring for Benchmark Materials 1,3, 7 and 10 after 60 minutes. [carbon dioxide, 172bar, 100°C]

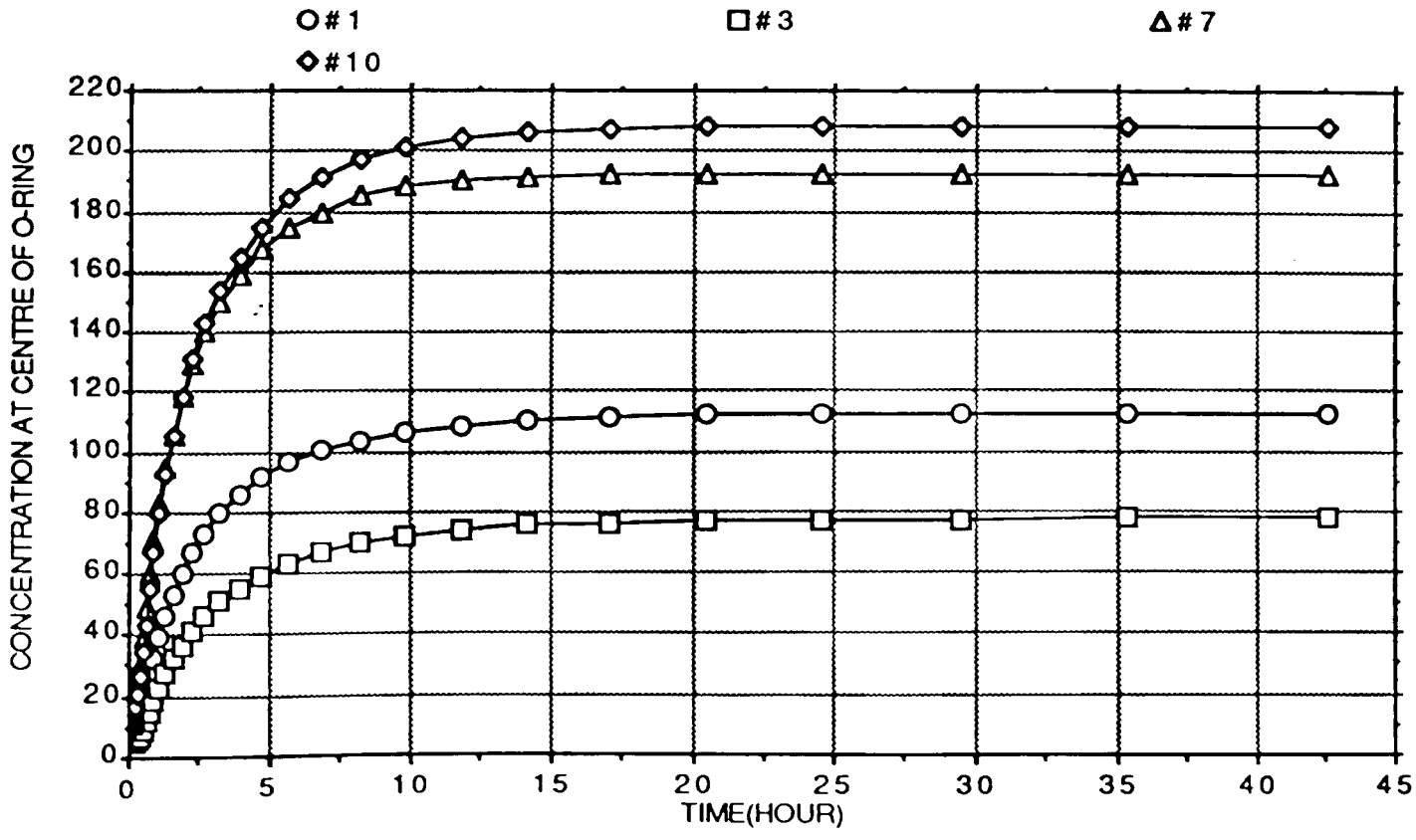

Figure 7.20 Gas uptake : Computed variation of concentration with time at the centre of an O-ring for Benchmark Materials 1, 3, 7 and 10. [carbon dioxide, 172bar, 100°C]

Benchmark no.	Material	Temp C	Pressure psi	Time to Equilibrium hour	Diffusion Coefficient sq cm /s	Solubility /bar	Equilibrium uptake vol s.t.p./ polymer vol
#1	EPDM	100	2500(173)	24.6	4.80	0.65	112
#3	high Nitrile	100	2500(173)	42.5	4.00	0.45	77
#7	Viton GFLT	100	2500(173)	20.4	6.40	1.12	192
#10	Aflas	100	2500(173)	24.6	5.30	1.21	208
#1	EPDM	100	2500(173)	24.6	4.80	0.65	112
#1	EPDM	100	10000(690)	20.5	5.90	0.19	131
#3	high Nitrile	100	2500(173)	42.5	4.00	0.45	77
#3	high Nitrile	130	2500(173)	61.1	2.00	1.10	190

Figure 7.21 Summary of computed times to saturation for an O-ring, for Benchmark Materials.
[carbon dioxide, 172 bar (2500 psi), 100°C]

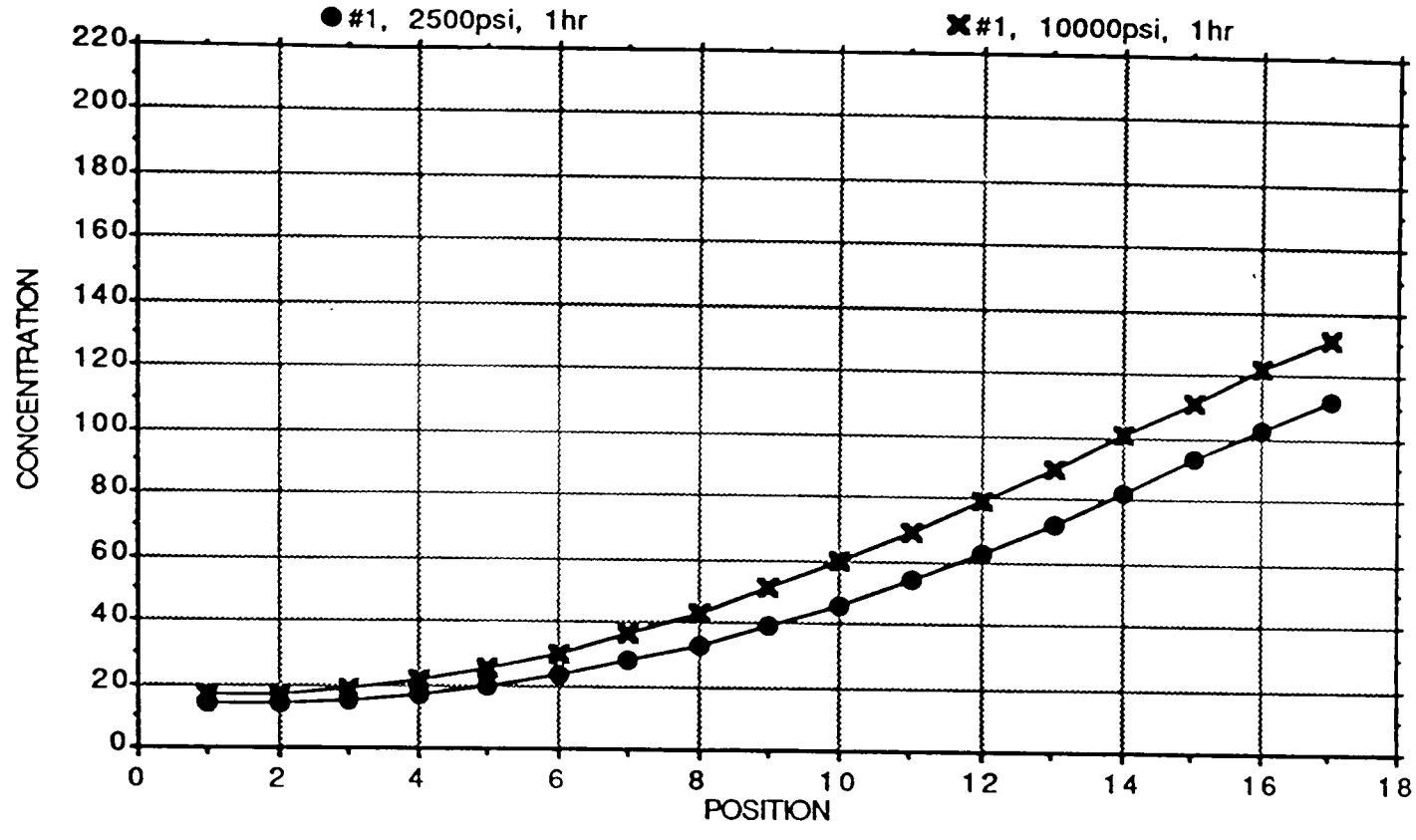

Figure 7.22 Gas uptake : Effect of pressure on concentration distribution in an O-ring of Benchmark #1 (EPDM), after 60 minutes. [carbon dioxide, 172bar and 690bar, 100°C]

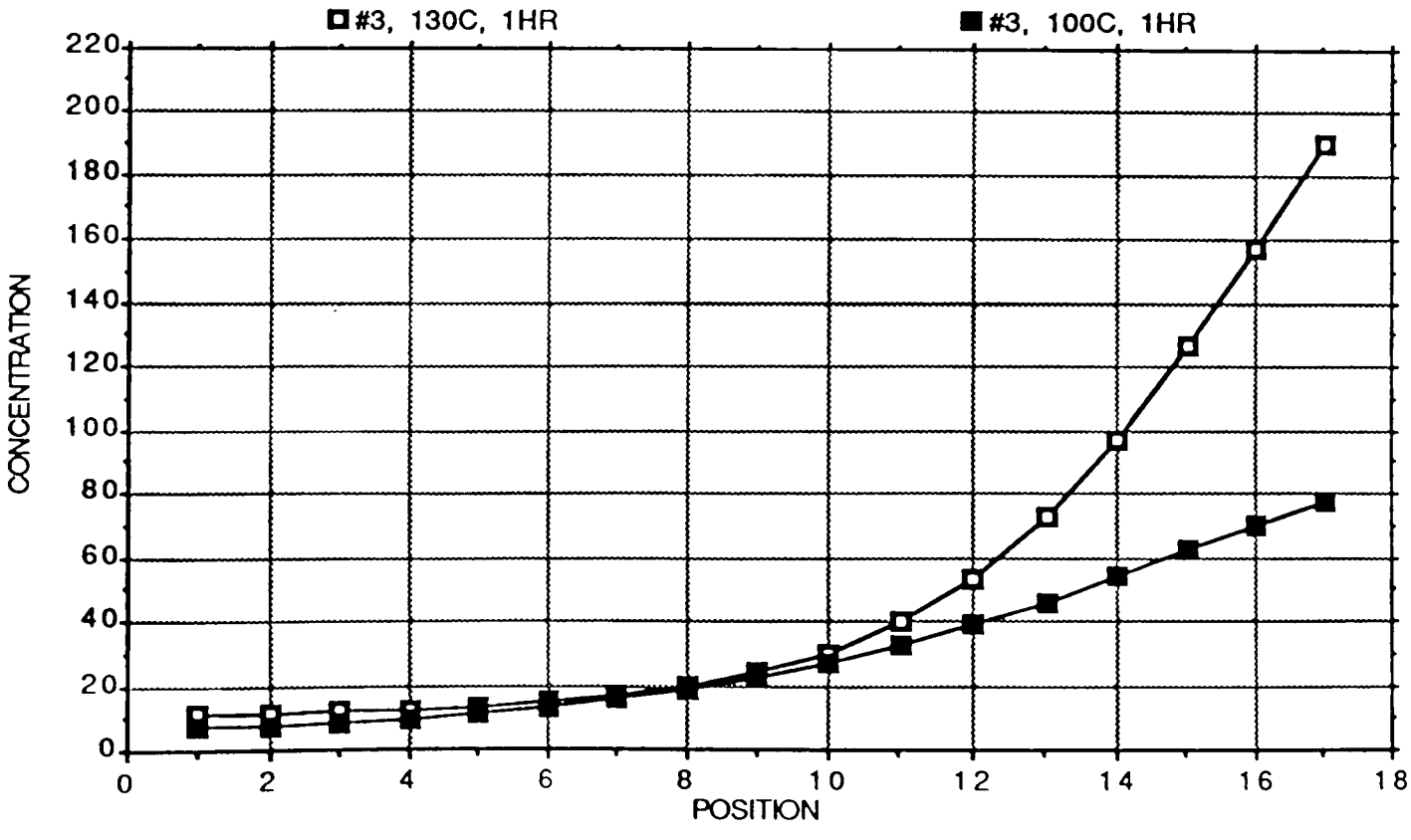

Figure 7.23 Gas uptake : Effect of temperature on concentration distribution in an O-ring of Benchmark #3 (high ACN NBR), after 60 minutes. [carbon dioxide, 172bar, 100°C and 130°C]

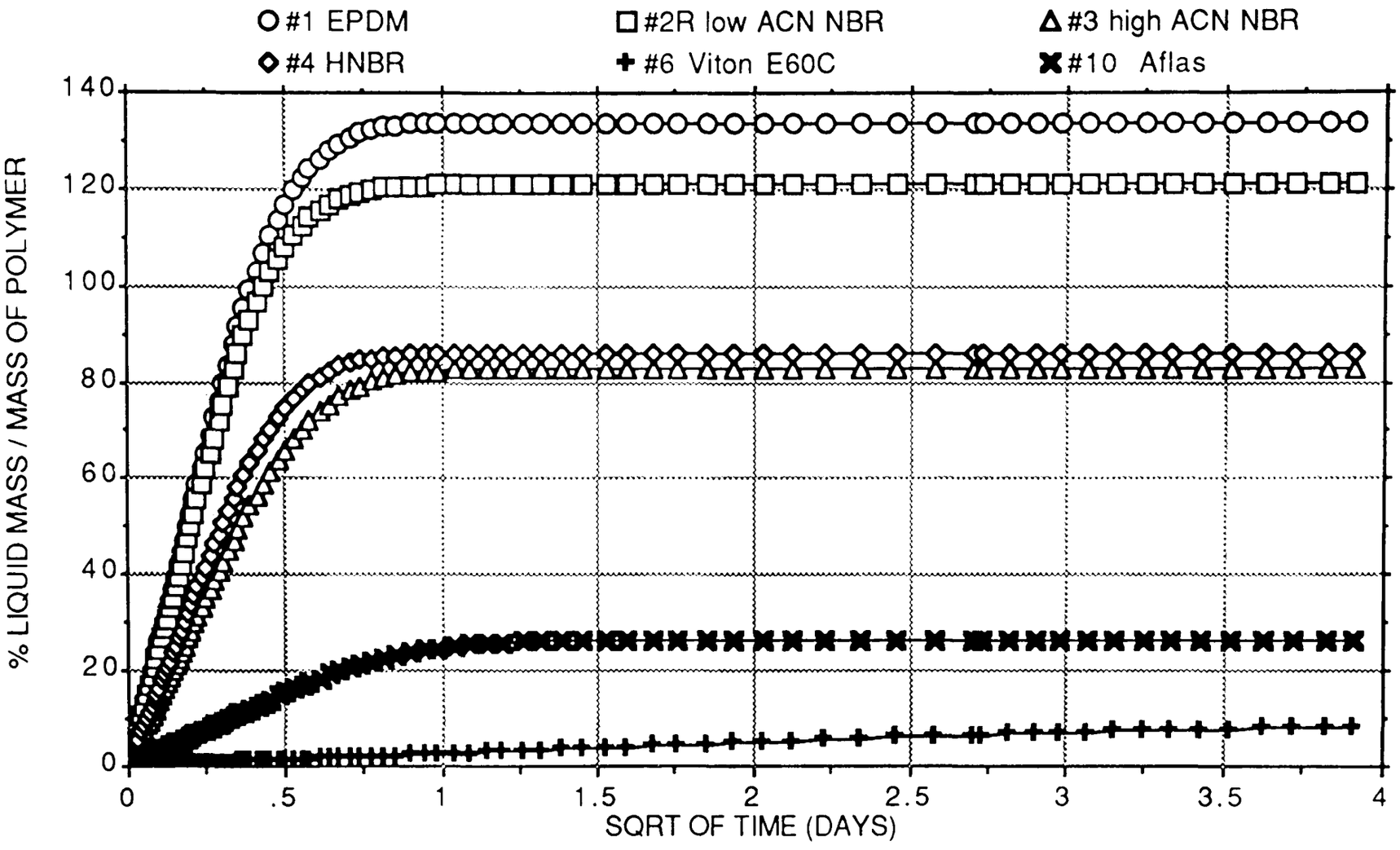

Fig 7.24 Liquid uptake : Computed variation with time of toluene uptake by a sheet sample for Benchmark Materials

Benchmark no.	Material	Experimental half period (sec)	Computed half period (sec)	Percentage Difference
# 1	EPDM	5515	5570	1%
#2R	low Nitrile	4983	5030	1%
# 3	high Nitrile	7437	7500	1%
# 4	HNBR Nitrile	5626	5680	1%
# 6	Viton E60C	280500	283200	1%
#10	Aflas	15835	15980	1%

Fig 7.25 Comparison of measured and computed toluene uptake by a sheet sample, for Benchmark Materials

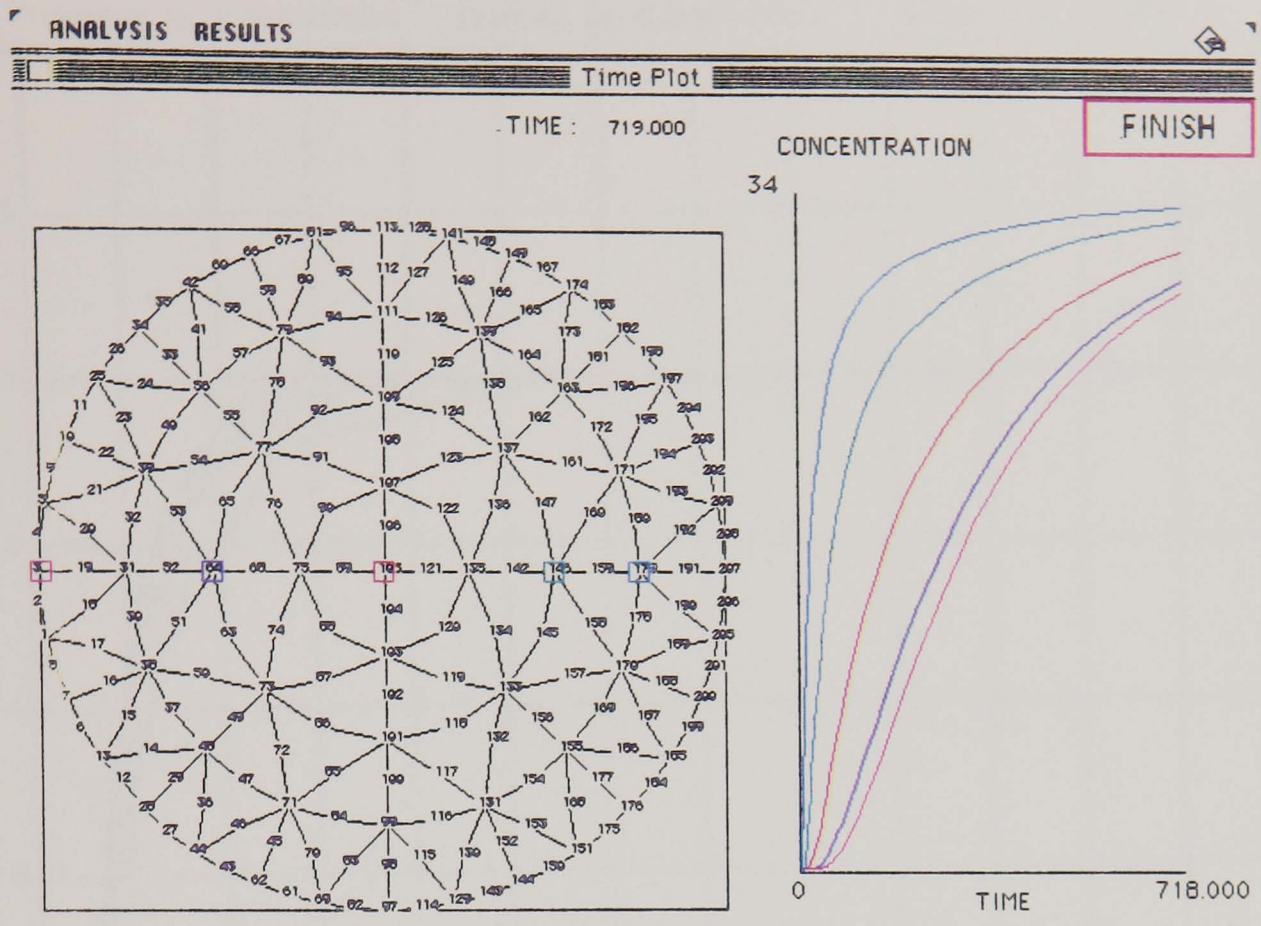

Figure 7.26 Computed concentration of methanol with time along the centreline of a Viton E60C O-ring

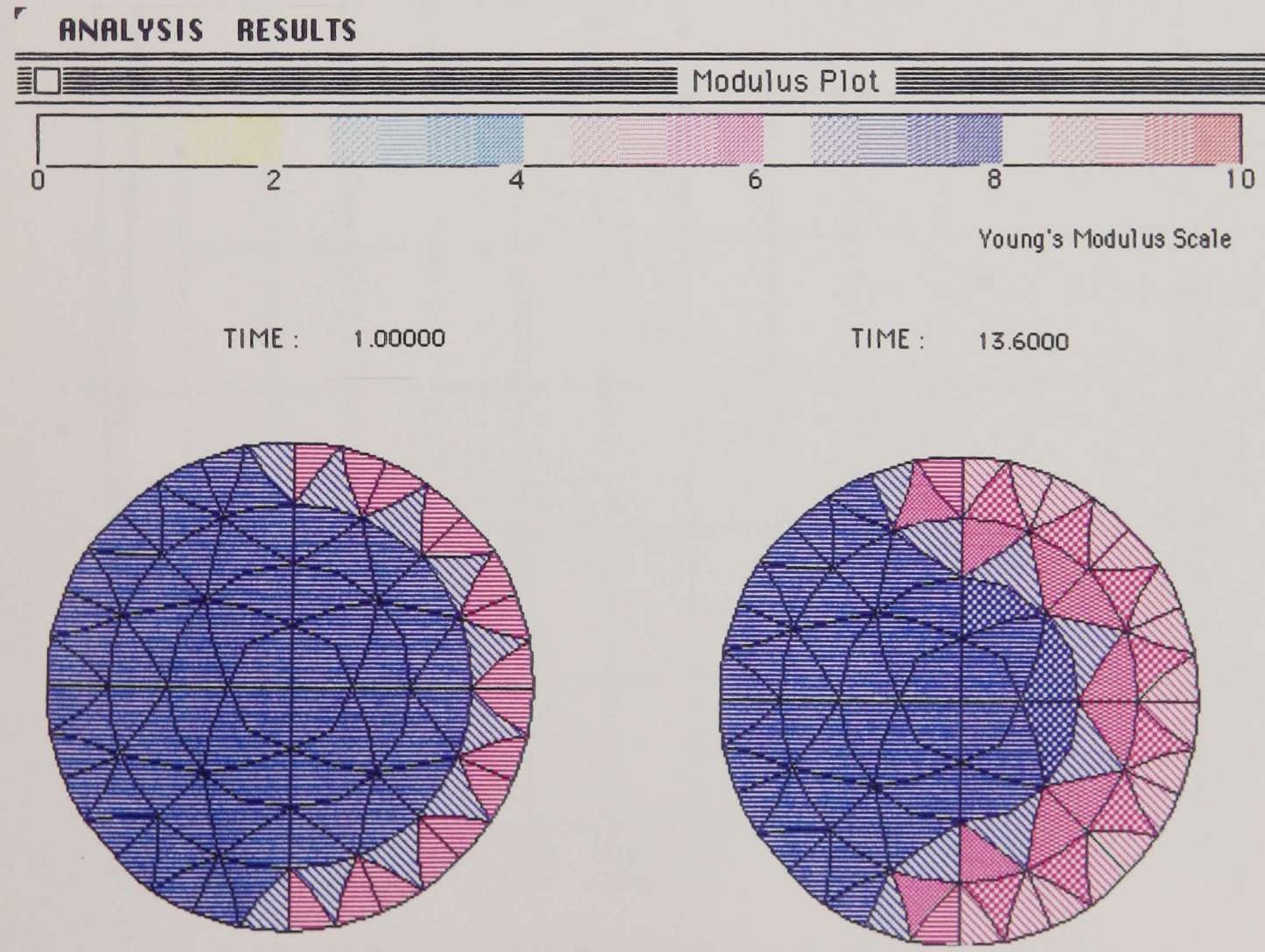

Figure 7.27 Computed modulus distribution of Viton E60C O-ring after 1 hour and after 14 hour soak in methanol

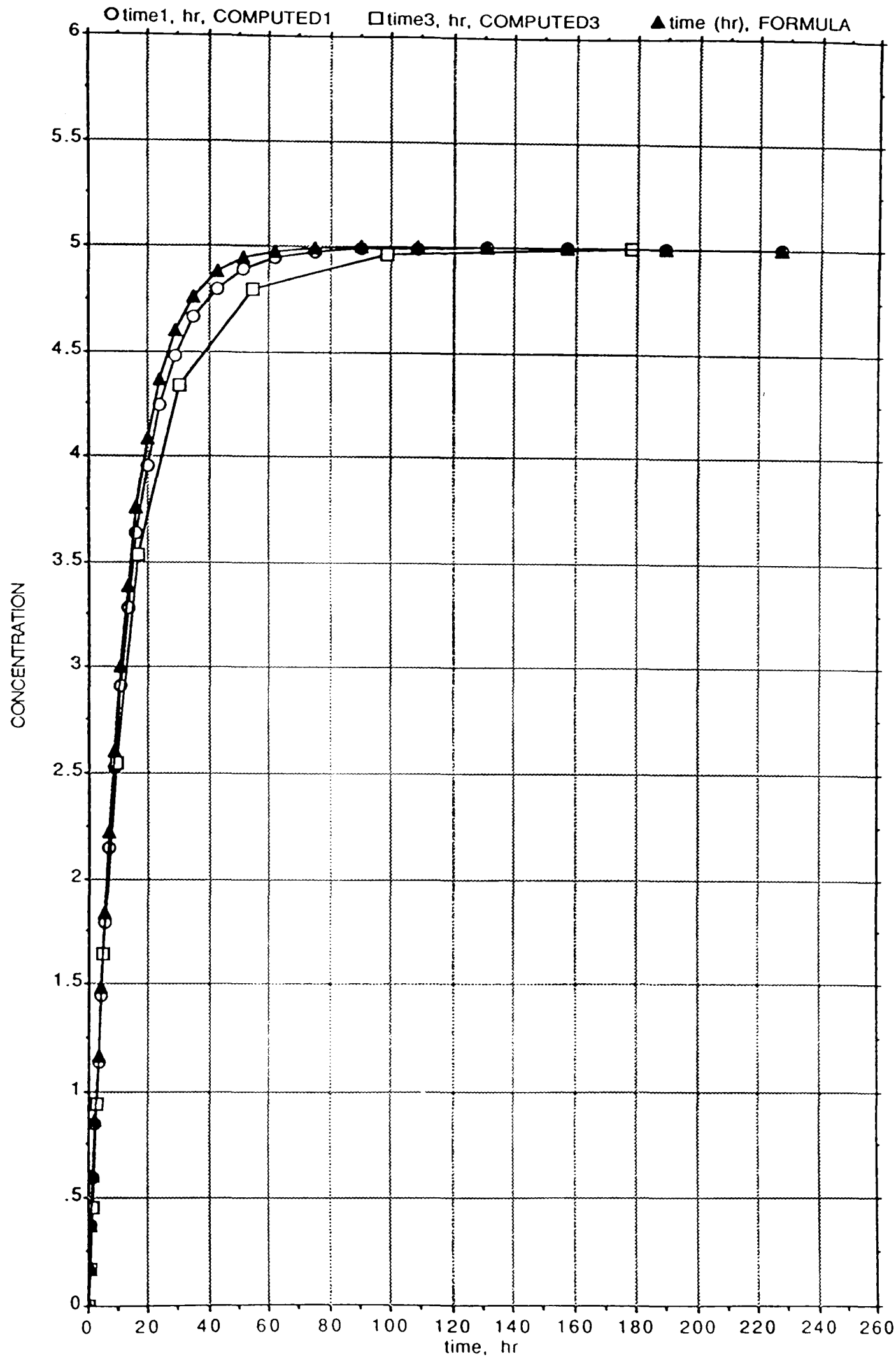

Figure 7.28 Chemical reaction model : comparison between computed and analytical solutions of reaction equation.

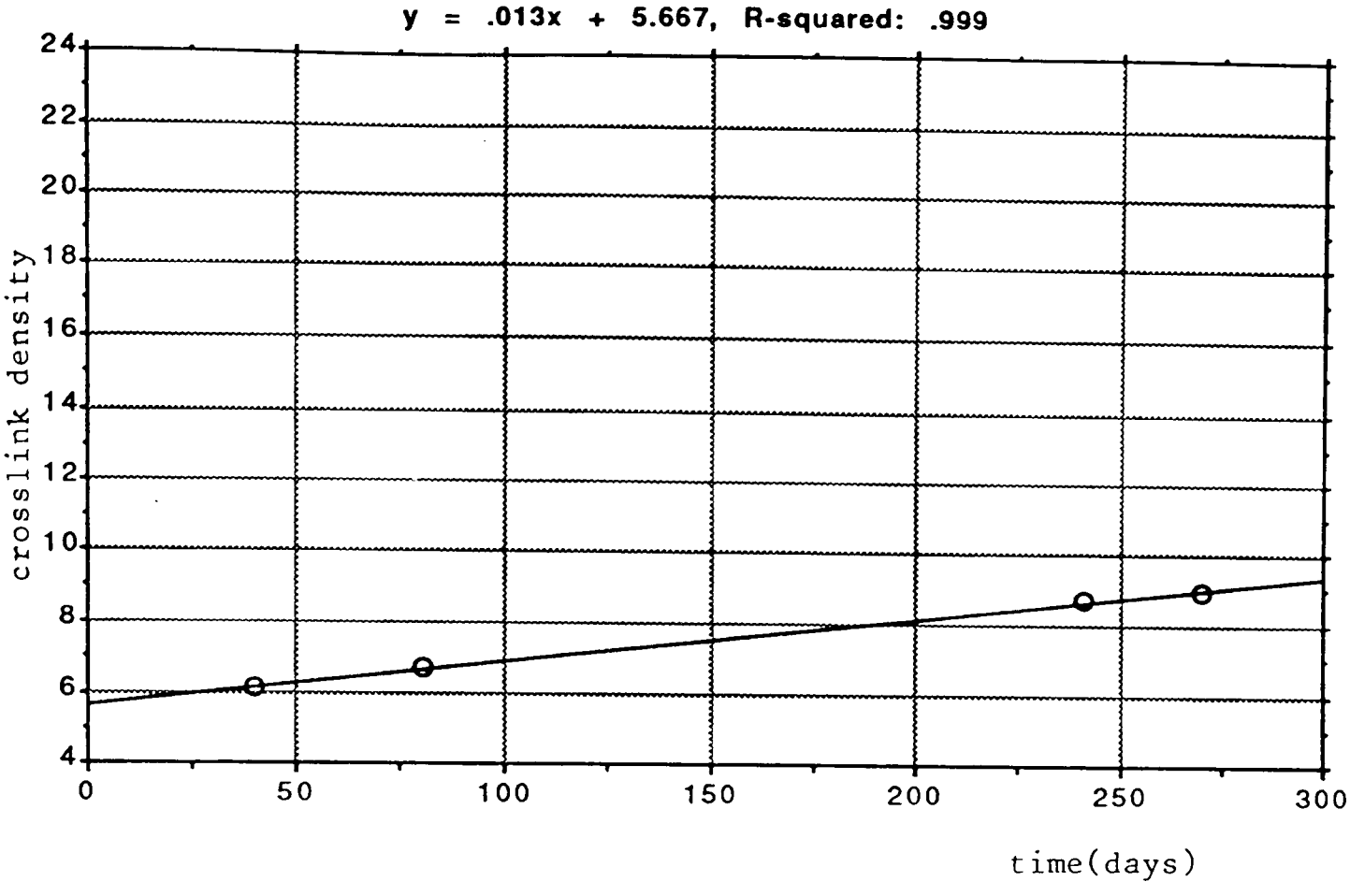

Fig 7.29 Measured crosslink density against time at 70 deg C

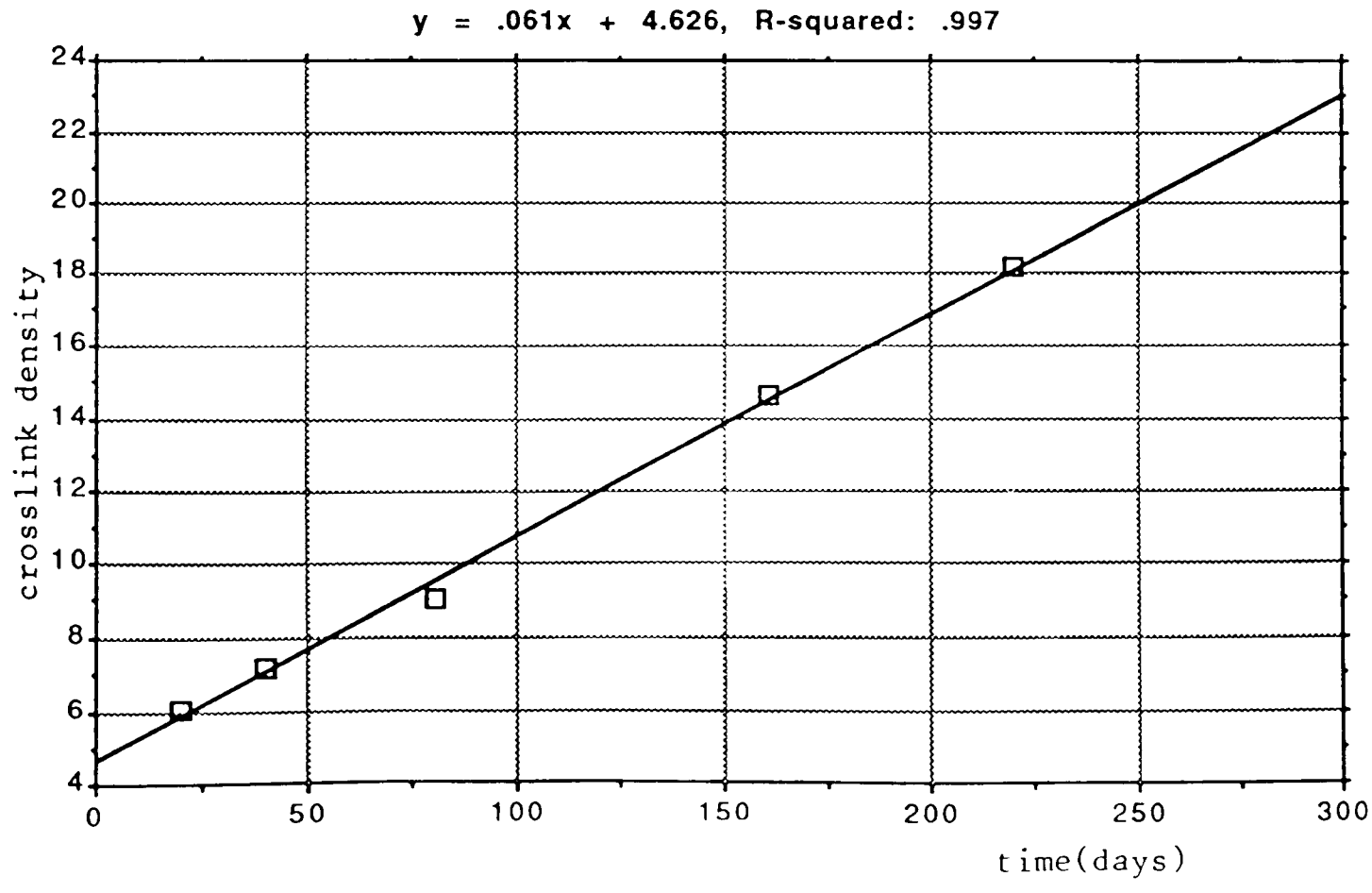

Fig 7.30 Measured crosslink density against time at 85 deg C

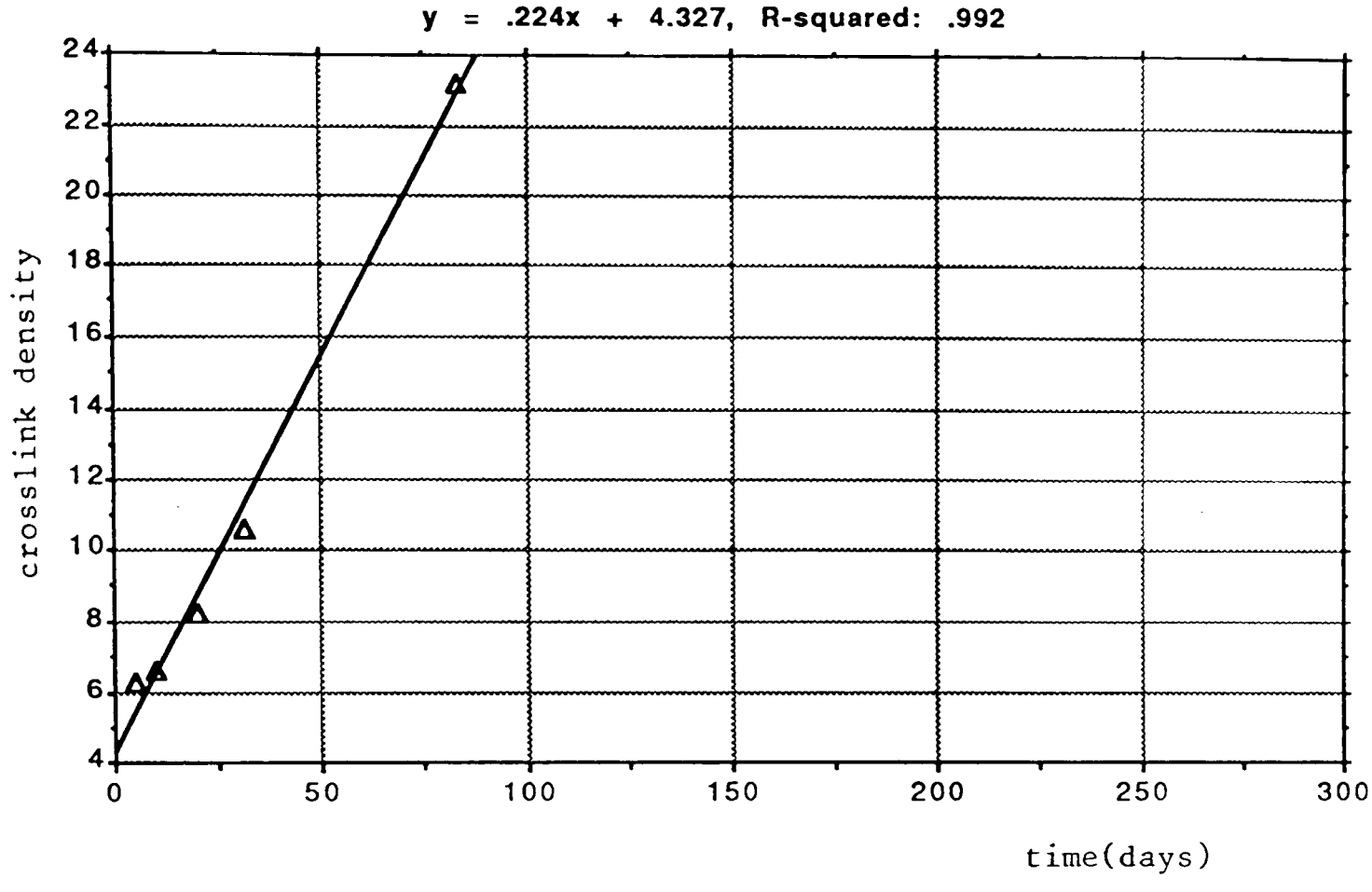

Fig 7.31 Measured crosslink density against time at 100 deg C

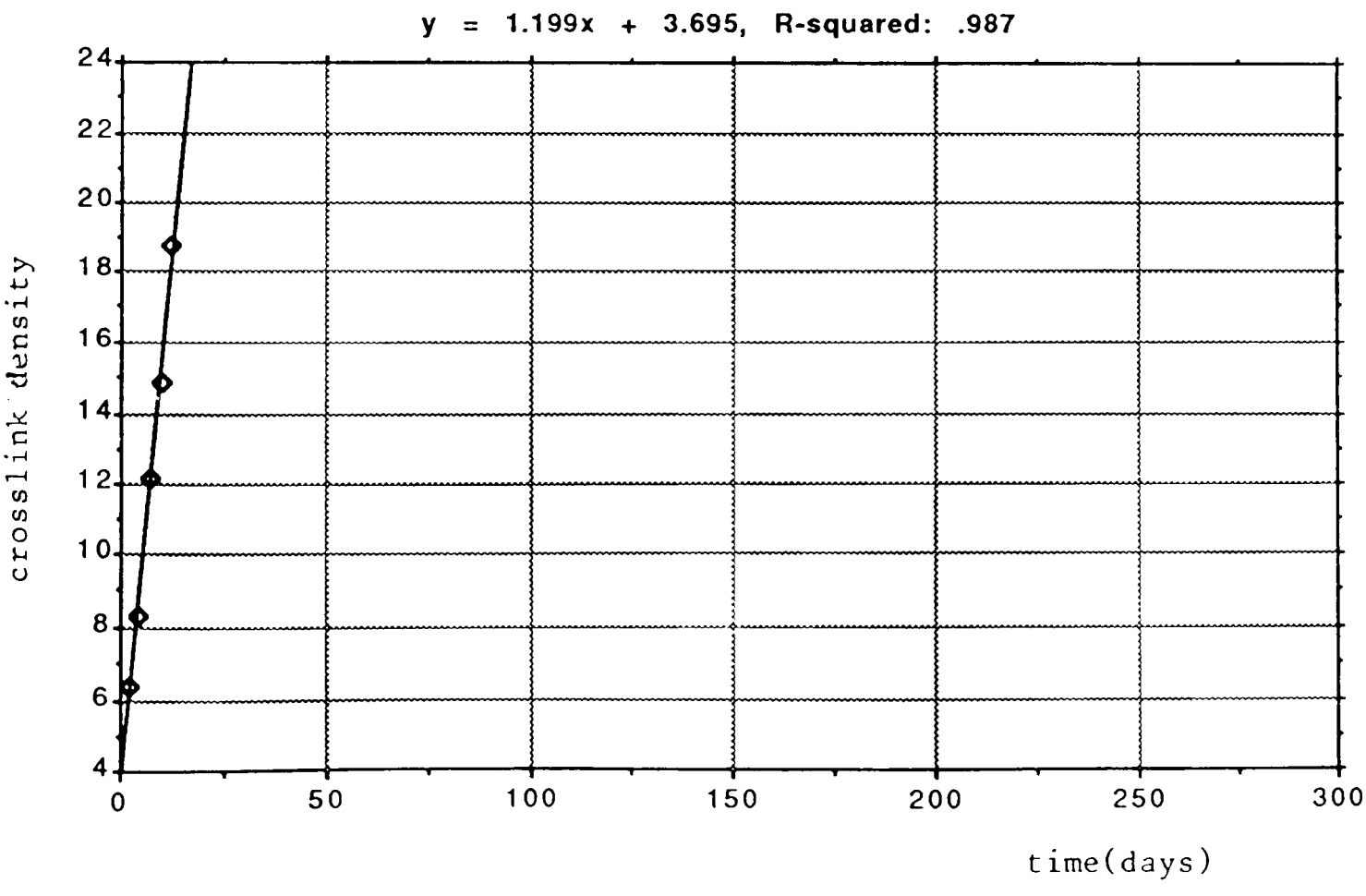

Fig 7.32 Measured crosslink density against time at 125 deg C

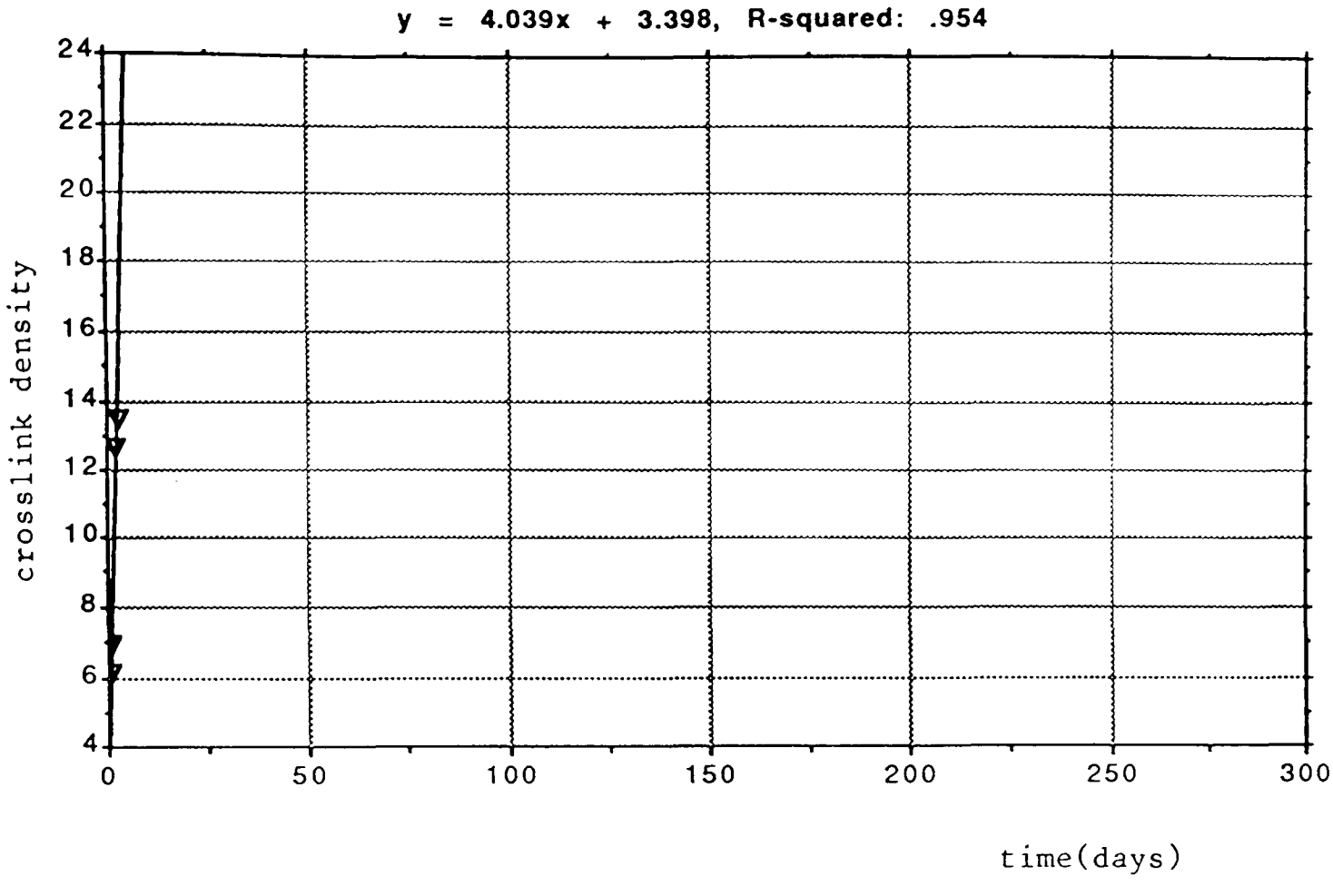

Fig 7.33 Measured crosslink density against time at 150 deg C

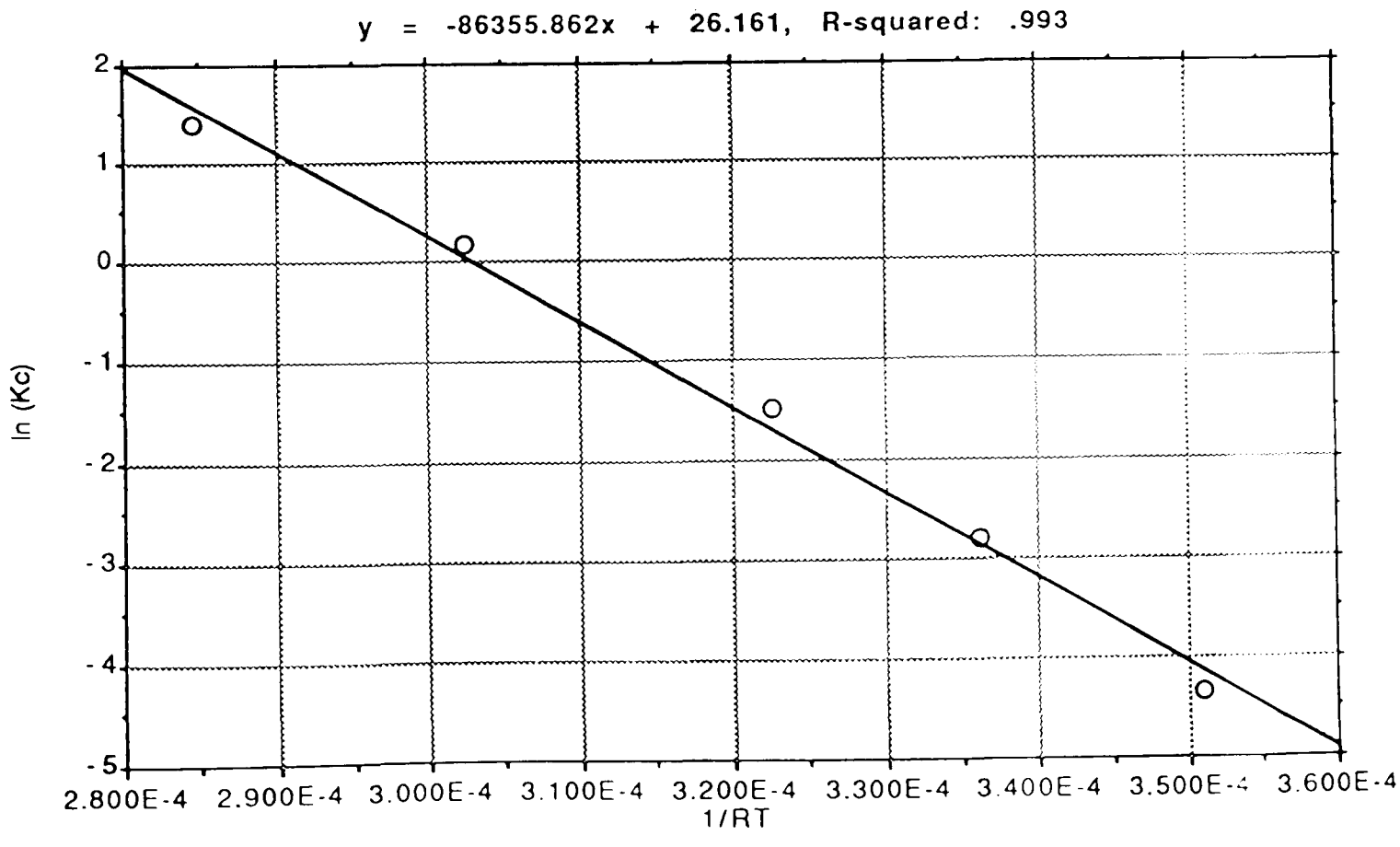

Fig 7.34 Arrhenius plot to determine coefficients for chemical reaction rates at all temperatures

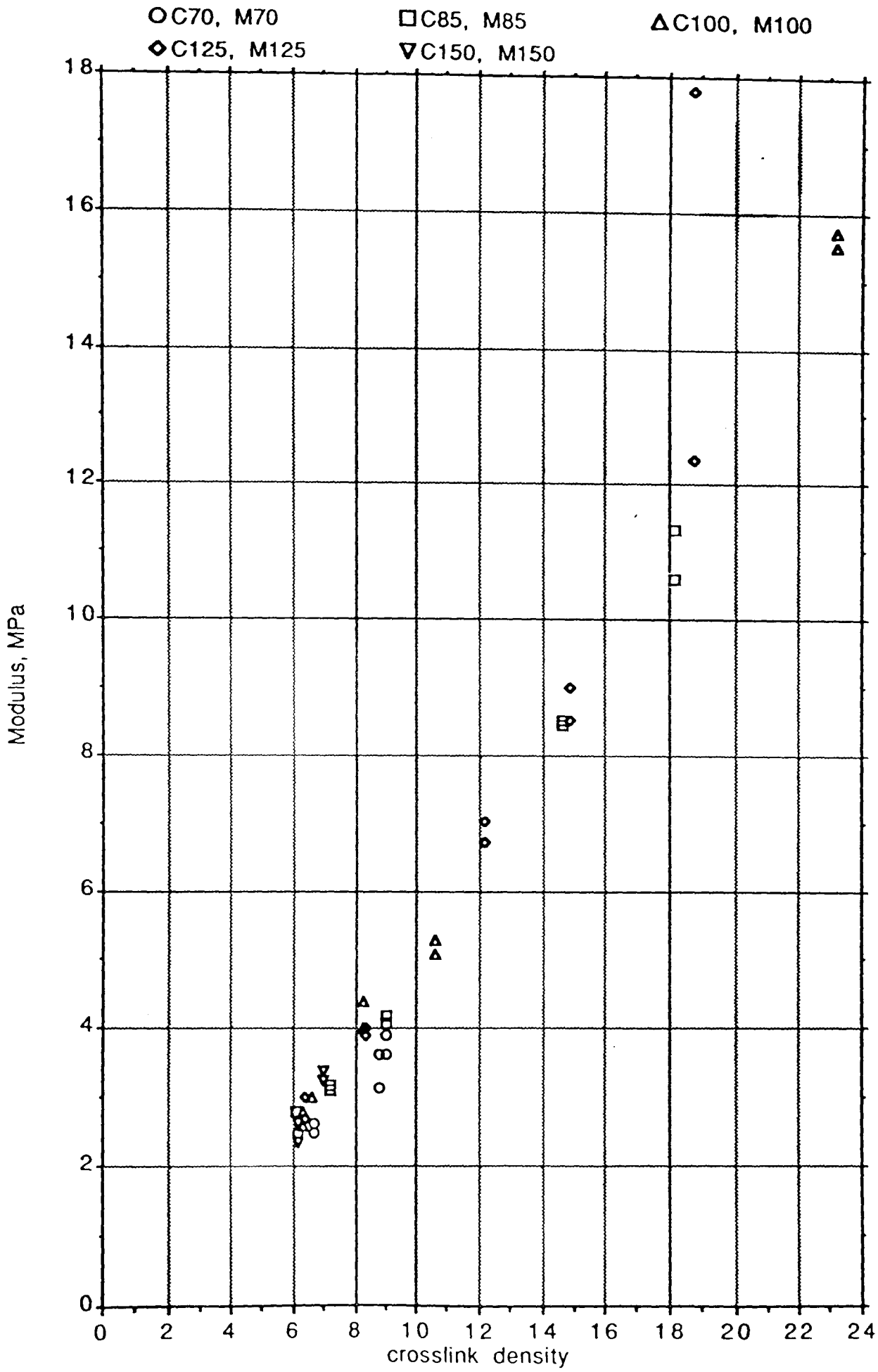

Figure 7.35 Modulus against crosslink density for a nitrile rubber

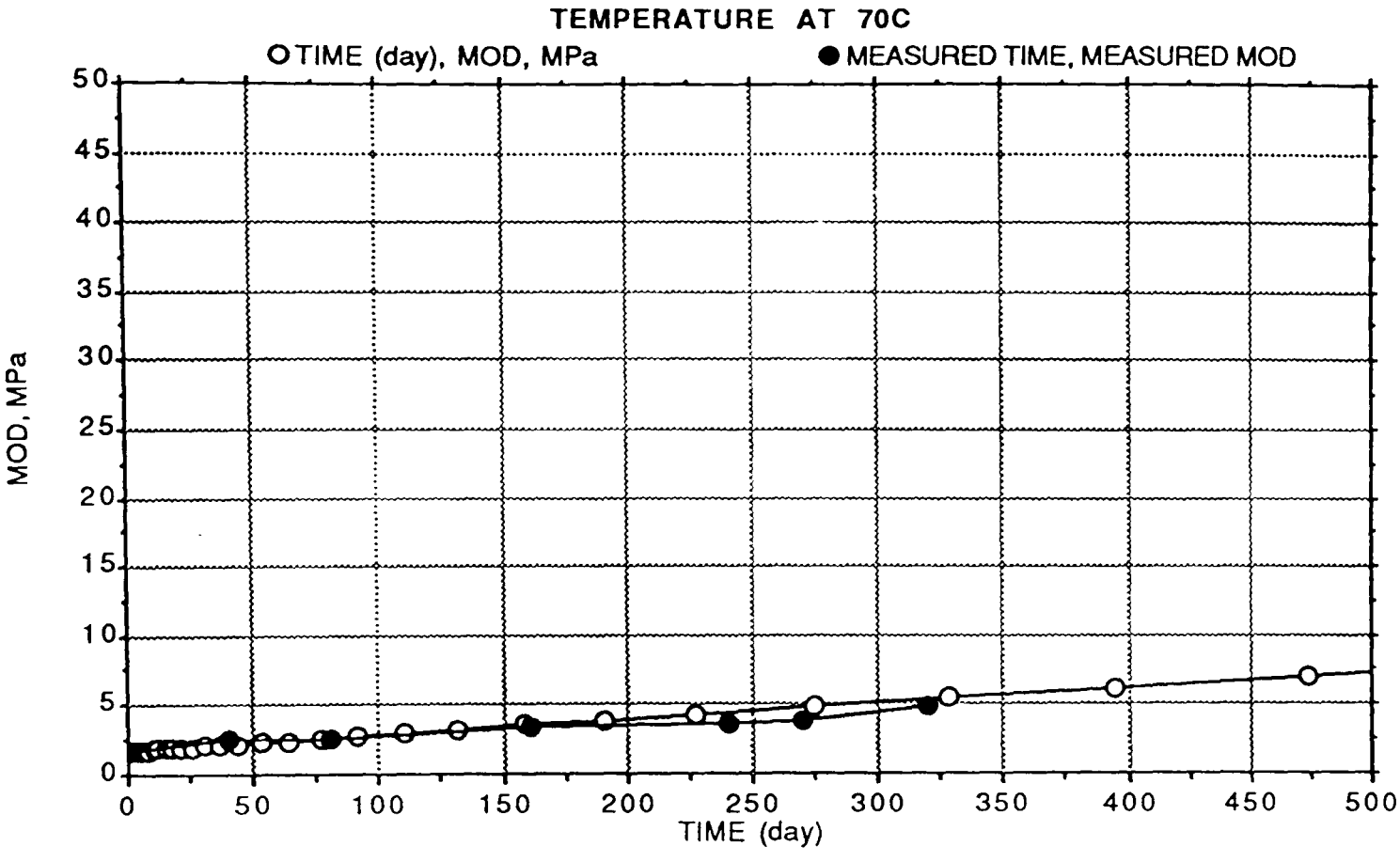

Figure 7.36 Chemical reaction model : comparison of air-ageing effect on measured (Ministry of Defence data) and computed Young's modulus in a NBR rubber, 70°C

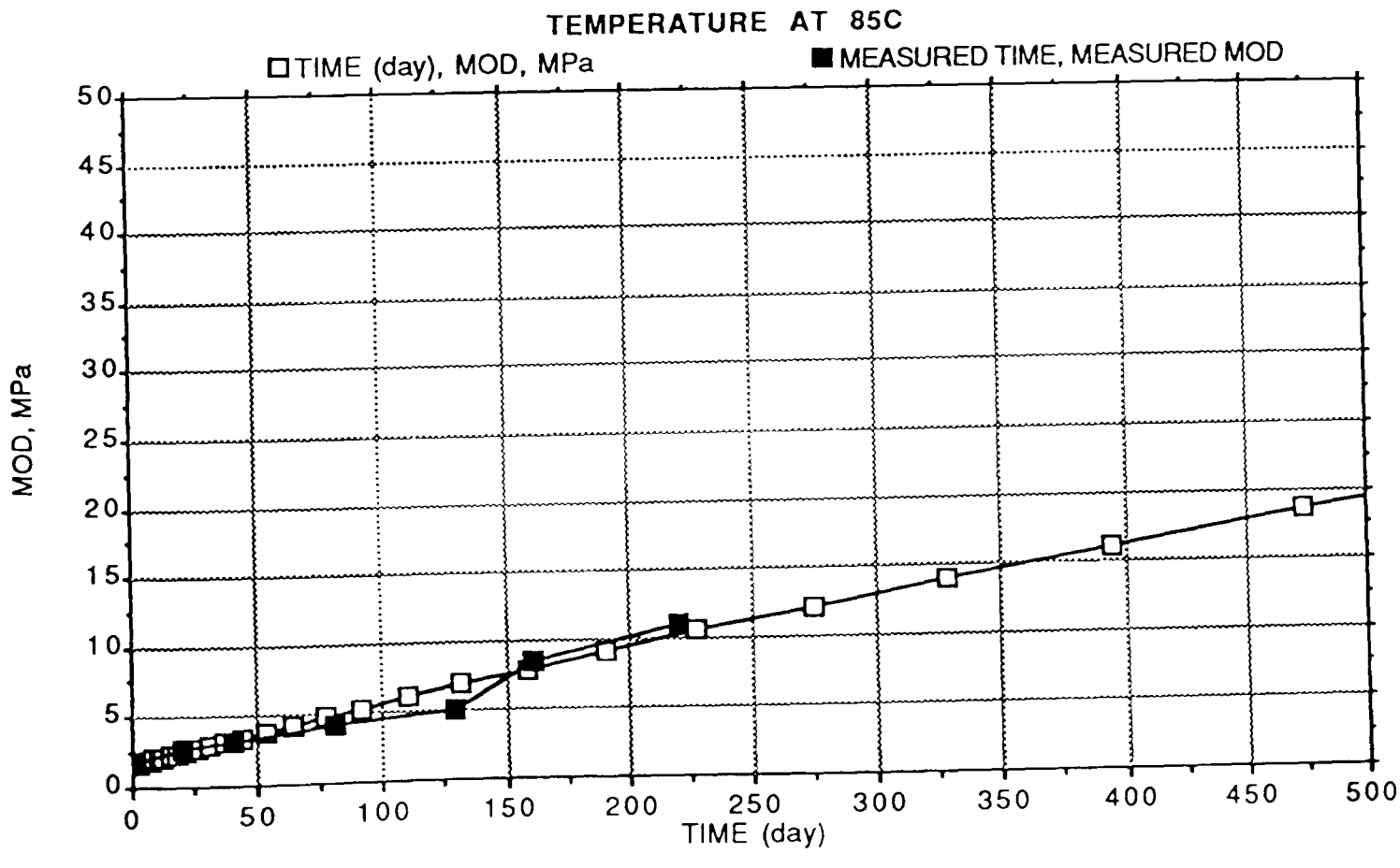

Figure 7.37 Chemical reaction model: comparison of air-ageing effect on measured (Ministry of Defence data) and computed Youngś modulus in a NBR rubber, 85°C

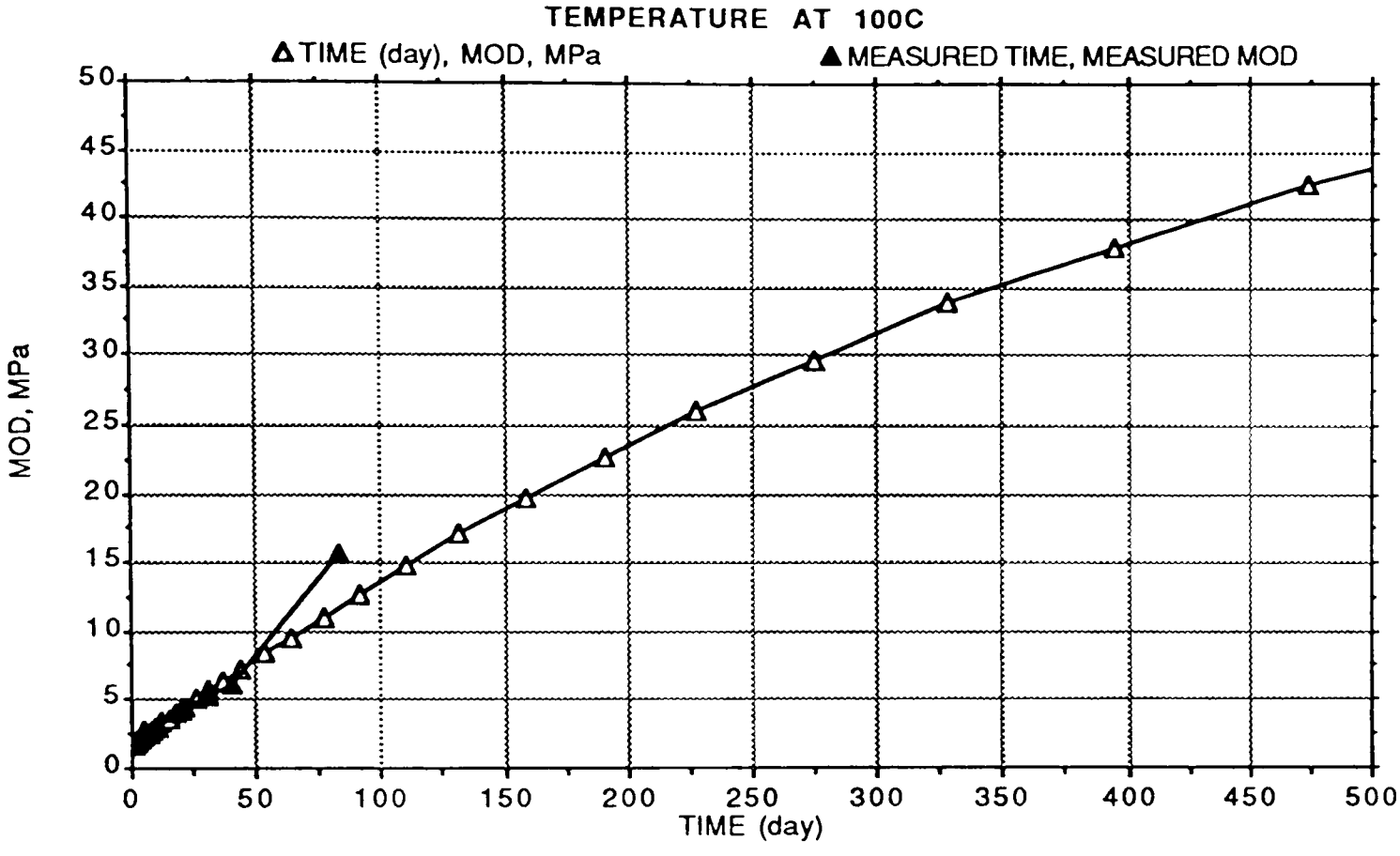

Figure 7.38 Chemical reaction model : comparison of air-ageing effect on measured (Ministry of Defence data) and computed Young's modulus in a NBR rubber, 100°C

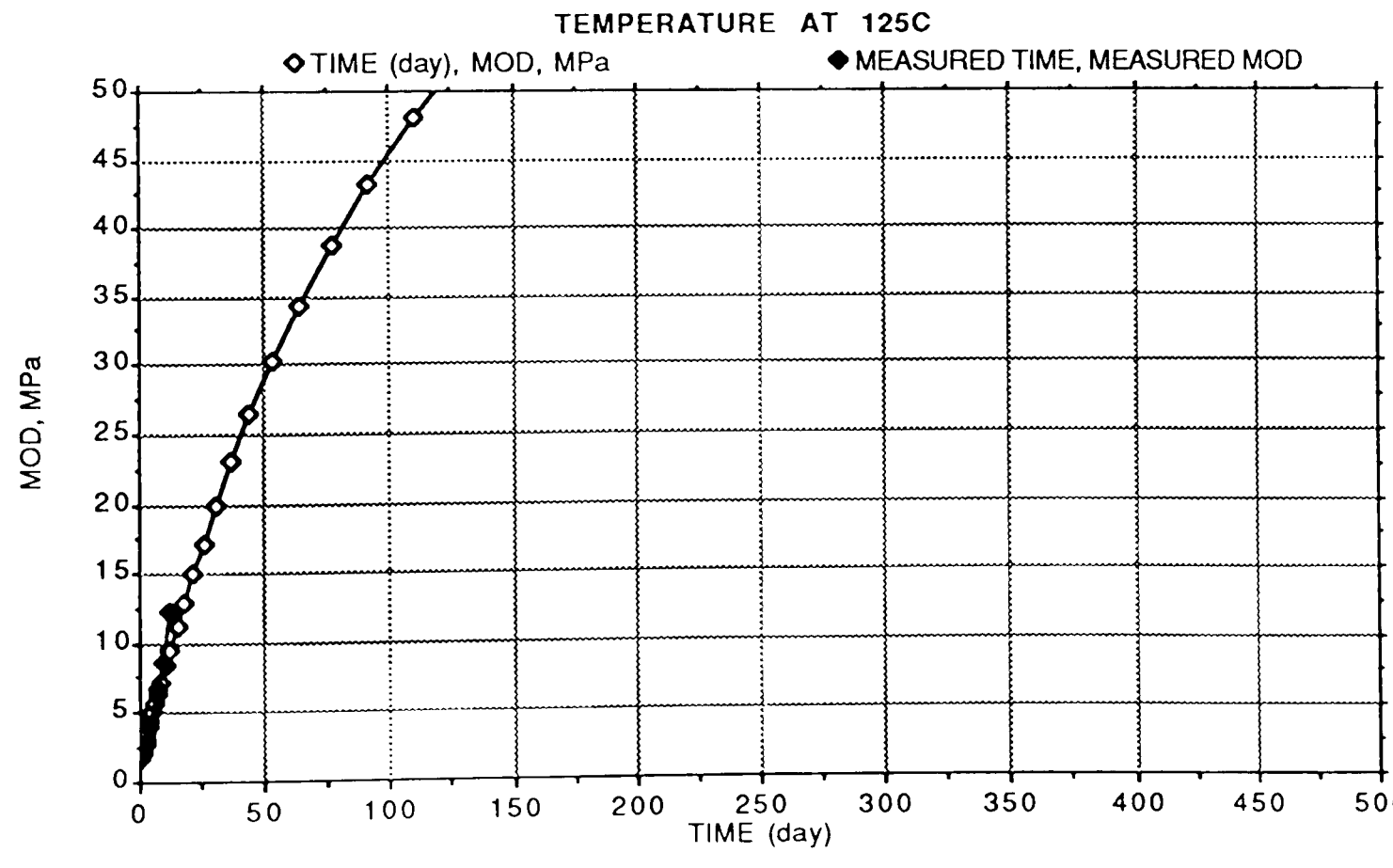

Figure 7.39 Chemical reaction model : comparison of air-ageing effect on measured (Ministry of Defence data) and computed Young's modulus in a NBR rubber, 125°C

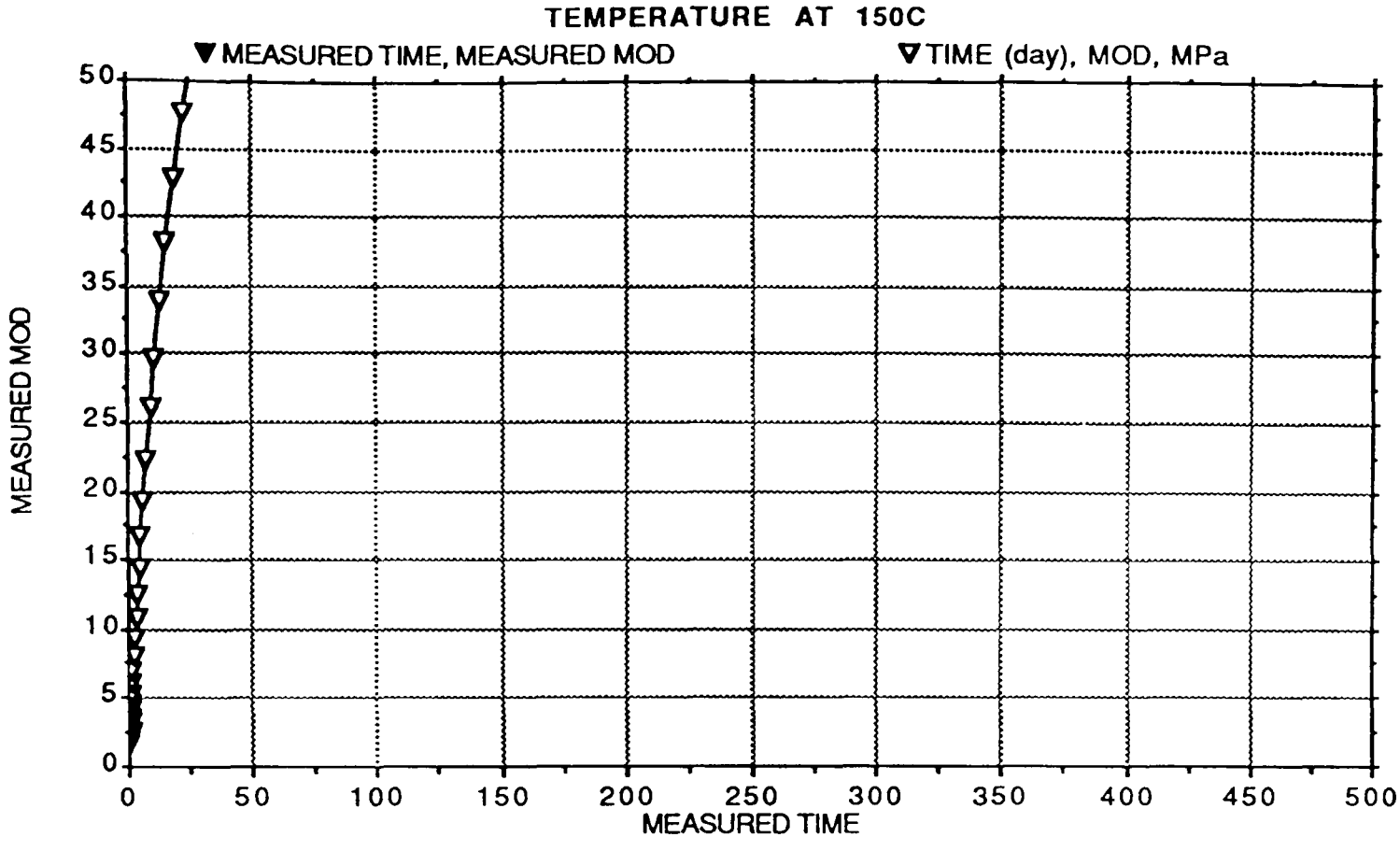

Figure 7.40 Chemical reaction model : comparison of air-ageing effect on measured (ministry of Defence data) and computed Young's modulus in a NBR rubber, 150°C

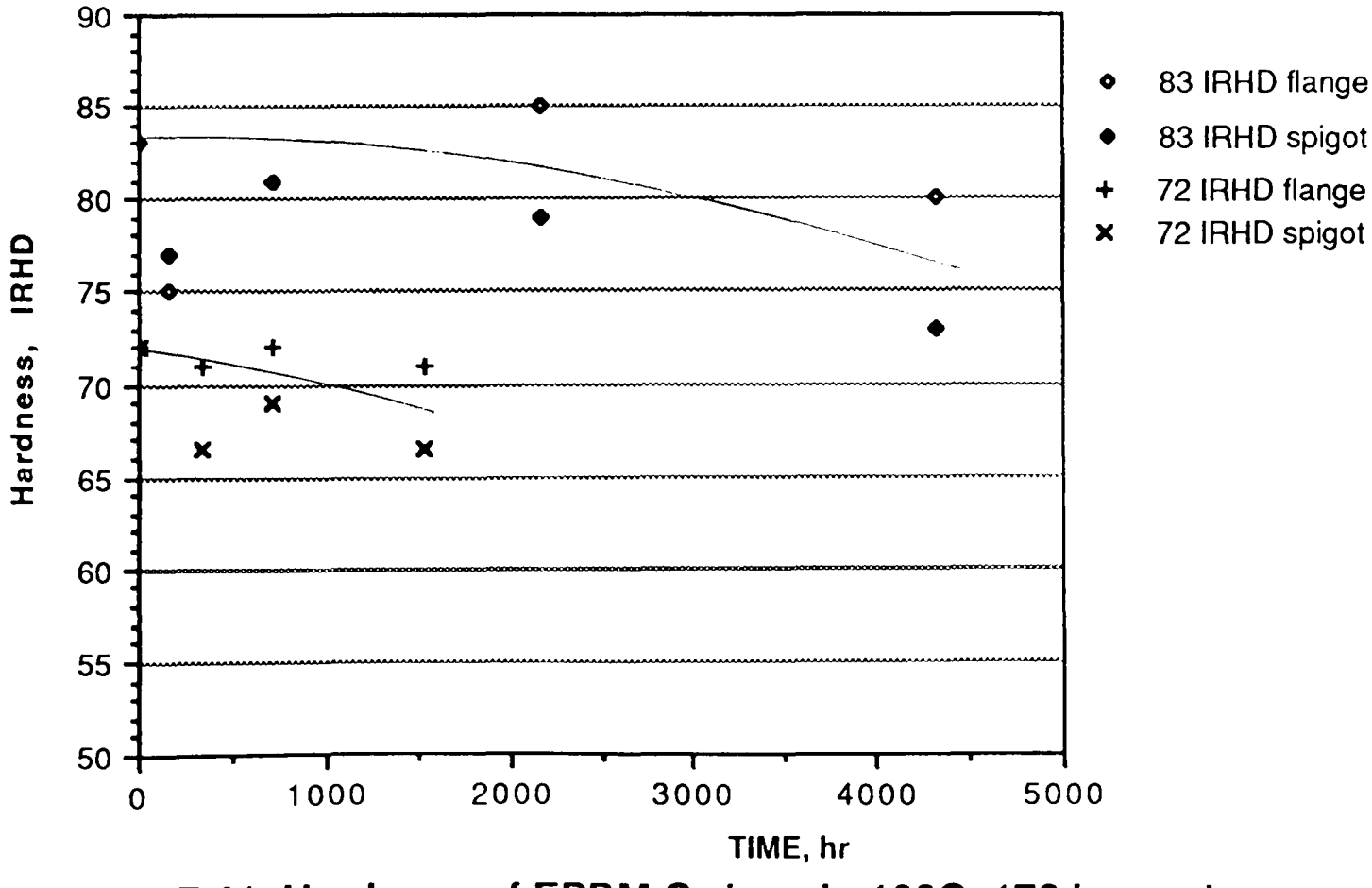

Figure 7.41 Hardness of EPDM O-rings in 100C, 173 bar water against time

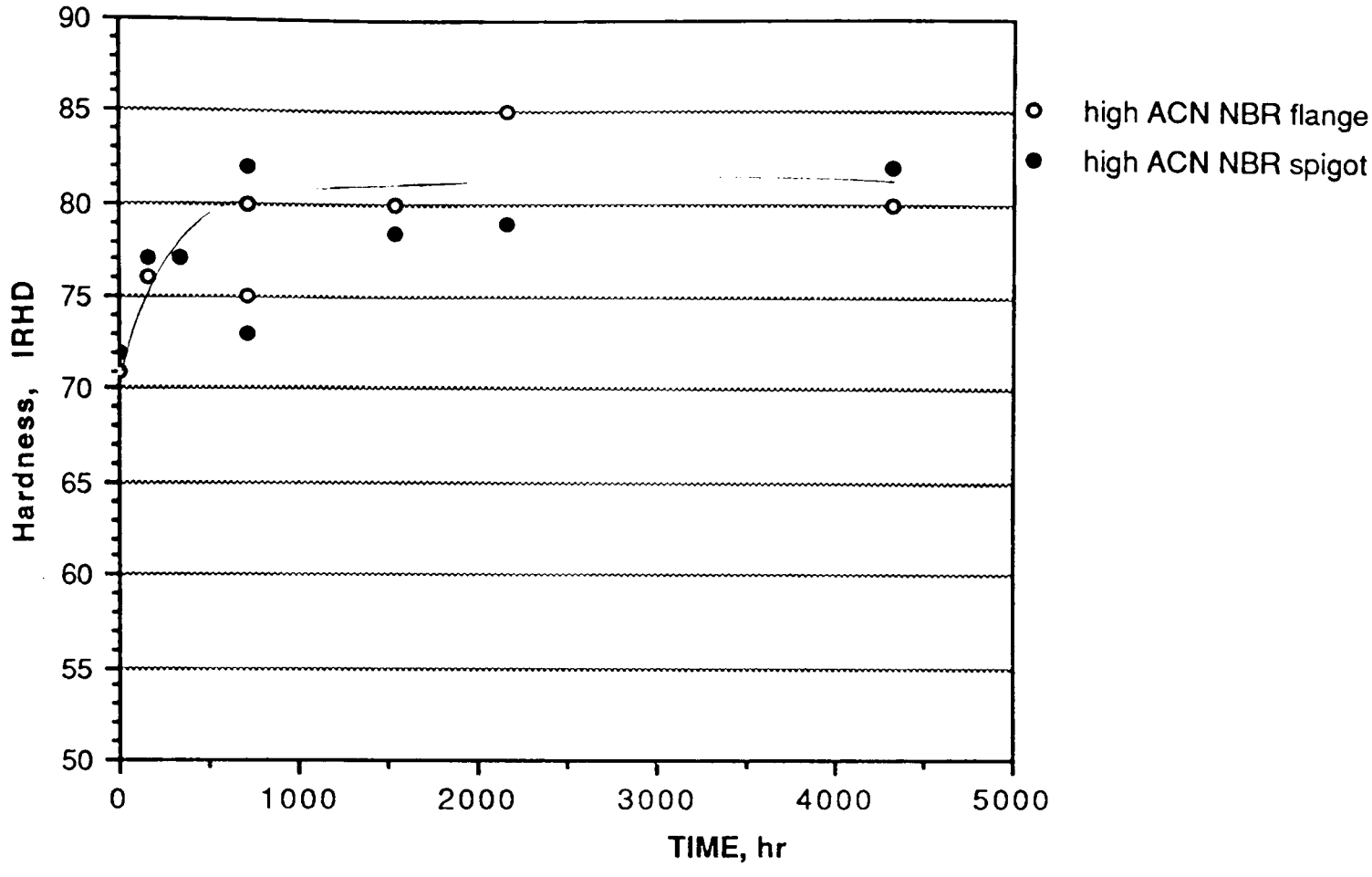

Figure 7.42 Hardness of high ACN NBR O-rings in 100C, 173 bar water against time

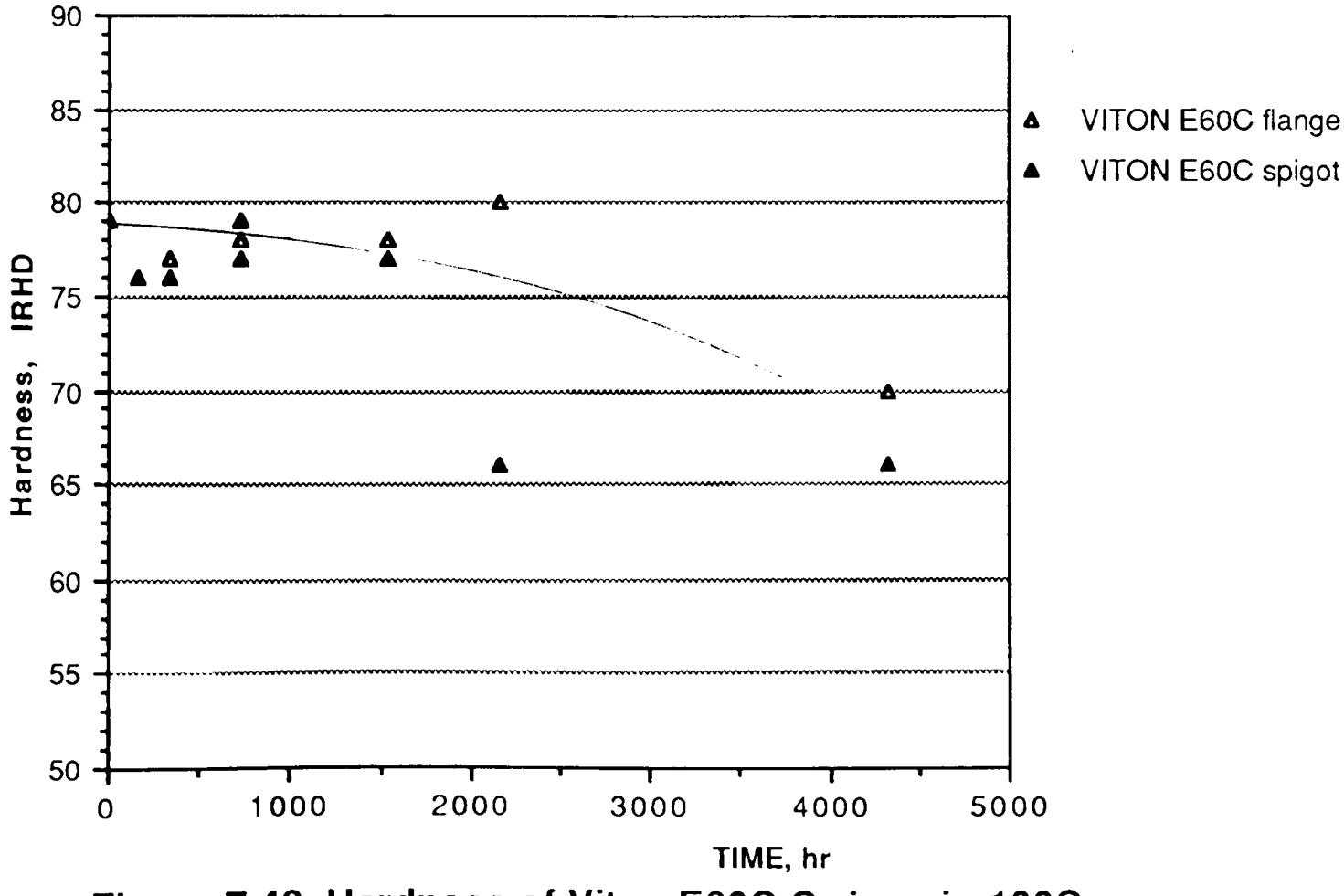

Figure 7.43 Hardness of Viton E60C O-rings in 100C, 173 bar water against time

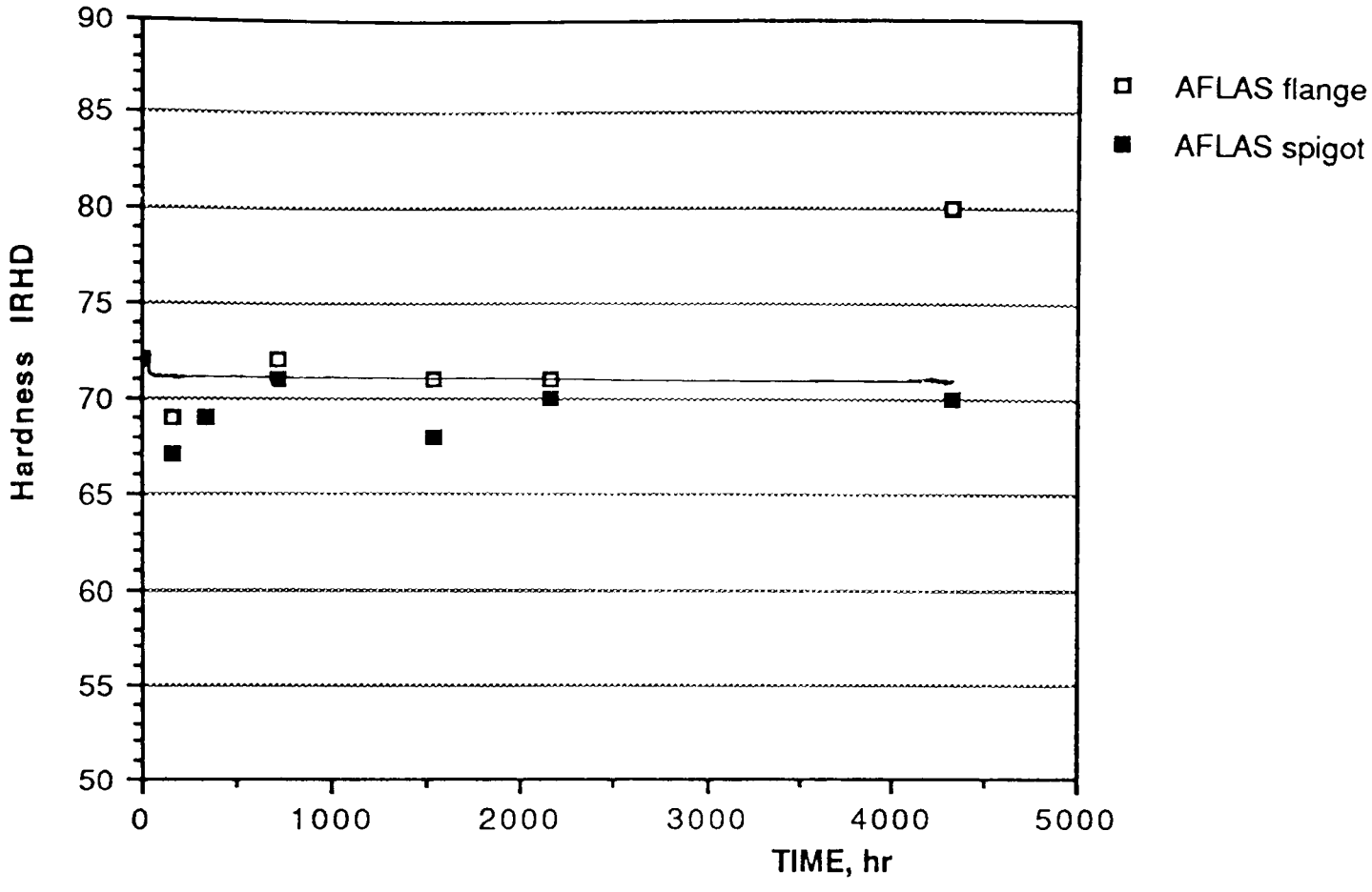

Figure 7.44 Hardness of Aflas O-rings in 100C, 173 bar water against time

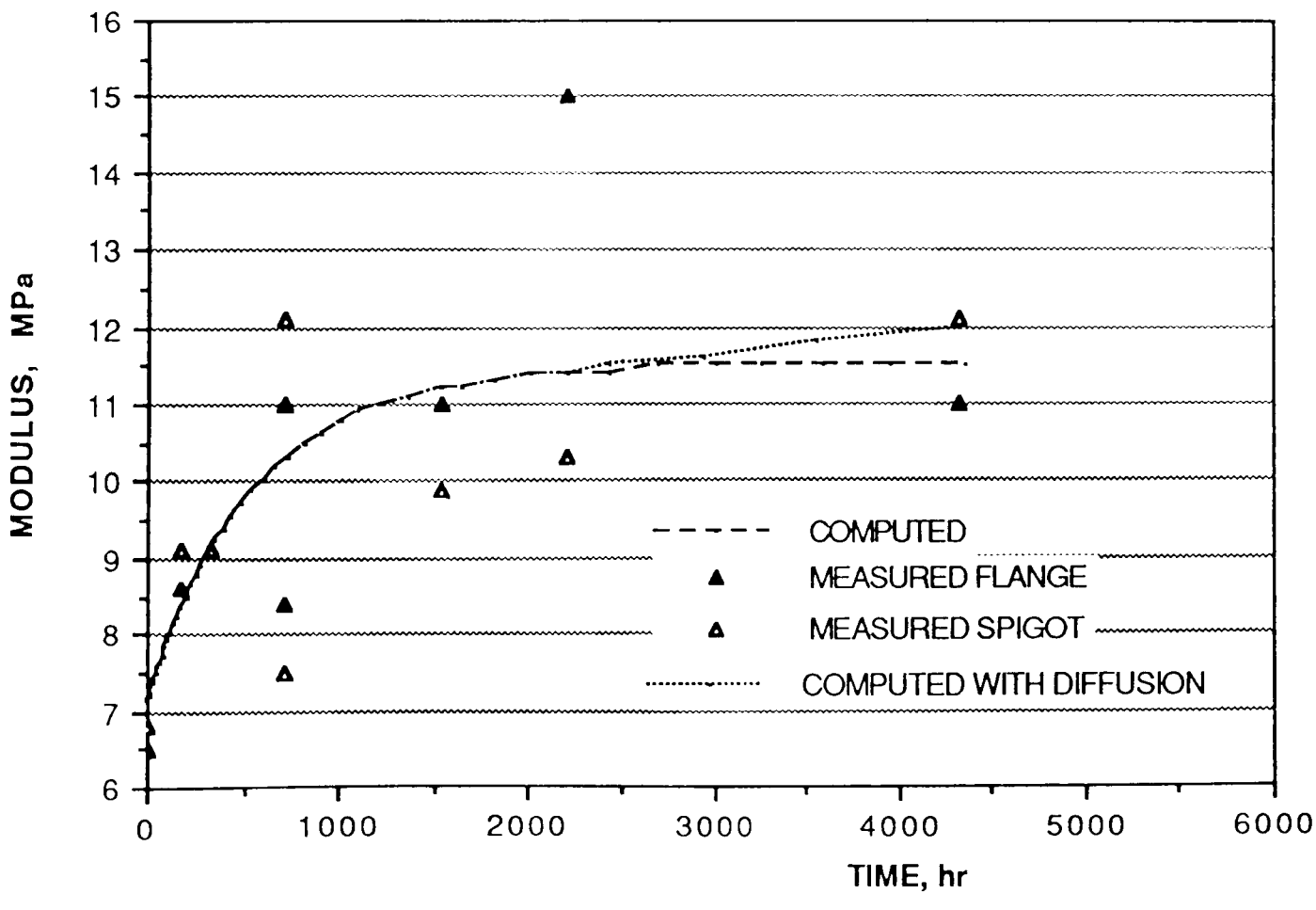

Figure 7.45 Predicted and Measured modulus of high ACN NBR in 100C, 173 bar water

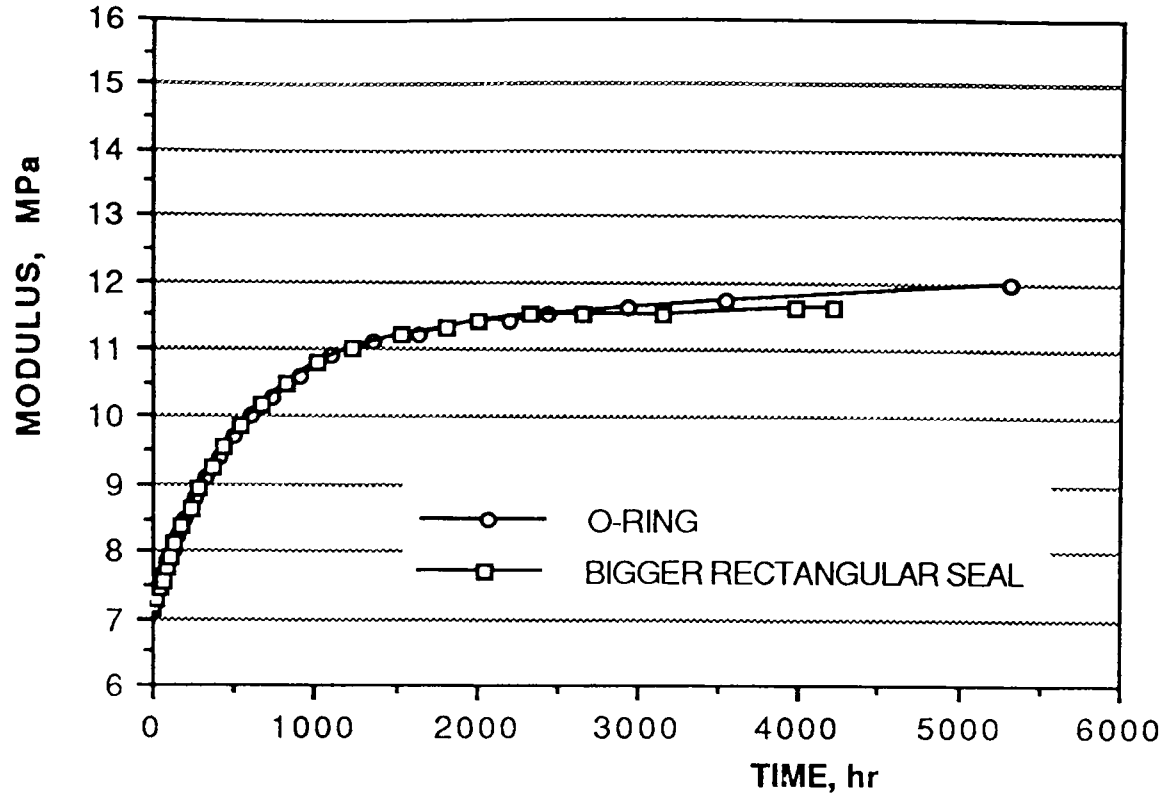

Figure 7.46 Predicted modulus of bigger size, high ACN NBR, rectangular seal

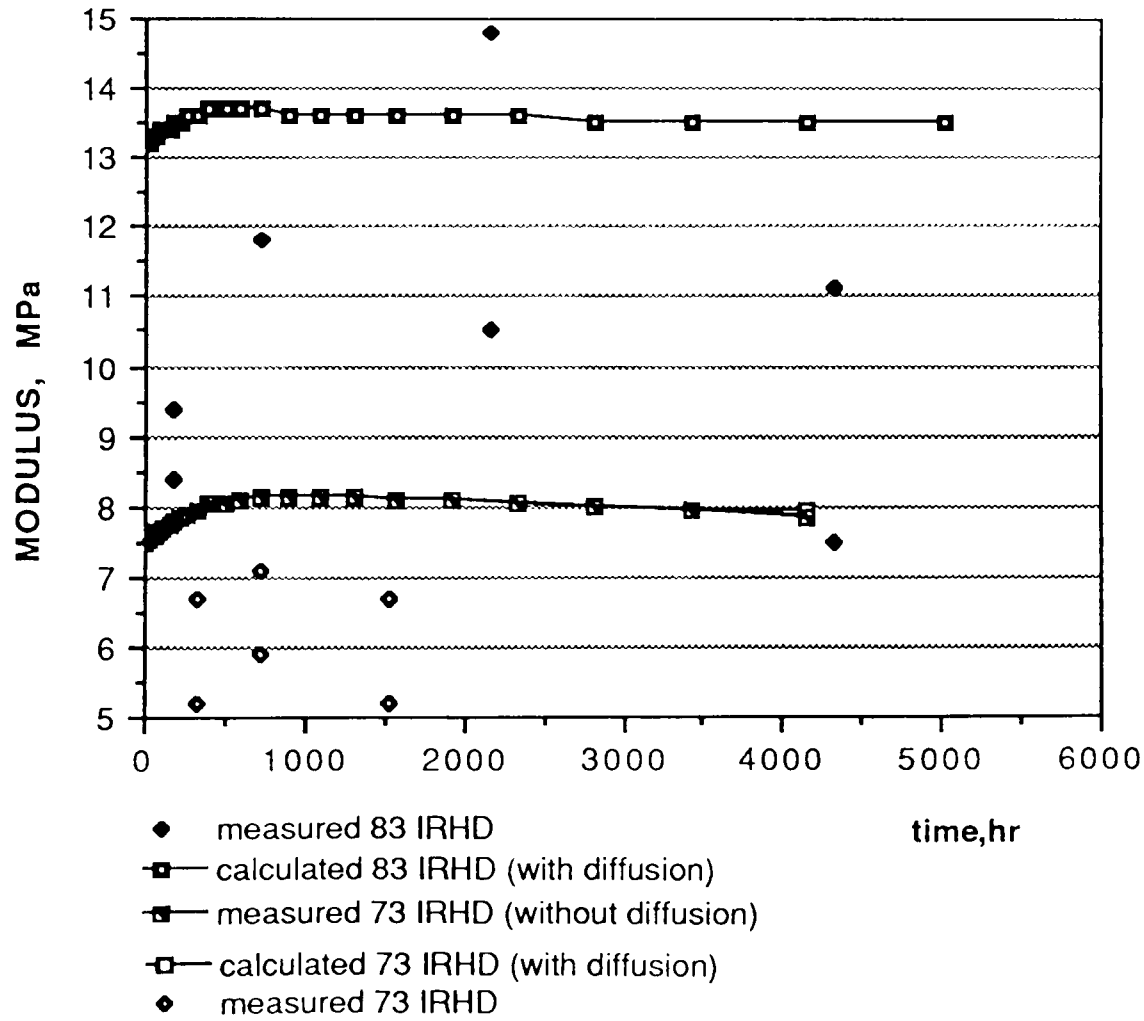

Figure 7.47 Predicted and Measured modulus of EPDM in 100C, 173 bar water

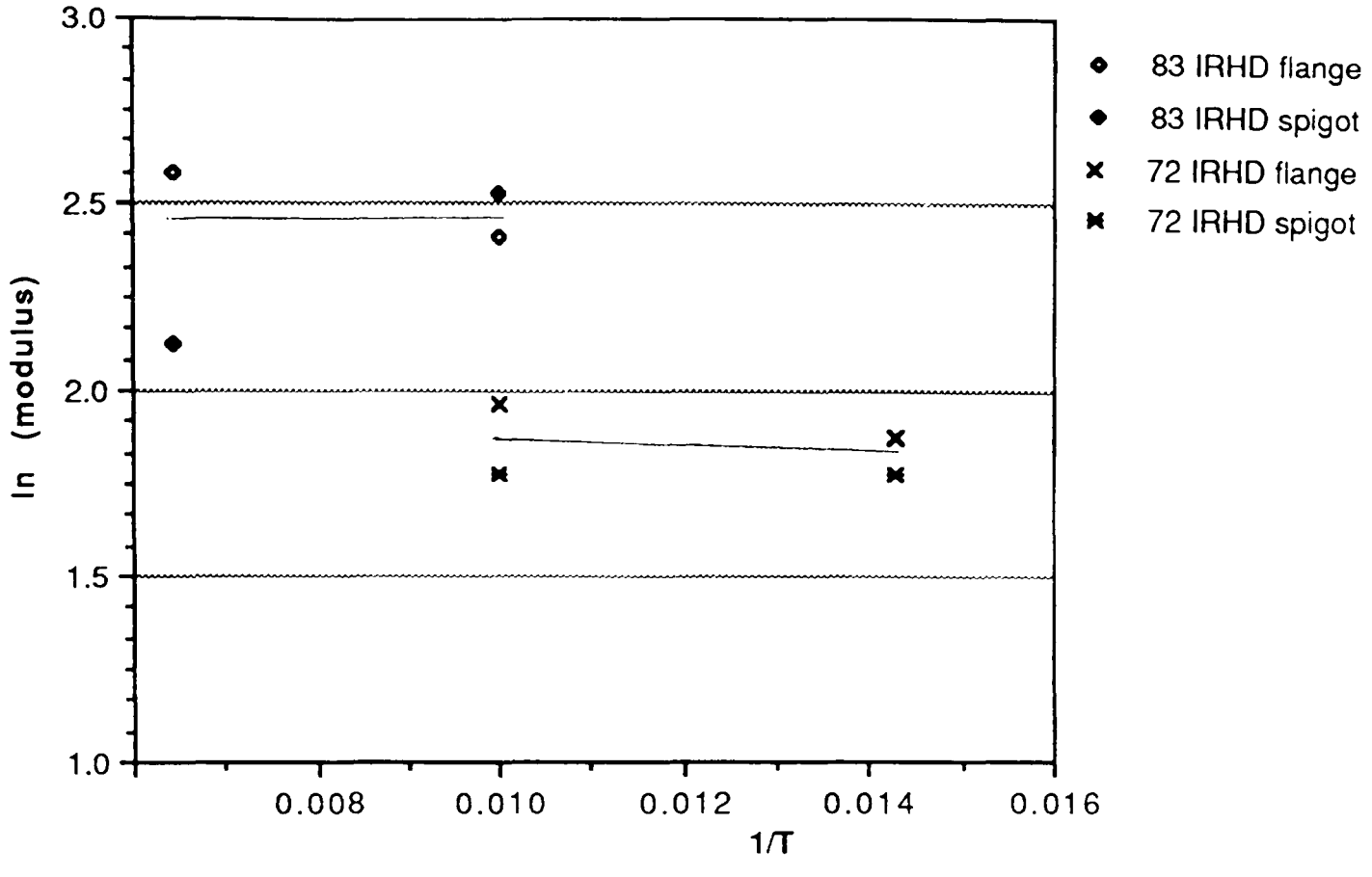

Figure 7.48 Arrhenius plot for modulus of EPDM in 100C, 173 bar water

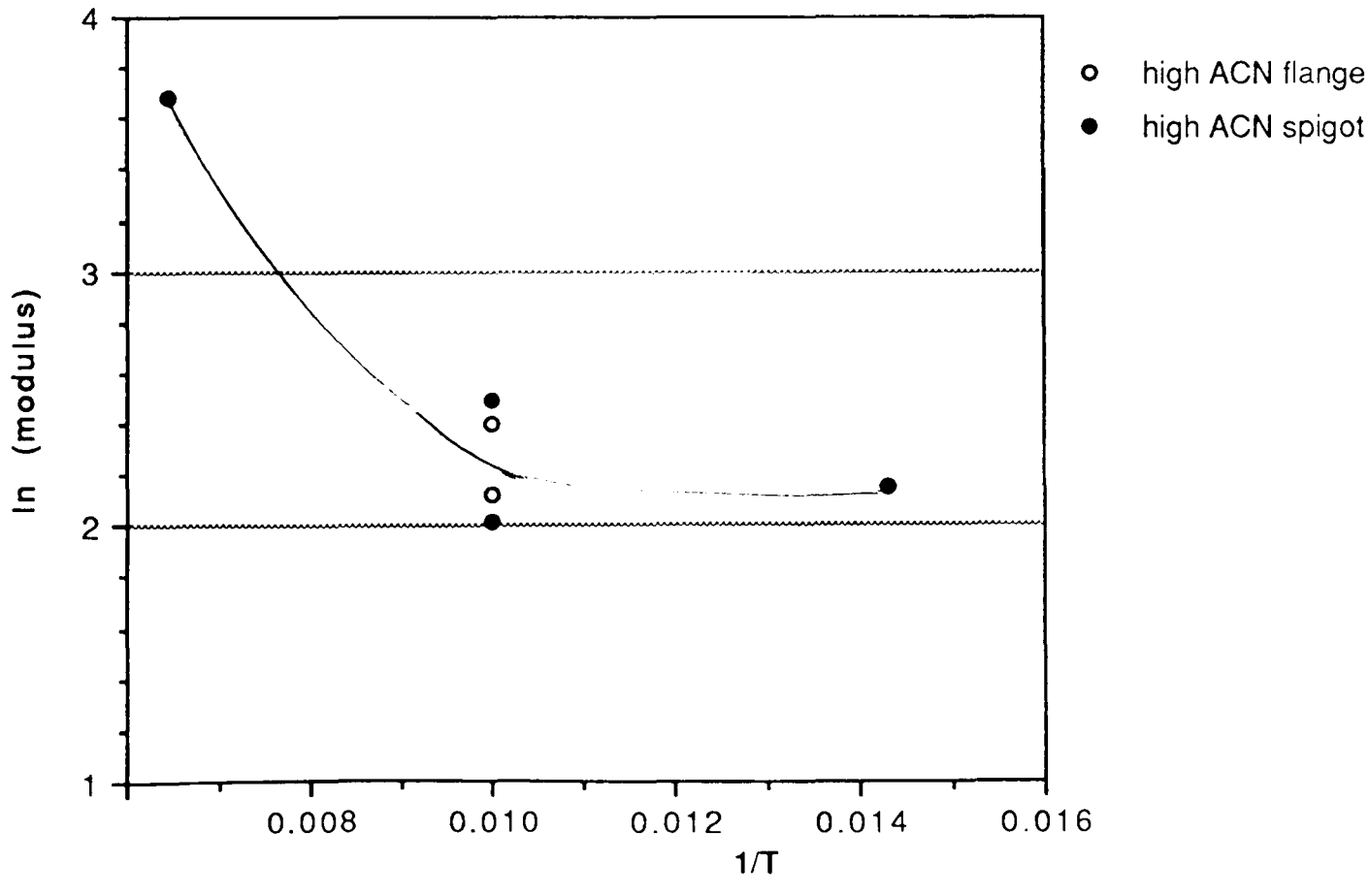

Figure 7.49 Arrhenius plot for modulus of high ACN NBR in 100C, 173 bar water

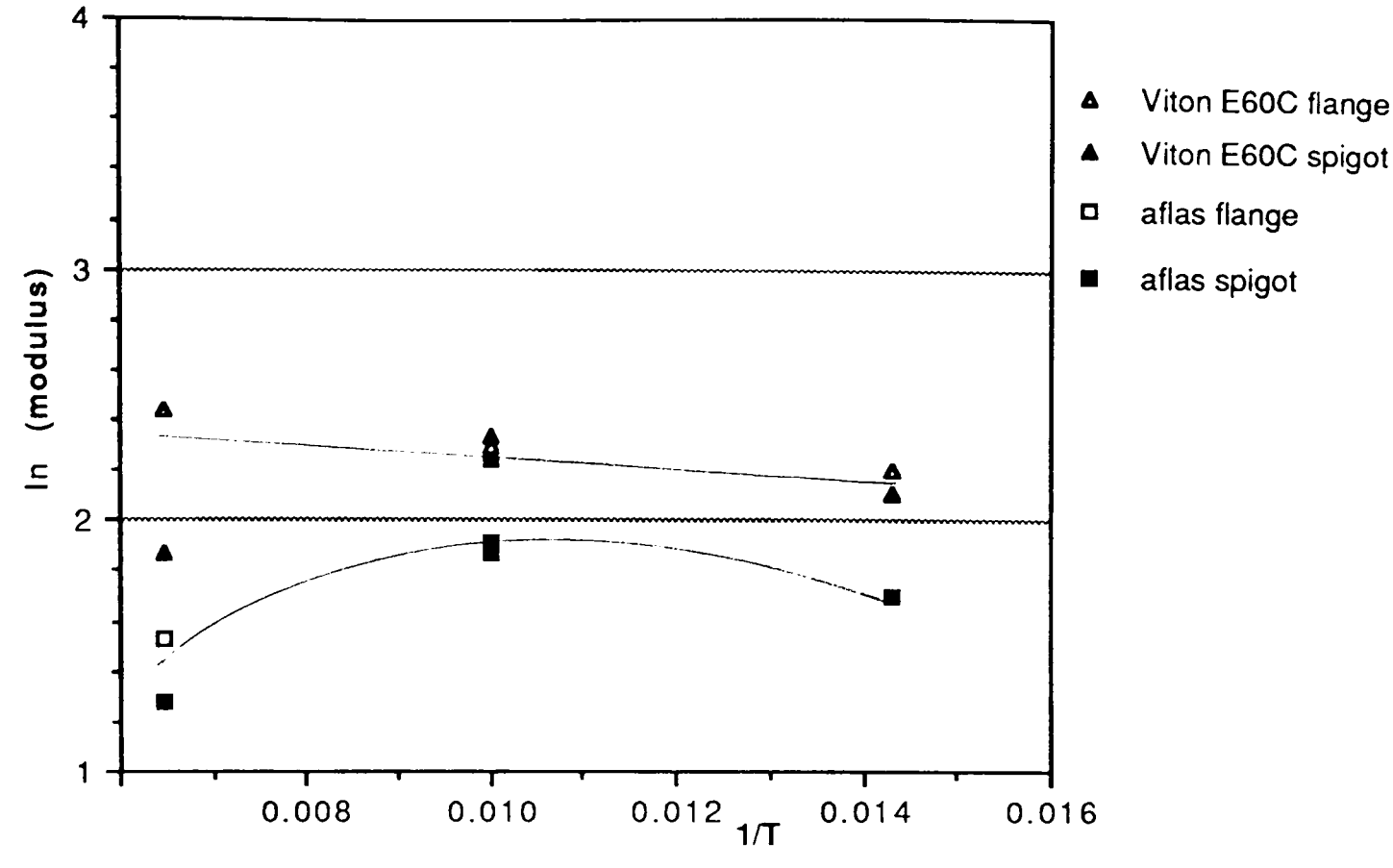

Figure 7.50 Arrhenius plot for modulus of Aflas and Viton E60C in 100C, 173 bar water

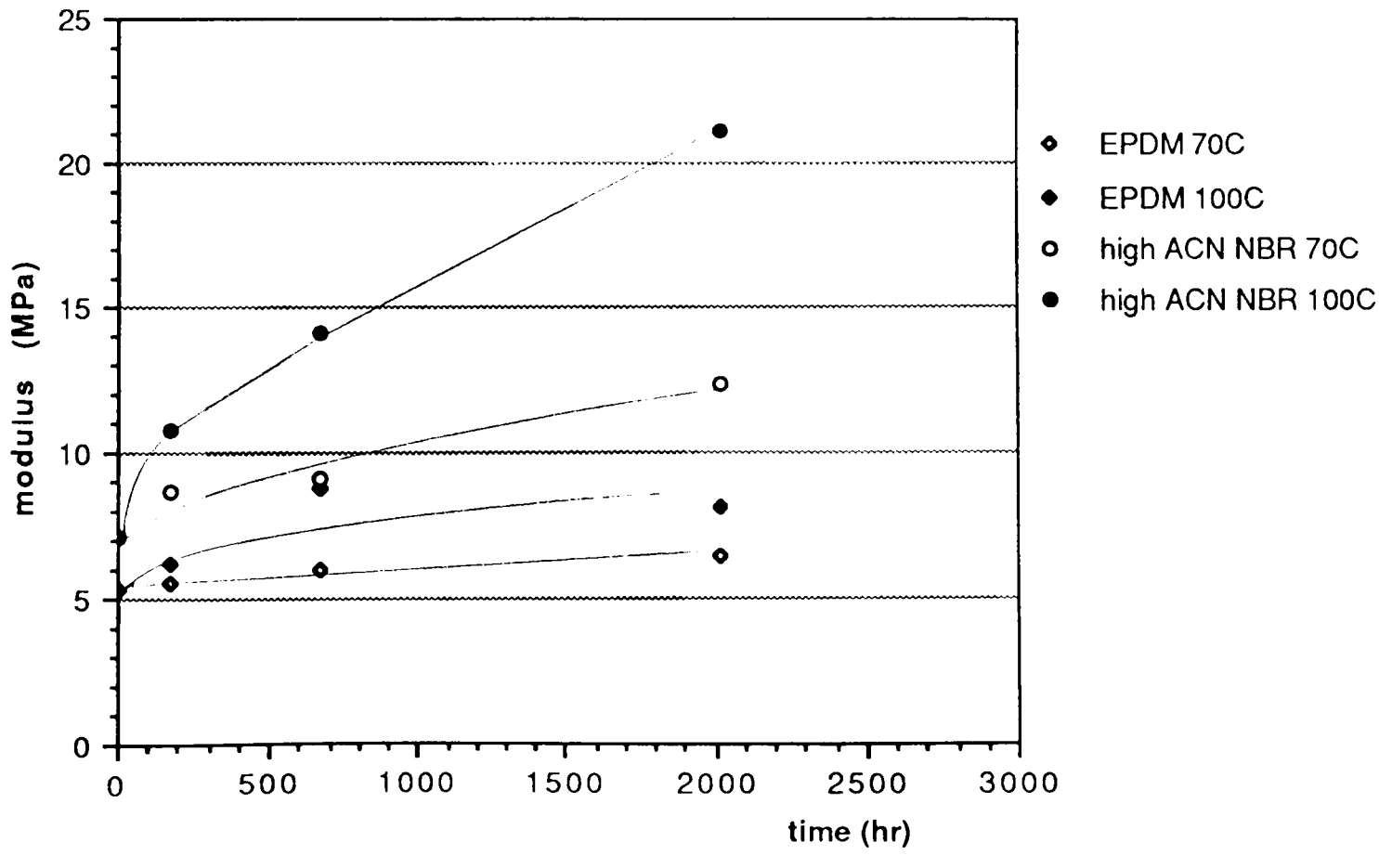

Figure 7.51 Modulus of EPDM and high ACN NBR in 70C, 100C air

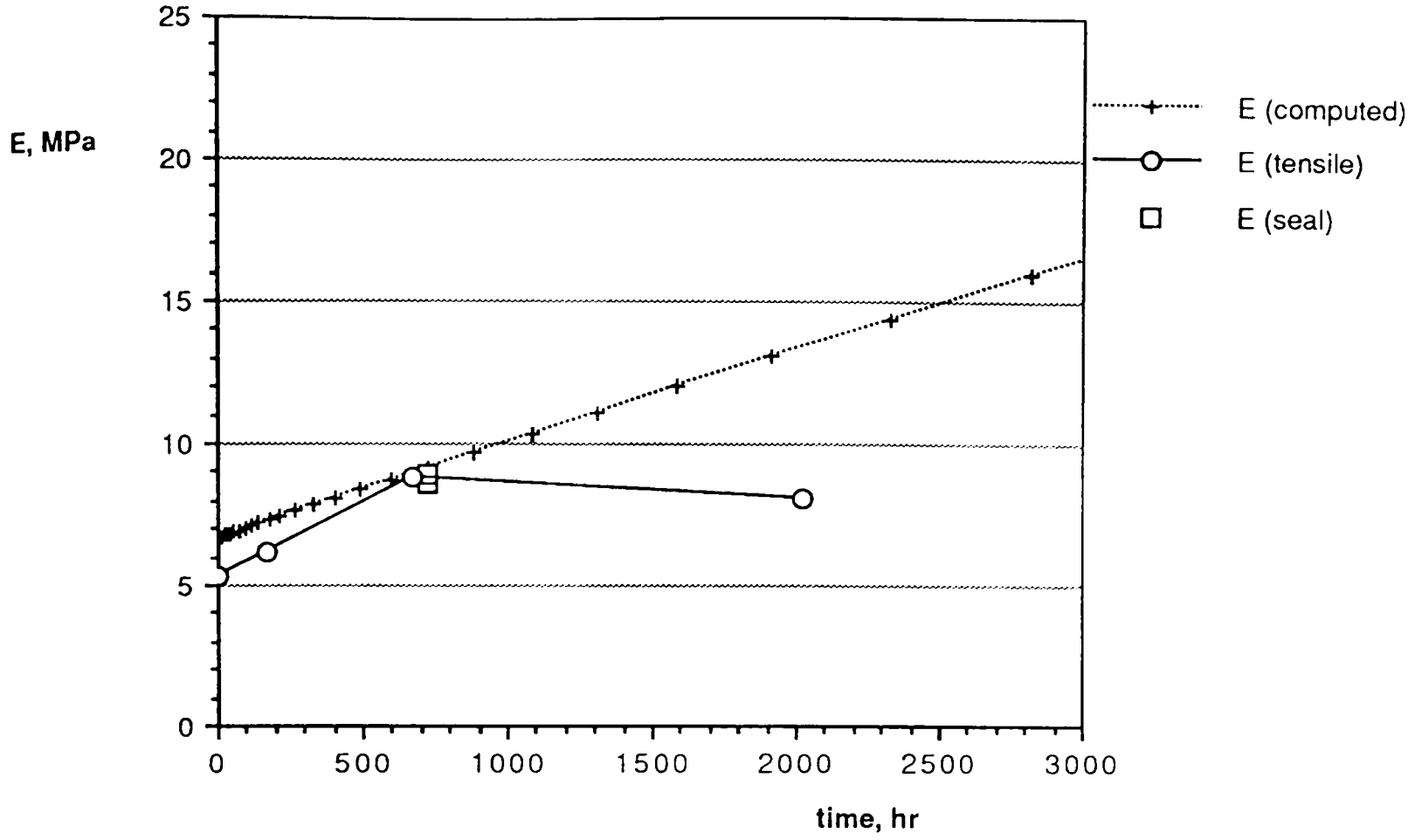

Figure 7.52 Predicted and Measured modulus of EPDM in 1 bar, 100C air

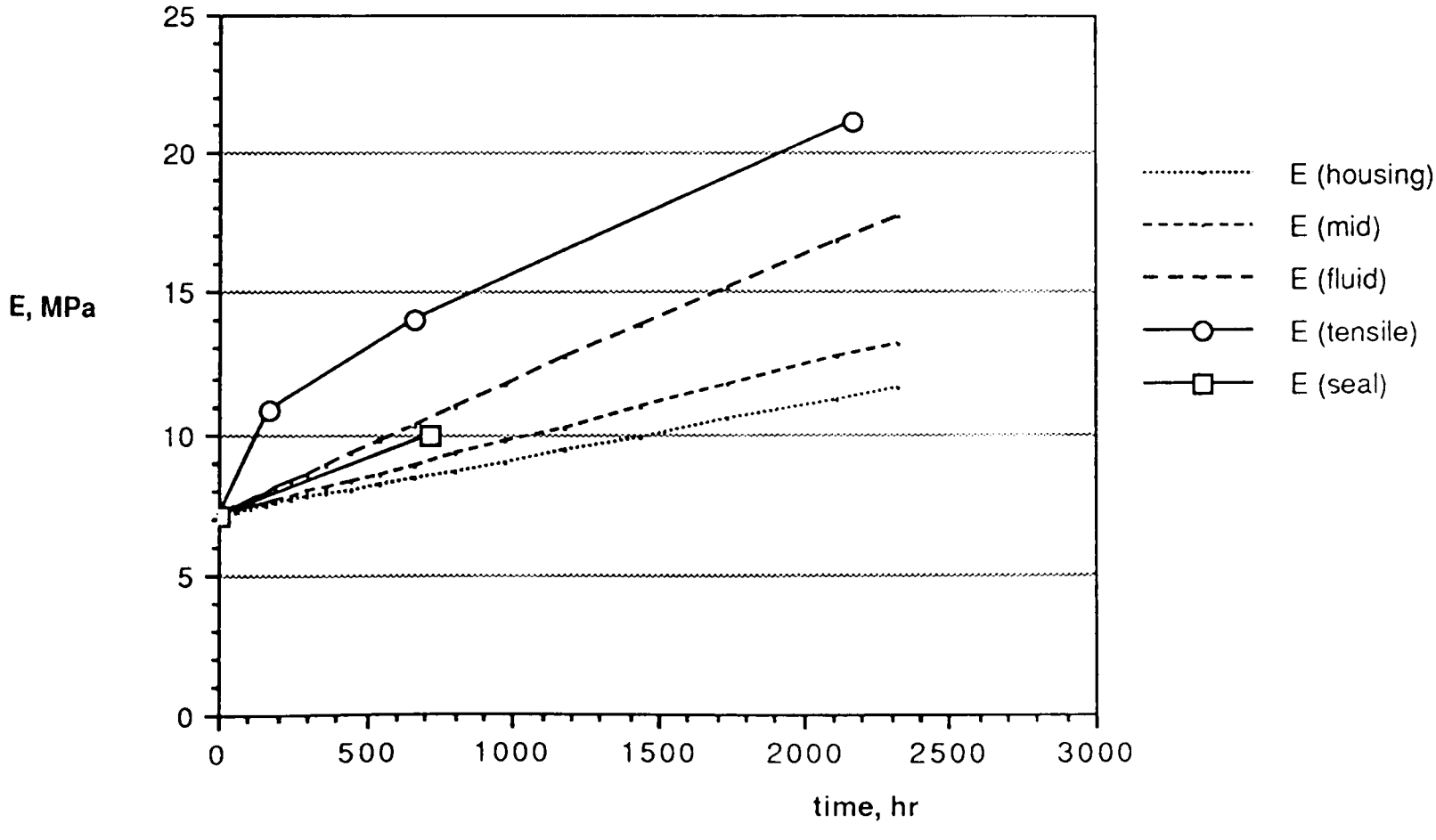

Figure 7.53 Predicted and Measured modulus of high ACN NBR in 1bar, 100C air

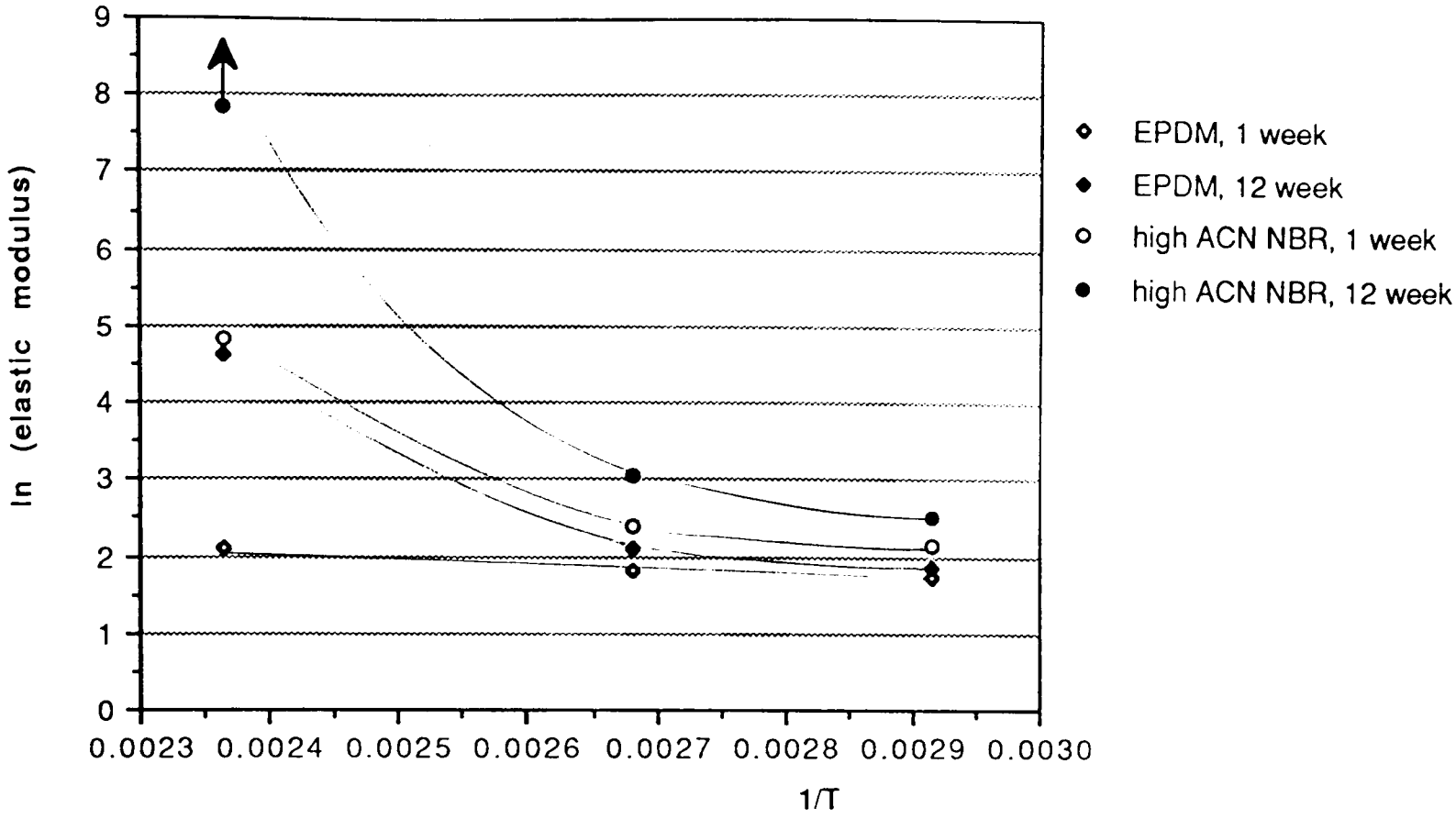

Figure 7.54 Arrhenius plot for modulus of EPDM and high ACN NBR in air

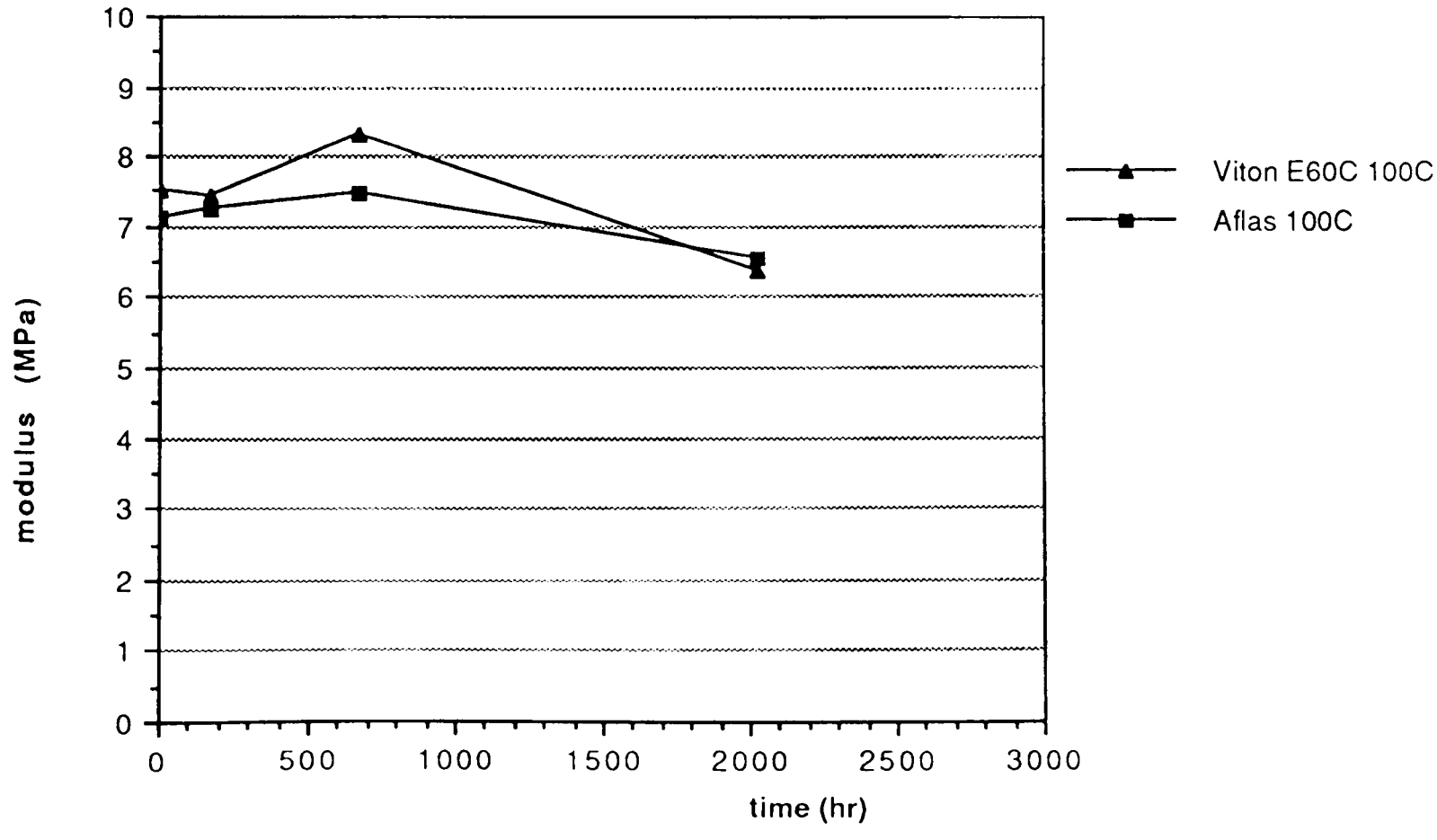

Figure 7.55 Modulus of Viton E60C and Aflas in 100C air

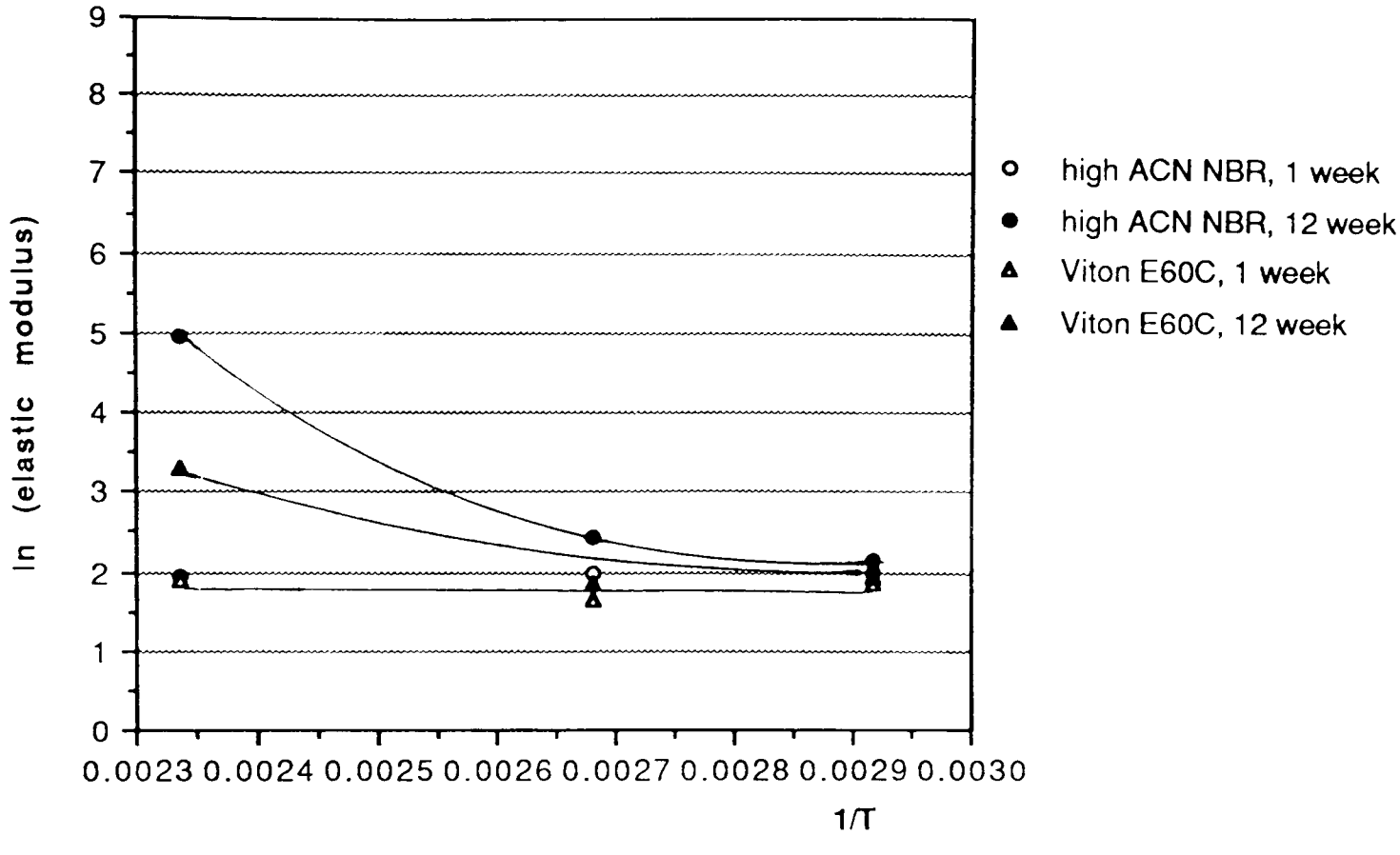

Figure 7.56 Arrhenius plot for modulus of high ACN NBR and Viton E60C in 10% toluene / 90% iso-octane

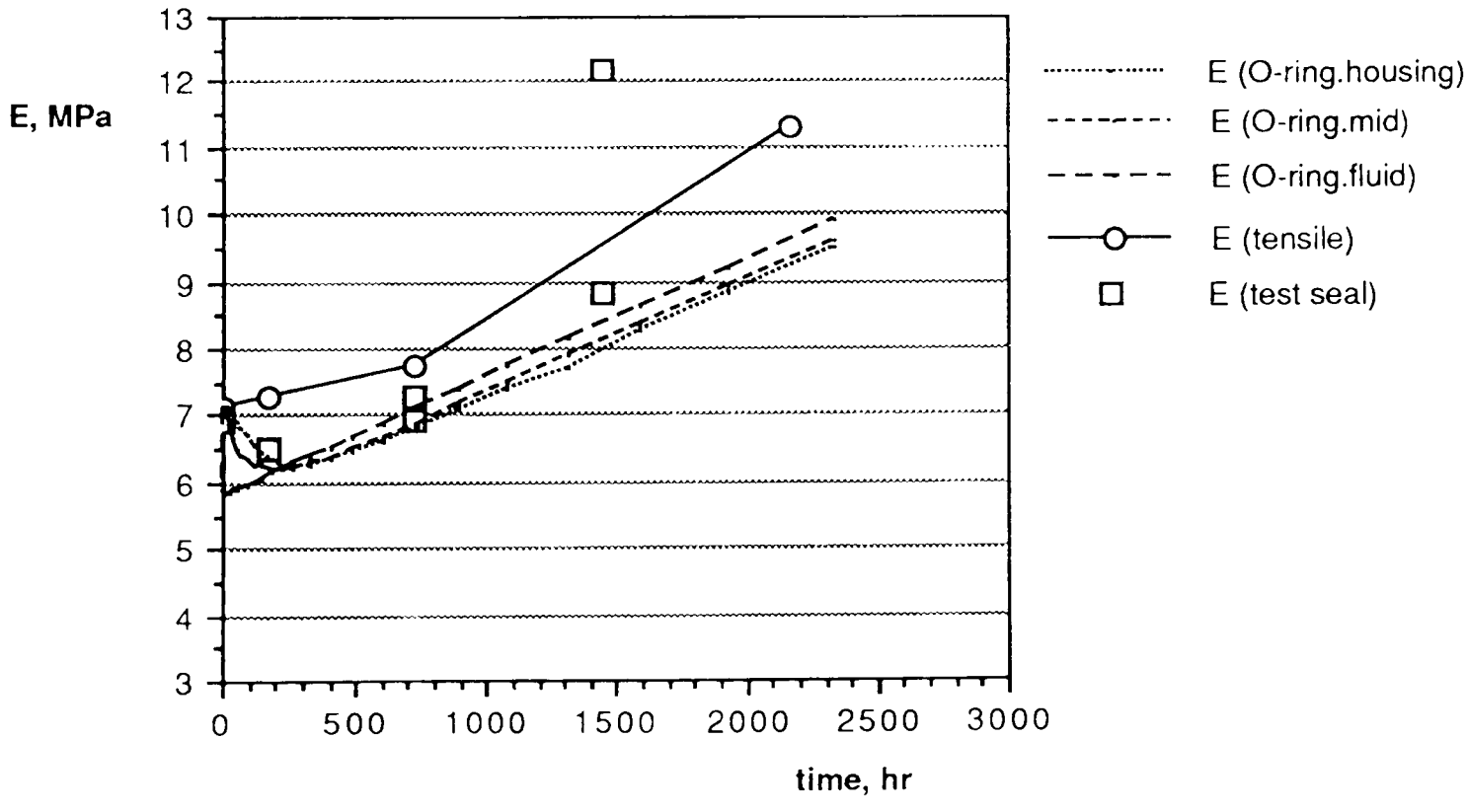

Figure 7.57 Measured and Predicted modulus (to 1st approximation) of high ACN NBR in 173bar, 100C 10% toluene / 90% iso-octane

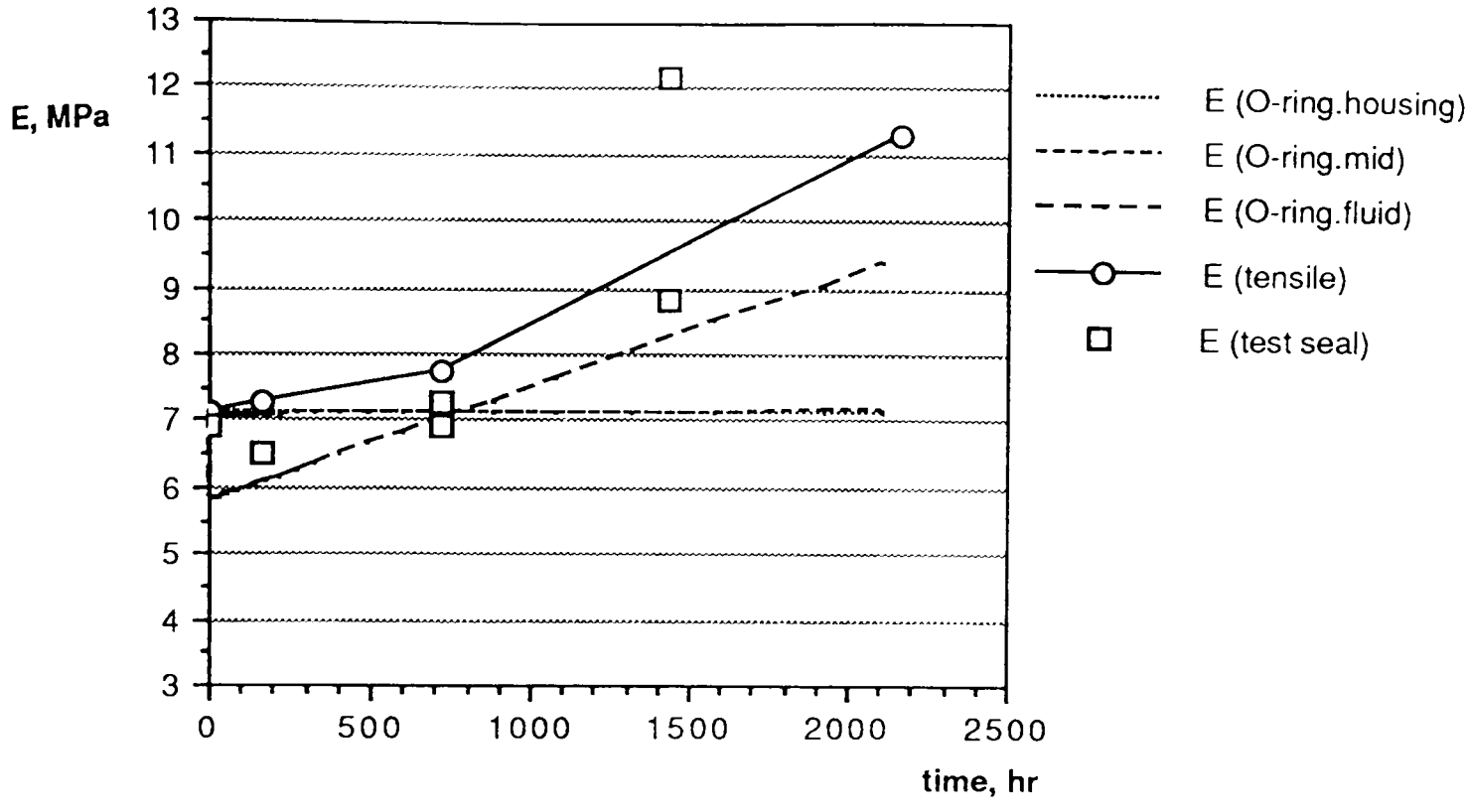

Figure 7.58 Measured and Predicted modulus (with significant fluid consumption of high ACN NBR in 173 bar 100C 10% toluene / 90% iso-octane

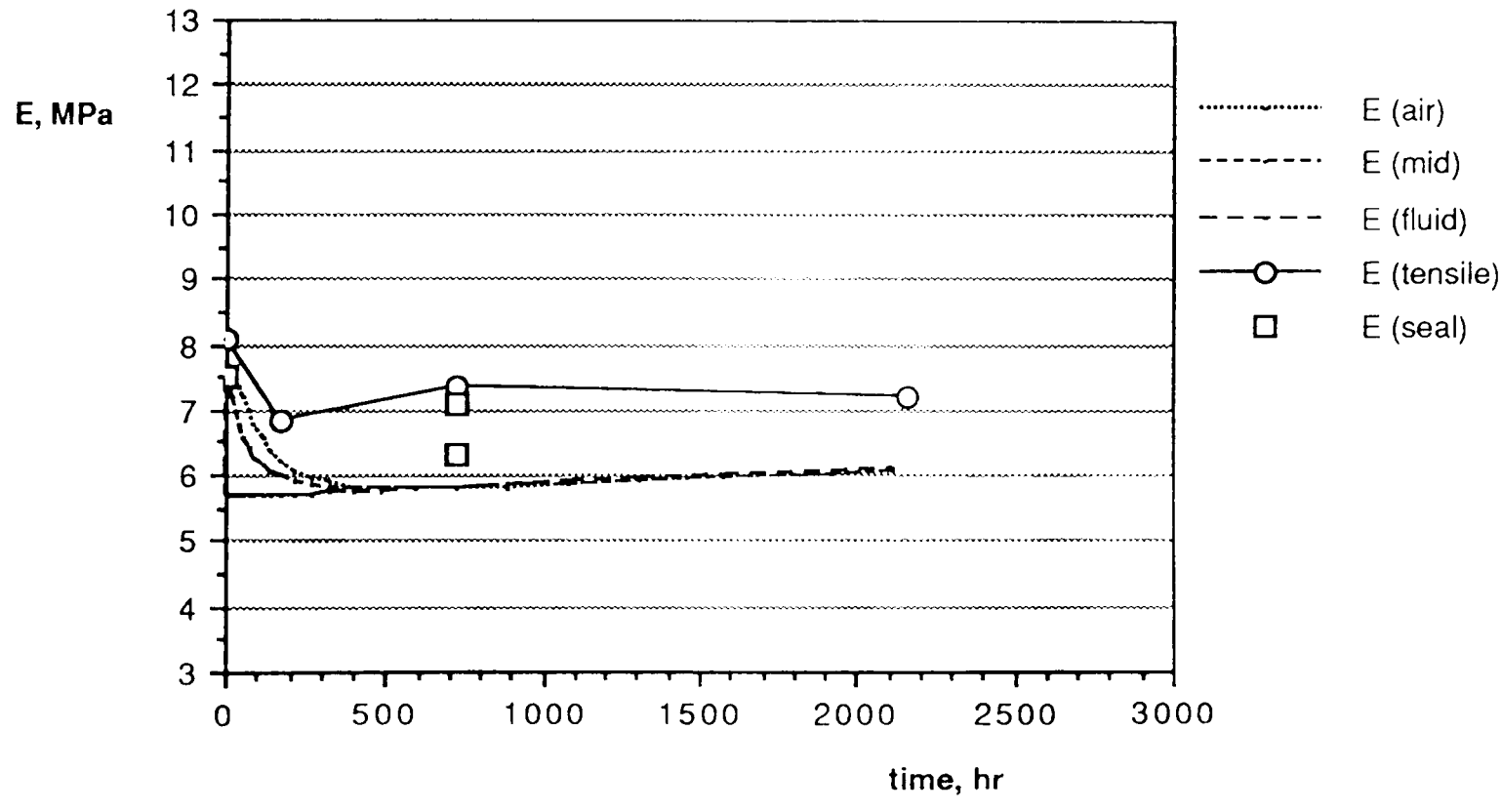

Figure 7.59 Measured and Predicted modulus (1st approximation) of HNBR in 173 bar, 70C 10% toluene / 90% iso-octane

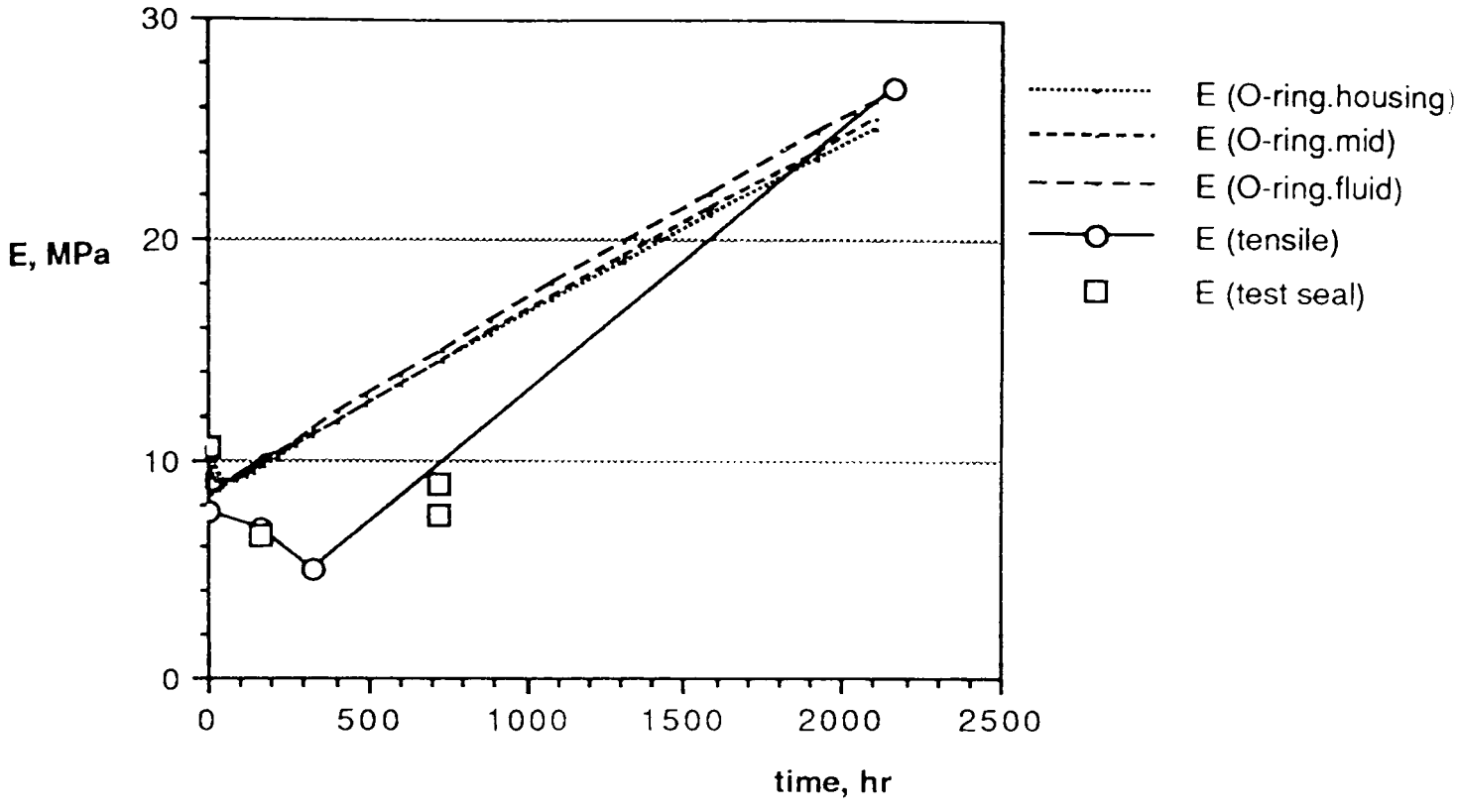

Figure 7.60 Measured and Predicted modulus of Viton E60C in 173bar, 155C 10% toluene / 90% iso-octane

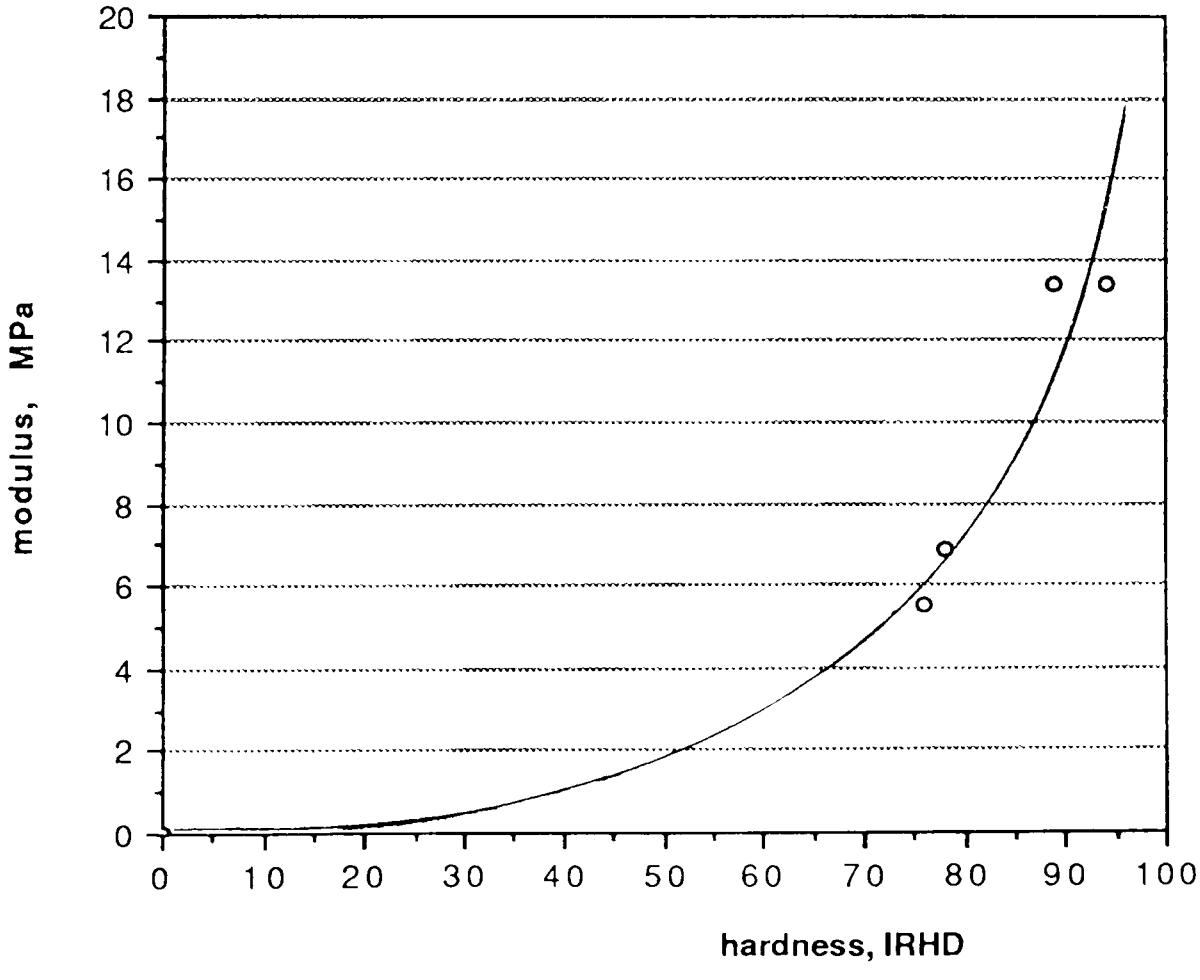

Figure 7.61 Modulus to hardness relationship for Viton E60C

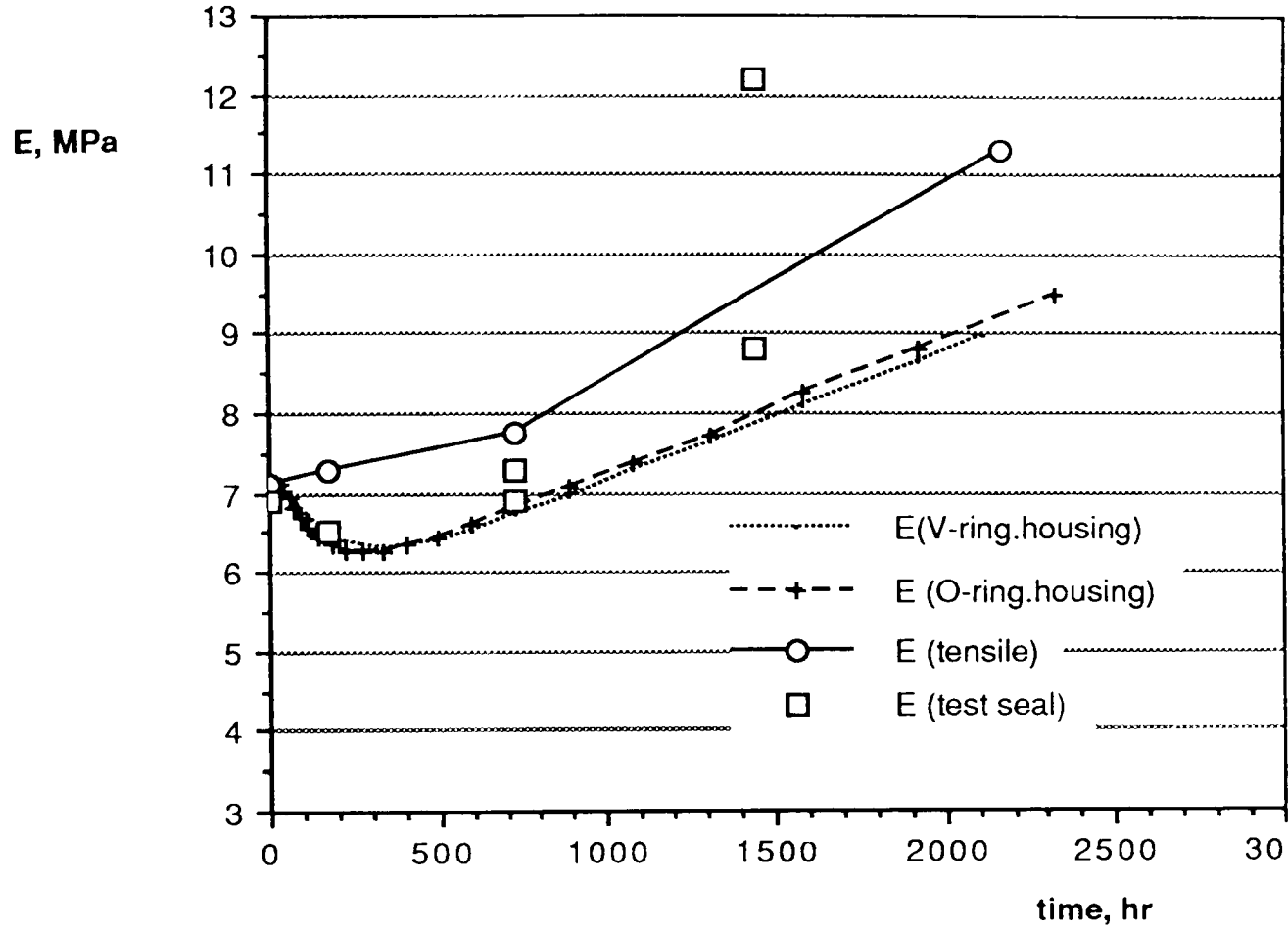

Figure 7.62 Predicted modulus of high ACN NBR V-ring in 173 bar, 100C 10% toluene / 90% iso-octane

8 SEMI-EMPIRICAL APPROACH TO O-RING INTERFERENCE FORCE PREDICTION

At present the computer model does not incorporate contact stress analysis calculations, therefore we consider the possibility of calculating retained interference force semi-empirically.

Retained interference force and compression set are important-quantities affecting seal performance. These have been measured for seals after each test performed in the BHR seal function rig. In this Chapter, simple formulae are derived empirically to describe the long term trends for both compression set and retained interference force of seals in high temperature-pressure water. A limitation of this approach is the scatter inherent in the experimental data, combined with the problem of generating sufficient data permits in tests of long duration.

All figures for Chapter 8 are presented at the end of the Chapter.

8.1 Empirical Representation of Compression Set

8.1.1 Time Effect

When O-rings were tested in 100°C, 173 bar water for 168 hour, 336 hour, 720 hour, 1560 hour, 2160 hour and 4320 hour, it is observed that :

i. EPDM performed very well in long term. It showed little increase with time in compression set even after a long period. Accelerated tests at higher temperature are justified in such case to study long term ageing.
ii. high ACN NBR showed significant increase of compression set with time.
iii. Viton E60C had the lowest initial set of about 15%. It however had the highest increase of compression set with time.
iv. Aflas had a high initial set at or above 50%. This is recognized as the physical compression set being 'frozen' at room temperature. Recovery of seals with high glass transition temperature are inhibited at room temperatures. When temperature increases, seals should be able to recover their physical compression set. The increase in compression

set (chemical dominating) of Aflas against time was however slow.

If linear compression set versus time curves (C_S,% -v- t,hr) are fitted to the experimental results in Fig 8.1-8.4, they have the following relationship :

i. $C_S = 30 + 0.0036t$ at 100°C for EPDM

ii. $C_S = 28 + 0.006t$ at 100°C for high ACN NBR

iii. $C_S = 15 + 0.010t$ at 100°C for Viton E60C

iv. $C_S = 51$ (independent of t) at 100°C for Aflas

8.1.2 Temperature Effect

Graphs of (ln C_S) against inverse of absolute temperature for the 336 hour tests at 70°C, 85°C and 100°C, and for the 720 hour tests at 70°C, 100°C and 155°C are plotted in Fig 8.5-8.8 to show the effect of temperature on compression set. For high ACN NBR, Viton E60C and Aflas, the compression set behaviour after 336 hour soak and those after 720 hour soak follow similar trends. From the graphs, we obtain the following relationships for temperature to 155°C:

i. $C_S = a_1\, e^{-4000/T}$ at 336-720 hour for high ACN NBR

ii. $C_S = a_2\, e^{-4760/T}$ at 336-720 hour for Viton E60C

iii. $C_S = 0.59\,(T-Tg)$ at 720 hour for Aflas

where a_1, a_2 are constants.

EPDM behaves differently in the 336 hour tests from the 720 hour tests, therefore no simple trend can be drawn.

Viton E60C is most affected by temperature. After 720 hour soak at 70°C, Viton E60C had the lowest compression set of below 10%, while both EPDM and high ACN NBR had 20-30% compression set, and Aflas had 30-40% compression set. However, at 155°C, Viton E60C and Aflas both had 80% compression set, high ACN NBR had 100% compression set, while EPDM had only 35% compression set. EPDM in general performed well with temperature.

8.1.3 Combined Effect

If we consider the present understanding of material ageing, the most likely form of equation for compression set is :

$$C_S = A(T-Tg)\log(t/to) + Btexp(-E/RT) \quad \text{..... (8.1)}$$

where the first term represents a physical effect, and the second term represents a chemical effect.

In the long term, the change of the physical term with time is small compared with the chemical term and to a first approximation we can assume the physical term is constant with time. i.e.

$$C_S = A(T-Tg) + Btexp(-E/RT) \quad \text{..... (8.2)}$$

The % compression set relationships for experimental data can therefore be arranged as follows for temperatures to 155°C :

i. $C_S = 0.27(T-Tg) + 273t\, e^{-4000/T}$ for high ACN NBR

ii. $C_S = 0.15(T-Tg) + 3500t\, e^{-4760/T}$ for Viton E60C

iii. $C_S = 0.59(T-Tg)$ for Aflas

8.2 Retained Force Measurements

8.2.1 Time Effect

The retained interference force (F, %) of O-rings tested in 100°C, 173 bar water for 168 hour, 336 hour, 720 hour, 1560 hour, 2160 hour and 4320 hour is plotted in Fig 8.9. For all four materials, retained force follows a linear relationship with time. The general performance characteristics are :

i. EPDM performed best in long term. It had a moderate physical relaxation, but the slowest decrease of force with time. Together with its high performance at higher temperature at 155°C, EPDM appears to be the outstanding performer in high temperature water tests.

ii. high ACN NBR had the lowest short term physical relaxation, but the highest rate of long term relaxation. Its application to long term and high temperature in water is not satisfactory.

iii. Viton E60C had similar trend in material properties change as in high ACN NBR, but its long term relaxation was slower than that of high ACN NBR. Therefore, it appears to perform better than high ACN NBR in longer term water applications.

iv. Aflas had the highest initial physical relaxation and high rate of long term relaxation, its performance in water is poor.

The following are the best linear fits to the experimental results :

i.	$F = 54 - 0.0057t$	at 100°C for EPDM
ii.	$F = 92 - 0.042t$	at 100°C for high ACN NBR
iii.	$F = 74 - 0.012t$	at 100°C for Viton E60C
iv.	$F = 36 - 0.050t$	at 100°C for Aflas

For the four materials, the compression set and retained force data generally agreed for EPDM and Viton E60C. Both types of measurement indicate EPDM performs well, while Viton E60C gradually deteriorates over long term. However, the two types of measurement disagree on the performance of high ACN NBR and Aflas O-rings. Measured retained force of Aflas O-rings had dropped to zero after 720 hour in 100°C water, and that of high ACN NBR had dropped to zero after 2200 hour. Compression set for the O-rings at the conditions were high, between 40% to 60%, but they were far from 100% set. No leakage had been recorded for all these test. This suggests the Aflas O-rings had no leakage while sitting at zero retained force for over 3500 hour (from 720 hour to 4320 hour), and the high ACN NBR O-rings had no leakage while sitting at zero retained force for over 2000 hour (from 2200 hour to 4320 hour). We therefore conclude that permanent compression set is a better indication of seal performance than the measured retained force after test. Long term seal life prediction based on permanent compression set is preferred.

One possible explanation for the poor correlation between the measured retained force after tests and seal performance, is that seals are not allowed to recover from strained position before retained force measurements. These measured retained force are highly determined by thermal expansion, physical sluggish of the seals at cool temperature, rather than by the chemical status of the seals. After test retained force measurement is useful to show possible seal failure at cool start, but not the long term performance of seals at constant high temperatures.

8.2.2 Temperature Effect

Retained force measured for high ACN NBR, Viton E60C and Aflas dropped to zero after 720 hours in water at 155°C, although the seals did not leak. These materials cannot be usefully analysed further. To study temperature effect on retained force of EPDM, which the quality of data allows, the logarithm of force relaxation (100% - F) is plotted against inverse of absolute temperature in Fig 8.10. The deduced Arrhenius equation for temperature to 155°C is :

i. $100\% - F = a_3 e^{-709/T}$ at 336-720 hour for EPDM

where a_3 is a constant

Arrhenius plots for force relaxation of high ACN NBR, Viton E60C and Aflas at 70°C, 85°C and 100°C are also shown in Fig 8.11 - 8.13. No definite trend can be drawn.

8.2.3 Combined Effect

Applying the format of the compression set equations to retained force, we have :

$$100\% - F = A(T-Tg) + Btexp(-E/RT) \quad \text{..... (8.3)}$$

the empirical equation for EPDM to temperature 155°C is :

$$100\% - F = 0.41(T-Tg) + 0.038te^{-709/T}$$

8.3 Retained Force Calculated from Compression Set

Another approach for predicting retained force for seals exposed to high temperature for long term is by calculation from compression set using equation 4.71. This has been done for EPDM, high ACN NBR, Viton E60C and Aflas in 100°C water. The results are compared with measured retained force after test in Fig 8.14. The calculated values are generally much higher than the measured values. As we have discussed in the previous section, the retained force calculated from compression set is likely to be a better indicator of performance of seals than direct measurement, which are subject to inaccuracies discussed above.

It appears from calculated retained force that high ACN NBR and Viton E60C are not suitable for long term (over 9 months) application in 100°C water. Aflas can seal for long term at constant high temperature, but will easily fail with temperature and pressure cycling for which the seals need to cool start. EPDM appears to be sealing well for 2-3 year.

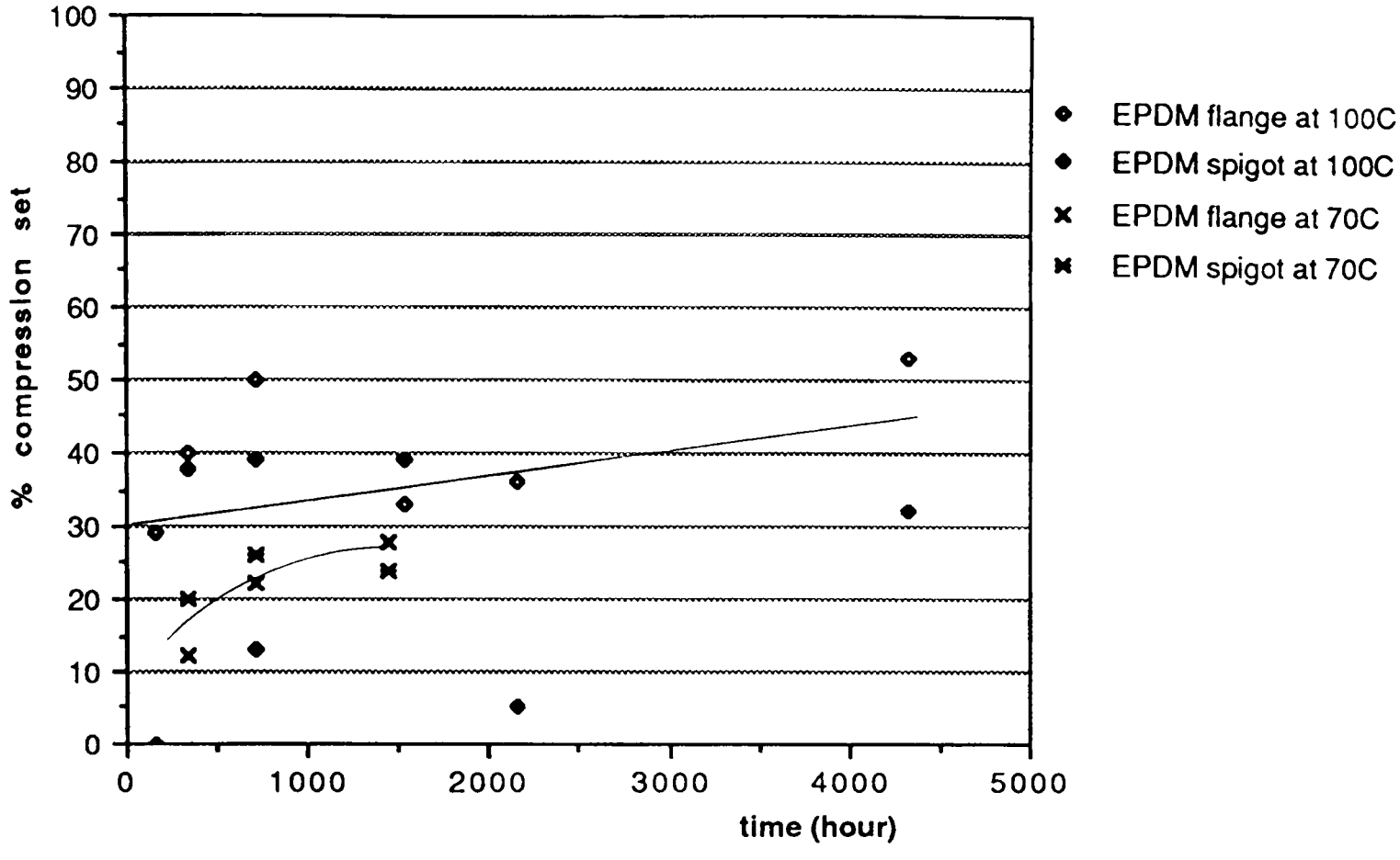

Figure 8.1 % compression set of EPDM in 70C and 100C, 173 bar water against time

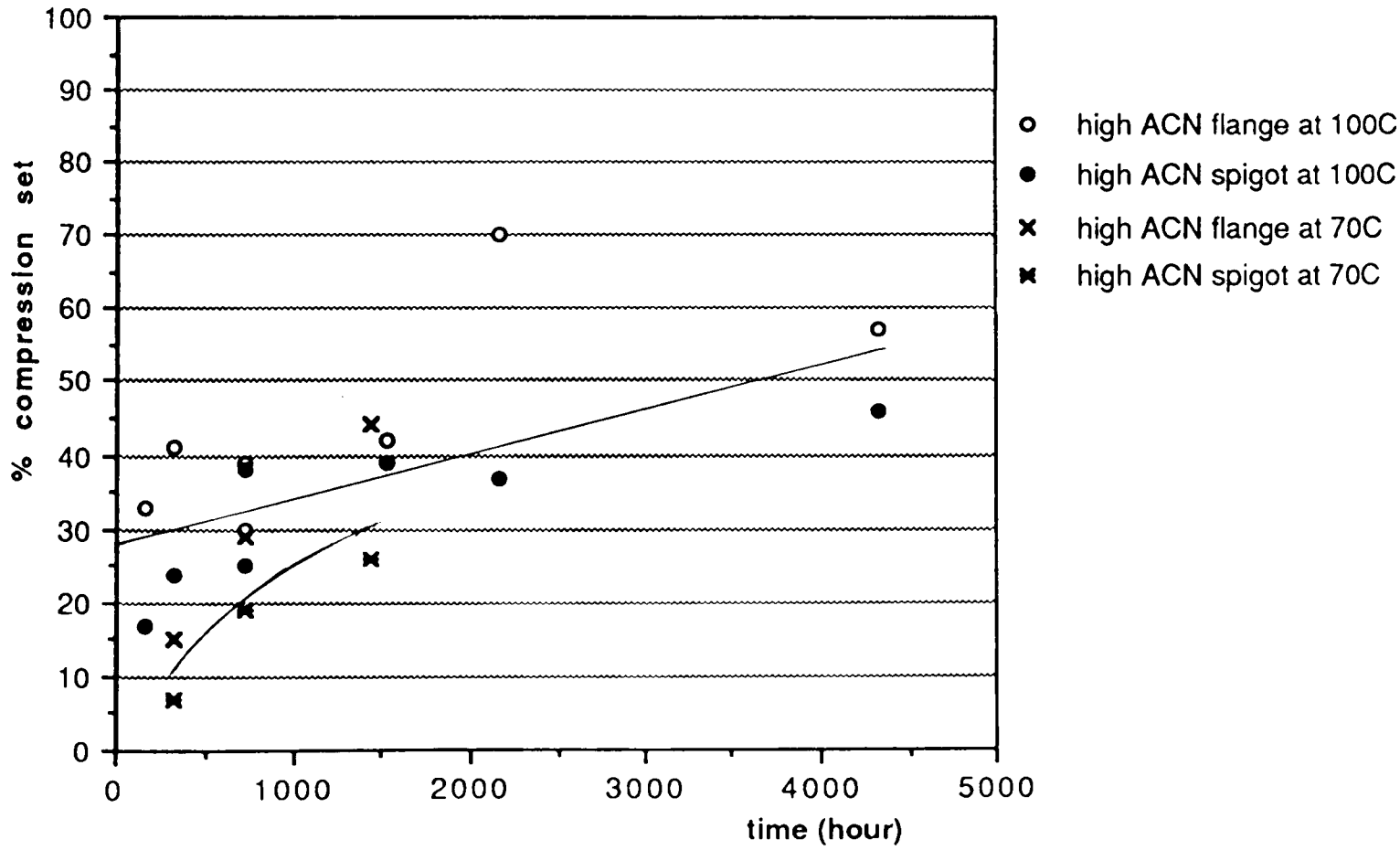

Figure 8.2 % compression set of high ACN NBR in 70C and 100C, 173 bar water against time

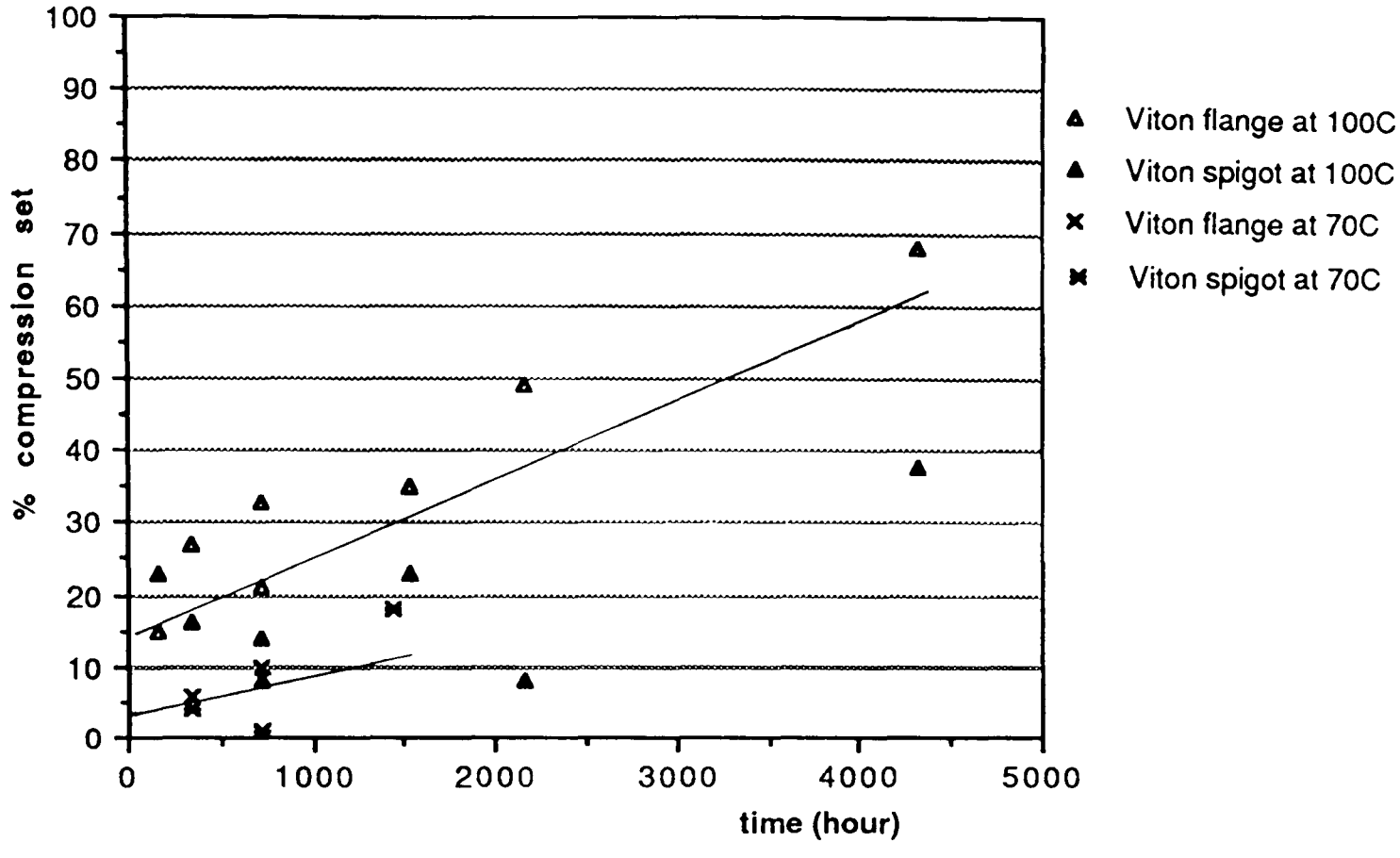

Figure 8.3 % compression set of Viton E60C in 70C and 100C, 173 bar water against time

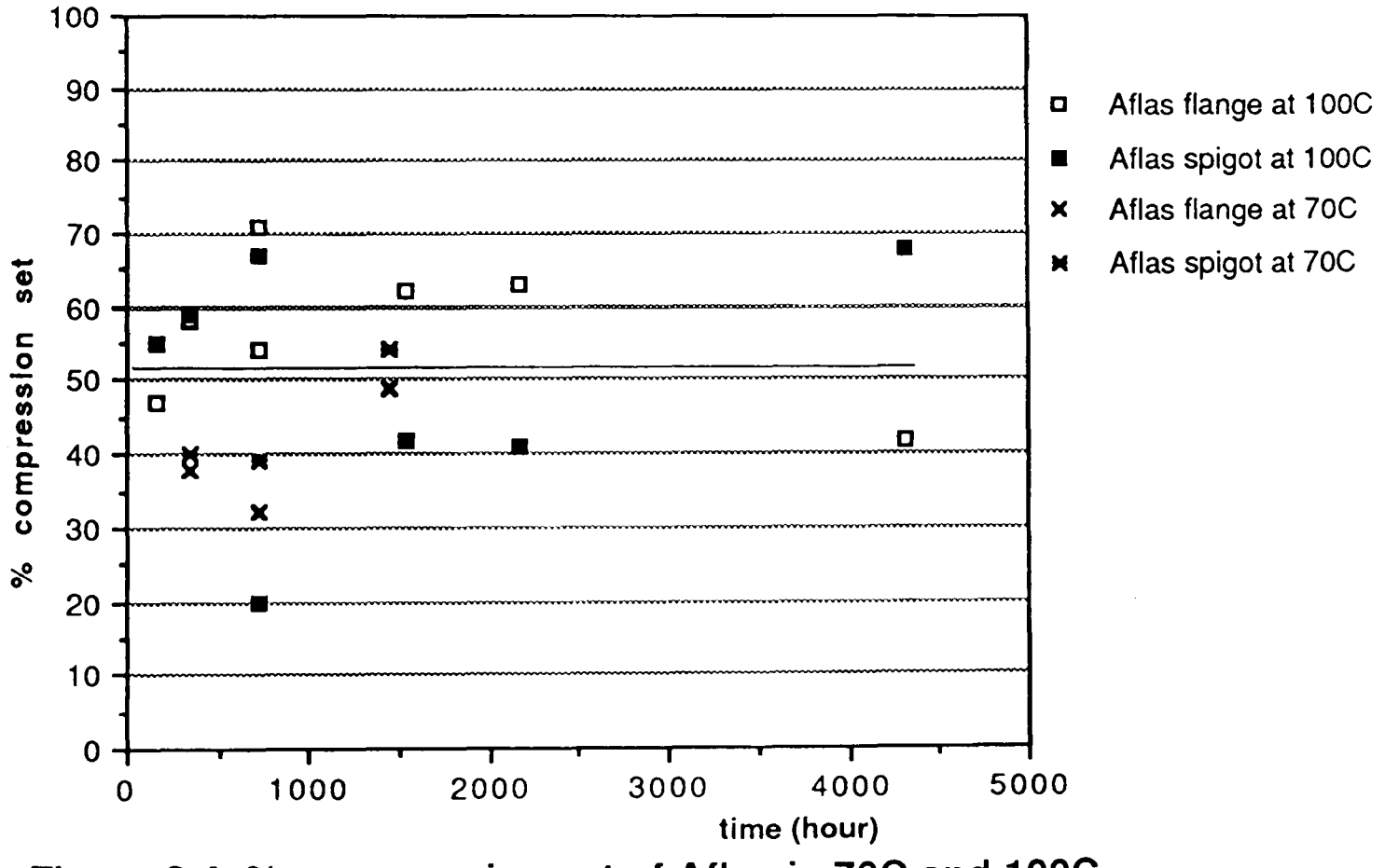

Figure 8.4 % compression set of Aflas in 70C and 100C, 173 bar water against time

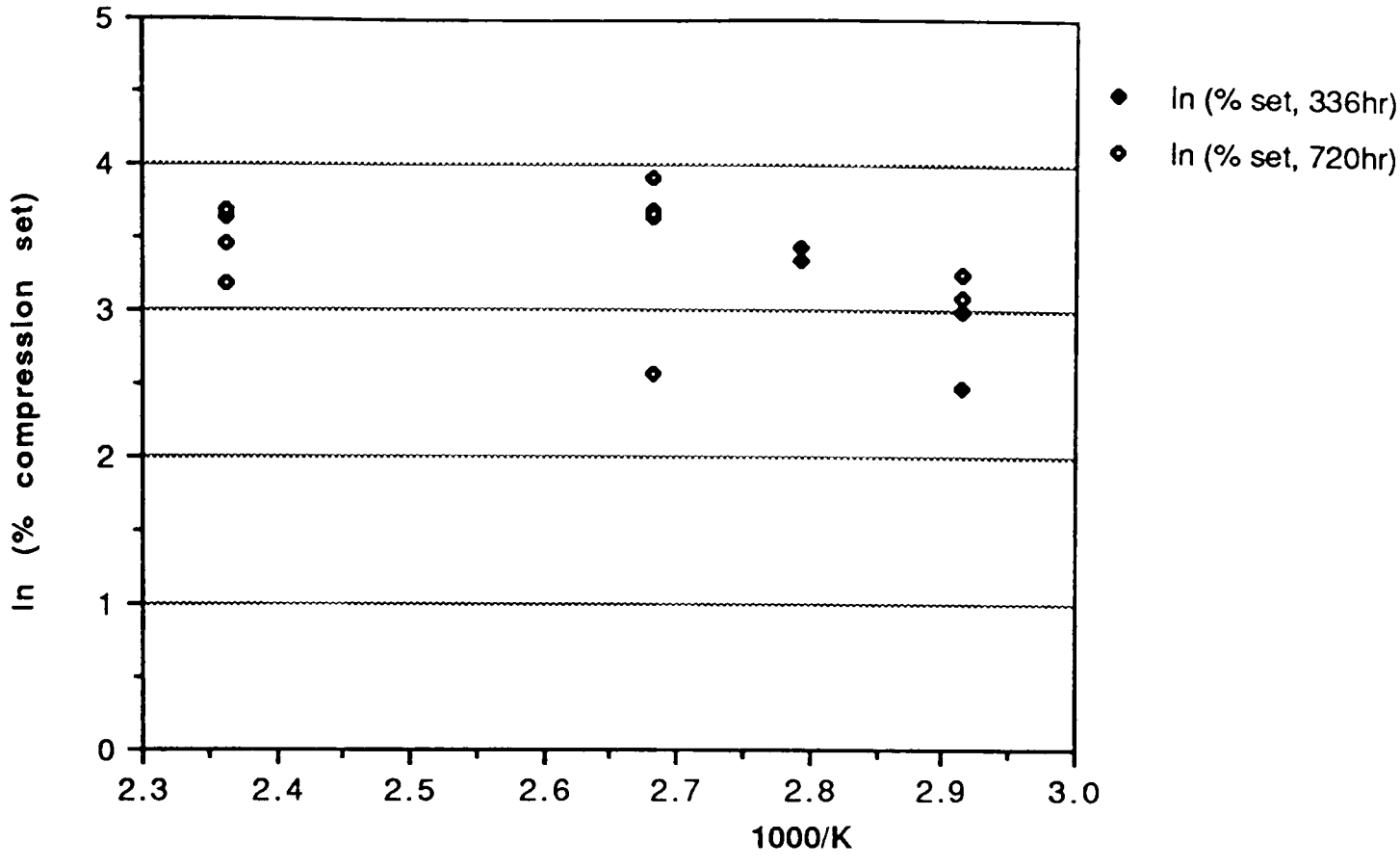

Figure 8.5 Arrhenius plot of compression set for EPDM after 336 hr and 720 hr in water

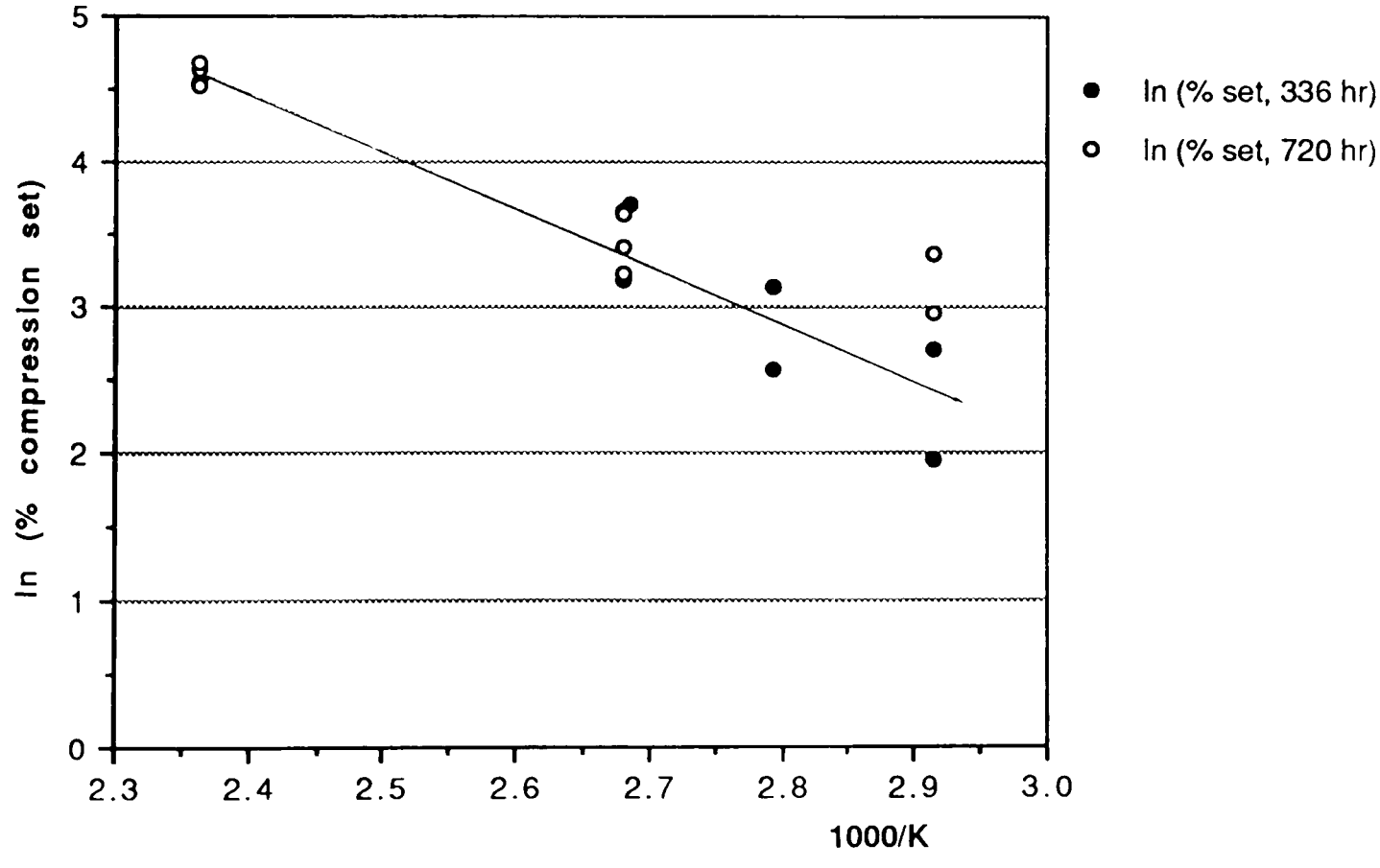

Figure 8.6 Arrhenius plot of compression set for high ACN NBR after 336 hr and 720 hr in water

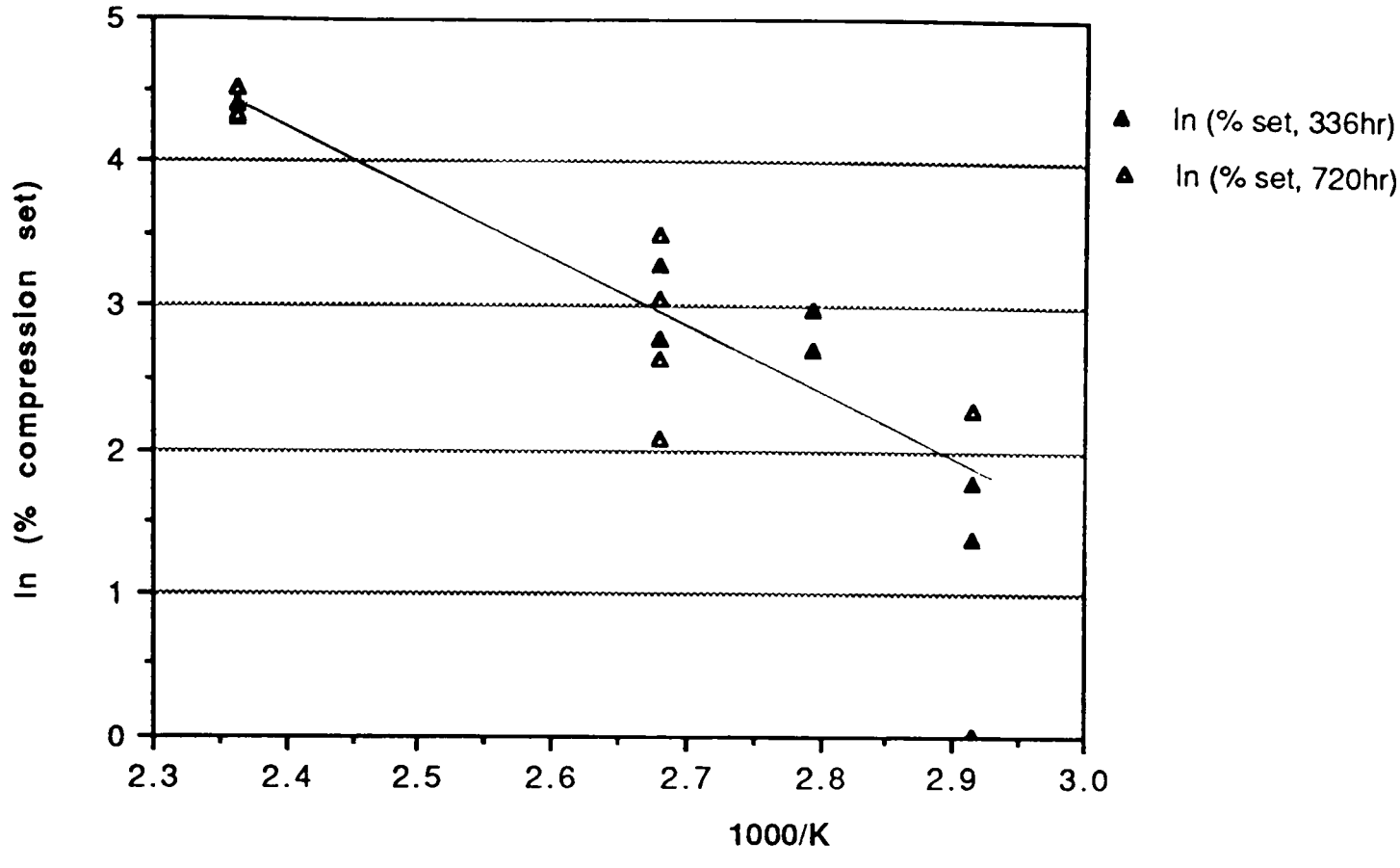

Figure 8.7 Arrhenius plot of compression set for Viton E60C after 336 hr and 720 hr in water

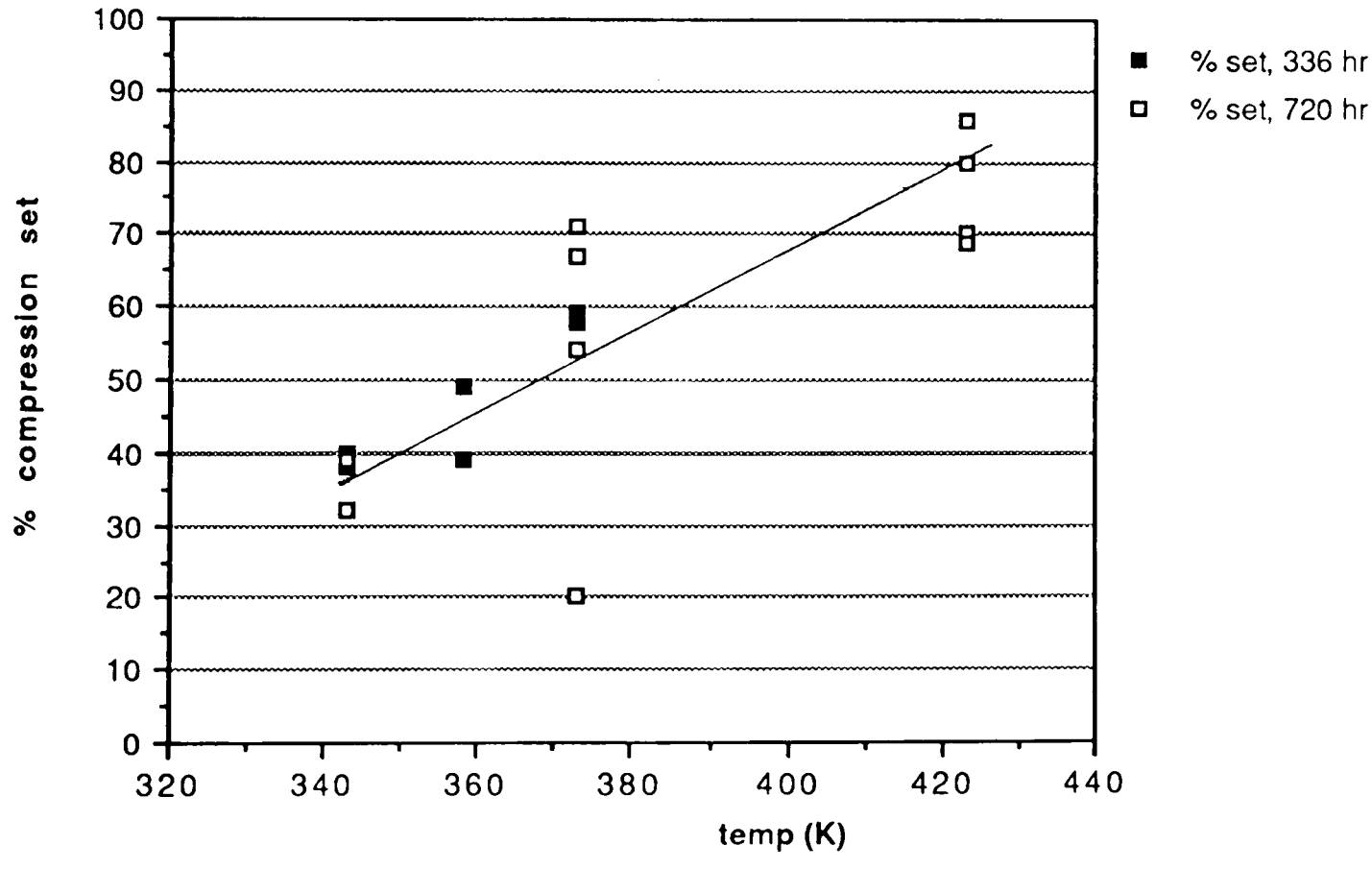

Figure 8.8 Compression set of Aflas against temperature after 336 hr and 720 hr in water

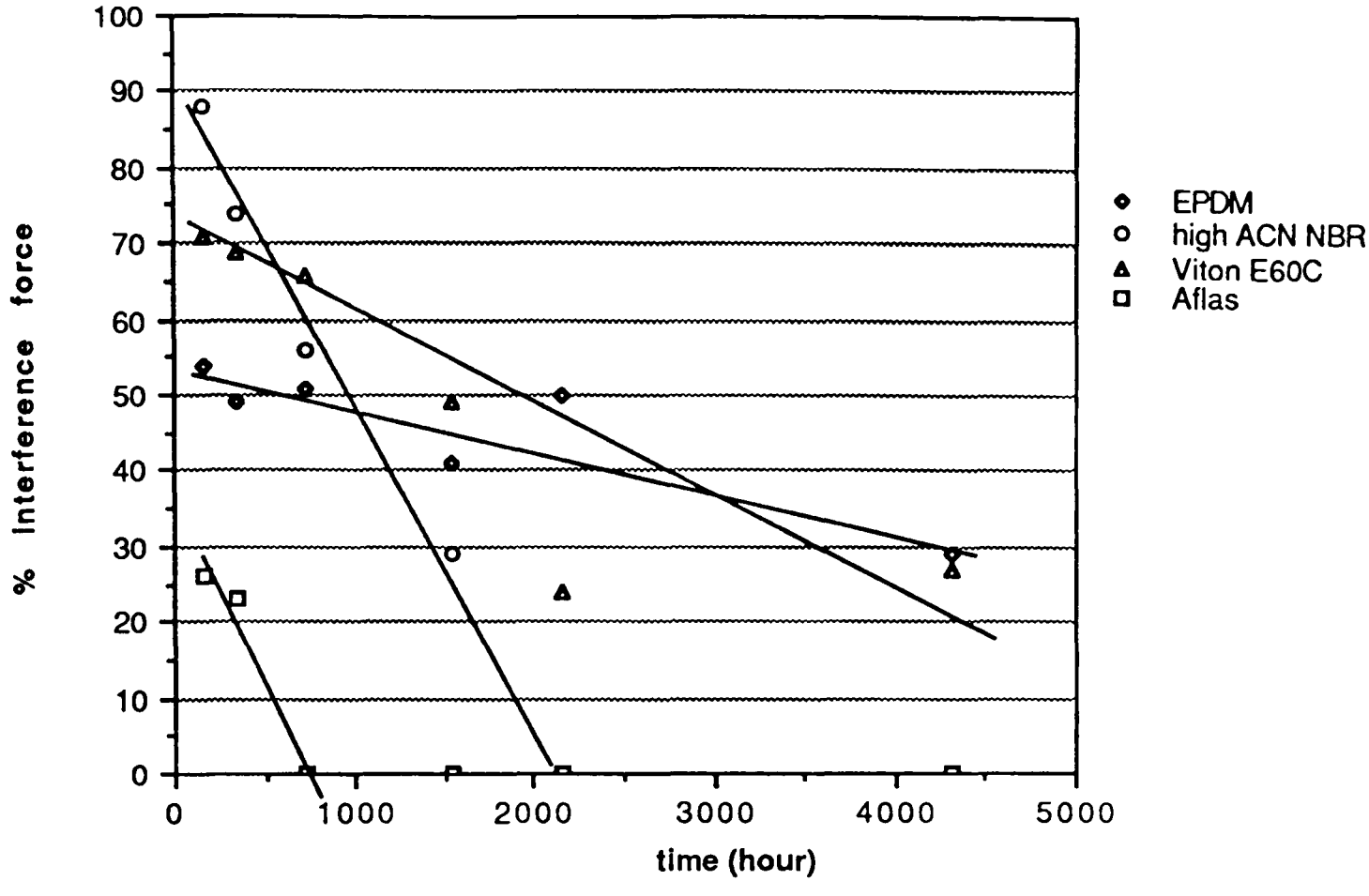

Figure 8.9 % retained force against time in water at 100C, 173 bar

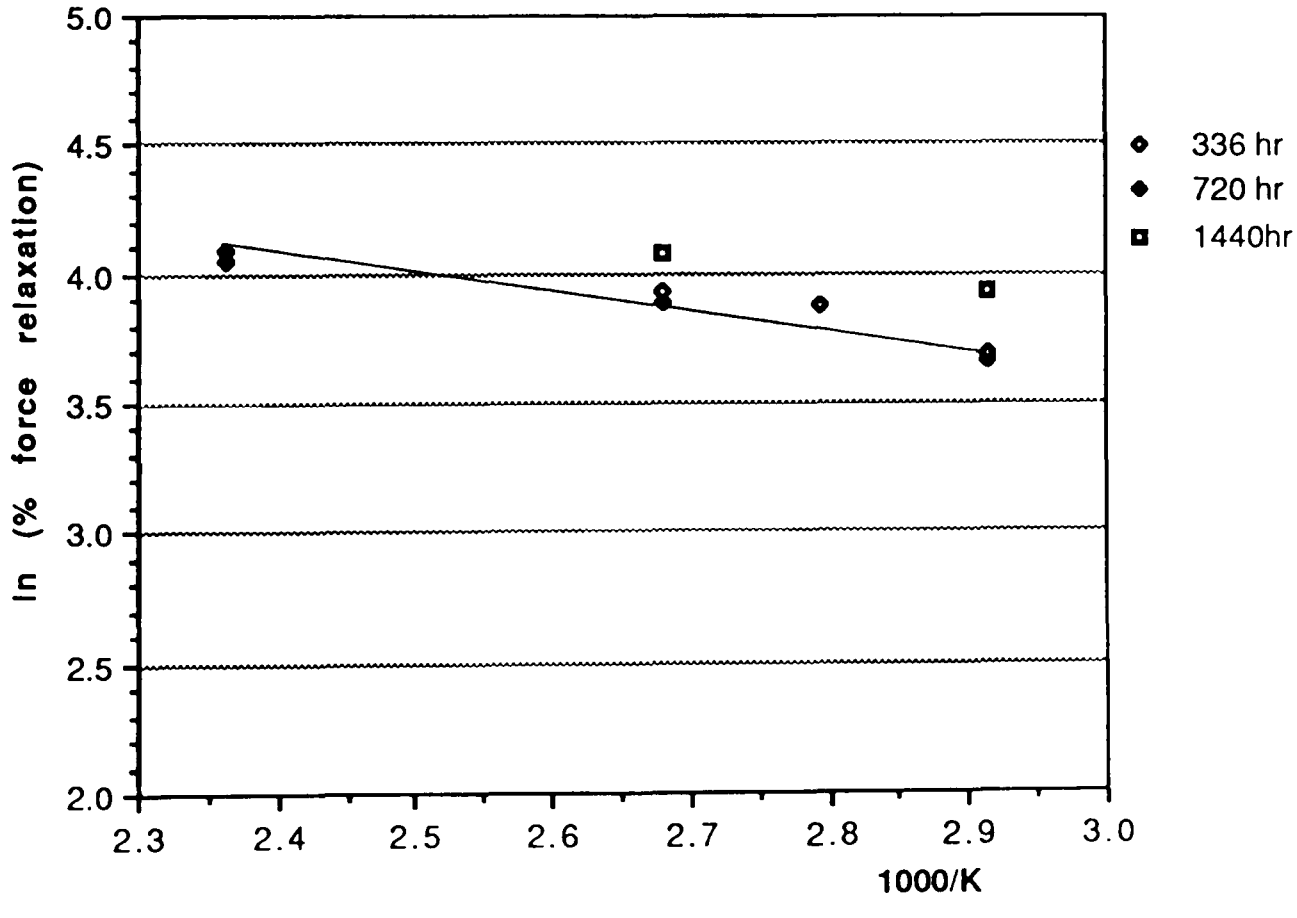

Figure 8.10 Arrhenius plot of force relaxation for EPDM after 336 hr, 720 hr and 1440 hr in water

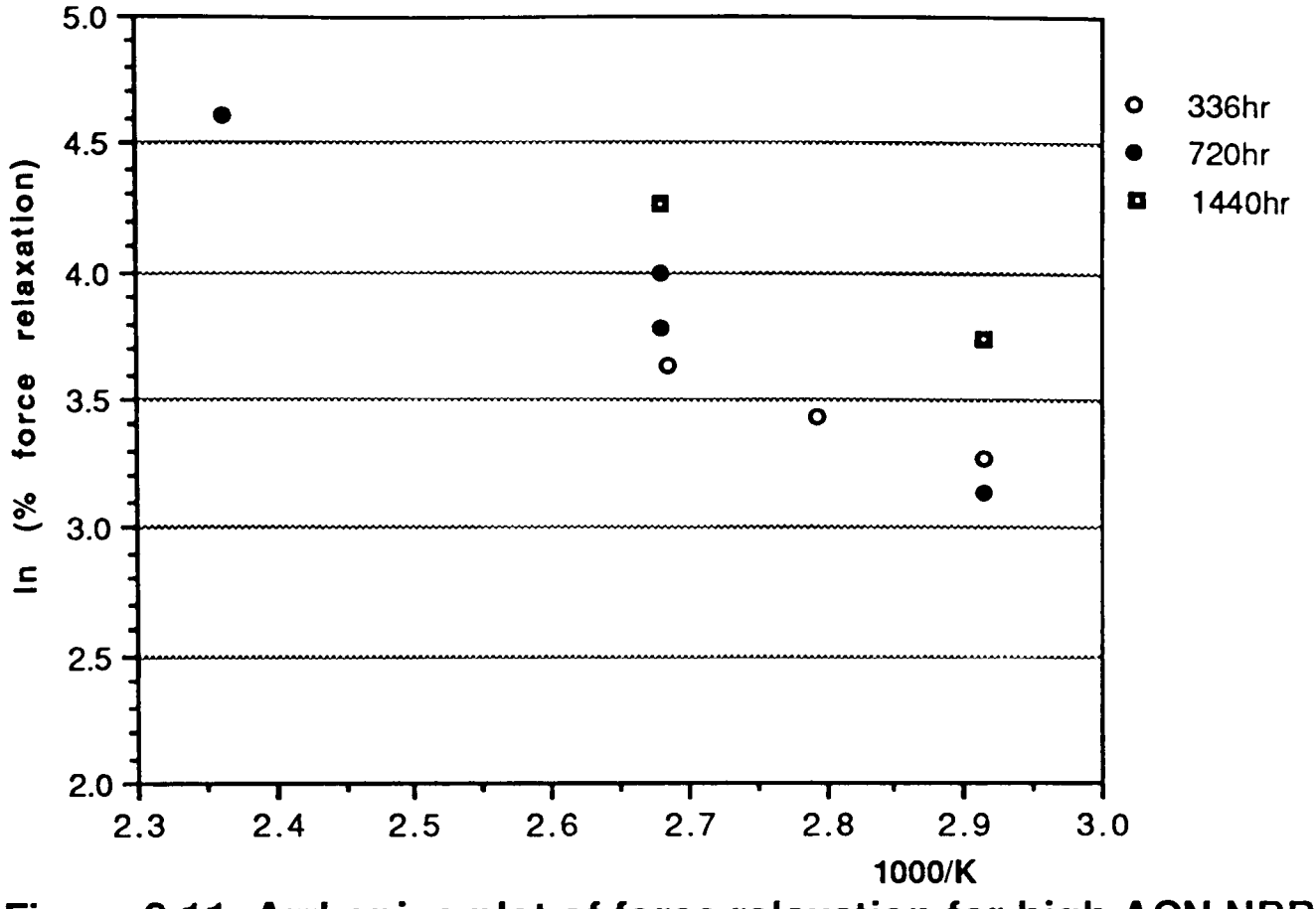

Figure 8.11 Arrhenius plot of force relaxation for high ACN NBR after 336 hr, 720 hr and 1440 hr in water

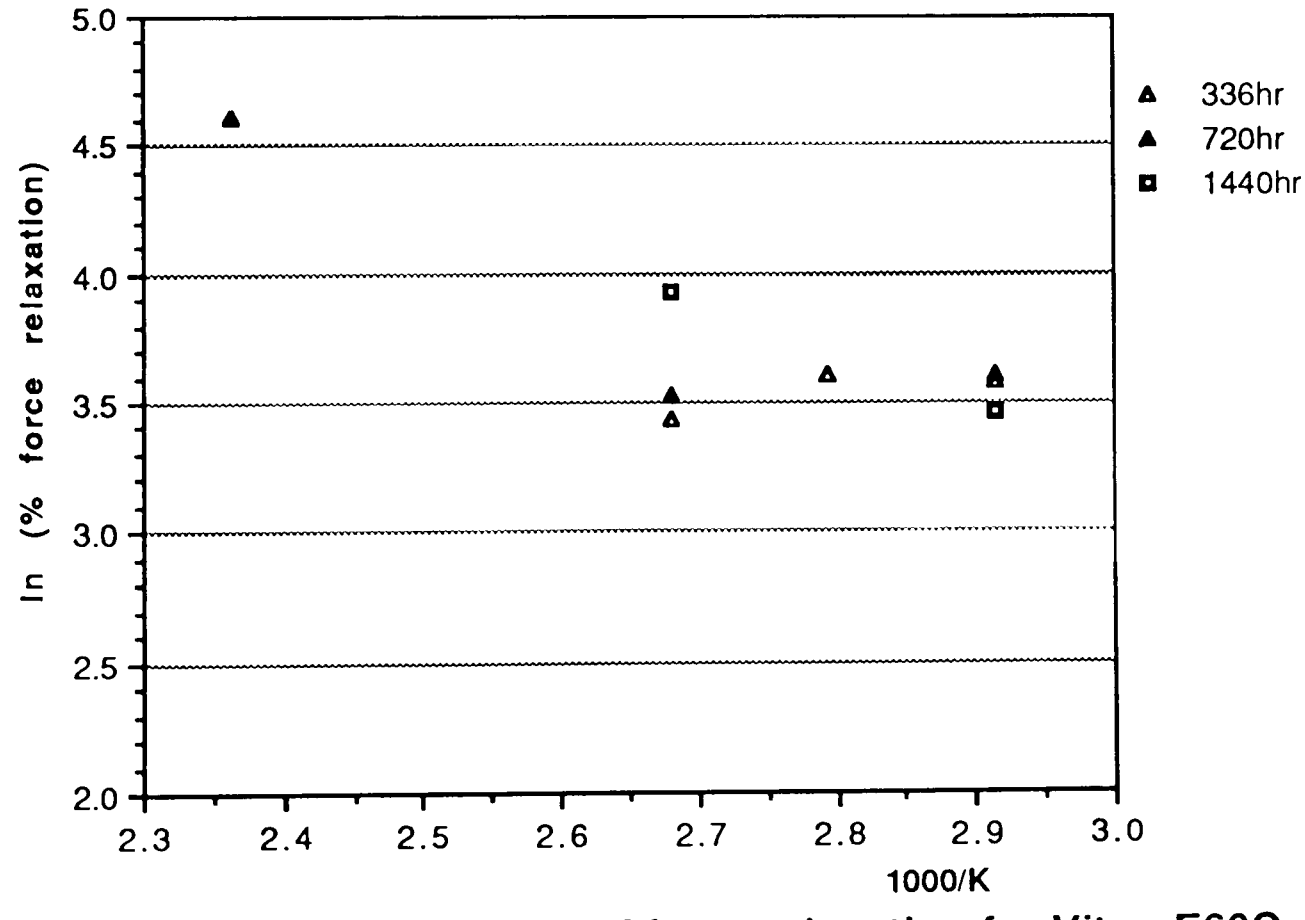

Figure 8.12 Arrhenius plot of force relaxation for Viton E60C after 336 hr, 720 hr and 1440 hr in water

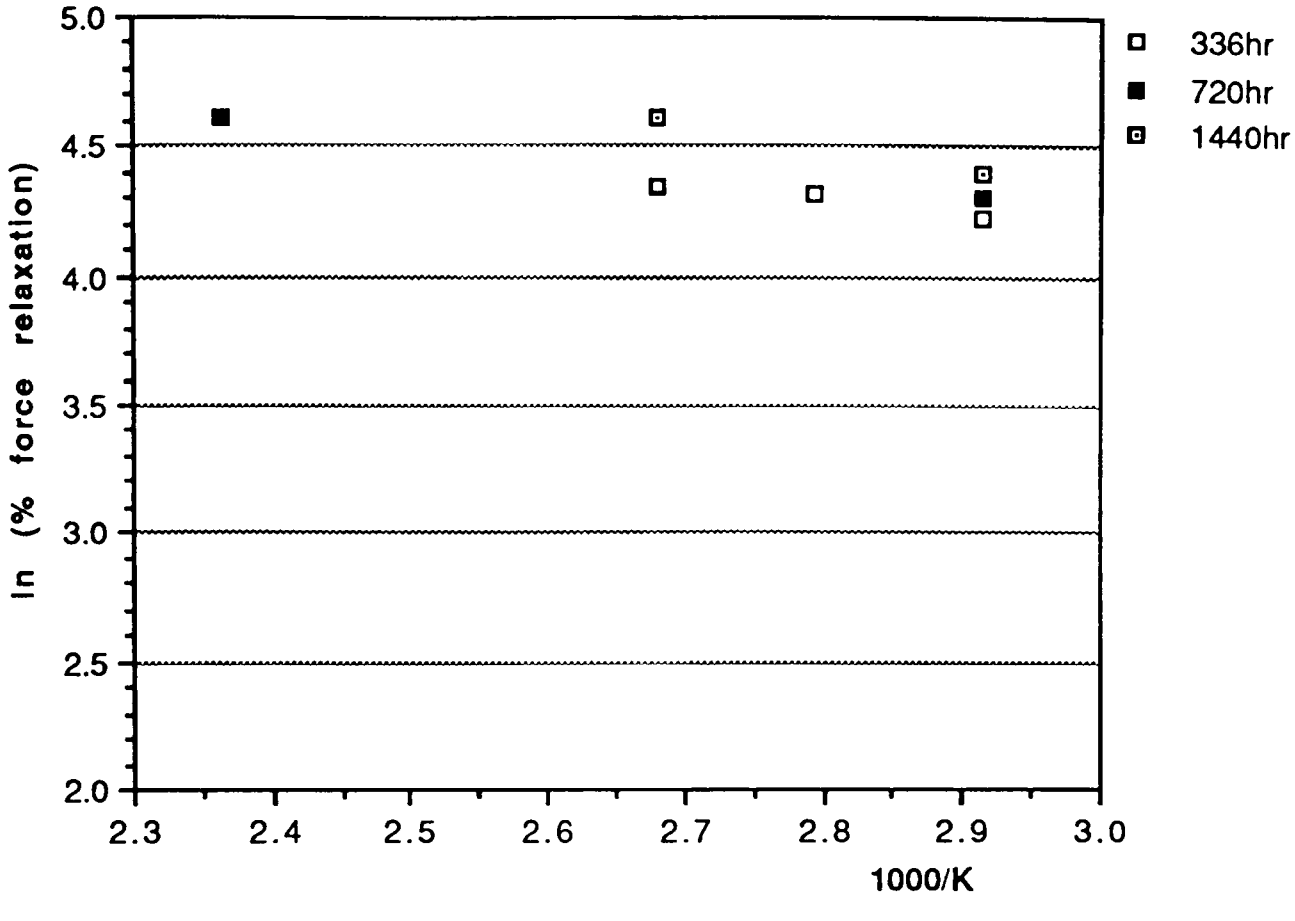

Figure 8.13 Arrhenius plot of force relaxation for Aflas after 336 hr, 720 hr and 1440 hr in water

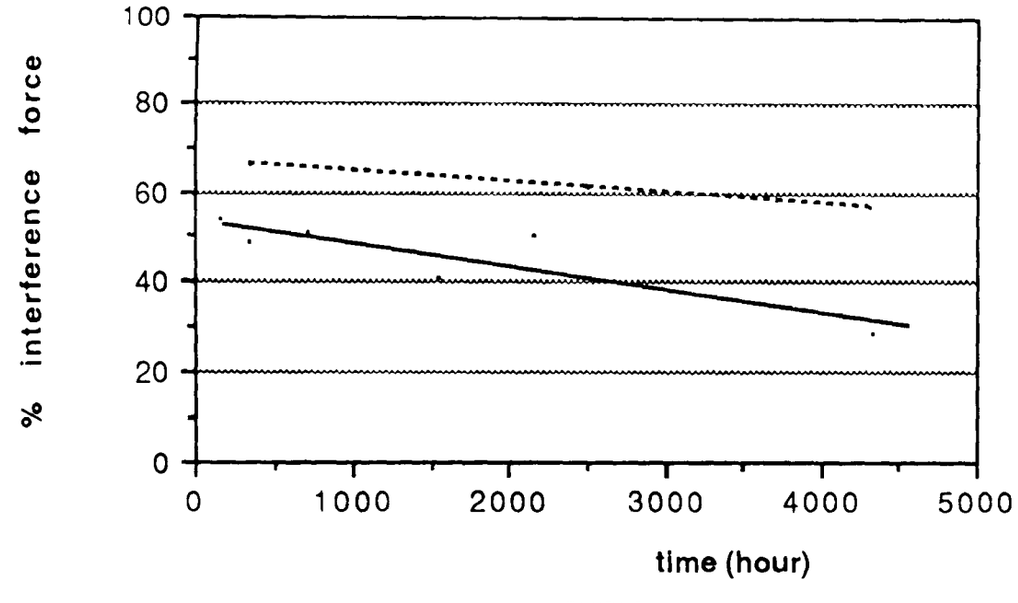

EPDM

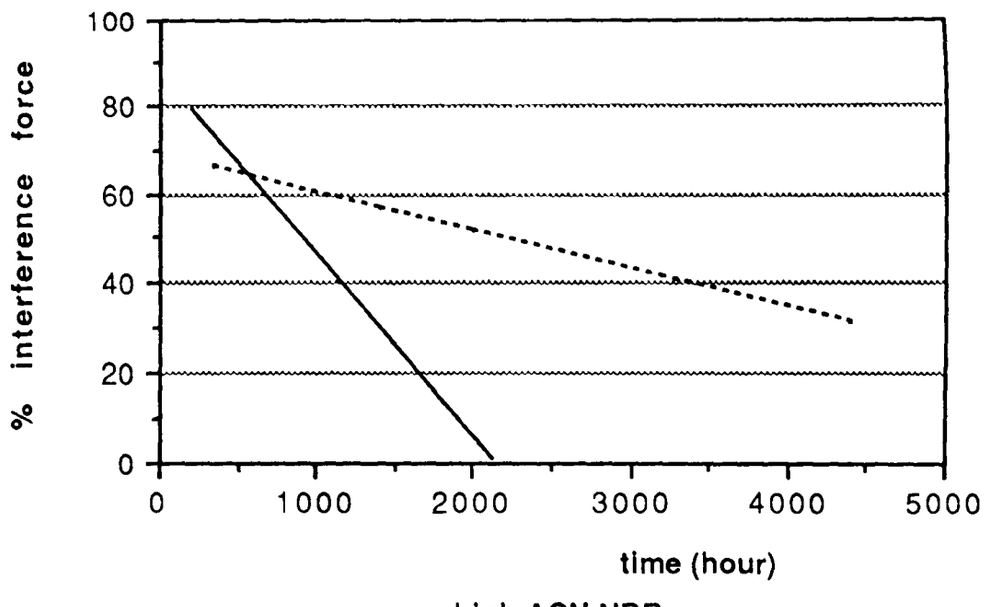

high ACN NBR

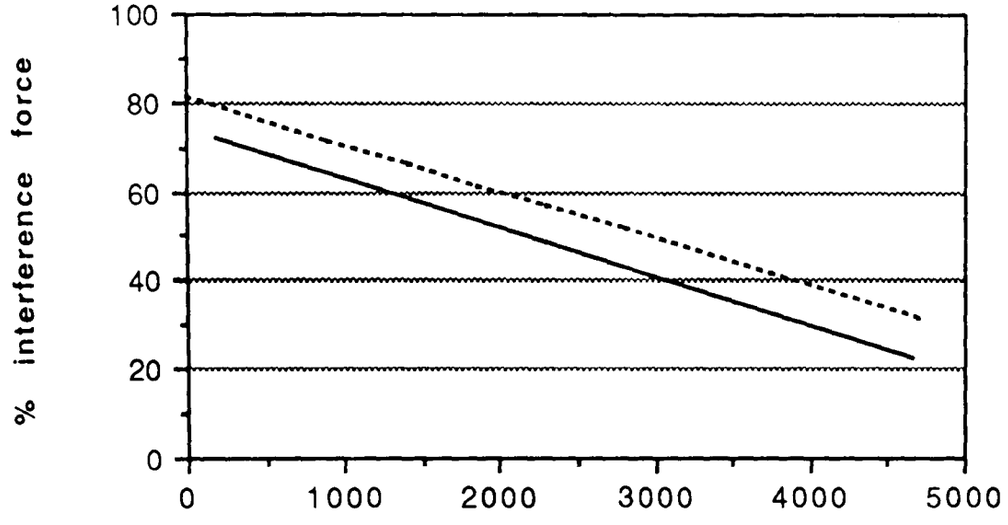

Viton E60C

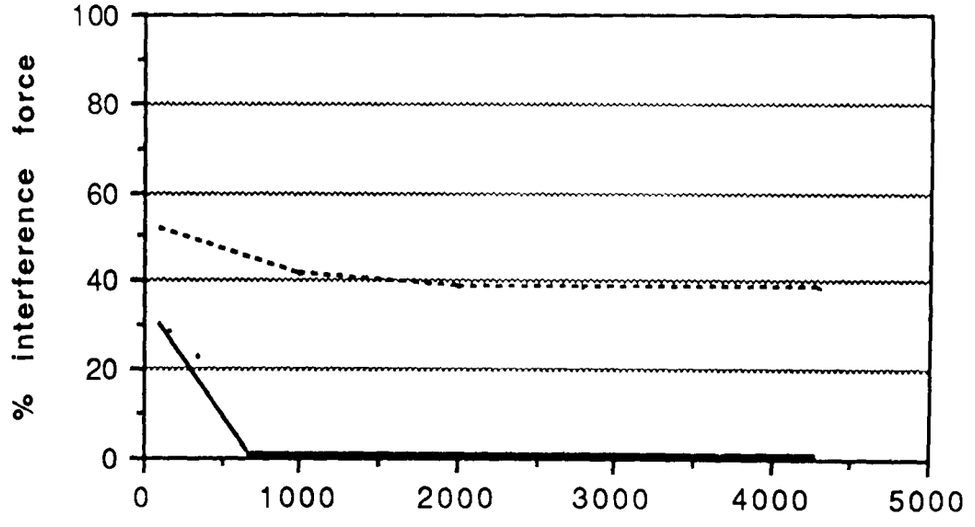

Aflas

— measured

----- by formula

Figure 8.14 **Measured and calculated force from compression set in water at 100C,173bar**

9. PROJECT MANAGEMENT

Management is the planning and organization of limited resources to achieve some specific goals and objectives. The non-technical aspect of the present PhD project is Project Management.

The Seal Life Project is a typical project which was relatively short-term (3 years in duration), and made up of interrelated tasks performed by various organizations, with a well-defined objective, schedule, and budget.

In chapter 1 - INTRODUCTION, the overall structure of the Seal Life Project was briefly presented in Fig 1.1, and three main deliverables were specified as :

i. Seal Performance Data for polymer seals under both simulated service conditions and laboratory benchmark conditions.
ii. A Seal-life Prediction Manual.
iii. A computer software package developed for predicting seals life from known material information.

The two research organizations, MERL and BHR group organized and carried out research work under the continuous monitoring from the industrial sponsors through progress reports, technical reports and project meetings. Project management is important within individual organizations to ensure all planned deliverables would be prepared on time.

The present PhD work which ran alongside the Seal Life Project was itself a project with fixed targets, limited time and resources. The objective of the PhD work was to develop the theoretical model and application software required to predict useful life of seals in service. Detailed definition of the software has been presented in Chapter 2 - OBJECTIVES. The prime functions of project management in the PhD project were to plan development, optimize labour resources, arrange computer and library resources, set up milestones, monitor progress and control production to ensure the completion of the project within schedule. It also included the organization of regular project meetings, once every 3 months with all supervisors; and the issue of short

minutes of the meetings to report progress, record discussion and decision.

Project management in research projects is different from other projects in the following ways:

i. The technique and knowledge known on the research topic is normally limited. Literature review is essential, but initial design involves setting up some assumptions, and initial development stage may need to perform testing to eliminate alternatives, or to confirm assumptions.
ii. High technology and new equipment or instrumentation may have to be used in research work. It is essential to look into the availability of this equipment and its impact on budget as early in the project as possible.
iii. The approach and method to achieve the defined objective cannot be fixed, but have to be adjusted in the light of new findings during the development stage. As a result, planning is an on-going process throughout the life of the project, and continuous effort needs to be put into project management.
iv. A research project normally involves a smaller team and less sub-contractors. However, most team members are key individuals with specialized skills, not easily exchangeable resources. This is particularly true once the project is well under way and the team members have acquired local knowledge.
v. Because of the specialization in manpower, informing progress to all parties concerned regularly is very important to co-ordinate team work.
vi. To quantify how much work is to be done can be very difficult in intermediate stages.
vii. The by-product from development can sometimes add value to the project. Slight diversion, subject to the request of the higher authority (end-users, sponsors, supervisors), may be justified in the early stage of the project;
viii. Because of the non-standard components in research, the involvement of the higher authority is very important. They are not only the decision-making people, but they can also provide positive inputs such as data, information and their knowledge.

Project management is made difficult in research projects by the non-

standard components and the unpredictable technical development in the scope of work. However, research and development projects in industry have strong market connections. These projects are aimed to have successful developments that can be beneficial to industry within economics favourable time periods. Therefore, project management is very important in research projects.

There are six main stages within the life cycle (ref. 72,73) of a project. They are:

i. Concept
ii. Definition
iii. Design
iv. Development
v. Application
vi. Final Completion

In this chapter, each of the individual stages in the Seal Life Project is looked into. Firstly, the economic initiation of the project, and the process to gain financial support are described. Then, project management is studied with details. These include the advantages and the drawbacks of the techniques and tools used to monitor time and budget, the change in approach and methods with time shown by the time-based critical path network charts. There are also discussions on the problems arising in the project, on the actions taken to solve the problems, and on the performance of project management as a whole. Lastly, the experience learnt from real application are summarized with suggestion for future improvement.

9.1 Concept

The conceptual stage is the preliminary evaluation of an idea. It means identifying existing needs and opportunities, studying initial technical, environmental, and economic feasibility and practicability.

For the Seal Life Project, it was based on the demand from oil companies,

equipment manufacturers and rubber suppliers to predict elastomer seal life reliably.

9.1.1 Benefit to Oil Industry

The rubber suppliers provide raw materials to seal manufacturers. It is common that these rubber suppliers dominate the market for their special blends of material, e.g. 3M in TFE/P, Du Pont in fluoro-elastomers and perfluoro elastomers. A rubber supplier will try to persuade the oil industry that its blends of material have higher performance than those of its competitors.

There are also new markets opening up for high performance elastomers. For example, the use of fluoroelastomers in the automotive market has more than doubled in the past ten years. Fluoroelastomers were once viewed as expensive materials only used in oil industry. However, it is increasingly accepted that the use of materials with good chemical resistance to engine oil, transmission fluids, gear lubricants, engine coolants and hydrocarbon fuels is cost-effective, even if the new materials are more expensive than the conventional ones.

An O-ring is normally of relatively low cost :

£1 - £10	oil-resistant material,
£20 - £50	fluoro-elastomer material,
£100 - £200	perfluoro elastomers (e.g. KALREZ)

In cases when special cross-section seals are used instead of O-rings, a new mould has to be designed and made. The mould can cause £500 - £2000.

The rubber seals are then supplied to oil-field equipment manufacturers to be installed into systems of oil-field machinery. The sales of one system is of the range of £10K to £100K. The cost of seals in their equipment is therefore of relatively low value, but an effective seal can be essential for the functioning of the whole system.

Because of the stringent technical requirements of the oil industry and the very high costs and the hazards of equipment failure, oil companies limit the purchasing of critical items to qualified suppliers. Suppliers need to maintain reliability for their own position in respect of future business. They can sometimes go to a lot of trouble to improve performance or to eliminate the use of rubber O-rings. Bestobell (74) developed a nitrogen pressure filled O-ring for their butterfly valves to provide drop tight sealing which it claimed to have little or no maintenance when in service for long periods of time and high resistance to erosion. Baker Oil (75) commented that O-ring seals are traditionally the most vulnerable parts of the hydraulically operated actuation systems - "When seals fail, leaks occur between the tubing and the casing. This costs money for repair, rig time and lost production." To enhance the long-term reliability of Baker Oil hydraulically operated tools, they combined two traditional downhole tool operating methods, electric line setting tools and hydraulics, to produce the Electronic Actuation System to control setting of packers as a replacement to traditional O-rings.

However, in a lot of cases O-rings cannot be eliminated technically or economically, and reliable rubber seals do make possible new development in oil-field tools. Hydra-Lok (76) publicized a newly-developed system that permitted isolated line-segment pressure testing. The system consisted of a steel mandrel with two rubber seals disposed along its axis. The key to the system was the seals which were manufactured from various grades of rubber so that they could withstand the high extrusion force applied to them.

In oil production, the oil and gas prices are determined by the world's demand. Oil companies can only minimize their cost to maximize profit. It is very much so in recent years when the world oil price is falling. A man-day labour offshore can cost £1000 or more. And the re-installation of failed seals can take couples of hours to a few days.

The even higher cost of failure is the loss of production. As building offshore platforms and installations to allow production is a capital-intensive business, the sum for interest payment is usually large, and continuous production is very important. One day loss of production on an average

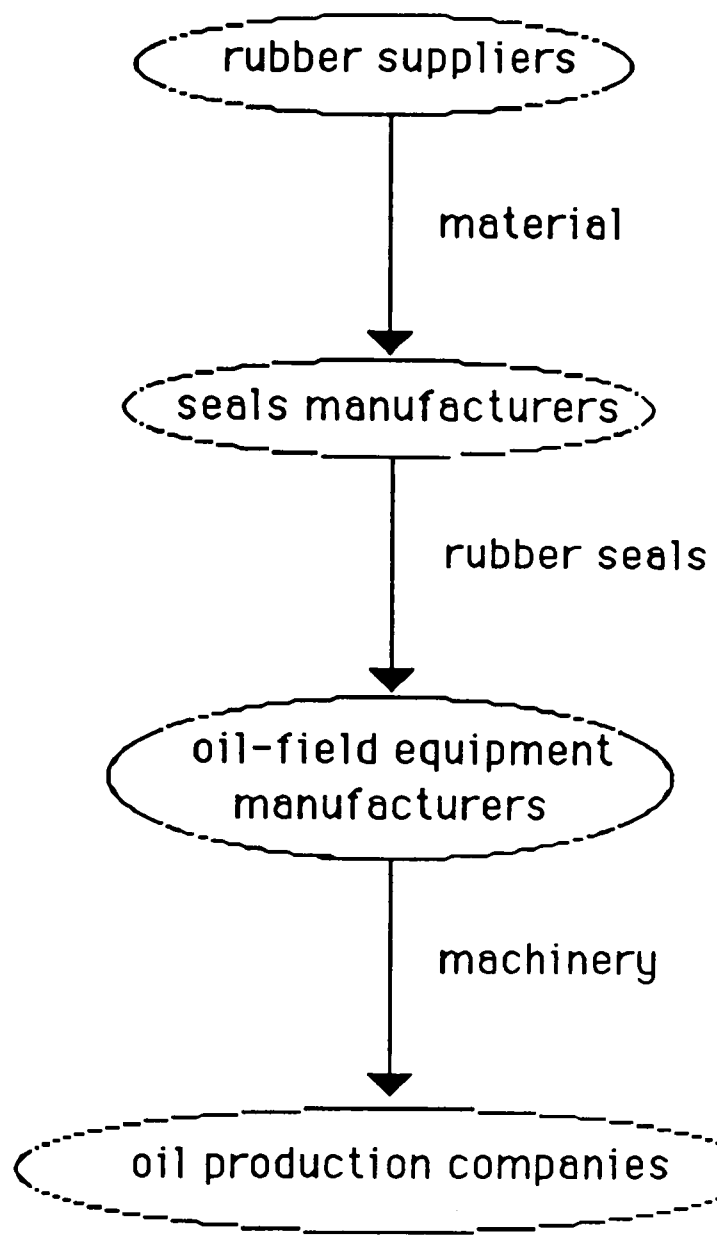

platform costs about £2 million. If a main pipeline has to be taken out of operation, it can affect 3 to 4 platforms which share the facilities. According to the data base for pipeline failures (77) in the period of 1967-87, about 6% of 650 pipeline failures were caused by equipment failures. And equipment failures were primarily due to leakage or malfunctioning of fittings such as flanges, clamps, valves, etc.

Another study (78) into the 150 largest losses caused by accidents and natural phenomena in the onshore hydrocarbon processing and chemical industry, during a period of 30 years ending Jan.1, 1989, shows that the cost and number of losses are increasing. Attempts to achieve economy of scale have had an undeniable effect on the size of potential losses. Piping systems including pipe and fittings are the most frequent type of equipment involved in the cause of large losses, causing 30% of the losses at an average cost of

US$42 million per loss. Pumps / compressors also responsible for 8 losses, causing US$19 million in total.

Keeping rotating machinery, such as compressors, pumps, turbines, and blowers, in top operating condition is a key activity that helps maintain efficient process operations in refineries and petrochemical plants. A process unit may run for 3 years before it is shut down for a turnaround period of only a few weeks. Predictive maintenance can help to organize servicing as well as stocking components. That is to ensure the new replacement seals are available and up to specification when required.

The traditional method of seal life prediction is to perform accelerated tests on potential seal materials before installation, and by continuous monitoring in service. Accelerated tests performed at high temperature are not completely reliable, as some chemical reactions occurred in accelerated tests do not operate at the lower service temperature. In service, if the last seal fails after two year operation, then one predicts a replacement seal of the same material will have a similar life. The method highly depends on individual experience or well-managed records, and provides low flexibility for the application of new materials.

The Royal Navy (79) is also interested in rubber ageing. They have to make sure the materials used will perform well in service, even after a long storage life. Their items are required to work with a very high reliability such as life-rafts and survival gear. The contact with hydrocarbon can be very important. As recently as the 1990 Gulf War when the sea was polluted with oil leakage, the seals in the mines laid by the Royal Navy had to seal hydrocarbon as well as water.

The British Government on the other hand is interested in the health and safety in oil production, and continuous export trade. It has to set up laws or regulations that are acceptable and practical for applications, but are effective in providing safety to offshore workers. It is also of government interest in revenue to ensure continual oil production in Britain.

9.1.2. Benefit to the Research Organizers

BHR group (previously known as BHRA) has been involved in sealing research for over 30 years. Its research area covers rotary (mechanical), reciprocating and static sealing applications such as bolted joint gaskets and elastomer seals. BHR group also specializes in test rig building and seal consultancy for industry. Consultancy include seal design and development, computer analysis of existing or proposed seal designs, performance comparison testing. However, both seal material behaviour and seal design affect elastomer seal performance. Existing information on seal material cannot be readily interpreted in terms of actual sealing performance in service. Therefore, a study in basic science of physical, chemical, diffusion and fracture properties of elastomer seal materials is essential within elastomer seal research to understand sealing technology and failure modes.

The Materials Engineering Research Laboratory (MERL) is an independent British company specializing in contract research and consultancy in elastomeric and related materials for engineering systems. They have worked on different rubber components, such as hoses and seals, used in offshore industry. Several of its engineers and scientists have 20 years experience on material properties research on elastomers.

By organizing a Seal Life Project, the two project organizers, BHR group and MERL, can increase income, broaden their market and further develop their technology based on their existing knowledge. In the conceptual stage, the two organizations worked together to draw up a 3-year programme for seal failure research, from basic principles to reliable prediction of seal life. The two organizations looked for the support from the industry. They arranged a seal consortium which could have 10 to 20 members, and each member paid an annual subscription up-front. The consortium would form a committee to control the direction of the research project.

The two organizations then arranged a press release, and two project launch meetings, one in U.S.A. and one in England, to introduce the project and discuss details with the oil industries.

9.1.3. Benefit of PhD Course

By following a PhD course, one can increase technical knowledge, develop creative thinking. Cranfield Institute is also in close proximity to a wide variety of the equipment and expertise necessary to support a PhD research. The Department of Fluid Engineering and Instrumentation (DFEI) is the closest interested group working in the area.

9.2 Definition

In the definition stage, elements considered under the conceptual stage are refined. It involves preparation of documentation, such as the preparation of R & D proposal, and receiving the award. It is at this stage that the sum of funding and the amount of deliverables are finalized.

I started my PhD study in September 1989. A PhD Support Panel was set up to monitor the progress of my PhD project. The Support Panel Member included :

i. the Head of Department of DFEI as Chairman,
ii. a Academic Supervisor from DFEI
iii. a Management Supervisor from the School of Management
iv. an Industrial Supervisor from BHR group
v. the Personnel and Training Manager from BHR group

On the Seal Life Project, BHR group and MERL drew up a proposal detailing the proposed activities and subscription fee for approval by clients. The original proposal based on an assumption of 15 members for a total budget of £ 700k, for which the two organizations equally shared the funding. However, the total amount of funding was not finalized at the start of the seal life project. The project proceeded when six or seven signatories were obtained, with a fairly firm commitment from several others. Clients continued to join within the first six months of the project. The final funding for the project was £520k, i.e. £260k for each organizer, from 11 companies.

BHR group and MERL also signed a formal collaboration agreement as co-principals of the project and BHR group as the contracts administer of the project.

For the seal life project, a Project Steering Committee was set up with representatives from each participant. The Committee had mandatory meetings every six months and controlled the direction of the project. The two organizations, BHR group and MERL provided expert guidance, technical leadership and advice in making recommendations to the Committee, but the Committee members decided what should be done within the scope of work based on funds available and research priority. The scope of work was subject to amendment by the Project Steering Committee throughout the project life.

At this stage, seal manufacturers reflected to the two organizers that they were interested in the offshore market. However, the relative high subscription was not justified in the case that elastomer seals were of relatively low price, at £1 to £100 per seal. The presence of seal manufacturers within the project could contribute valuable advice, and supply specially designed seals to the research project. The Steering Committee therefore agreed to invite seal manufacturers to join the Seal Life Project as associate sponsors with a lower subscription fee, and with provision of materials, seals and services supplied to the project. These associate sponsors however were non-voting, had no property rights, and the deliverables were limited to progress reports and non proprietary test data.

9.3 Design and Development

Production begins in the design stage. Detailed plans are prepared for future product development. A literature review started the Seal Life Project in January 89. The design of the seal life rig commenced in May 90. The PhD course began in September 89 by defining a plan for software development in coordination with other research work.

The implementation of the established design started in the development stage when BHR group and MERL built test rigs, carried out preliminary benchmark tests, developed theories and computer modules, analyzed and documented results.

The development of the computer software in the PhD project took up 2/3 of the full project time. It involved establishing theories and numerical methods, coding of several 'stand alone' functional modules, and then combining them to predict elastomer seals with consideration of fluid diffusion, material properties and stress relaxation.

Because prediction of seal life involved studying a large number of relevant processes, and computer modelling of changing material properties in polymers was a relatively new technique, the Seal Life Sponsors agreed that the development of seal life software should be concentrated on modelling deterioration of the rubber due to its reaction with diffused fluid. Such data would then be transferred to a general purpose FE package to interpret the effects on sealing contact stress. The decision to concentrate on material deterioration in the development stage was to ensure the most useful deliverable to sponsors would be completed within the project schedule and budget. The incorporation of incompressible stress-strain facilities and the ability to handle undetermined contact boundaries are to be included in phase 2 of the current project as another 'stand alone' project.

BHR group and MERL had monthly meetings throughout the project to exchange information, co-ordinate research and discuss ideas. It is essential to link material testing to appropriate scientific theory to provide the basic

theoretical model for computer modelling. MERL characterized material using both experimental and theoretical studies. The results are then used as computer input for modelling seals of specific shapes. Results from functional seal tests in BHR group also provided data for software validation.

Both organizations circulated regular technical reports to sponsors, prior to each six-monthly meeting of the Steering Committee. Well informed sponsors could then follow discussions and contribute technical information in the Committee Meeting. Regular technical reports helped researchers to summarize facts, review performed work, organize thoughts and plan for future work.

The issue of insufficient time for the original proposed PhD content was also presented to the PhD Support Panel in the beginning of the second academic year, as soon as the problem was confirmed. I proposed a revised PhD content for the Support Panel to assess. The Panel agreed that the proposed content was enough for a PhD project, and therefore authorized the change.

Yearly PhD reports are prepared for the Support Panel and SERC. Supervisors reviewed the reports, identified scope of work need improvement, and advised on future work plans to ensure the PhD project would be on time, and up to quality standard.

9.4 Application and Final Completion

To establish financial support for the next phase of the Seal Life Project, BHR group and MERL worked together to prepare an overview of the project, and a proposal for a two-year extension to develop further seal life prediction skills. The preparation of follow-up on contracts for the second phase work had to be brought forward, so as to allow more time for discussion among the participants, and for the sponsors' organization to arrange financial contracts.

In the application phase, the product or service of the project is integrated to the existing organization. MERL concluded their basic research with material tests in service fluids at service temperature and pressure. BHR group conducted service fluids tests which included corrosion inhibitors, hydrogen sulphide gas, etc. The computer modules were applied to practical service conditions which included both physical swell and chemical ageing. User-interface was also improved and a user-manual was prepared to be delivered to sponsors with the software. The finalization of a methodology document for predicting seal life with cross-reference to the other technical area was also undertaken .

For the final completion of the Seal life Project, MERL established the theory for physical material properties and chemical material deterioration. They tabled or graphically summarized all test results, and defined the experimental procedures for testing material properties that could be readily interpreted in terms of actual sealing performance in service. BHR group presented all the simulated test results with the derived correlations, and delivered a software package with a report on theory and validation, and a user-manual. There was also the methodology document which linked the different areas of work together, and explained conclusively how to use the research information for seal life prediction.

At the end of the PhD project, a thesis will be submitted, recording the established theory behind the seal life software and work examples to demonstrate the application of the software in seal life prediction. It should also provide some insight into computer elastomer seals and some suggestions on perspective future research work on the subject.

9.5 Time Management

There are different methods for monitoring time schedules (ref. 80,81). Graphical presentations such as bar charts or critical path network charts can be used. They aim to highlight spare time and pinpoint potential bottlenecks. They can also give an up-to-date picture of progress. In the

beginning of the Seal Life project, a bar chart was drawn for showing the planned start time and duration of scheduled events. At the end of the first year, a time-based critical path network chart was drawn instead, as it is easier for highlighting critical events, and the link between different process. The chart has then been updated regularly to incorporate the latest development, and record any variations from plan. The original bar chart and all the network charts are included in the next few pages.

It can be seen in the first two network charts, that there were some refinements in the presentation technique as well as updating information. These included :

i. adding the program of the partner organization MERL to the chart;
ii. adding links between material testing, functional rig testing and computer modelling to show their inter-relations;
iii. shading the completed functions.

Within the contents of the charts, there have been a few major changes :

i. the starting date of the design and development of the Seal Life Software was three months later than the original plan, due to the availability of manpower;
   - Manpower is always a limited resource. Because of the delay in completion of another project, manpower was not available in the first three months to design and develop software. As explained in the beginning of this project, specialized skill is required for research. Temporary staff cannot perform satisfactorily, while an increase in permanent staff requires long term, stable income.

ii. report and validation of computer program need to be done regularly, rather than at the end of the project only;
   - There are the various interrelated processes involved in seal life prediction. Validation of individual module of the computer program is important to identify problems or inaccuracy, so as to gain confidence for further development. Regular reports help individuals to review performed work, and inform partners in different aspects of the project on the results and development of research.

iii. longer time required for the design and build of the Seal Life Test Rig to install the safety devices for running hazard fluids;
- There were conflicting design requirements for the Seal Life Test Rig as discussed in appendix 4.3.3. Sponsors were consulted to make the final decision. It was also found that the commission of the Test Rig was best carried out in three stages : a) for non-hazard fluids, b) for inflammable fluids, c) for toxic fluids. Three stage commission allowed itemized equipment testings, opportunity to build up experience and confidence, establishing testing procedures, and the starting of seal testing as early as possible. The expense of time spent on building test rigs did reduce time available for long term seal testing in the project.

iv. longer time required to develop the theoretical model of physical and chemical degradation of material properties, including swell, ageing etc.
- to establish the theoretical model for computer modelling required basic information on each of the processes involved in seal failure. These required a lot of basic material testing and data analysis. Computer modelling was originally scheduled to develop in parallel with other tasks of the project. In practice, it had to follow the theory established from material testing, it required material properties data, and seal data for validation.

The milestones of the seal life project were set with some functional tasks, e.g. the seal life rig commission, the completion of the diffusion modules etc. BHR group and MERL also prepared bimonthly progress reports and six-monthly written technical reports to inform participants on the status of work done.

In a project when a delay occurs, some modifications in the project plan have to be taken for ensuring the completion of the project. One approach is to extend the project life when the resources allow. It is usually impractical or limited in application. The other approach is to reduce the amount of work to be done with minimum sacrifice in the quality or quantity of the deliverables.

Or a combination of both of the above methods has to be taken.

When delay occurs in developing the seal life software, the most important point is to complete an useful software which can be delivered to the sponsors at the end of the project. Sponsors' companies are likely to have finite element stress-strain package. Therefore, it is most important to be able to model material properties degradation in the seal life software. To avoid delay in the delivery of the final products, three measures have been made :

i. The end of the project has been postponed by 3 months to allow the completion of the longer term ageing tests.
ii. The incompressible stress-strain facilities and the ability to handle undetermined contact boundaries are to be handled by commercial stress- strain package within the current phase of the project.
iii. The number of validation tests on the final program with service conditions are reduced.

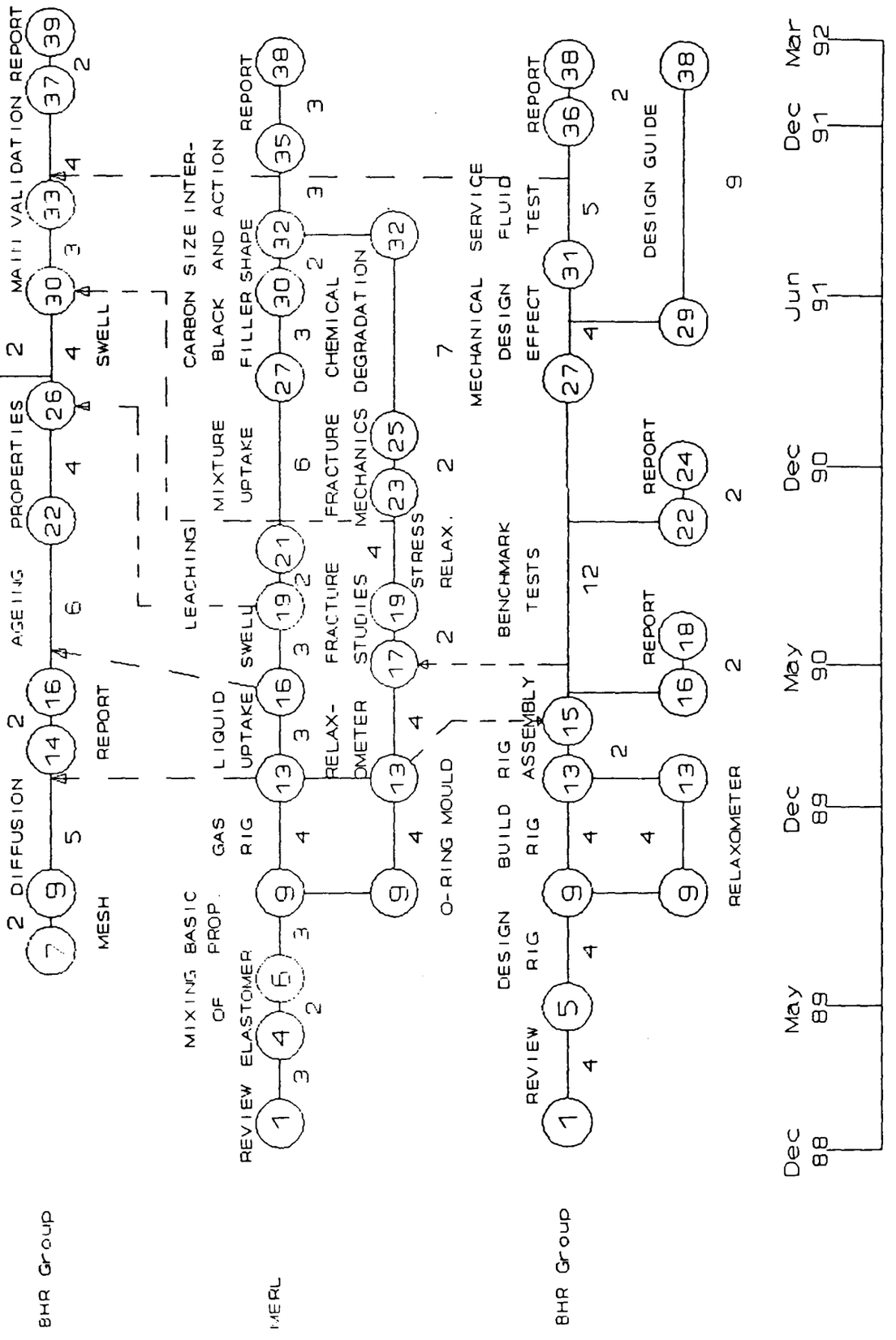

Fig 9.1 Time based critical path network chart in July 1991

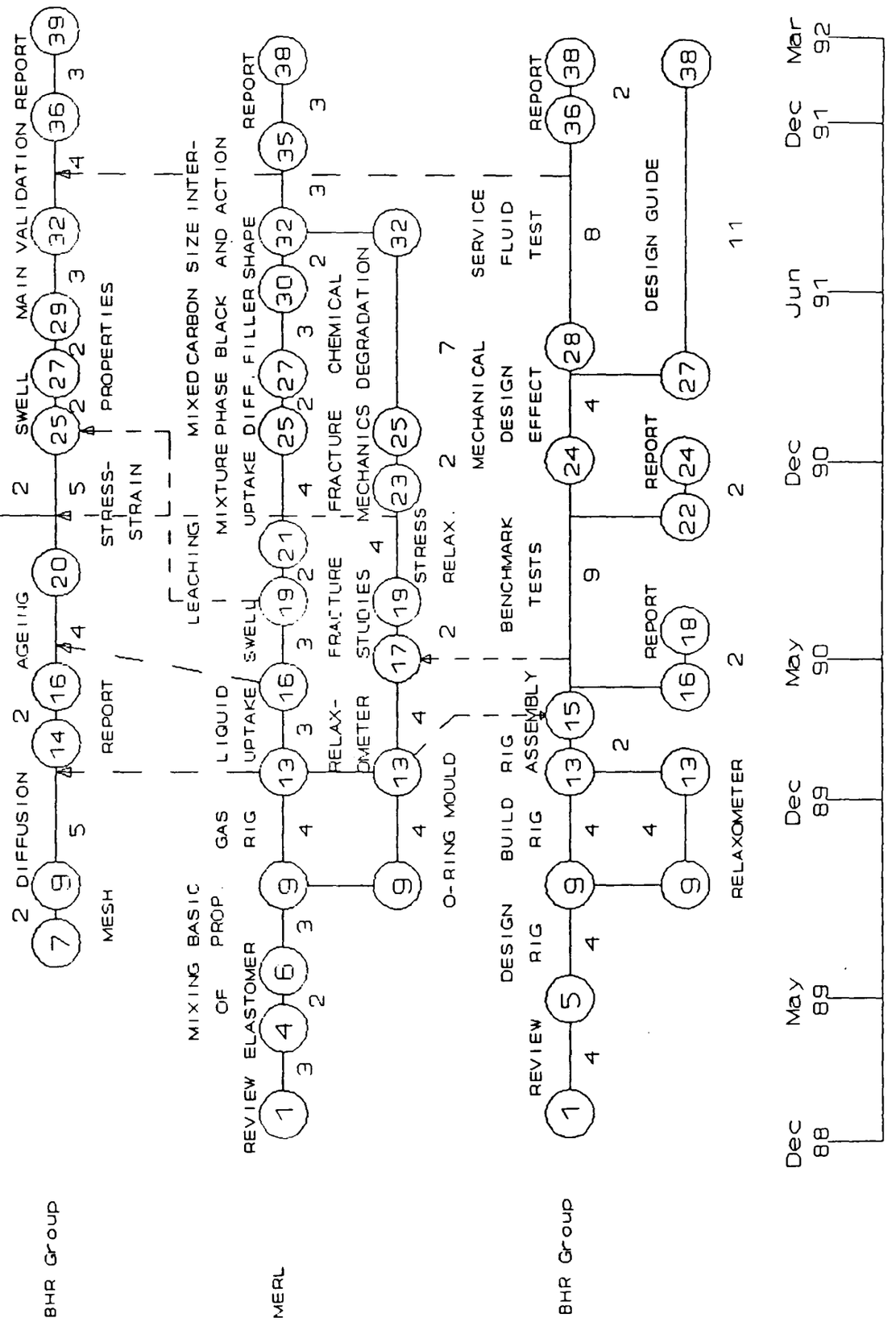

Fig 9.2 Time based critical path network chart in December 1990

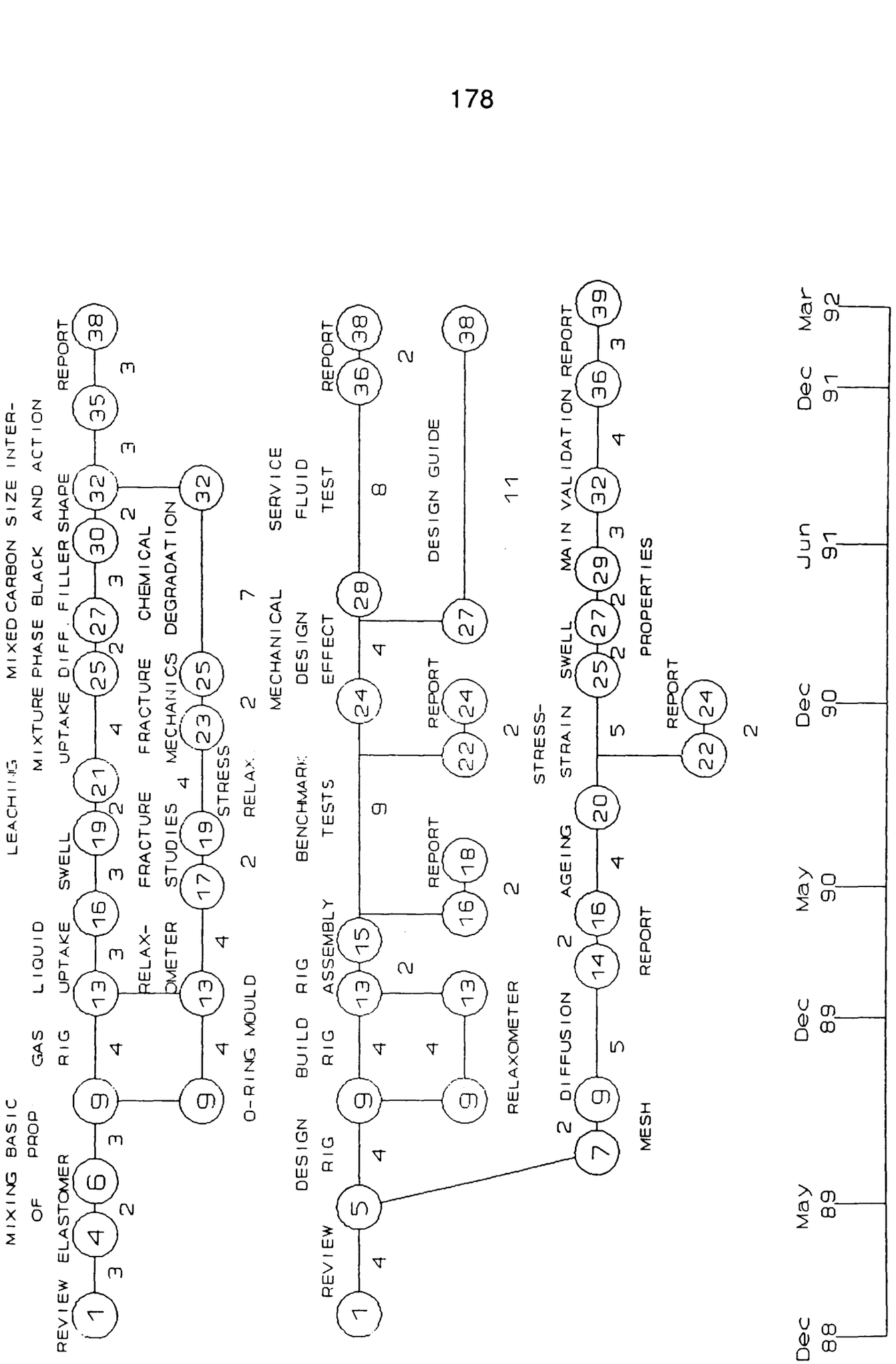

Fig 9.3 Time based critical path network chart in June 1990

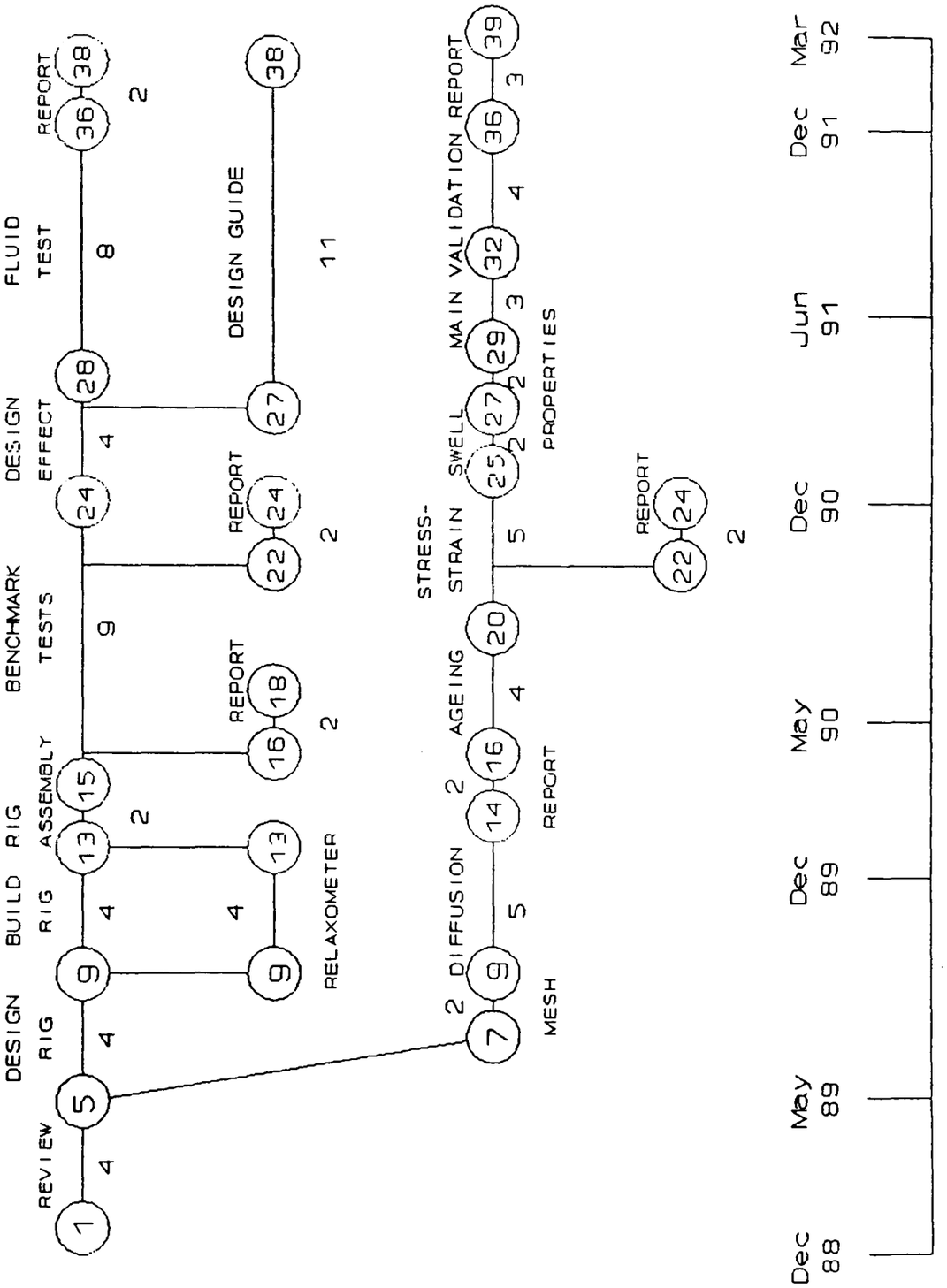

Fig 9.4 Time based critical path network chart in February 1990

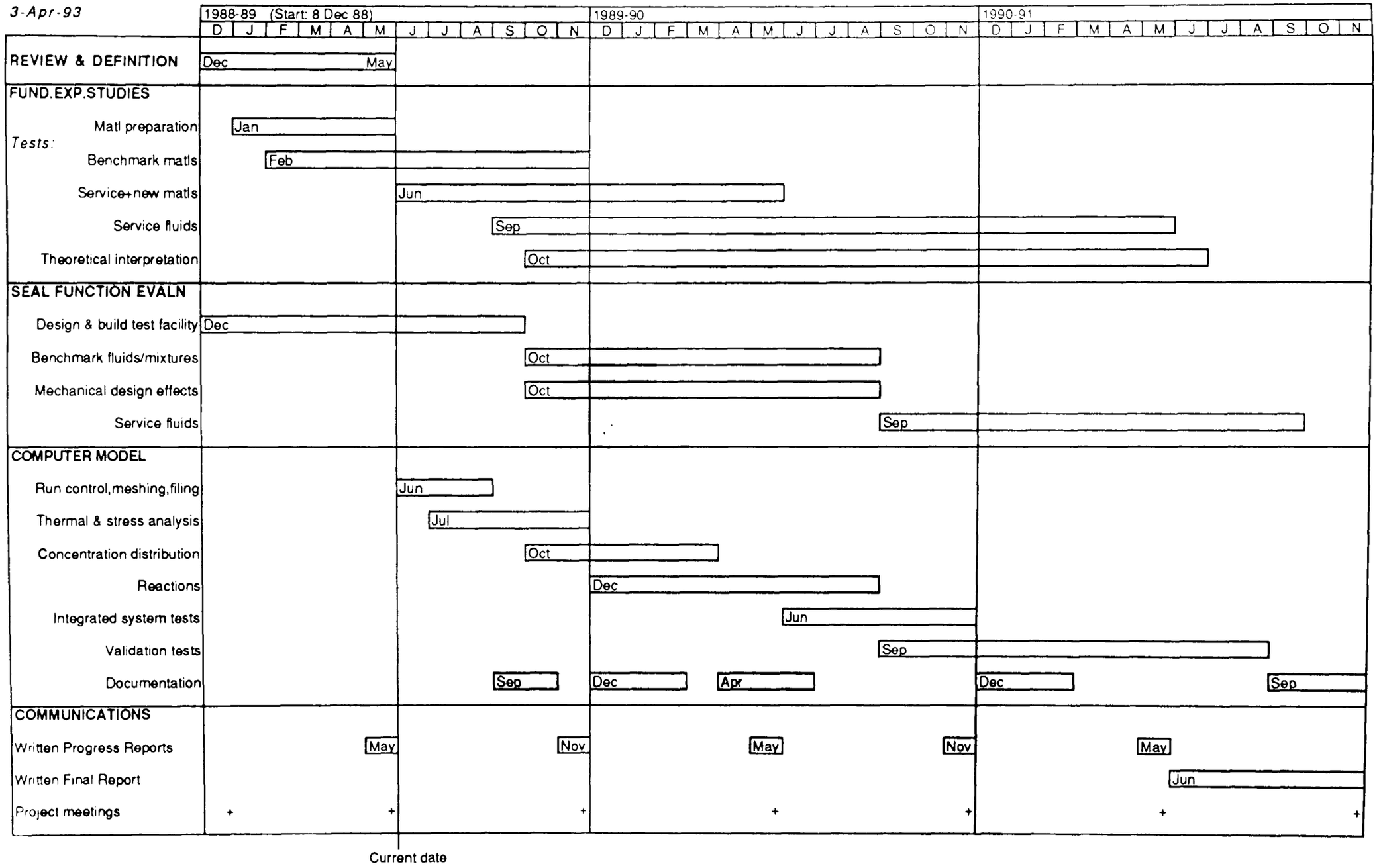

Fig 9.5 Bar chart for seal life project in November 1989

9.6 Budget Management and Financial Performance

Financial situation of a project can be represented by graph and table as shown at the end of this chapter. A graph can show the current cash flow condition and an overall view on the cost and income balance. However, it does not include the degree of completion of the project, and therefore cannot represent the performance of the project as a whole. A table of expected time and actual time is the better method in viewing performance in % of completion. Itemization of activities can also help to visualize the resources required for future work. In real applications, it is most likely that both graph and table have to be used to get a complete picture of the status of a project.

At the end of the seal life project, it had a 10% financial loss. That is about £30k over-spend in labour, after taking into account of company overhead, but excluding capital investment. This is due to a number of reasons :

i. There were less participants than the initial estimation. There were only eleven members in the consortium, not fifteen as estimated.
ii. The proposed time period for the completion of all the research work was very tight. Extra cost incurred to keep up time schedule.
iii. The administration work for the initial signing-up process had taken up a longer time than expected. Some participants did not complete their initial payment until 6 months after the starting of the project.
iv. The building of the seal life rig was more complicated than expected. There was a three month delay in the delivery of the machined parts. To reduce commission time, seal testing had to start before optimum function of the rig was achieved.
vi. There were more short term tests, less long term tests than planned.
vii. The running cost for testing hazard fluids was higher than initial estimation.
viii. Additional effort had been put in to use the established computer software for real application.

Most committee members of the Seal Life Project agreed that the two organizers, MERL and BHR Group had done very useful work on a relatively

tight budget; and there were new questions arising from the three years work needing to be addressed. Therefore, the committee members agreed to a further 2 year extension to carry out new areas of research, and welcome new participants to join the committee for the second phase work. These new participants have to pay a joining fee of £25,000 for the benefit of having the first phase project reports, and the full annual fee for 2 years without discount. The joining fee could help the two organizers to recover some of their first phase loss, while the annual fee will contribute to the cost of the second phase work.

To avoid the repeat occurrence of the financial problems in the second phase, the following steps have been taken:

i. the budget was estimated with the assumption of 11 members only;
ii. the discussion on proposal for the second phase work started 12 months before the launch of the project to allow administration time;
iii. allow time in the beginning of the programme to improve the seal life rig to reduce running cost;
iv. strictly assess the necessity for short term tests;
v. the capability of running service fluids is essential to the development of the seal life methodology, but hazard fluid tests have to be minimized;
vi. The application of existing software to service conditions has added value to the project. However, future application of existing software has to be limited to a fixed budget.

The PhD project is also at its conclusion phase, part of its programme has been altered with the Seal Life Project. However, it has the benefit of learning from the Seal Life Project to ensure the completion within time and manpower restraints.

Fig 9.6 Example of cash flow graph

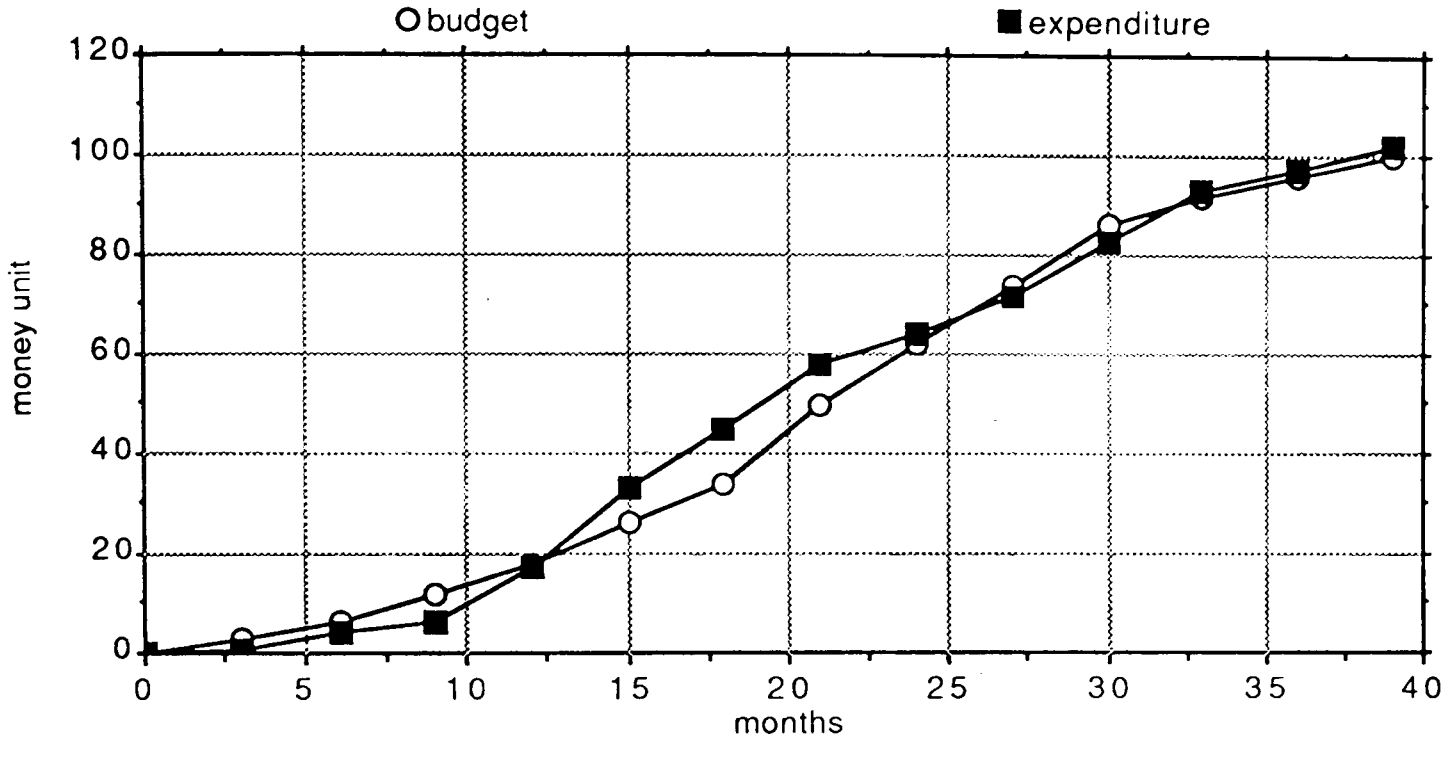

Fig 9.7 Table for cost control

Activity	Budget (£ unit)	% Complete	Expected (£unit	Actual (£unit)
A	5.0	100.0	5.0	5.0
B	24.0	50.0	12.0	15.5
C	17.0	100.0	17.0	17.0
D	D1+D2+D3=68	100.0	68.0	103.0
E	13.0	100.0	13.0	13.0
F	6.0	100.0	6.0	20.0
G	35.0	15.0	5.3	10.5
H	7.5	0.0	0.0	0.0
I	10.0	0.0	0.0	0.0
J	5.0	0.0	0.0	0.0
K	10.0	100.0	10.0	16.0
L	10.0	0.0	0.0	0.0
M	12.0	20.0	2.4	3.5
N	4.0	0.0	0.0	0.0
O	12.0	0.0	0.0	0.0
P	15.0	10.0	1.5	1.5
Total	253.0		140.2	205.0
%	100.0		55.0	81.0

10. DISCUSSION AND CONCLUSIONS

Prediction of elastomeric seal life in specified applications is a very complex exercise, due to the variety of failure modes and ageing processes. In the present work, computer software to assist in the prediction of seal life has been developed. Using the software, we can accurately calculate the fluid concentration in each section of a seal, and therefore the time required for ingressing fluids to saturate seals of different sizes and shapes. This provides a basis for the better understanding of the mechanisms of explosive decompression, and the factors affecting loss of sealing contact stress, such as the loss of strength (modulus), and changing dimensions (set and swell).

The most significant part of the present work focused on long term material ageing - chemical reaction of the seal material with fluid throughout the seal. This is traditionally less studied and slow in development because time consuming experiments or well recorded long term seal histories are required for theoretical validation. The main step forward using computer simulation, rather than conventional extrapolation of material specification measurements, is that it takes into account diffusion, shape and size of seals.

In particular, when crosslinks are formed in aged rubber, the modulus of the rubber increases and compression set occurs. Excessive hardening enbrittles and ruptures rubber seals. Compression set reduces the elasticity of rubber seals and therefore their ability to cope with movement in housing. In another situation, when chain-scissions occur, the modulus of the rubber decreases. Too much softening reduces contact stress between the rubber and its housing, to such an extent that leakage may occur. Chapter 7 has shown success for predicting modulus of high ACN NBR seals in air, water and hydrocarbon liquids, as well as for EPDM seals in air and water. The process still requires laboratory testing to specify material data for program input. Potential source for these laboratory results, and the mechanism to prepare the data for input into Seal-Life Software are explained with examples in chapter 7. It is important that material tests are performed in the service fluids, as experimental results and existing service data show that the same material can behave significantly differently in different environments.

A benefit of the computer software is that it permits use of geometrically simple test samples for characterizing material behaviour. This has the advantages :

i. fluid supply for chemical reaction is plentiful, allowing chemical reaction to start earlier.

ii. test samples are easier to obtain - manufacturers may not stock the specific size of O-rings that suit existing seal test rigs. Before a firm commitment to buy a large amount of seals, manufacturers may not provide seal test samples.

In some cases, there are already some field data available on the selected material. These data can be used by the Seal-Life Software to predict longer term material change or functional life of seals of the same material, but of other sizes and shapes, possibly at different temperatures.

However, we have seen from examples in Section 7.3 that the Seal-Life Software is not appropriate for all seal applications. The following approaches are recommended :

i. If the dominating failure mode of the material in the application is :

decompression - then use diffusion calculation by Seal Life Software to determine saturation time as a basis for explosive decompression test duration.

swell - then use diffusion and modulus change calculation by Seal Life Software.

ageing - short term physical - then use laboratory data since tests are very short

- long term chemical - then use :
  - diffusion and chemical reaction calculation of modulus by Seal Life Software, and
  - compression set calculation by empirical formula (section 8.1),
  - retained interference force by the semi-empirical relation based on a combination of theory and the above empirical treatment of compression set (section 8.3).

ii. If ageing at temperature for which data is not available :

- interpolate using Arrhenius formulation : with caution,

- extrapolation to lower temperature : with caution,
- extrapolation to higher temperature : not advisable.

Representation, measurement and interpretation of rubber properties in non-linear stress-strain analysis are complex problems. Uni-axial or biaxial experiments can only approximately characterize the elastic behaviour of filled rubber compounds. Even greater difficulties appear in the specification of rubber material properties for seal-life prediction, particularly in fluoroelastomers which have high physical material properties change initially, but slow chemical material properties change in long term service.

Validation tests for the Seal Life Software have been performed on :

i. benchmark polymer compounds versus single-species gas,
ii benchmark polymer compounds versus single-species liquid,
iii. benchmark polymer compounds versus multi-species service fluids.

The Seal Life Software has closely predict material property changes for nitrile, EPDM and HNBR in air, water and a mixture of hydrocarbon liquids. However, results for Viton E60C are less satisfactory. The ability of the software to predict material property change depends more on elastomers than fluids.

There is, probably, scope for improvements in the theory of rubber ageing. The present work has explained and quantified some of the behaviour observed from seals in service. The developed software are able to assist understanding on more seal behaviours, such as the hardening of EPDM in hot air, but not in hot water.

The study of incompressible elastic behaviour and dimensional change is reported in Section 4.3, based on Neo-Hookean formulation. The development of computer program for stress analysis is not included in the scope of the present work. However, the semi-empirical representation of experimental results for compression set and retained seal force has been presented. Their correlation with time and temperature in water are established in chapter 8. This confirms that experimental data on compression set generally follow the theoretical model :

$$\% \text{ permanent compression set} = A\,(T-Tg) + B \exp(-E/RT)$$

This is encouraging as the model is based on rubber property concepts. Permanent compression set provides a good indication to the elasticity of aged seals. Measured retained force after test represents the cool start performance of a seal. Good performance in both hot and cold environment is important as seals need to function in both cases whenever it occurs in operation.

11. RECOMMENDATIONS FOR FURTHER WORK

Further work is required in the following main areas :
- generation of more extensive or better input data for the model;
- extension of computer model capabilities;
- elucidation of fundamental processes;
- execution of parameter scans.

11.1 Input Data

There are gaps in existing data from test pieces and from seals. Fluoro-elastomers, such as Viton and Aflas, are normally quite resistant to chemical attack. Their chemical reaction properties are therefore particularly difficult to define from relatively short term tests. More longer term tests, from 3 to 6 months, are therefore required to better define the long term material behaviour of fluoroelastomers.

More material property data for different elastomers, including EPDM, nitrile rubber and fluoroelastomers, for a range of additional fluids, such as methane, hydrogen sulphide and corrosion inhibitors would be very useful for seal application in petroleum industry. Such data is required over a wide range of temperatures and pressures, and for extended exposure periods.

The Seal Life Software has the ability to continuously update material properties with the change in crosslink density in the polymer. There is however little material data available to make use of these facilities, therefore measurements are required for a range of elastomers and conditions to provide the required input data. For example, the relationship between Young's Modulus of nitrile rubber and crosslink density has been established, but other material properties, such as diffusion coefficient, solubility factor of gases and equilibrium concentration for liquid uptake can also change with crosslink formation / scission in aged rubber. Measurements of these effects will therefore provide a good basis for the validation of analogous relationships. There can also be chemical reactions involving the polymer chains which also need consideration.

11.2 Extension of Software

A semi-empirical correlation between compression set and retained force of O-rings has been presented. It provides a preliminary indication of contact stress in aged O-rings. The method is however not yet sufficiently accurate, nor does it cover seals of different shapes, such as V-rings, U-rings, T-rings etc. The problem needs addressing. Commercial finite element stress analysis packages with the ability to handle contact boundaries offer a solution to this problem, but it would be much more convenient if stress-strain analysis were incorporated into the program.

11.3 Fundamental Processes

The effect of Tg on permeation and possibly, elastic characteristics of seals at high pressure need to be established since the Seal Life Software requires users to input material properties at the operational conditions. For example, compaction occurs at high pressures and can raise the glass transition temperature (Tg) close to the operational temperature, changing material characteristics. Again, saturation concentration of carbon dioxide in high ACN NBR at 100°C goes beyond the limit to Henry's law, but not at 130°C.

The Seal Life Software assumes that there is a dominating consistent ageing process occurring in a seal throughout its life. Laboratory tests show that occasionally a seal can exhibit a delayed sudden acceleration in deterioration during a long term test, resulting in sudden failure. For example, we have seen delayed (36 days) sudden uptake of water by test pieces of Viton E60C at 155°C, followed by blistering. This is possibly due to water reacting with certain metal oxides and hydroxides present in the Viton E60C test pieces. It is important therefore that the possibility of this type of sudden deterioration is recognised and the circumstances under which it may occur be clearly defined.

11.4 Parameter Scans

Parameter scans using the Seal Life Software, within validated limits, should be run to develop design guide charts. Trends in seal behaviour can then be studied to provide insight into seal performance.

REFERENCES

LITERATURE REVIEW

1. Hindmarch, R.S., "Rubber Offshore",
   Rubber & Plastics Processing and Applications, 1985, Vol 1

2. MRPRA, "Comparison of Natural and Synthetic Rubbers",
   Materials & Design, Vol.10, No.1, January/February 1989, pp39-41

3. Allen, G., "Speciality Polymers : Prospect - Retrospect",
   Materials & Design, Vol 7, No.4, July/August 1986, pp179-181

4. Evans, R.K., "Selection of the Optimum Synthetic Seal",
   Materials & Design, Vol. 7, No.3, May/June 1986, pp120-123

5. Parker B. and Raines C., "Status report on Life Prediction tests
   Covering High Performance Elastomers in Severe Environments",
   3rd International Conference Polymers in Offshore Engineering,
   Scotland, June 1988, Paper 7

6. Palmer, K.P.,
   "High Temperature Elastomers in Gas Turbine Engine Fuel Sealing",
   8th International Conference on Fluid Sealing, University of Durham,
   UK, September 1978, Paper F1.

7. Seregely Z., Nagy T. and Pfisztner N.,
   "Ageing of Elastomers Under Simulated Offshore Conditions",
   3rd International Conference Polymers in Offshore Engineering,
   Scotland, June 1988, Paper 15

8. Stevenson, A.,
   "An Overview of the Requirements for Seal Life Prediction",
   Corrosion 92, the NACE Annual Conference and Corrosion Show,
   Paper No. 65.

9. Blakeston, M.L., Tomblin, K.A. and Ward J.,
"The Testing of Elastomers for Channel Seal Plugs in a Steam Generating Heavy Water Nuclear Reactors",
8th International Conference on Fluid Sealing, University of Durham, UK, September 1978, Paper G1.

10. Metcalfe, R., Baset, S.B., Lesco R. and Selander W.N.,
"Modelling of Space Shuttle Solid Rocket O-rings",
12th International Conference on Fluid Sealing, Brighton, UK, May 1989, Paper AI, pp3-25.

11. Ferry, J.D.,"Viscoelastic Properties of Polymers", John Wiley & Sons, 1961.

12. Wadiak, D.T., Bond, P.M., Cyr, N.A., Fields S., Ferguson, G.H., Swenson, L.W.,
"A Finite Element Methodology to Predict Age-related Mechanical Property and Structural Performance Changes in High Performance Polymers",
International Journal for Numerical Methods in Engineering, Vol.29, 1990, pp1159-1175.

13. Treloar, L.R.G., "The Physics of Rubber Elasticity", 3rd Edition, Clarendon Press, 1975.

14. Cowie, J.M.G., "Polymers : Chemistry and Physics of Modern Materials", International Textbook Company Ltd., 1973.

15. Flory, P.J., "Principles of Polymer Chemistry", Cornell University Press, ITHACA, NEW YORK, 1953.

16. Van Amerongen G. J., "Diffusion in Elastomers",
Rubber Chem. Technology 37, 1964, pp1065 - 1152

17. Southern, E.,"Diffusion of Liquids through Rubbers",
Rubber in Offshore Engineering, MRPRA, Proceedings of a conference,
London, April 1983, pp262-274

18. Rodriguez, F., "Principles of Polymer Systems", 3rd edition,
Hemisphere Publishing Corporation, 1989.

19. Bateman, L., "The Chemistry and Physics of Rubber-Like Substances",
Maclaren & Sons Ltd., London, 1963.

20. Young, R.J., "Introduction to Polymers", Chapman and Hall, London,
1981.

21. Beerbower, A., Kaye L.A., Pattison D. A.,"Picking the Right Elastomer to
Fit Your Fluids", Chemical Engineering, December 18, 1967

22. Adkins, P.W., "Physical Chemistry", 3rd Edition, Oxford Univ. Press,
1988, pp654, 677-678

23. Crank, J., "The Mathematics of Diffusion", 2nd Edition, Oxford Univ.
Press, 1975.

24. Zienkiewicz, O.C., "The Finite Element Method in Engineering
Science", McGraw-Hill, 1971, pp38-42

25. Zienkiewicz, O.C., "The Finite Element Method", 3rd Edition, McGraw-
Hill, 1977, pp44-58

26. Hinton, E and Owen, D. R. J.,
"An Introduction to Finite Element Computations", Pineridge Press,
1979, pp223-224

27. Hinton, E and Owen, D. R. J.,
"A Simple Guide to Finite Element", Pineridge Press, 1980, pp19-24, 70-71

28. Conner, Brebbia,
"Finite Element Techniques for Fluid Flow", pp166-168

29. Burnett, David S., "Finite Element Analysis from Concept to Application", A T & T Bell Laboratories, 1987, pp465-466

30. Ellis, N.S., McCauley, A.M., Mark, J.W.,
"Mathematical modelling of the diffusion of liquids in stressed polymers" Proceeding of the Plastics & Rubber Institute Conference Diffusion in polymers, Reading, Mar1988, Paper 19

31. Crank, J. and Park, G., "Diffusion in Polymers", Academic Press, London, 1968.

32. Harper, J.F., and Naeem, M., "The Moisture Absorption of Glass Fibre Reinforced Vinylester and Polyester Composites", Materials & Design, Vol. 10, No. 6, November/December 1989, pp 297-300.

33. Van Krevelen, D.W., "Properties of Polymers", 2nd edition, Elsevier Scientific Publishing Company, Amsterdam, 1976

34. Roy, S. and Reddy, J.N.,
"Finite-Element Models of Viscoelasticity and Diffusion in Adhesively Bonded Joints",
International Journal for Numerical Methods in Engineering, 1988, Vol 26, pp2531-2546

35. Campion, R.P. and Morgan G.J.,
"High Pressure Permeation and Diffusion of Gases in Polymers of Different Structures", Journal for Plastics Rubber & Composites : Processing & Applications, 17, 1992, No.1, pp51-58

36. Derham, C.J., "Elastomeric Sealing", Engineering, May 1977, pp405-407

37. Derham, C.J., "The effect of moisture on the creep and stress relaxation of natural and synthetic general purpose rubbers", Proc. International Rubber Conference, Brighton, May 1972, Paper F1

38. Derham, C.J., "Creep and stress relaxation of rubbers - the effects of stress history and temperature changes", Journal of Materials Science 8, 1973, pp1023-1029

39. Brydson, J.A., "Rubber Chemistry", Applied Science Publishers Ltd, 1978, pp198-205, 270-279

40. Blow, C.M., "Elastomers for Seals - a Review", Review and Bibliography on Aspects of Fluid Sealing, BHRA, Cranfield, UK, 1972, Paper D, pp41-105.

41. Southern, E., and Thomas, A.G., "Diffusion of Liquids in Crosslinked Rubbers", Part 1, Transactions of the Faraday Society, No.536, Vol 63, Aug 1967, pp1913-1921.

42. Hermann, R., "Environmental Degradation in Fuselage Aircraft Windows", Materials & Design, Vol. 10, No.5, September/October 1989, pp241-247.

43. Sperling, L.H., "Introduction to Physical Polymer Science", John Wiley & Sons, 1986.

44. Sheehan, C.J., and Bisio, A.L., "Polymer/Solvent Interaction Parameters", Rubber Chem Technology 39, No.1, Feb 1966, pp149-192

45. Johannesson, Hans L., "Calculation of the Pressure Distribution in an O-ring Seal Contact", Proceedings of the 5th Leeds-Lyon Symposium on Tribology, 1978, Paper XI (ii), pp379-384.

46. Johannesson, Hans L.,
"Calculation of the Pressure Distribution in an Arbitrary Elastomeric Seal Contact", Wear, 130 (1989), pp3-15

47. Herrmann, L.R., 1965
"Elasticity Equations for Incompressible and Nearly Incompressible Materials by a Variational Theorem",
AIAA Journal, Vol.3, no.10, pp1896-1900

48. Kikuchi, N., "Finite Element Method in Mechanics",
Cambridge Univ. Press, 1986.

49. Zienkiewicz, O.C.,
"the Finite Element Method - Basic Formulation and Linear Problems",
4th Edition, Vol 1, McGraw-Hill, pp 334-363

50. Salita, M.,
"A Simple Finite-Element Model of O-ring Deformation and Activation during Squeeze and Pressurization",
AIAA-87-1739, AIAA/SAE/ASME 23rd Joint Propulsion Conference, San Diego, California, June 1987.

51. Eirich, F.R., "Rheology : Theory and Applications", Vol. 1, 1956,
Academic Press, New York, Chapter 10, "Large Elastic Deformation" by Rivlin R.S., pp351-386

52. Williams, J.G., "Stress Analysis of Polymer", 2nd edition, Ellis, 1980.

53. Oden, J.T., "Finite Elements of Nonlinear Continua", McGraw-Hill, 1972.

54. Medri, G., Molari, P.G. and Strozzi, A.,
"Numerical and Experimental Stress-Strain Analysis on Rubber-like Seals in Large Elastic Deformations under Unilateral Contact",
8th International Conference on Fluid Sealing, Durham, England,
Sept. 1978, Vol 1, Paper F2, pp19-30.

55. George, A. F., Strozz A., and Rich, J.I.,
"Stress Fields in a Compressed Unconstrained Elastomeric 'O' Ring Seal and a Comparison of Computer Predictions with Experimental Results.", 11th International Conference on Fluid Sealing, Cannes, Frances, Paper B1, April 87, pp117-137

56. Green, Itzhak, and English, Capel,
"Analysis of Elastomeric O-ring Seals in Compression Using the Finite Element Method", Tribology Transactions, Volume 35 (1992),1, pp83-88

57. Pascoe, S.K., Mottershead J.E. and Hellen T.K.,
"A Comparison of Finite Element Techniques for Contact Stress Analysis", Proceeding of the Conference, Stress and Vibration, Liverpool, April 1989, pp299-312

58. Rizzo, A.R., "FEA Gap Elements : Choosing the Right Stiffness", CIME, Mechanical Engineering, June 1991, pp57-59

59. Derby, T., Collins, F. and Moses, C.,
"Finite Element Analysis in the Manufacturing and Design of Rubber Engineering Components",
Rubber in Offshore Engineering, MRPRA, Proceedings of a conference, London, April 1983, pp89-113

60. Nelson, Norman W.,
"Finite Element Analysis in the Design of Rubber Components",
Symposium on Engineering Design with Elastomers, August 20-24,1989

61. Morman, Kenneth N., and Pan Tsung Y.,
"Application of Finite-Element Analysis in the Design of Automotive Elastomeric Components",
Rubber Chemistry and Technology, July-Aug 1988, Vol. 61, pp503-533

62. Fursdon, P.M.T.,
"Finite Element Analysis in the Design of Rubber Components",
Rubbercon 92, Brighton, June 92.

63 . Ho, E., Flitney R.K. and Nau B.S.,
"Elastomeric Seal Life - Prediction",
Elastomers in oil recovery, RAPRA Seminar, Manchester, Sep 1991.

DEVELOPMENT OF THEORETICAL METHOD

64. Campion, R. P. and Morgan, G. J.,
MERL Seal Life Report SL/M4, January 92,
"High Pressure Gas Permeation and Related Properties"

65. Campion, R. P. and Morgan, G. J.,
MERL Seal Life Report SL/M6, January 92,
"Liquid Diffusion Studies of Benchmark Elastomers"

66. Berry, J.P., Scanlan, J. and Watson, W. F.,
"Cross-Link Formation in Stretched Rubber Networks", August 1956,
the Transactions of the Faraday Society, No. 404, Vol. 52, Part 8.

NUMERICAL METHOD

67. Zienkiewicz, O. C.,
"The Finite Element Method in Structural and Continuum Mechanics",
McGraw-Hill, 1968, p166-168

PROGRAM VALIDATION AND APPLICATION

68. Carslaw, H.S. and Jaeger, J.C.,
"Condition of Heat in Solids", 2nd Edition, Oxford University Press, 1959, pp101-102

69 Tom Pugh and Jim Goodson,
"Elastomers for Subsea Safety Valve Flapper Seals",
Corrosion 91, the NACE Annual Conference and Corrosion Show, Paper No. 457.

70. Fagg S.V., "Differential Equations", Hodder and Stoughton, 1977, pp27-29

71a. Perry H.J., "Chemical Engineers' Handbook", 2nd Edition, McGraw-Hill, 1974

71b. Potts, D. J.,
"Explosive Decompression Resistance of Elastomers in Gas Duties", Offshore Engineering with Elastomers, Aberdeen, Scotland, Paper 15, June 85.

PROJECT MANAGEMENT

72. Archibald, R.d.,
"Managing High-Technology Programs and Projects", Wilney, 1976.

73. Kerzner, H. and Thamhain, H.J.,
"Project Management for Small and Medium Size Business",
Van Nostrand Reinhold Company Inc.,1984

74. "Pump & Valve Products", Offshore Engineer, February 1990, pg 51.

75. Fox, C., "Completion Technology Embraces the Computer Age", Offshore Engineer, August 1991, pg 36.

76. Lowes, J.M., "Pressure-Testing Method Permits Line-Segment Isolation", Oil & Gas Journal, December 1990, pp121-123.

77. Nandke, J. S., "Corrosion Causes Most Pipeline Failures in Gulf of Mexico", Oil & Gas Journal, October 1990, pp40-44

78. Krembs, J. A., and Connolly, J. M., "Analysis shows Process Industry Accident Losses Rising", Oil & Gas Journal, August 1990, pp40-45.

79. Dukes, R., "Materials Research for the Royal Navy", Materials & Design, Vol. 8, No. 4, July/August 1987, pp198-203.

80. Lester A., "Project Planning and Control", Butterworth, 1982.

81. Lock, D., "Project Management", 3rd edition, Gower, 1984.

APPENDIX 1 DIFFERENTIAL EQUATIONS GOVERNING FLUID DIFFUSION IN POLYMERS

A1.1 Cartesian Coordinate

According to Fick's 1st Law of Diffusion, the fluid mass flow (J_x) in the x direction is proportional to the concentration gradient ($\partial c/\partial x$) in the same direction.

$$J_x=-DA(\partial c/\partial x) \quad \text{(A1.1)}$$

where D is the diffusion coefficient, A is the cross-sectional area, and c is the concentration of fluid in its host.

Consider a thin slab of cross-sectional area A extending from x to dx, the left hand side inflow is

$$J_x = -DA(\partial c/\partial x) \quad \text{(A1.2)}$$

the right hand side outflow is

$$J_{x+dx} = -DA\partial/\partial x\{c+(\partial c/\partial x)dx\} \quad \text{(A1.3)}$$

The rate of mass uptake in the slab during a time interval $d\tau$ is therefore

$$(\partial c/\partial \tau)\, Adx = J_x - J_{x+dx} = DA\{\partial^2 c/\partial x^2\}dx$$

$$\partial c/\partial \tau = D\{\partial^2 c/\partial x^2\} \quad \text{(A1.4)}$$

known as Fick's 2nd Law of Diffusion

In a 3-dimensional field

$$\partial c/\partial \tau = D_x(\partial^2 c/\partial x^2) + D_y(\partial^2 c/\partial y^2) + D_z(\partial^2 c/\partial z^2) \quad \text{(A1.5)}$$

If there is a fluid source or sink in the media, +ve or -ve, for example due to reaction of the fluid with rubber constituents, an additional term S_i expressed as the change of concentration per unit volume is added to equation (A1.5)

$$\partial c/\partial \tau = D_x\{\partial^2 c/\partial x^2\} + D_y\{\partial^2 c/\partial y^2\} + D_z\{\partial^2 c/\partial z^2\} + S_i \quad \text{(A1.6)}$$

For steady state application, the mass of substance in an element volume does not change with time, i.e. the net mass uptake is zero at each time interval. Therefore,

$$D_x\{\partial^2 c/\partial x^2\} + D_y\{\partial^2 c/\partial y^2\} + D_z\{\partial^2 c/\partial z^2\} + S_i = 0 \quad \text{(A1.7)}$$

A1.2 Axisymmetric Coordinates

Consider an elemental cylindrical tube with internal radius r and external radius (r+dr), the rate of radial diffusion through the inner face ($2\pi rdz$) is

$$J_r = - D_r (2\pi rdz) (\partial c/\partial r) \quad \text{(A1.8)}$$

The rate of radial heat inflow through the outer face $2\pi(r+dr)dz$ is

$$J_{r+dr} = - D_r * \{2\pi dz (r+dr)\} * \partial(c + (\partial c/\partial r)\, dr\,) /\partial r$$

$$= - D_r * 2\pi dz (r+dr) * (\partial c/\partial r + (\partial^2 c/\partial r^2)dr) \quad \text{(A1.9)}$$

The radial diffusion from the cylinder is

$$J_r - J_{r+dr}$$

$$= D_r (2\pi dz) [- r(\partial c/\partial r) + r(\partial c/\partial r) + r(\partial^2 c/\partial^2 r)dr + dr(\partial c/\partial r) + dr^2(\partial^2 c/\partial^2 r)\,]$$

$$= D_r (2\pi dzdr) [r(\partial^2 c/\partial^2 r) + (\partial c/\partial r)] \qquad \text{neglecting 2nd derivative}$$

$$= D_r (2\pi dzdr)\, \partial/\partial r\, [r(\partial c/\partial r)] \quad \text{(A1.10)}$$

The longitudinal diffusion through the cylinder is

$$J_{1z} - J_{2z}$$

$$= -D_z(2\pi rdr)(\partial c/\partial z) + D_z(2\pi rdr)\{(\partial c/\partial z) + dz(\partial^2 c/\partial z^2)\}$$

$$= D_z(2\pi rdrdz)(\partial^2 c/\partial z^2)$$

$$= D_z (2\pi dzdr)\, \partial/\partial z\, [r(\partial c/\partial z)] \quad \text{(A1.11)}$$

The net mass inflow into the axisymmetric cylindrical tube must be equal to the mass uptake by the tube during the time interval $d\tau$, therefore

$$2\pi rdrdz\, (\partial c/\partial \tau) = D_z (2\pi dzdr)\, \partial/\partial z\, [r(\partial c/\partial z)] + D_r (2\pi dzdr)\, d/dr\, [r(\partial c/\partial r)]$$

$$\partial c/\partial \tau = \partial/\partial z\, [\, D_z(\partial c/\partial z)] + 1/r\, \{\partial/\partial r\, [D_r r(\partial c/\partial r)]\} \quad \text{(A1.12)}$$

To include the possibility of a source of change of concentration in the media, the full equation would be

$$\partial c/\partial \tau = \partial/\partial z\, [\, D_z(\partial c/\partial z)] + 1/r\, \{\partial/\partial r\, [D_r r(\partial c/\partial r)]\} + S_i \quad \text{(A1.13)}$$

where r is the radius, z is the longitudinal length

At steady state, there is no net change of concentration in the media, equation (A1.13) can be simplified to

$$\partial/\partial z\,[\,D_z(\partial c/\partial z)] + 1/r\,\{\partial/\partial r\,[D_r r(\partial c/\partial r)]\} + S_i = 0 \quad \text{..... (A1.14)}$$

Reference: Adkins, Physical Chemistry 3rd Edition, pp654, 677-678
Conner and Brebbia, Finite Element Techniques, pp258-259
Zienkiewicz, The Finite Element Method, pp434-435
Roger & Mayhew, Engineering Thermodynamics, Work and Heat Transfer pp495-496

APPENDIX 2 Shape (Interpolation) Functions and their Derivatives of Isoparametric Quadratic Triangular Element

Shape functions for isoparametric elements can be found in most of the finite element test books. They are formulated based on area coordinates. Isoparametric quadratic triangular elements are chosen for higher ability to fit curved boundary. Their shape functions are:

$N_1 = \beta * (2 * \beta - 1)$

$N_2 = \eta * (2 * \eta - 1)$

$N_3 = \zeta * (2 * \zeta - 1)$

$N_4 = 4 * \eta * \zeta$

$N_5 = 4 * \beta * \zeta$

$N_6 = 4 * \beta * \eta$

The derivatives with respect to β are

$\partial N_1 / \partial \beta = 4 * \beta - 1$

$\partial N_2 / \partial \beta = 0$

$\partial N_3 / \partial \beta = 0$

$\partial N_4 / \partial \beta = 0$

$\partial N_5 / \partial \beta = 4 * \zeta$

$\partial N_6 / \partial \beta = 4 * \eta$

The derivatives with respect to η are

$\partial N_1 / \partial \eta = 0$

$\partial N_2 / \partial \eta = 4 * \eta - 1$

$\partial N_3 / \partial \eta = 0$

$\partial N_4 / \partial \eta = 4 * \zeta$

$\partial N_5 / \partial \eta = 0$

$\partial N_6 / \partial \eta = 4 * \beta$

The derivatives with respect to ζ are

$\partial N_1 / \partial \zeta = 0$

$\partial N_2 / \partial \zeta = 0$

$\partial N_3 / \partial \zeta = 4 * \zeta - 1$

$\partial N_4 / \partial \zeta = 4 * \eta$

$\partial N_5 / \partial \zeta = 4 * \beta$

$\partial N_6 / \partial \zeta = 0$

Reference: Zienkiewicz, The Finite Element Method in Engineering Science,pp115-119

Zienkiewicz, The Finite Element Method, third edition, pp164-167

Desai and Abel, Introduction to the Finite Element Method, pp98

APPENDIX 3 FULL CONVECTION BOUNDARY MATRIX

Writing $h\int_{\varphi}\{N\}^T\{N\}d\varphi$ in full

$$= h_1/4 \{w_1 \sqrt{[(2x_6 - 2x_2) + (x_1 - 2x_6 + x_2)z_1]^2 + [(2y_6 - 2y_2) + (y_1 - 2y_6 + y_2)z_1]^2}$$

$$\begin{bmatrix}
(z_1+1)^2(z_1-1)^2/64 & (1-z_1)^2(1+z_1)(z_1-3)/64 & 0 & 0 & 0 & (z_1+1)^2(z_1-1)(3-z_1)/32 \\
(z_1-3)(1-z_1)^2(z_1+1)/64 & (3-z_1)^2(1-z_1)^2/64 & 0 & 0 & 0 & (3-z_1)^2(1-z_1)(z_1+1)/32 \\
0 & 0 & 0 & 0 & 0 & 0 \\
0 & 0 & 0 & 0 & 0 & 0 \\
0 & 0 & 0 & 0 & 0 & 0 \\
(z_1+1)^2(3-z_1)(z_1-1)/32 & (3-z_1)^2(1-z_1)(z_1+1)/32 & 0 & 0 & 0 & (z_1+1)^2(3-z_1)^2/16
\end{bmatrix}$$

$$+ \{w_2 \sqrt{[(2x_6 - 2x_2) + (x_1 - 2x_6 + x_2)z_2]^2 + [(2y_6 - 2y_2) + (y_1 - 2y_6 + y_2)z_2]^2}$$

$$\begin{bmatrix}
(z_2+1)^2(z_2-1)^2/64 & (1-z_2)^2(1+z_2)(z_2-3)/64 & 0 & 0 & 0 & (z_2+1)^2(z_2-1)(3-z_2)/32 \\
(z_2-3)(1-z_2)^2(z_2+1)/64 & (3-z_2)^2(1-z_2)^2/64 & 0 & 0 & 0 & (3-z_2)^2(1-z_2)(z_2+1)/32 \\
0 & 0 & 0 & 0 & 0 & 0 \\
0 & 0 & 0 & 0 & 0 & 0 \\
0 & 0 & 0 & 0 & 0 & 0 \\
(z_2+1)^2(3-z_2)(z_2-1)/32 & (3-z_2)^2(1-z_2)(z_2+1)/32 & 0 & 0 & 0 & (z_2+1)^2(3-z_2)^2/16
\end{bmatrix}$$

$$+ h/4 \{w_1 \sqrt{[(2x_1 - 2x_6) + (x_1 - 2x_6 + x_2)z_1]^2 + [(2y_1 - 2y_6) + (y_1 - 2y_6 + y_2)z_1]^2}$$

$$\begin{bmatrix}
(z_1+1)^2(z_1+3)^2/64 & -(1-z_1)(1+z_1)^2(z_1+3)/64 & 0 & 0 & 0 & (z_1+3)^2(1+z_1)(1-z_1)/32 \\
(z_1-1)(1+z_1)^2(z_1+3)/64 & (1-z_1)^2(1+z_1)^2/64 & 0 & 0 & 0 & -(1-z_1)^2(1+z_1)(z_1+3)/32 \\
0 & 0 & 0 & 0 & 0 & 0 \\
0 & 0 & 0 & 0 & 0 & 0 \\
0 & 0 & 0 & 0 & 0 & 0 \\
(z_1+3)^2(1+z_1)(1-z_1)/32 & -(1-z_1)^2(3+z_1)(z_1+1)/32 & 0 & 0 & 0 & (z_1+3)^2(1-z_1)^2/16
\end{bmatrix}$$

$$+ w_2 \sqrt{\ [(2x_1 - 2x_6) + (x_1 - 2x_6 + x_2) z_2]^2 + [(2y_1 - 2y_6) + (y_1 - 2y_6 + y_2) z_2\ ]^2}$$

$$\begin{bmatrix}
(z_2+1)^2(z_2+3)^2/64 & -(1-z_2)(1+z_2)^2(z_2+3)/64 & 0 & 0 & 0 & (z_2+3)^2(z_2+1)(1-z_2)/32 \\
(z_2-1)(1+z_2)^2(z_2+3)/64 & (1-z_2)^2(1+z_2)^2/64 & 0 & 0 & 0 & -(1-z_2)^2(1+z_2)(z_2+3)/32 \\
0 & 0 & 0 & 0 & 0 & 0 \\
0 & 0 & 0 & 0 & 0 & 0 \\
0 & 0 & 0 & 0 & 0 & 0 \\
(z_2+3)^2(1+z_2)(1-z_2)/32 & -(1-z_2)^2(3+z_2)(z_2+1)/32 & 0 & 0 & 0 & (z_2+3)^2(1-z_2)^2/16
\end{bmatrix}$$

APPENDIX 4 SEAL LIFE TEST RIG

A4.1 OBJECTIVES

Rubber seals were tested to generate data for comparison with predictions, using computer modelling and data from physical tests on simple test pieces. Test facilities were required to accommodate two types of test :

(i) Ageing tests - to generate data on the progressive degradation of seals with time under carefully controlled conditions. Tests fluids were to include:

simple benchmark fluids, either liquid or gas.
mixed phase benchmark fluids, liquid+gas.
simulated service fluids

(ii) Gas decompression tests - to generate data on explosive decompression behaviour of seals. Test fluids were to include:

simple benchmark gases
mixtures of benchmark gases
mixtures of benchmark liquids and gases

Since most major operational specifications for each type of test were similar, the two types of test can be accommodated by a single type of test rig. To provide for ageing tests of extended duration for 1-6 months in non-hazardous fluids up to 100°C, 2500 psi, two simpler test rigs were also provided.

A4.2 PERFORMANCE ENVELOPE

Tests over a wide range of fluid pressures were planned. Although not necessary to cover all possible service pressures, it was important that the range be sufficient to include all major pressure phenomena which were expected to occur in service. Target maximum working pressure was therefore set at 15 000 psi.

Tests over a range of fluid temperature were planned, up to 230°C and down to 4°C. The former based on oil wellhead considerations and the latter on seabed conditions.

In December 1989, six reference liquids and three reference gases were employed for this project.

The reference liquids are
- Toluene
- iso-Octane
- Sea water (standard, BS3900/2011)
- Demineralised water (conductivity <2μs)
- Methanol
- Ethylene glycol (ethanediol)

The reference gases are
- Carbon dioxide
- Methane
- Nitrogen

These standard test fluids and their mixtures would be used to establish material behaviour and seal performance for the project.

Functional rig tests on service fluids, including hydrogen sulphide, corrosion inhibitors etc., would be carried out on the last stage of the project.

A4.3 DESIGN CONSIDERATIONS

The design of the test facility evolved through iterative discussions with sponsors, at Project Meetings and by mail. Key issues addressed during the design process are discussed below.

A4.3.1 Primary constraints

The critical constraint was safety, initially the policy was to keep test fluid (including leakage) physically separated from the primary heating equipment. Whilst having the advantage of being intrinsically safe, this approach involves an intermediate heat transfer fluid and separate ducts within the test unit, the result being that valuable test fluid volume is sacrificed. Despite exploring many possibilities, it did not proved possible to achieve significant increase in test fluid volume with this concept. The problem is that to maintain safe stress levels at 15000psi, 230°C, the structure rapidly escalates in size, weight and cost as test fluid volume is increased.

An adequately large fluid volume is important to avoid significant chemical change during tests. Such change may result from differential adsorption of chemical species by the seals or leaching of various substances from the the seals into the fluid. In view of this the original policy was changed. The new concept was based around electric heaters fitted directly to the test unit, the entire assembly enclosed by an inert gas blanket, to control the fire/explosion hazard. This is more complex in operation but results in a worthwhile increase in fluid volume.

A4.3.2 Operational considerations

Operational considerations affecting rig design were:

i) The main object was to determine the progressive degradation of test seals as a function of time, under controlled conditions. For this it is required to be able to remove seals from test after defined periods of

time for measurement and analysis. Once removed, seals would not normally be returned to the test rig for further testing.

ii) It was <u>not</u> intended to 'test to failure' in order to compile 'definitive' performance data for specific seal materials and service fluids, although some useful information of this kind was expected to be generated incidentally.

iii) Tests with a variety of fluid media were planned. It was not required to cover all service fluids of possible interest , however it was important that fluids used should be likely to cause measurable seal degradation under test conditions, reproducing different degradation mechanisms of practical importance.

iv) Since multiple fluids and fluid phases were to be tested, it was necessary to make provision for mixing constituents before introduction to the test chamber and minimizing stratification subsequently.

v) For operational simplicity and economy it was desirable to have as many test stations on the pressure vessel as possible. Individual test stations should be easily dismountable for individual replacement of test seals. The dismounted module should be capable of retaining the face seal in compression for offline measurement of residual sealing stress and compression set.

vi) Test fluid should be rechargeable in the course of a test, to make up leakage or restore changed fluid composition.

A4.3.3 Test chamber volume

Substances can be leached from test seals and affect other seals on the same rig, if not identical; care is therefore needed to minimize possible interactions of this type. This can be achieved by not mixing, in the same test, materials likely to cause interactions and by maximizing fluid volume. There is also concern that, if the volume of gas in a test fluid mixture is small, its

volume could be comparable with the volume of rubber in the system and might therefore change significantly due to absorption in the rubber. This again requires maximum fluid volume.

There are conflicting design requirements in that while test chamber volume should be as large as possible, for the reasons above, structural stresses increase with size and rapidly necessitate impracticably massive housings to handle fluid at maximum rated working conditions, 15 000 psi at 230°C. The design concept does provide for on-line replenishment of test fluid during tests(see piping diagram) but the fluid volume in the test chamber at any given time is nevertheless limited.

Another factor bearing on this issue is the method of heating. For safe operation with flammable fluids it is preferable to use an intermediate heat transfer fluid, so that there are no high temperature heaters exposed to leaking vapor. This also facilitates cooling to required sub room temperature tests, at 4°C. This approach requires provision of separate channels in the test unit, which has strength and volume implications. On this basis the test fluid volume available actually within the test unit, as distinct from connecting pipework etc., would have been about 200ml.

However, the chamber volume requirement is considered over-riding and for this reason the rig concept was modified to allow direct electric heating, the space otherwise occupied by heating channels now being incorporated into the test fluid volume. A nitrogen blanket system was introduced to handle the flammability problem. The chamber was also lengthened to accommodate the heaters and this also provided extra volume. With this approach the final test unit fluid volume was about 700ml.

A4.3.4 Test seal sizing

Test seals were required to be a standard size, to facilitate procurement; they should also be available in several thicknesses to permit study of section size effects. In view of this and the requirement that they be of reasonable size in relation to the test housing, this narrows the choice. A 25.4 mm o.d.

size was therefore selected which is available in four section thicknesses. To give the maximum size range, the largest and smallest of these are the Preferred Sizes : 1.8 mm and 5.33 mm. The stress analysis of the housing was based on the groove size required for the larger of these.

A4.3.5 Test seal interference

This is a test variable to be explored in the test program. Since most tests are planned for high temperatures, a low squeeze value was initially designed in. However, as there is considerable interest in high squeeze the initial design values have now been increased to be just above the maximum recommended in BS 1806 .

A4.3.6 Test-vessel material selection

The table below summarizes pros and cons of shortlisted materials. Both strength and fluid compatibility requirements are met in their entirety only by Hastelloy C276 and Inconel 625, although both are expensive, and on long delivery. Ferralium is of a more economical price, strong enough to permit a chamber fluid volume approaching 700ml, and allows low percentage hydrogen sulphide gas to be tested. Ferralium was therefore chosen as the fabricated material.

Table 1: Vessel material comparisons.

Material	**Compatibility with**	**Cost / availability test fluids**
Hastelloy C276	all	expensive. £9000 per vessel, long delivery.
Ferralium 255-3SF duplex stainless steel. £3000 per vessel ex stock	low temperature hydrogen sulphide	moderate cost
Inconel 625	all	very expensive.
S61 = high-strength stainless steel	not hydrogen sulphide, crevice corrosion in sea-water	low cost, £800 per vessel
S31 = Ti-stabilized stainless-steel	seawater-resistant	no supplier located, strength poor

A4.4 MAIN TEST RIG

The main seal life test rig was commissioned in January 1990 for running non-hazardous fluids. Instrumentation was fine tuned and seal testing started with carbon dioxide, nitrogen and demineralised water, while the installation of safety devices continued. The rig was commissioned for running inflammable fluids in July 1990. A general description of the rig is given below :

A4.4.1 Pressure vessel

The main pressure vessel made of Ferralium is capable of a slow oscillation mechanism through 180° to ensure even exposure of the tested seals to fluid mixtures (see fig A4.1). Its central chamber contains most of the test fluid, while two sets of four test stations are bolted to the central unit (see fig A4.2 and A4.3). Fluids in the vessel are not circulated, but any small loss in pressure is made-up from an external fluid reservoir by the pressurizing pumps.

To withstand high pressure up to 15000psi (1000 bar), the vessel has thick walls. The vessel is heated by band-heaters fixed at the middle of the vessel and near to its two ends. A pair of thermocouples is situated next to the middle band-heater on the external surface of the metal, for detecting the metal temperature. It can then control all the heaters to maintain steady rig temperature.

A4.4.2 Test seal housings

A total of eight test stations are fixed to the main vessel. Each station has a test flange and a thick end cap. Eight flanges and eight end caps were made of Ferralium. Each flange can accommodate two test seals in different configurations, flange and spigot (see fig 4 and 5). To withstand high test pressure, relative high bolt tension is applied to the end caps - a minimum of 62N bolt tension on each of the eight 12mm nominal diameter bolts. Anti-extrusion rings are also installed at the atmospheric side of each spigot

seal. After assembly, the nominal flange seal interference is 20% and the nominal spigot seal interference is 13%.

Another set of eight 316 stainless steel flanges were fabricated in March 1991, providing an alternative extrusion gap in the spigot groove (see fig A4.6). Extrusion on flange is provided by spacer. After assembly, the nominal flange seal interference is 16% and the nominal spigot seal interference is 13%.

A4.4.3 Fluid supply system

High pressure pipework is installed for supplying fluids to the rig (see fig A4.7). A gas booster and a liquid pump are used to build up system pressure. Both of them are operated by compressed air. The value of the system pressure is shown on a pressure gauge. A pressure transducer in the pipework also sends signals continuously to a chart recorder as a permanent record.

Normally, venting of fluids is carried out by a manual vent valve installed in the system. In case of emergency, when high pressure has built up, the system is automatically vented off by a relief valve. Rig pressure can also be 'dumped' in an emergency by a remotely operated valve.

A4.4.4 Leakage collection system

A leakage collection system was designed and built for monitoring slow leakage from the test seals (see fig A4.8). Collection channels are linked to the low pressure side of each test seal. These channels guide leakage from the seals to eight low pressure glass chambers by sixteen flexible pipes. Each chamber has two separate fluid inlets, and four of these chambers are piped to a vent valve and a sensitive pressure transducer. The transducers continuously monitor any pressure fluctuations. An increase in pressure indicates leakage. The vent valves open when a pre-determined pressure has built up in the leakage chambers.

The glass chambers are filled with water in gas tests. Leakage from an individual inlet can therefore be seen as bubbles, indicating the origin of the leakage. In liquid tests, the glass chambers are initially purged clear with nitrogen, so that vapour condensed on the glass walls can be seen. A large gas or liquid leak would exceed the flow capacity of the liquid hydropump or gas booster and the resultant pressure drop would stop the test.

A4.4.5 Instrumentation

In addition to the heat-control thermocouple situated next to the middle band-heater, two thermocouples are located in the test fluid. Fluid temperatures are about 10°C lower than the external metal temperature, at or above 100°C.

Continuous test parameters are logged by a chart recorder situated outside the test room. These parameters include :

i) pressure detected by the main pipework pressure transducer,
ii) pressure from the leakage chamber pressure transducers,
iii) room temperature from thermocouples,
iv) fluid temperatures from in-situ thermocouples,
v) readings from hydrocarbon sensors,
vi) nitrogen level in the test cabinet.

A4.4.6 Safety systems

The Seal Life Test Rig is situated in an isolated test room . There are escape doors at each end of the room. The Seal Life Test Rig is situated in a cabinet inside the room, with emergency shut down switch on the cabinet. The cabinet is filled with nitrogen during test of inflammable liquids, to reduce internal level of oxygen to 5%. All electronics in the room outside the test cabinet are flameproof. An automatic sprinkler system and hydrocarbon gas sensors are installed in the test room and cabinet. Piping and ventilation ducting are incorporated to purge the cabinet with nitrogen before opening in case of leakage of flammable or toxic fluids.

A small volume (9 litre) liquid reservoir for storing test fluid is situated in the same isolated room, and is blanketed with nitrogen.

The main control panel and instrumentation are remote from the test rig. They are situated outside the room, separated from the rig by a fire resistant wall. The rig will automatic shut down in the following conditions:

i) high or low test pressure,
ii) high or low test temperature,
iii) loss of nitrogen in the cabinet blanket,
iv) high hydrocarbon concentration in the cabinet or room,
v) high ambient temperature in the cabinet or room.

The instrumentation also allows full manual control from outside the test room.

A4.5 SIMPLIFIED TEST RIG

Two simplified test rigs were fabricated for running 3 to 6 month ageing tests in non-flammable fluids, such as water, carbon dioxide or nitrogen. The design test temperature is 100°C, and the test pressure is 2500psi (173 bar).

A4.5.1 Test vessels and flanges

The two test rigs are both made of 316 stainless steel. Each has a central fluid passage and four test flanges bolted together (see Fig A4.9). The geometry of each test flange is the same as those in the main seal life test rig. Therefore, two test seals of different configuration, flange and spigot, can be situated in each flange. A total of eight seals are tested in each rig at one time. The test flanges are assembled axially in the main body, no oscillation is required.

A4.5.2 Fluid supply system

The two simplified test rigs share a common fluid supply system which is similar to that in the main seal life rig (see Fig A4.10). A liquid pump is used for building up system pressure. They are operated by compressed air. System pressure can be read from a pressure gauge. A pressure transducer sends signals continuously to a chart recorder. An open reservoir is used for storing test liquid - normally distilled water.

A manual vent valve is installed to vent fluids. A relief valve is fitted as a precaution against system over-pressure.

A4.5.3 Leakage collection system

The leakage collection system of the two simplified rigs is designed for monitoring slow leakage from test seals. A collection channel is linked to the low pressure side of each test seal. These channels guide leakage fluids to individual measuring cylinders.

The measuring cylinders are filled with water in gas tests. Leakage can be visualized as bubbles. In liquid tests, the measuring cylinder can collect small amount of leaked liquid. A large gas or liquid leak would however lose pressure and stop the test.

A4.5.4 Instrumentation

Instrumentation on the two simplified rigs are very similar to those on the main seal life rig. Heating to the rigs are applied by two electric band-heaters attached to the outer surface of the pressure vessels and monitored by a pair of thermocouples between the heaters which operate a pre-programmed temperature controller. An additional pair of thermocouples are installed in the test fluid of each rig to detect in-situ fluid temperature which is logged onto the chart recorder.

Test parameters logged by the chart recorder for the two simplified rigs are :

i) pressure detected by the main pipework pressure transducer,

ii) fluid temperatures from in-situ thermocouples.

A4.6 GENERAL COMMENTS

The main seal life test rig has been running satisfactorily on both ageing and gas decompression tests. Specified test procedures are used (see section A4.7). The dimensions, hardness and interference force of O-rings tested in the rigs are measured before and after testing. By July 1991, a total of over 600 seals had been tested in BHR Group test rig. The experimental results from these tests are essential in building up the basic understanding in seal failure, contributing seal life material information, and providing data for validating the computer software.

A4.7 SEAL LIFE TEST RIG GENERAL OPERATING PROCEDURES

SEAL LIFE TEST RIG
GENERAL OPERATING PROCEDURE

1. Clean and purge the system and the bare test vessel.
2. Clean test modules.
3. Measure the test seals: dimensions, hardness etc. (parallel material tests on seals and material samples will be carried out at MERL).
4. Assemble test seals onto spigot and flange (application of assembly lubricants when necessary).
5. Measure the interference force on the flange seal.
6. Fit auxiliary leakage-collector seals.
7. Assemble test modules into vessel.
8. Purge the assembled test vessel with nitrogen.
9. Fill vessel with test fluid.
   For 'liquid-only' tests the vessel to be filled but unpressurized,
   for gas the relevant partial pressures of test gasses to be introduced.
10. Close vent valve.
11. Fill test cabinet with nitrogen for inflammable fluid tests.
12. Bring the vessel up to test temperature, release pressure if it goes higher than the test pressure.
13. Set test pressure and commence housing oscillation.
14. During the test monitor: test pressure, temperature, oscillation and leakage.
    (If leakage occurs this is piped individually to a collector vessel with facilities for observation of leakage and measurement of pressure

build up in the collector. Small levels of leakage is made up by the test fluid pumps to maintain the test conditions. In the event of excessive leakage the test will be terminated.)

15. At end of test period: Reduce temperature and pressure as prescribed in the relevant additional test procedure - **Depressurization test operating procedure or Ageing test operating procedure.**
16. Turn off nitrogen supply to test cabinet when the rig is cooled to room temperature.
17. Close vent valve and apply low pressure, less than 500psi, for cold leak test of the seals. Inspect all seals for leakage. Vent pressure.
18. Purge test chamber of any hazardous test fluid.
19. Remove the test modules.
20. Remove the spigot seals for inspection.
21. Remove flange shim and leakage collector seal form the flange seal arrangement.
22. Measure residual seal interference force.
23. After interference measurements remove flange seal for inspection.
24. Measure dimensions and hardness of the seals.

SEAL LIFE PREDICTION RIG

DEPRESSURIZATION TEST

OPERATING PROCEDURE - 20Feb90

1. Follow **SEAL LIFE TEST RIG GENERAL OPERATING PROCEDURE**, (Appendix 1), steps 1 to 8 for assembling test modules into vessel, and connecting all pipings.

2. Fill the vessel with test fluid (carbon dioxide, nitrogen, methane, ...etc.), apply a low pressure ~**150psi** (=10bar)

3. Bring the vessel up to test temperature, normally one of the below: 195°C, 155°C, 130°C, 100°C, 70°C

4. Apply test pressure. Inspect all seals for leakage.

5. Soak in test temperature and pressure for **half an hour**. Inspect all seals for leakage.

6. Turn off heater.

7. Turn off pump.

8. Depressurization - Open vent valve to allow test pressure to be released in about **15 minutes.**

9. Allow vessel to cool to room temperature.

10. Low pressure test
    - close vent valve
    - apply low pressure, less than **500 psi (~30 bar)**
    - keep low pressure for **10 to 15 minutes**
    - inspect all seals for leakage
    - vent pressure

11. Return to **SEAL LIFE TEST RIG OPERATING PROCEDURE** (see Appendix 1) steps 16 to 23 for post-testing procedure

SEAL LIFE TEST RIG
AGEING TEST OPERATING PROCEDURE

1. Follow **SEAL LIFE TEST RIG GENERAL OPERATING PROCEDURE**, (Appendix 1), steps 1 to 14 for assembling test modules into vessel, and running test.
2. At end of test period, turn off pump.
3. Turn off heater, let the rig to cool overnight to room temperature.
4. Open throttle vent valve to allow remaining fluid pressure to be released at about 2psi/min.
5. low pressure test
   - close vent valve
   - apply low pressure, less than **500psi (~30bar)**
   - keep low pressure for **10 to 15 minutes**
   - inspect all seals for leakage
   - vent pressure
6. Return to **SEAL LIFE TEST RIG GENERAL OPERATING PROCEDURE** (see Appendix 1) steps 16 to 24 for post-test procedures.

Fig A4.1 Seal life prediction rig

Fig A4.2 Assembly of seal life prediction rig

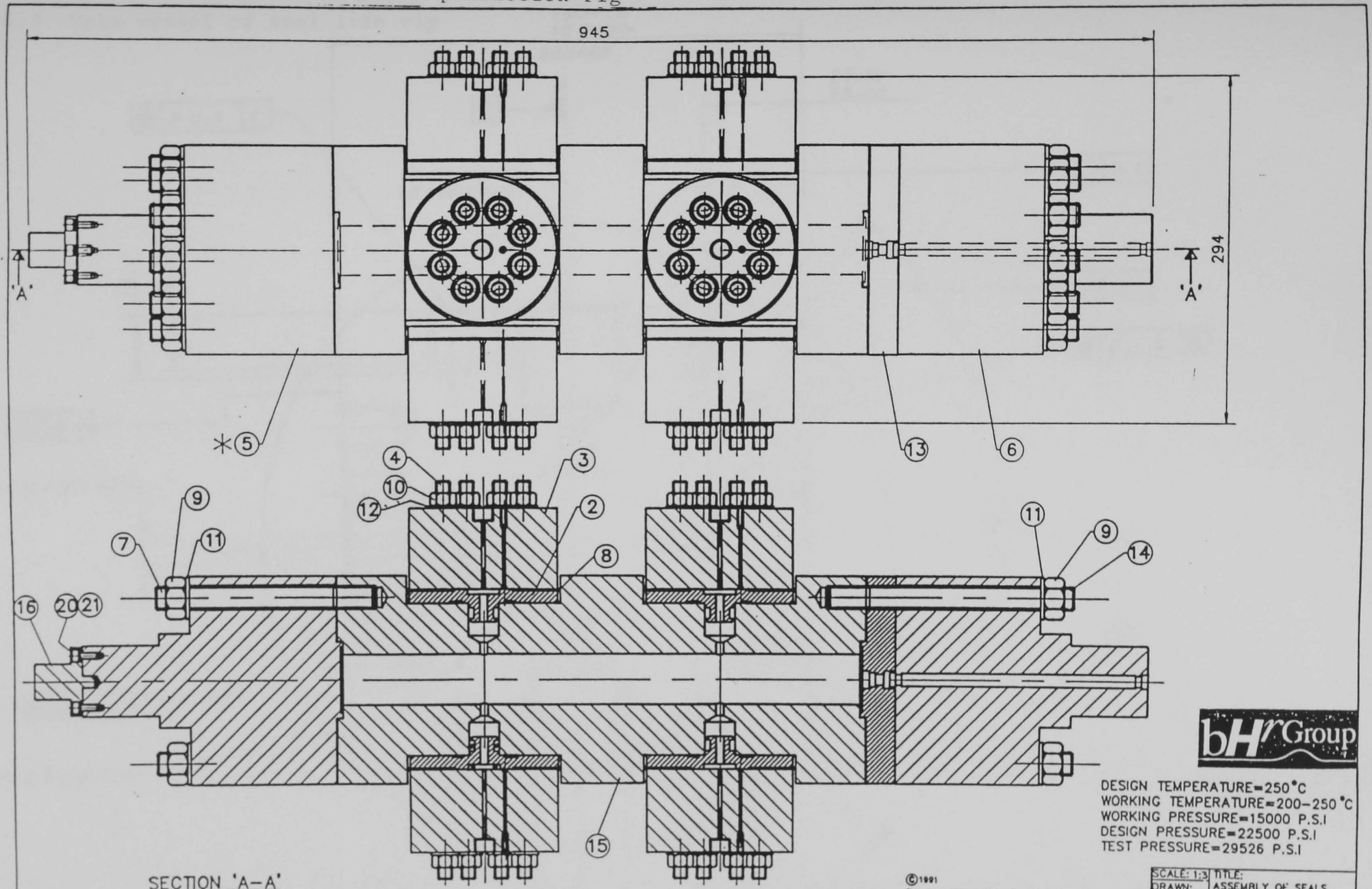

Fig A4.3 Main vessel of seal life rig

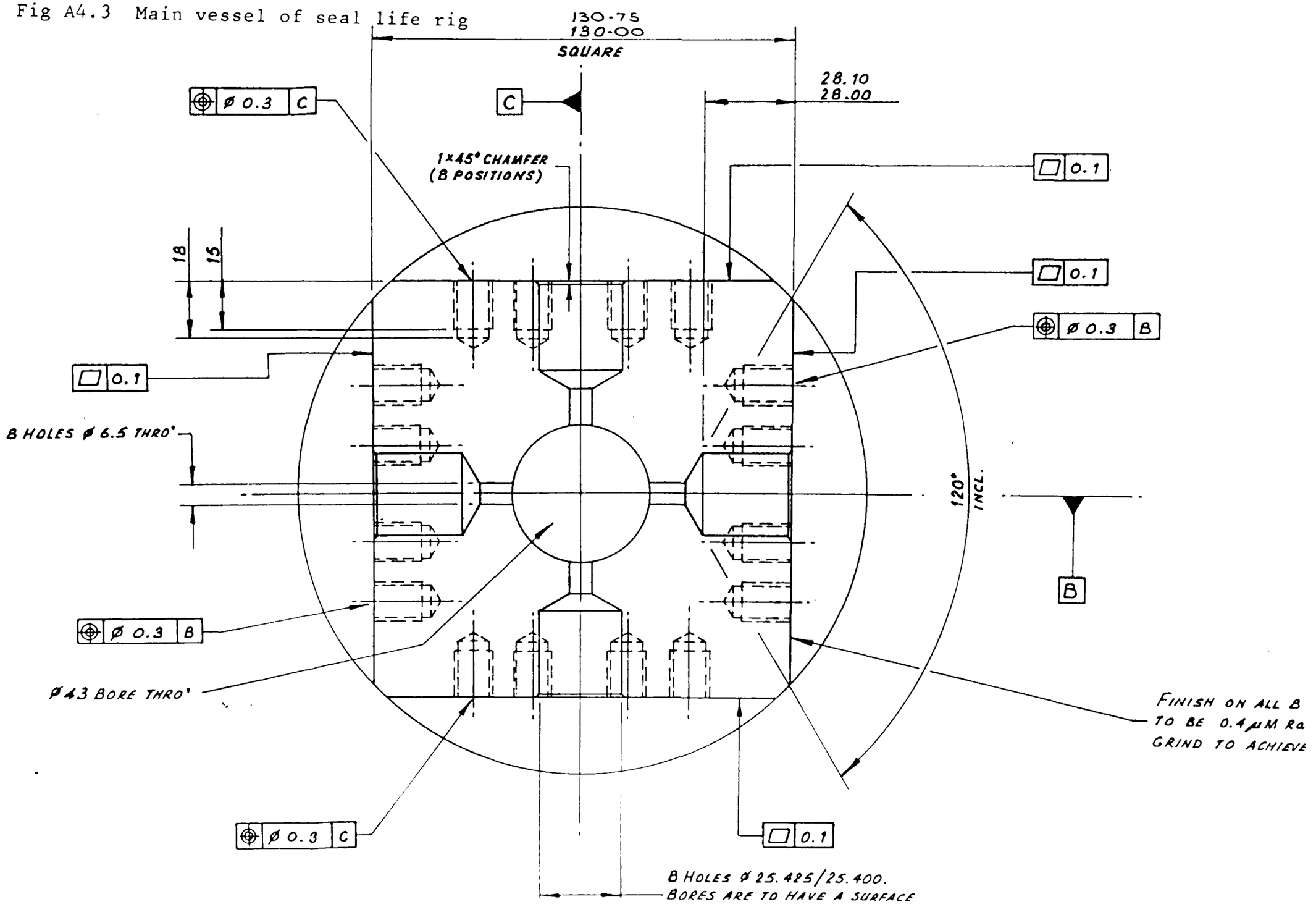

Fig A4.4 Flange of seal life rig

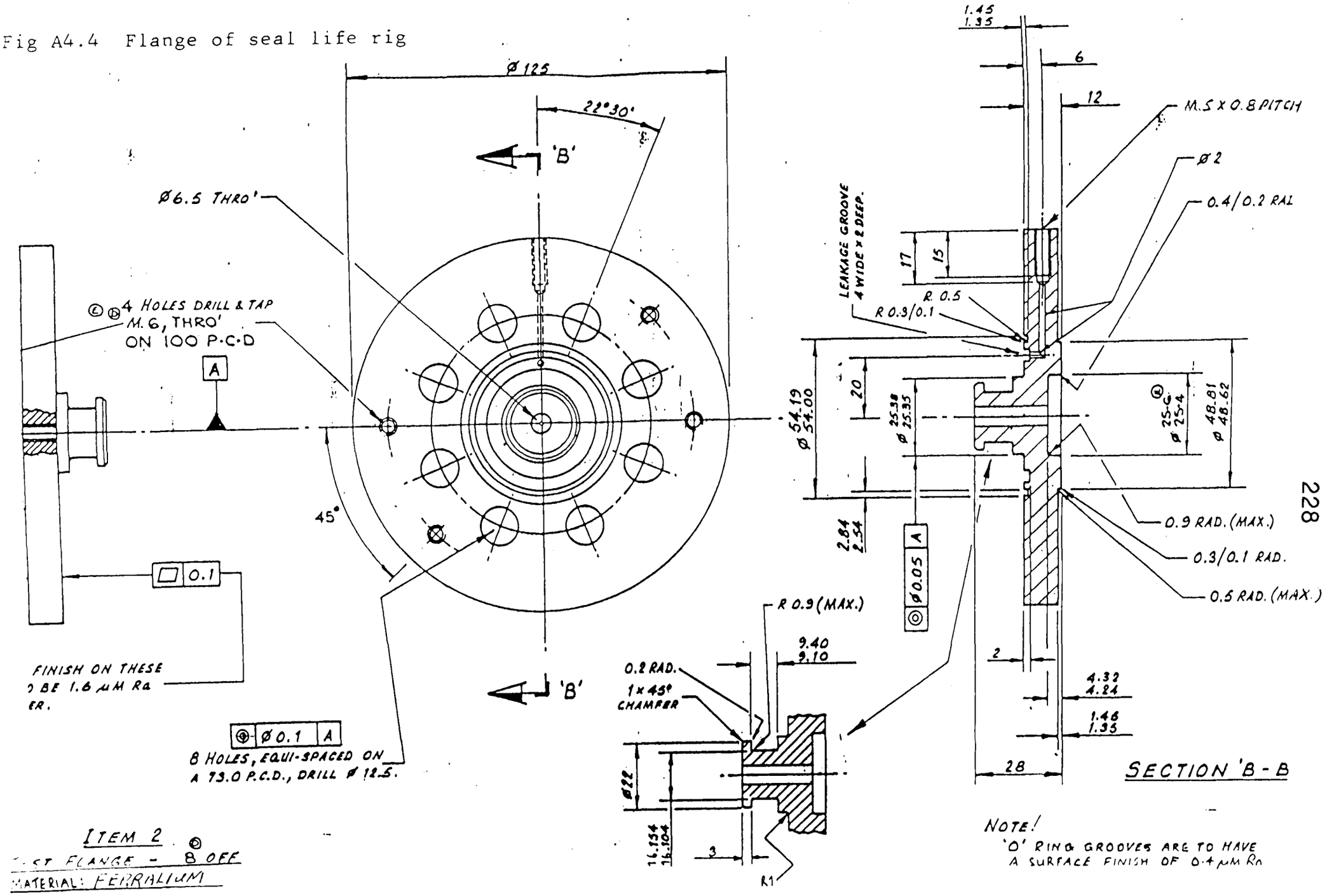

ITEM 2

FLANGE - 8 OFF

MATERIAL: FERRALIUM

NOTE!
'O' RING GROOVES ARE TO HAVE
A SURFACE FINISH OF 0.4 µM Ra

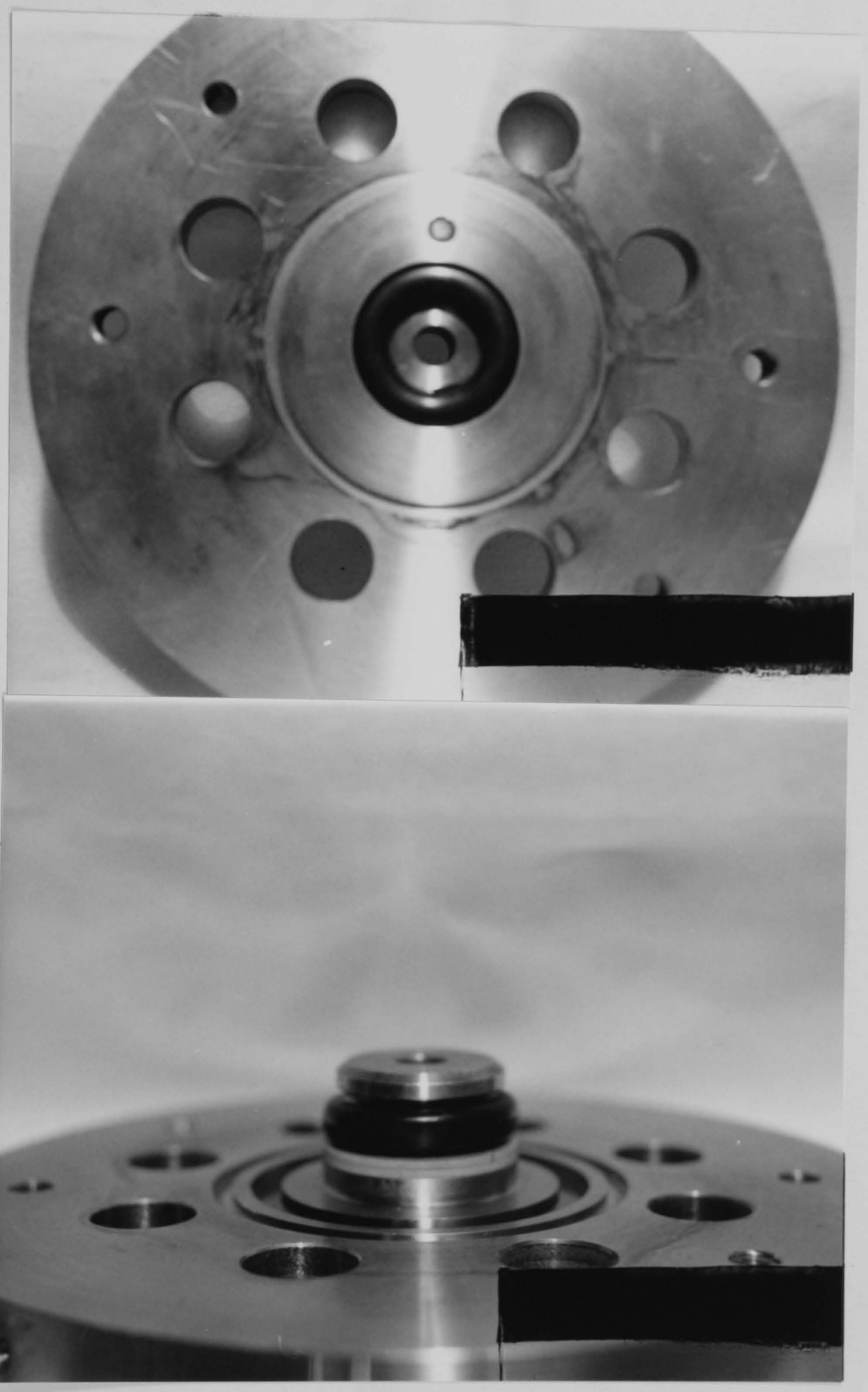

Fig A4.5 O-rings in flange and spigot locations

Fig A4.6 Additional flanges with 0.2mm extrusion gap

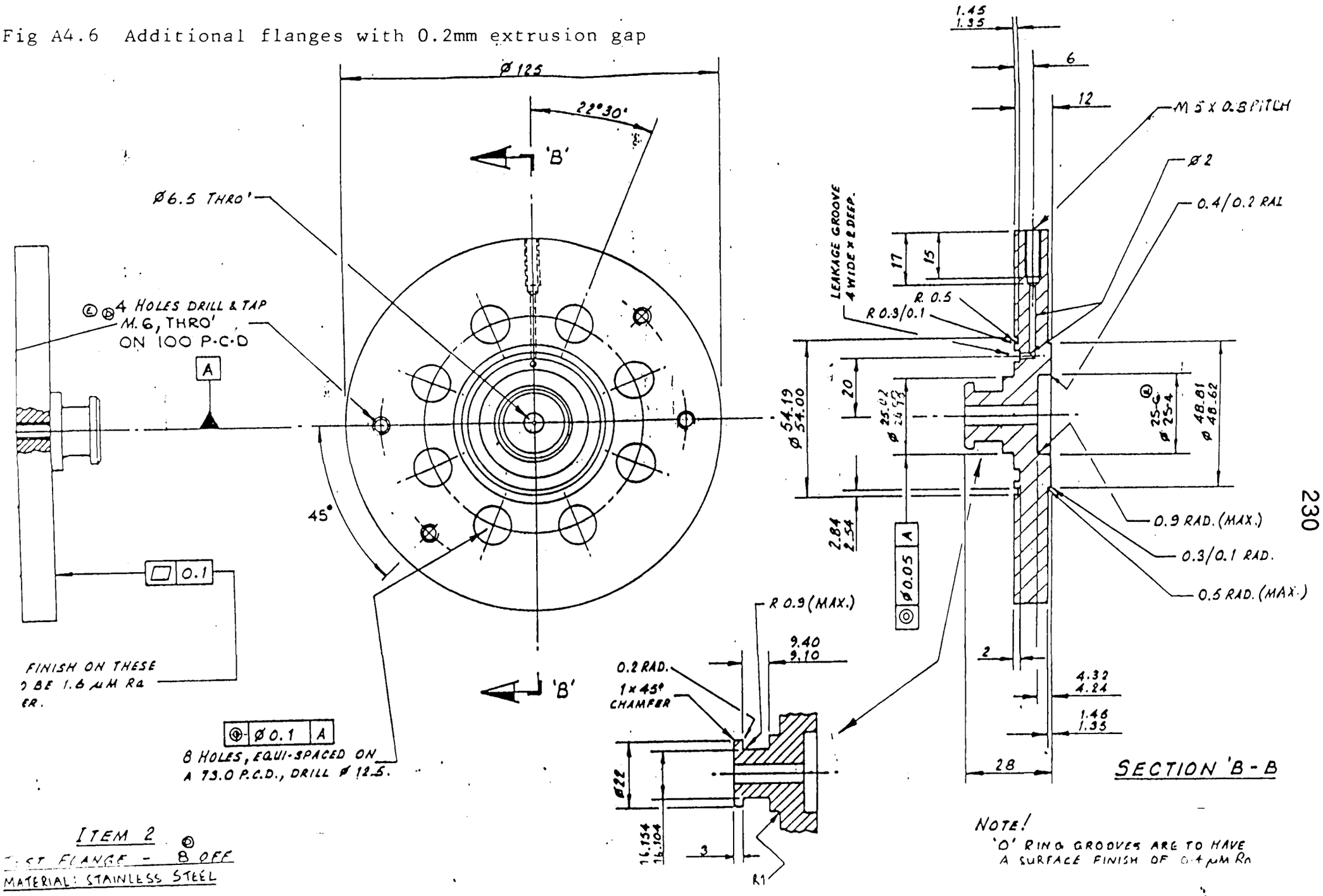

ITEM 2

TEST FLANGE - 8 OFF

MATERIAL: STAINLESS STEEL

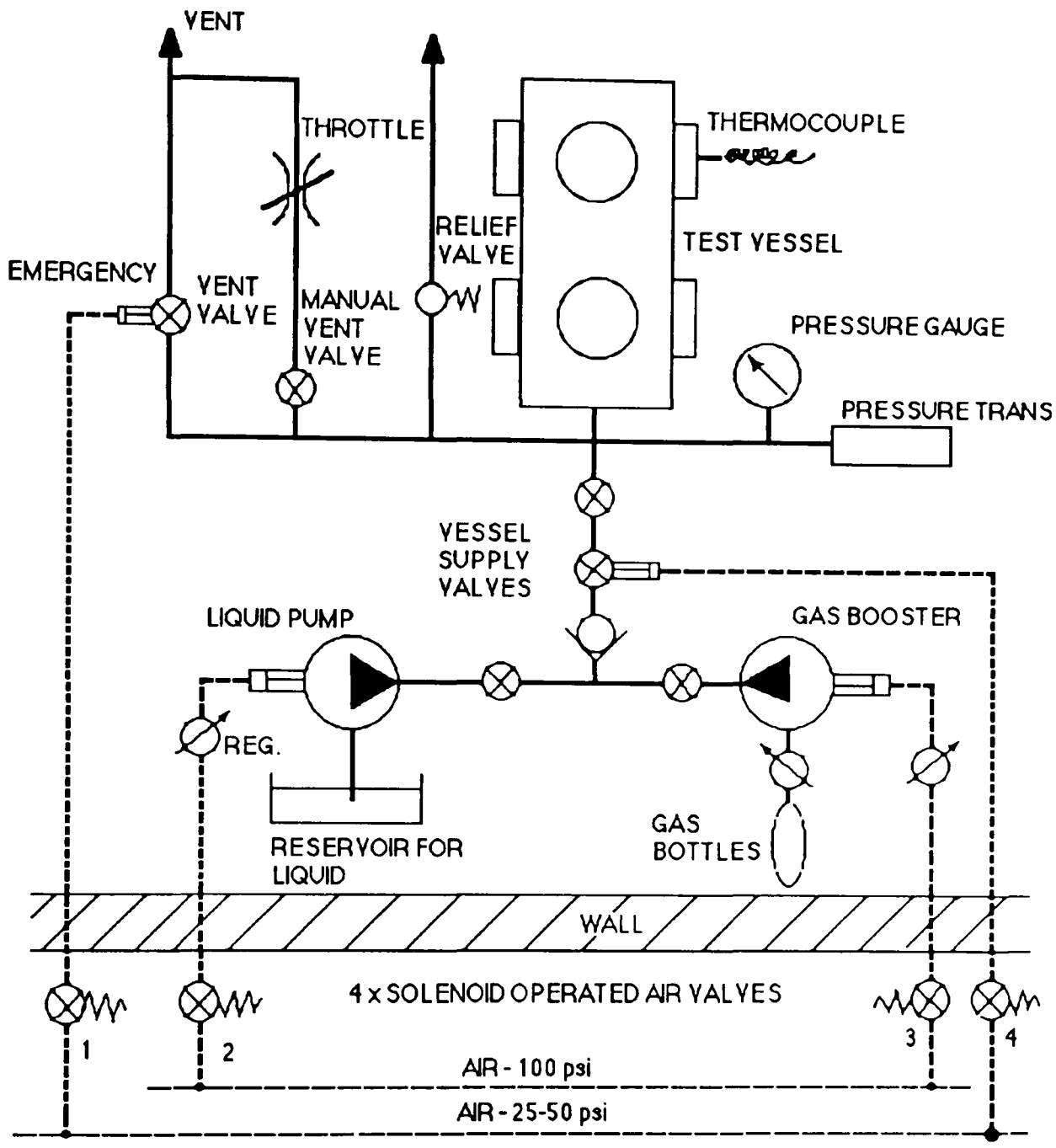

Fig A4.7 Seal life prediction test circuit

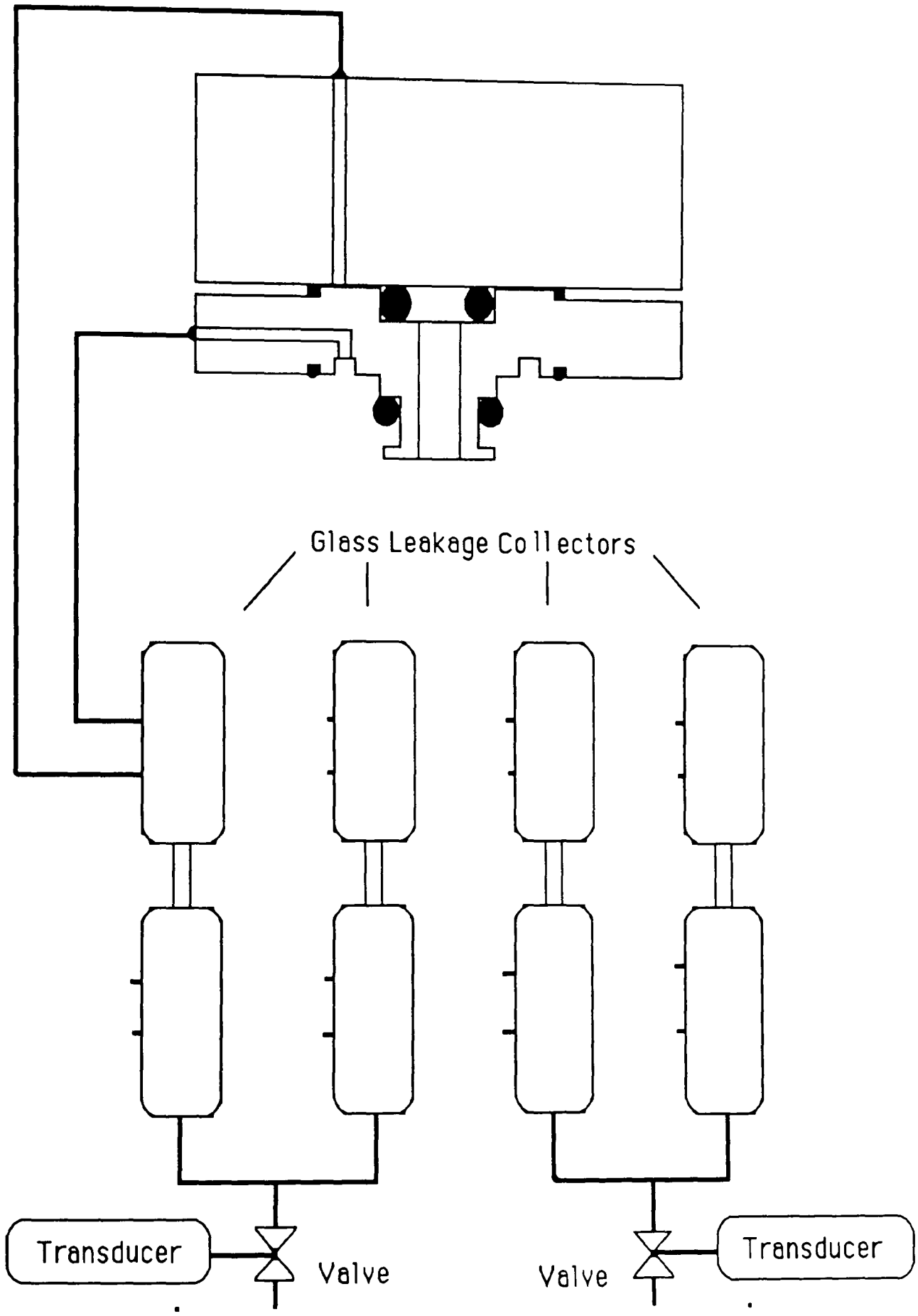

Fig A4.8 Leakage collection system for main seal life rig

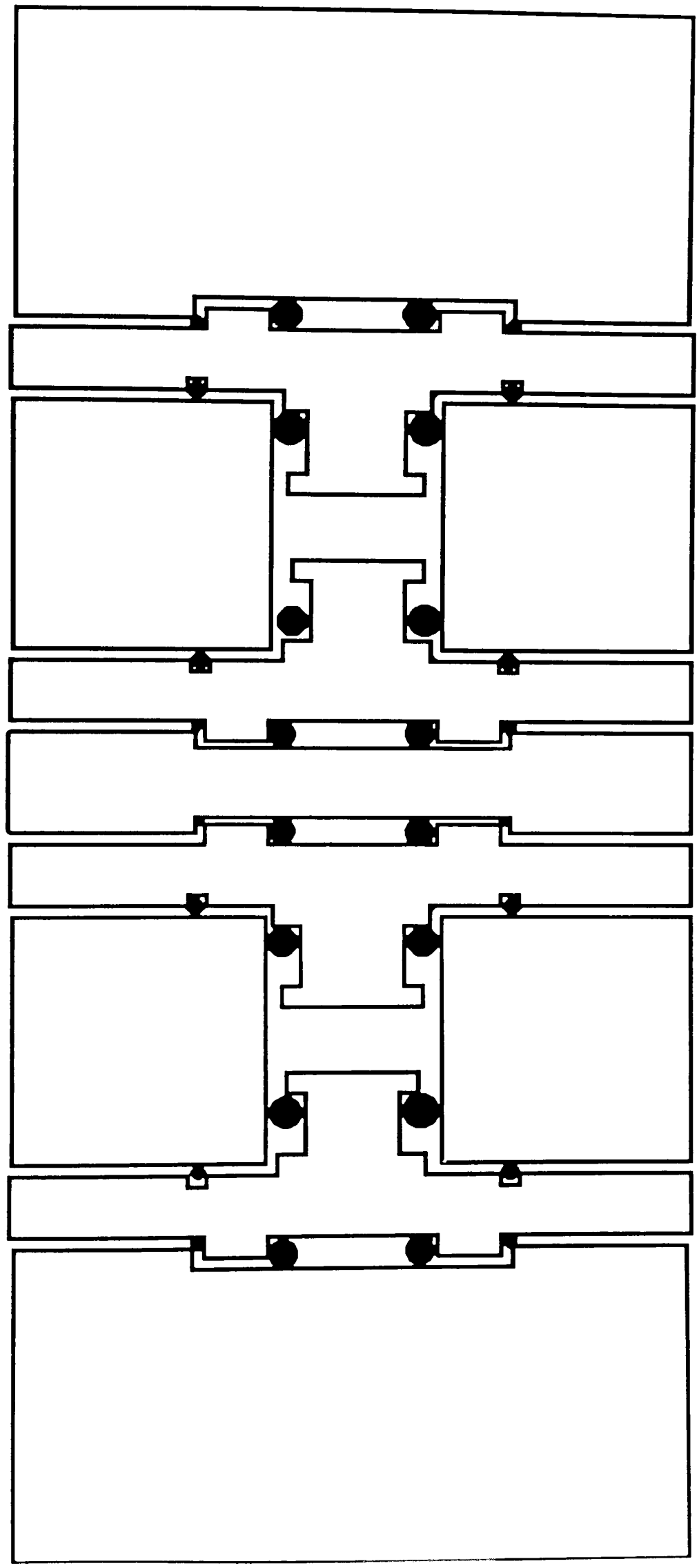

Fig A4.9 Simplified rig for long term test

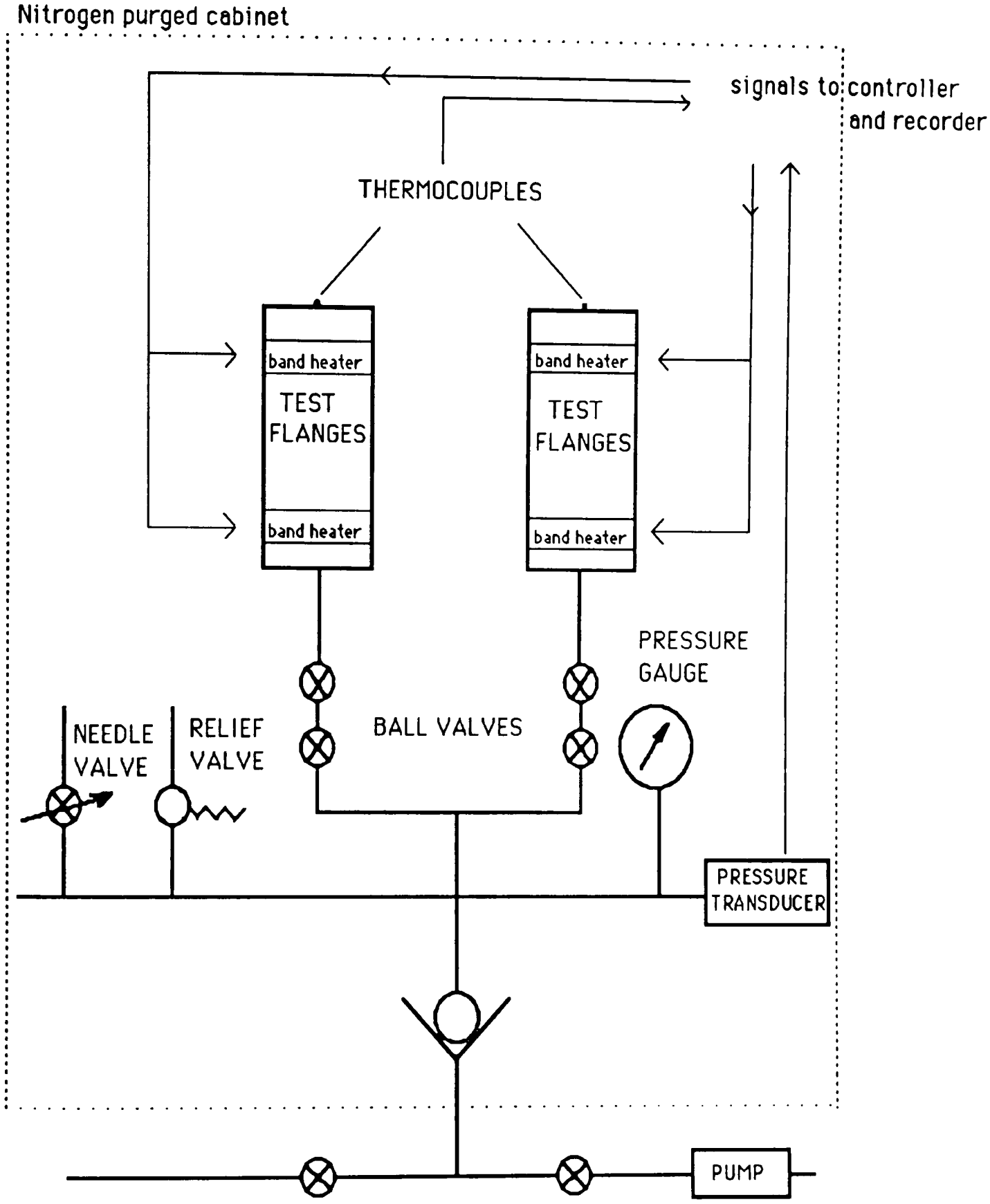

Fig A4.10 Fluid supply system for simplified test rig